F-THEORY REALIZATIONS OF EXACT MSSM MATTER SPECTRA

Muyang Liu

A DISSERTATION

in

Physics and Astronomy

Presented to the Faculties of the University of Pennsylvania

in

Partial Fulfillment of the Requirements for the

Degree of Doctor of Philosophy

2021

Supervisor of Dissertation

Mirjam Cvetič, Professor of Physics and Astronomy

Graduate Group Chairperson

Jonathan Heckman, Professor of Physics and Astronomy

Dissertation Committee

Mirjam Cvetič, Professor of Physics and Astronomy

Ron Donagi, Professor of Mathematics

Jonathan Heckman, Associate Professor of Physics and Astronomy

Justin Khoury, Professor of Physics and Astronomy

Evelyn Thomson, Associate Professor of Physics and Astronomy

F-THEORY REALIZATIONS OF EXACT MSSM MATTER SPECTRA

Muyang Liu

This thesis is dedicated to my mom

Acknowledgments

First of all, I would like to express my sincere gratitude to my advisor Mirjam Cvetič for guiding me through the fantastic world of string theory. I greatly benefited from her profound knowledge, not only as a young physicist who attempts to touch the exploring of our universe since the early days of my research life, but also as a person greatly supported by her extensive patience and continuous encouragement, which influence me deeply on the aspects of both academically and non-academically. It is my great pleasure to become a student of Mirjam, and the treasured discussion with her will motivate me forever in the pursuit of future research.

Furthermore, many thanks go to Ling Lin for leading me through the understanding of basic F-theory compactification in my early days of graduate study, which gives rise to our fruitful collaborations thereafter. I would like to especially thank Martin Bies for patiently listening to all of my questions. His insights and suggestions guide me throughout scientific exploration as well as benefits me in developing numerous skills from an amateur. I would also like to thank Paul-Konstantin Oehlmann, Fabian Ruehle, Jiahua Tian, Hao Zhang, and Gianluca Zoccarato for their friendly advice and collaboration. Many thanks also delivery to my office mate Thomas Rochais for our enjoyable and interesting discussions as well as strong supports between us.

I would like to thank Prof. Ron Donagi, Prof. Jonathan Heckman, Prof. Justin Khoury, and Prof.Evelyn Thomson at the University of Pennsylvania for their constant help, as well as their parts on my thesis committee. It is my great honor to have them on my committee and eventually evaluate my research. I would also like to thank Prof. James Halverson at Northeastern University for his shared interests and collaborations with me as well as his supports as referee of my postdoc searching.

I am thankful to the University of Pennsylvania and the many institutions that have hosted me over the past five years: Harvard University, the Simons Center for Geometry

and Physics at Stony Brook, CERN, International Solvay Institutes, and the University of Oxford. It is my great pleasure to meet so many amazing researchers there.

Finally, and most importantly, I would like to express my deepest thanks to my family and friends for their supports and love, which make my every day joyful. Thank you indeed!

ABSTRACT

F-THEORY REALIZATIONS OF EXACT MSSM MATTER SPECTRA

Muyang Liu

Mirjam Cvetič

F-theory is remarked by its powerful phenomenological model building potential due to geometric descriptions of compactifications. It translates physics quantities in the effective low energy theory to mathematical objects extracted from the geometry of the compactifications. The connection is built upon identifying the varying axio-dilaton field in type IIB supergravity theory with the complex structure modulus of an elliptic curve, that serves as the fiber of an elliptic fibration. This allows us to capture the non-perturbative back-reactions of seven branes onto the compactification space B_3 of an elliptically fibered Calabi–Yau fourfold Y_4. The ingredients of Standard model physics, including gauge symmetries, charged matter, and Yukawa couplings, are then encoded beautifully by Y_4's singularity structures in codimensions one, two, and three, respectively. Moreover, many global consistency conditions, including the D3-tadpole cancellation, can be reduced to simple criteria in terms of the intersection numbers of base divisors.

In this thesis, we focus on searching for explicit models in the language of F-theory geometry that admit exact Minimal Supersymmetric Standard Model (MSSM) matter spectra. We first present a concrete realization of the Standard Model (SM) gauge group with $\mathbb{Z}_2$ matter parity, which admits three generations of chiral fermions. The existence of this discrete symmetry beyond the SM gauge group forbids proton decay. We then construct a family of $\mathcal{O}(10^{15})$ F-theory vacua. These are the largest currently known class of globally consistent string constructions that admit exactly three chiral families and gauge coupling unification.

We advance to study the vector-like spectra in 4d F-theory SMs. The 4-form gauge back-

ground G_4 controls the chiral spectra. This is the field strength of 3-form gauge potential C_3, which impacts the vector-like spectra. It is well known that these massless zero modes are counted by line bundle cohomologies over matter curves induced by the F-theory gauge background. In order to understand the line bundle cohomology's dependence on the moduli of the compactification geometry, we pick a simple geometry and create the database consisted of matter curves, the line bundles and the vector-like spectra. We analyze this database by machine learning techniques and ugain full understanding it via the Brill-Nother theory. Subsequently, we present the appearance of root bundles and how they enter as significant ingredients of realistic F-theory geometries. The algebraic geometry approaches to root bundles allow combinatoric descriptions, which facilitate the analyze of statistics on the vector-like spectra at the end of this thesis.

LIST OF TABLES

LIST OF ILLUSTRATIONS

Part I

Motivation

CHAPTER 1: Motivation

From natural philosophy to modern physics Due to the rise of universities in medieval times, the concepts of mass, energy and motion slowly shaped into the form we are familiar with today. Those conceptual developments prompted physics to evolve from the rubric of natural philosophy. During the renaissance, scholars devoted themselves to the foundation of modern science. For instance, Galileo Galilei realized that the leading criteria of a successful physics theory is the extent to which its predictions agree with empirical observations. Since then, theoretical physicists endeavor to apply proposed models to explain phenomena in nature that have been observed in experiments and predict new phenomena. Meanwhile, they undertake great efforts to explore the connection between mathematical theorems and physics objects. The vision provided by pure mathematical systems can provide clues to how a physical system might be modeled. For instance, the notion of differential geometry that spaces can be curved, had a significant impact on the theory of general relativity (GR). Entering the 19th and 20th centuries, the most significant conceptual achievements were the laws of thermodynamics as well as the electromagnetic force, which was initially explained by Maxwell's equations. Moving forward, the revolution of modern physics lies on the root of two branches: relativity theory and quantum mechanics. The theory of GR describes the gravitational dynamics of large-scale objects like galaxy clusters. In contrast, quantum mechanics attempts to understand the internal structures and interactions of atoms and molecules at small scales.

To date, in the framework of quantum field theory (QFT), the Standard Model (SM) of particle physics has combined effects of three of the four known fundamental forces. It contains electromagnetism, weak and strong interactions described by a QFT with $SU(3)_C \times SU(2)_L \times U(1)_Y$ gauge symmetry. However, if we bring GR naively to the quantum scale, the theory is not renormalizable. To that end, string theory is one of the promising candidates for a theory of quantum gravity. It provides various applications which range from heavy ion physics to condensed matter, black hole physics, or early

universe cosmology. It has also stimulated a number of outstanding developments in pure mathematics.

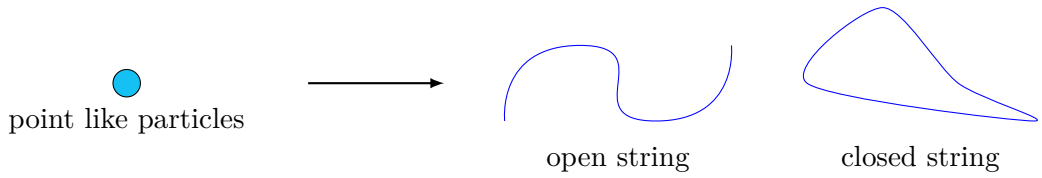

Figure 1: Strings behave as ordinary point-like particles at the energy well below M_s.

String theory – A consistent theory of quantum gravity String theory proposes that the building blocks of elementary particles are *not* point-like. Instead, they are small one-dimensional objects, *strings*, of typical size $l_s = 1/M_s$, with M_s known as the string scale. As we have not observed strings in experiments, the string scale must be incredibly large compared to any experimentally probed energy scale. Many string models believe that the string scale M_s is of the order of the Planck energy $M_{\rm Planck} \sim 10^{19}$ GeV. On the distance at least several magnitudes larger than the string length l_s (at the energy well below M_s), strings behave as ordinary point-like particles, with dynamics described by the low energy effective theory of particle physics. Different vibrational states of strings determine various properties (mass, charges, spin, etc.) of the oscillation states and behave as distinct particles.

There are two types of strings: they can be either open or closed as depicted in Figure 1. A closed string is topologically equivalent to a circle and has no end-points. On the other hand, an open string has two end-points and is topologically equivalent to a line interval of a closed string. One of the many oscillation states corresponds to a spin two particle – graviton, the force carriers of gravity. Moreover, a string perturbation series can provide its UV-completion – the string scattering amplitudes are finite at each loop, hence are already renormalizations of the underlying effective field theory amplitudes. [1] Thus, it is commonly believed that string theory is a UV-finite quantum description

[1] It is commonly argued that the string is UV-finite to all orders. However, IR-finiteness is only discussed much more recently at low loop order.

including a graviton, which makes it a consistent theory of quantum gravity. In addition, string theory also leads to significant progress in other aspects of gravity, like accounting for the microscopic degrees of freedom of certain black holes, and explicitly realizing holography in terms of the AdS/CFT correspondence. Most remarkably, string theory is not a purely gravitational theory, but contains the basic building blocks of the SM, naturally including non-abelian gauge interactions, charged chiral fermions in replicated families, fundamental scalars, Yukawa couplings, etc. [3, 4, 5, 6, 7, 8]

The earliest version of string theory, bosonic string theory, incorporated only the class of particles known as bosons. It has good behavior at high energy only if the spacetime has the critical dimension $D = 26$. If we include fermionic excitations and enforce supersymmetry between bosons and the fermions, consistency of string theory requires $D = 10$. This physical theory is known as superstring theory. Prior to the mid 1990s, five consistent versions of superstring theories in flat 10-dimensional Minkowski spacetime, were known. These are termed type I, type IIA, type IIB, heterotic $E_8 \times E_8$ and heterotic $SO(32)$ string theory. They were seemed to be independent of each other. However, Edward Witten realized [9] that they were different perturbative limits of a single underlying theory in 11 dimensions, which is today known as M-theory. This insight uncovered relations among these perturbative string theory formulation by so-called dualities.

Compactification As fermions are observed in our daily experience, we focus on superstring theories in this thesis. In order to explore the connections between the constructed string models and the observed physics in the 4 dimensional spacetime, we employ the mechanism of compactification as a generalization of Kaluza–Klein (KK) theory [10, 11, 12]. The theory of KK was an extension of GR. It is a classical unified field theory of gravitation and electromagnetism built around the idea of an extra fifth dimension depicted as a circle beyond the common 4 dimensional spacetime. It turns out that the 5d field equations can be reinterpreted in terms of physics in the four non-compact dimensions as 'ordinary' GR coupled to an electromagnetic gauge field. Furthermore, the

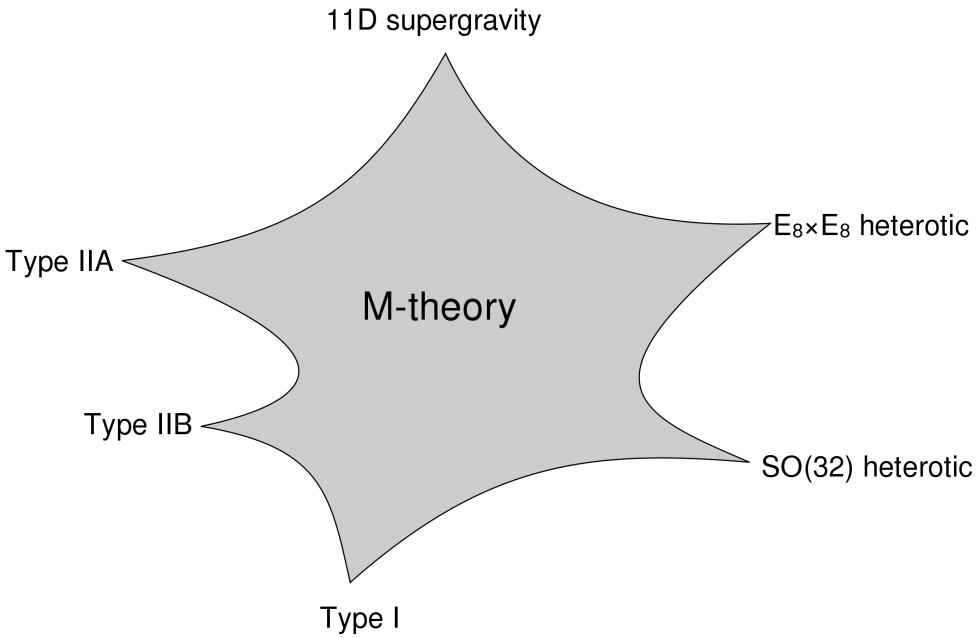

Figure 2: A schematic visualization of the relationship amongst M-theory, the five superstring theories and eleven-dimensional supergravity. The shaded region represents possible physical configurations of M-theory (also known as its 'moduli space'). The five different superstring theories sitting at certain corners represent certain limits of the moduli space of M-theory.

coupling strength can be related to the size of the extra dimension, which is a so-called (Kähler) modulus. Each modulus gives rise to a massless scalar field that freely propagates in 4D spacetime. Hence, KK theory is considered an important precursor to string theory, where we introduce compact dimensions to obtain a higher-dimensional manifold with much richer structure of the moduli space compared to the simple circle applied by KK theory. This mechanism is referred to as string compactification.

The string compactification is defined on a spacetime $M_{10} = M_4 \times X_6$. X_6 is called the *internal space*, which is a 6-dimensional compact manifold. The size of the internal space is taken small enough so that at energies well below M_s, the 4d effective theory agrees with the physics of our everyday experience. Calabi-Yau manifolds were first considered [13] for compactifications of six dimensions in superstring theory because they leave some

of the original supersymmetry unbroken. The unbroken $\mathcal{N} = 1$ supersymmetry requires that the manifolds have, for perturbatively accessible configurations, $SU(3)$ holonomy and that the four-dimensional cosmological constant vanishes. The existence of spaces with $SU(3)$ holonomy was conjectured by Calabi [14] and proven by Yau [15]. Many Calabi–Yau varieties/orbifolds can be found as weighted complete intersections in a weighted projective space. Various constructions of Calabi-Yau varieties allow us to explore possible embeddings of the SM of particle physics in the 4 dimensional spacetime in string theory. Such questions are interested in a field commonly known as string phenomenology, and this thesis is part of it.

D-brane Objects called Dp-branes are extended objects of p spatial dimensions, which at weak coupling can be defined as $(p+1)$-dimensional subspace of the spacetime on which open strings end. These Dp-branes feature prominently in string compactifications and obey non-perturbative dynamics [16]. It is crucial to observe that stacks of coincident Dp-branes realize gauge algebras [3, 4, 5, 6, 7, 8] and thus make it possible to engineer non-trivial gauge theories in string compactifiations. In braneworld models, systematic studies of D-brane configurations in a Calabi-Yau manifold leads to various approaches of SM building in string theory. Past work on intersecting branes models in type II include [17, 18, 19, 20, 21, 22, 23] (see also [24] and references therein).

The most important ingredient in type IIA brane world models are the D6-branes as well as their intersection patterns. We consider a flat 10d space, decomposed as $M_4 \times \mathbb{R}^2 \times \mathbb{R}^2 \times \mathbb{R}^2$ and two stacks of D6-branes. [2] These D6-branes are "flat" (considered as straight lines) in each $\mathbb{R}^2$-factor and fill all of the external Minkowski space. Their relative position is therefore completely specified by the enclosed angle θ_i in the i-th $\mathbb{R}^2$ factor.

$\mathcal{N} = 1$ supersymmetry is preserved if $\sum_i \theta_i = n \cdot 2\pi, n \in \mathbb{Z}$. Chiral fermions are localized at the intersection of the brane volumes. Perturbative type IIB superstring theory is

[2] In fact, many constructions consider T^2 instead of $\mathbb{R}^2$ (the 2-dimensional torus). Generalization considers the orbifold quotients of this space.

closely related to type IIA via T-duality. The engineering of desired gauge groups can easily be realized in compactifications with D3- and D7-branes [24, 25] Unfortunately, backreactions of the D7-branes cause a breakdown of the perturbative theory as reviewed in [26]. Consequently, people began to push beyond the perturbative limits of M-theory to handle such compactifications. One of the most prominent non-perturbative frameworks of constructing string compactifications is F-theory.

F-theory As a branch of string compactifications, F-theory encodes the back-reactions of the seven branes in IIB theory in the geometry of an elliptically fibered Calabi-Yau space $Y_{n+1} \to B_n$. [3] By studying this space Y_{n+1} with well-established tools of algebraic geometry, one can then ensure the global consistency conditions of the physics in $10-2n$ non-compact real dimensions. Developed by Cumrun Vafa.[27], F-theory provides a very flexible tool to cover the to date largest set of consistent vacua [28, 29, 30, 31, 32](see [33, 34, 35, 26] for some reviews). This flexibility follows from the systematic engineering of gauge theories coupled to gravity by use of powerful tools of algebraic geometry.

Motivated by the capability of F-theory constructions, this thesis focuses on an important characteristic of 4d $\mathcal{N}=1$ F-theory compactifications (i.e.,n= 3). Namley, by following the philosophy of string phenomenology, we search for geomemtries such that the 4d low energy effective theory closely resembles the MSSM. As a first step beyond the gauge group, we focus on a chiral fermionic spectrum. It is fixed by a background gauge flux, which is specified by the internal C_3 profile in the dual M-theory geometry. Namely, the chiral spectrum only depends on the flux $G_4 = dC_3 \in H^{(2,2)}(Y_4)$. By now, there exists an extensive toolbox for creating and enumerating the so-called primary vertical subspace of G_4 configurations [36, 37, 38, 39, 40, 41, 42]. The application of these tools led to the construction of globally consistent chiral F-theory models [40, 42, 43, 44], which recently culminated in the largest class of explicit , globally consitent string vacua which realize the Standard Model gauge group with its exact chiral spectrum and gauge coupling

[3] n is the complex dimension

unification [32].

However, these methods are insufficient to determine the exact vector-like spectrum of the chiral zero modes (i.e., not just the difference between chiral and anti-chiral fields). This is because the zero modes depend not only on the flux G_4, but also on the flat directions of the potential C_3. The complete information of the gauge potential is encoded in the so-called *Deligne cohomology*. In [45, 46, 47], methods for determining the exact vector-like spectra were put forward. This approach exploits the fact that (a subset of) the *Deligne cohomology* can be parameterized by Chow classes. By use of this parameterization, one can extract line bundles $L_{\mathbf{R}}$ that are defined on curves $C_{\mathbf{R}} \subset B_3$. In the dual IIB picture, this can be interpreted as localization of gauge flux on matter curves, which lifts some vector-like pairs on these curves. Explicitly, the zero modes are counted by the sheaf cohomologies of $L_{\mathbf{R}}$ and we have $h^0(C_{\mathbf{R}}, L_{\mathbf{R}})$ massless chiral and $h^1(C_{\mathbf{R}}, L_{\mathbf{R}})$ massless anti-chiral superfields in representation $\mathbf{R}$ on $C_{\mathbf{R}}$. Based on this motivation, the goal of this thesis is to find a realistic F-theory geometry with situable line bundle cohomology on each matter curve $C_{\mathbf{R}}$ such that the produced spectrum exactly matches the massless matter spectrum of the MSSM.

Outline of the thesis Part I provides a broad summary of techniques used throughout this thesis, which experts may skip. In section 1 we review generalities of String theory. Subsequently, we explain in section 2 how F-theory encodes the physics of B_n in an elliptic fibraton $Y_{n+1} \to B_n$.

In Part II, we discuss the model building of the exact chiral spectrum in the F-theory realizations. Different gauge symmetries are realized by different fiber geometries, as presented in chapter 3 and chapter 4. We advance to seek the approaches towards complete matter spectra in 4d $\mathcal{N} = 1$ F-theory compactifications in Part III. First, we introduce how line bundle cohomologies dependen on the complex structure moduli of the compactification geometry. To this end, we focus in chapter 5 on a simple geometry, for which we can compute the vector-like spectrum by brutal force. We generate a database and

analyze this data with machine learning techniques. We find that jumps in the vector-like spectrum ca somtimes, but not always, be predicted from topology. A complete understanding of our data is acheived with Brill-Nother theory. Equipped with this understanding, we turn back to fully F-theory steups in chapter 6. In QSM geomemtries, we notice that root bundles are significant ingredients of realistic F-theory SMs. We prove existence of root bundles on all/but the Higgs matter curve with cohomologies required for F-theory MSSMs. The algebraic geometry approaches and the programming scanning of root bundles give rise to key outputs of statistics that are heavily applied in chapter 7. We focus on searching for explicit models in our landscape of F-theory Standard Models that have a realistic vector-like spectrum. The results of chapters 3 to 7 have been presented in the publications [44, 32, 48, 49, 50].

Part II

Introduction

In this chapter we start with the motivations for string compactifications followed by a brief introduction to M-theory. For a detailed review of string theory, see [3, 4, 5, 6, 7, 8]. Then we follow with a very short review of F-theory [27] as a non-perturbative extension of type IIB string theory and as a decompactification limit of M-theory compactifications. With these ingredients, we will then present the appearance of gauge symmetries, matter states and Yukawa couplings along singularities in 4D F-theory compactifications.

2.1 String Theory Basics

2.1.1 Warm up - the bosonic string

As a string propagates in spacetime, it sweeps out a two-dimensional surface Σ, known as the worldsheet. Any point in the worldsheet is labeled by two coordinates (t, σ), where t denotes the "time" coordinate analogous to that in point particle worldlines, and with σ parameterizing the extended spatial dimension of the string at fixed t. A classical string configurations in D-dimensional Minkowski space M_D is given by a set of functions $X^M(t, \sigma)$ with $M = 0, \cdots, D-1$, which specify the spacetime position of the worldsheet point (t, σ). More precisely, the functions $X^M(t, \sigma)$ provide an embedding of the surface Σ (worldsheet) into D-dimensional spacetime M_D (target space).

The string dynamics is defined by an action $S[X(t, \sigma)]$. A natural proposal for the classical string action is called Nambu-Goto action, [1] which is the total area spanned by the worldsheet (analogous to the point particle action given by the worldline interval)

$$S_{NG} = -\frac{1}{2\pi\alpha'}\int_\Sigma dA = -\frac{1}{2\pi\alpha'}\int_\Sigma \sqrt{-\det h} d\sigma dt\,, \tag{2.1.1}$$

where $1/(2\pi\alpha') \simeq M_s^2$ is the string tension. As for the second equality, we have express the action in terms of $X^M(t, \sigma)$ by using the 2d worldsheet metric (which is the pullback

[1] The Polyakov action with a suitable worldvolume cosmological constant term added is classically equivalent to the Nambu-Goto action.

of the spacetime metric to the string worldsheet along the embedding $\Sigma \hookrightarrow X^M(t,\sigma)$)

$$h_{tt} = \partial_t X^M \partial_t X_M, \quad h_{\sigma\sigma} = \partial_\sigma X^M \partial_\sigma X_M, \quad h_{t\sigma} = \partial_t X^M \partial_\sigma X_M \,. \tag{2.1.2}$$

Many remarkable properties of string theory emerge from the subtle relations between the physics in 2d worldsheet and physics in spacetime. Different string theories are defined by different worldsheet structures.

UV finiteness and critical dimensions A fundamental property of string theory is that the scattering amplitudes are unitary, and moreover finite, order by order in perturbation theory. It defines consistent quantum theories, which are free of the ultraviolet (UV) divergences of quantum field theory. String theory provides a regularization of quantum field theory, with the effective cutoff M_s, above which the amplitudes soften rather than diverge. In a quantum field theory, UV divergences occur when two interaction vertices coincide in spacetime; however, in string theory, they are delocalized in a region of size $L_s \simeq 1/M_s$, which acts as an effective position space cutoff for the amplitude.

The conformal symmetry of the worldsheet action is the single reason we can fully solve the quantum string (at least for flat target space). The conservation of the conformal symmetry at quantum level restricts the dimension of the target space M_D to a critical value, called *critical dimension*. The Nambu-Goto action 2.1.1 can be extended by addition to the bosonic scalar fields X^M fermionic fields in a natural way. This leads to the action of the so-called superstring, for which the critical dimension is $D = 10$.

2.1.2 Superstrings

In order to have fermionic string excitations in the target space, one needs to modify the worldsheet field content. Concretely, there is a set of 2d fermionic fields $\varphi^M(\xi)$ (spinors) as superpartners of bosonic fields $X^M(\xi)$. In addition, there is a worldsheet gravitino $\varphi_a(\xi)$, related to $g_{ab}(\xi)$. Supersymmetry relates the worldsheet fermions to their bosonic cousin fields in spacetime. Subtle exceptions include type 0 theories, which are omited

here since these theories have no application to construct particle physics models and deviate away from our focus in this thesis. The appearance of spacetime supersymmetry guarantees the absence of spacetime tachyons, and thus provide stable string vacua. The five superstring theories have a high degree of spacetime supersymmetry, with the same number of supercharges as 4d $\mathcal{N} = 8$ in type II theories and as of 4d $\mathcal{N} = 4$ in heterotic and tyoe I theories. In 4d compactifications, the degree of supersymmetry can be reduced, leading to theories with 4d $\mathcal{N} = 1$ (or no) supersymmetry, with potential particle physics model building applications.

D-brane In particular, objects called Dp-branes feature prominently in string compactifications when studying interesting non-perturbative dynamics [16] as well as its low-energy limit towards gauge theories with non-perturbative effects. In short words, Dp-branes are extended objects of p spatial dimensions, which at weak coupling can be defined as $(p+1)$-dimensional subspace of the spacetime on which open strings end. It is crucial to observe that stacks of coincident Dp-branes realize gauge algebras [3, 4, 5, 6, 7, 8] and the gauge bosons are open strings that start and end on the same stack of D-branes. Those observations thus make the string engineering of non-trivial gauge theories more flexible. In braneworld models, we are confined to consider a small subset of the Calabi-Yau manifold on which it intersects a D-brane. The systematic study of D-brane configurations in Calabi-Yau manifolds leads to various approaches to realize the SM in string theory models/geometries.

As open string modes on D-brane describe the dynamics of the D-brane, one can generalize 2.1.1 to the so called Dirac-Born-Infeld (DBI) action. The DBI action describes the coupling of the D-brane to the NSNS fields, and in particular to gravity. By using the gauge transformations of the Kalb-Ramond field B_2 in the DBI-action, one can derive the Yang–Mills action for world worlume gauge field as well as its supersymmetric completion, which involves the world-volume scalars X^M and the world-volume fermions ψ^M. However, there exists no similar symmetry on the brane like conformal symmetry on

the worldsheet. Thus, we lack the ability to quantize the solutions to the D-brane action. This can be understood as result of the non-perturbative nature of Dp-branes.

2.1.3 Compactification

The string compactification is defined on a spacetime $M_{10} = M_4 \times X_6$. X_6 is called the *internal space*, which is a 6-dimensional compact manifold. The size of the internal space is taken small enough to agree with current experimental observations, and we expect that the physics at energy well below M_s reduces to an effective 4 dimensional theory which is in agreement with our everyday experience. Calabi-Yau manifolds were first considered in [13] for compactifications of six dimensions in superstring theory because they leave some of the original supersymmetry unbroken. The unbroken $\mathcal{N} = 1$ supersymmetry requires that the manifolds have, for perturbatively accessible configurations, $SU(3)$ holonomy.

Calabi-Yau Manifolds The condition that compactifiations on X_6 leads to some unbroken supersymmetry can be described as follows. Around each point P in $M_4 \times X_6$, the spacetime is locally isomprphic to $\mathbb{R}^{10}$ and we have a local set of 10d supercharges, which transform as spinors of $SO(10)$. As Dirac spinor of $SO(n)$ has $2^{(n/2)}$ components with the same amount of supercharges. Thus, we can naively argue that the Dirac spinor of $S0(10)$ is composed by that of $SO(6)$ and $SO(4)$. Supercharges of the 4d theory correspond to supercharges which are well defined globally on X_6. Since X_6 is curved, local supercharges at different points in X_6 are related by parallel transport with the $SO(6)$ spin connection induced from the metric of X_6. Supercharges which are rotated upon parallel transport do not lead to globally well defined supercharges. Hence, the condition that compactifiation on X_6 preserves some supersymmetry is that there exist sufficiently many [2] non-trivial spinors on X_6, which remain constant upon parallel tranport. Such covariantly constant spinors are called killing spinors. The existence of such spinor can be recasted into demanding X_6 to be a manifold with special holonomy, i.e. its holonomy

[2] 'sufficiently many' means that we want to demand the holonomy group of the Calabi–Yau threefolds X_6 is identical to $SU(3)$. However, some authors introduce Calabi–Yau threefolds by the condition that the holonomy group is allowed to be a proper subgroup of $SU(3)$.

group must be a subgroup of $SO(6)$. This is satisfied by the Calabi–Yau manifolds with $SU(3)$ holonomy. According to the conjecture of Calabi [14], followed by its proof by Yau [15], an N-dimensional complex Kähler manifold with vanishing first chern class admits a metric with $SU(N)$ holonomy.

The constructions of Calabi-Yau manifolds rely heavily on the computational power of algebraic geometry and the model building potential benefited from programming skills. In fact, a large portion of the geometry is encoded in the descriptions of vanishing loci, which specify the Calabi-Yau spaces as hypersurfaces or even higher complete intersections of the ambient manifolds. For instance, many Calabi-Yau varieties/orbifolds can be found as complete intersections in a weighted projective space. Those combinatoric data derived from the applications of the toric geometry method upon Calabi-Yau manifolds allows us to calculate many physically relevant quantities (i.e., charges, chiral indices) or verify various physical conditions (e.g., tadpole cancellation for the global consistency, quantization conditions). In this thesis, we will employ both toric geometry methods and program scanning skills to systematically construct and study Calabi-Yau manifolds.

M-theory It turns out that the consistent formulation of superstring theory is not unique in flat 10 dimensional Minkowski spacetime. Five superstring theories are related by the so-called S-duality and T-duality. Moreover, they can be seen as different limits of an 11 dimensional supergravity theory, which preserves $\mathcal{N} = 1$ supersymmetry. It is believed that there exists a UV-completion of 11 dimensional supergravity. This compactifiation is called M-theory. Thus the 11 dimensional supergravity theory is comprehended as the low energy limit of *M-theory*. Its bosonic part is governed by the metric G and an anti-symmetric 3-tensor, i.e. 3-form C_3. Denote the 11 dimensional Planck mass as M_{11D} and R being the Ricci scalar, the dynamics of M-theory is described by the action

$$S_{11D} = \frac{M_{11D}^9}{2} \int_{M_{11}} d^{11}x \left(\sqrt{-\det G} R - \frac{1}{2} G_4 \wedge *G_4 - \frac{1}{6} C_3 \wedge G_4 \wedge G_4 \right),$$

where $G_4 = dC_3$. In analogy to the gauge transformations in Yang–Mills theory, the action of dynamic is invariant under a gauge transformation: $C_3 \to C_3 + d\Lambda_2$, which allows us to interpret G_4 as the field strength of the gauge potential C_3 followed from F-M-theory duality. Moreover, there exist similar brane configurations in *M-theory*, which are called M2-branes and M5-branes. They are charged electrically and magnetically, respectively, under C_3. M-branes and the G_4-flux are prominent features of the F-theory regime. Later in this thesis, we will parameterize a subset of G_4-fluxes by the so-called *Chow ring* [45] and the gauge potential C_3 by *Deligne Cohomology*.

We emphasize that this thesis focuses on F-theory. This is because F-theory compactifications provide physicists a large number set of compactifiations in the so-called string theory landscape. We devote the following section to a brief review of type IIB theory, followed by the approaches to F-theory as a non-perturbative formulation of Type IIB compactifications.

2.1.4 Type IIB theory

The low energy description of type IIB string theory in flat 10d spacetime admits an effective formulation, which preserves $\mathcal{N} = (2,0)$ supersymmetry. The bosonic part of this classical action is [26]

$$\begin{aligned}\frac{1}{2\pi}S_{\text{IIB}} = \int d^{10}x\, e^{-2\phi}\sqrt{-g}\,(R + 4\partial_\mu\phi\,\partial^\mu\phi) - \frac{1}{2}\int e^{-2\phi}H_3 \wedge *H_3 \\ - \frac{1}{4}\sum_{p=0}^{4}\int F_{2p+1}\wedge *F_{2p+1} - \frac{1}{2}\int C_4 \wedge H_3 \wedge F_3\,.\end{aligned} \tag{2.1.3}$$

The relevant equation of motion is completed by the duality relation $F_5 = *F_5$ since this action 2.1.3 is pseudo.It is conventional to define field strengths as follows:

$$\begin{aligned}&H_3 = dB_2, \quad F_1 = dC_0, \quad F_3 = dC_2 - C_0\,dB_2, \\ &F_5 = dC_4 - \frac{1}{2}C_2\wedge dB_2 + \frac{1}{2}B_2\wedge dC_2, \quad F_9 = *F_1, \quad F_7 = -*F_3\,.\end{aligned} \tag{2.1.4}$$

field	symbol	type	electric BPS state	magnetic BPS state
dilaton	ϕ	scalar	–	–
metric	$G_{\mu\nu}$	symmetric 2-tensor	–	–
B-field	B_2	2-form	F1-string	NS5-brane
RR 0-form	C_0	0-form	D(-1) instanton	D7-brane
RR 2-form	C_2	2-form	D1-string	D5-brane
RR 4-form	C_4	4-form	D3-brane	D3-brane

Table 1: Bosonic field content of 10-dimensional type IIB supergravity – based on [1].

The vev of the dilaton ϕ affects the string coupling constant, $g_s = e^{\langle\phi\rangle}$, which plays a key role in the perturbative description of type IIB strings[3, 4, 5, 6]. D7-branes, on the other hand, are magnetic sources for the IIB Ramond-Ramond (RR) axion C_0. Together with the dilaton ϕ, we introduce the complex axio-dilaton field

$$\tau = C_0 + ie^{-\phi}. \tag{2.1.5}$$

This allow us to rewrite 2.1.3 in the Einstein frame as

$$\frac{1}{2\pi}S_{\text{IIB}} = \int d^{10}x\sqrt{-g}\left(R - \frac{\partial_\mu\tau\partial^\mu\bar{\tau}}{2(\text{Im}\tau)^2} - \frac{1}{2}\frac{|G_3|^2}{\text{Im}\tau} - \frac{1}{4}|F_5|^2\right) + \frac{1}{4i}\int \frac{1}{\text{Im}\tau}C_4 + G_3\wedge\bar{G}_3, \tag{2.1.6}$$

where $G_3 = dC_2 - \tau dB_2$ and $|F_p|^2 = \frac{1}{p!}F_{\mu_1\cdots\mu_p}F^{\mu_1\cdots\mu_p}$. This action enjoys an $SL(2,\mathbb{R})$ symmetry [51] under the transformations

$$\begin{pmatrix} C_4 \\ G \end{pmatrix} \mapsto \begin{pmatrix} C_4 \\ G \end{pmatrix}, \quad \tau \mapsto \frac{a\tau + b}{c\tau + d}, \quad \begin{pmatrix} C_2 \\ B_2 \end{pmatrix} \mapsto \begin{pmatrix} a & b \\ c & d \end{pmatrix}\begin{pmatrix} C_2 \\ B_2 \end{pmatrix}, \quad \begin{pmatrix} a & b \\ c & d \end{pmatrix} \in SL(2,\mathbb{R}), \tag{2.1.7}$$

and even breaks to an $SL(2,\mathbb{Z})$ subgroup upon quantizaion[3]. It is believed that this remant group persists as a symmetry of the full non-perturbative IIB string theory.

Seven branes in type IIB Since seven branes are electric and magnetic sources for the form fields C_8 and C_0 in the action, their presence will alter the fields by backreactions

[3]The breaking is induced by the factor $exp(2i\pi\tau)$ contributed by D(-1) instantons to the partition function. This factor is only invariant under $SL(2,\mathbb{Z})$ of τ.

in a similar way as a classical electron backreacts onto the electromagnetic field. Consider a D7-brane along $\mathbb{R}^{1,7} \subset \mathbb{R}^{1,9} \simeq \mathbb{R}^{1,7} \times \mathbb{C}$. The Bianchi identity of F_9 implies

$$\int_{S^1} *F_9 = \int_{S^1} dC_0 = 1\,, \tag{2.1.8}$$

where S^1 is a circle around the D7-brane in the normal space $\mathbb{C}$. Let z_0 denote the position of D7-brane in the normal space with coordinate z. To preserve supersymmetry, in the vicinity of the D7-brane we must have a field profile

$$\tau(z) = \frac{1}{2\pi i}\ln(z - z_0) + \text{terms regular at } z_0\,. \tag{2.1.9}$$

In the complex plane, as we encircle z_0, the logarithmic branch cut induces a monodromy of the axio-dilaton profile

$$\tau \to \tau + 1 \ .$$

This monodromy can be interpreted by the $SL(2,\mathbb{Z})$ symmetry 2.1.7, namely, one D7-brane induces an $SL(2,\mathbb{Z})$ transformation given by the matrix $M_{[1,0]} = \left(\begin{smallmatrix} 1 & 1 \\ 0 & 1 \end{smallmatrix}\right)$. There are other types of seven branes specified by different monodromy matrices. In the perturbative regime of type IIB description, we define a (p,q) string as a BPS bound state of p fundamental strings and q D1-strings, which ends on a $[p,q]$ 7-brane. These strings are invariant under the $[p,q]$-brane induced monodromy $M_{[p,q]} = \left(\begin{smallmatrix} 1+pq & p^2 \\ -q^2 & 1-pq \end{smallmatrix}\right)$. Depending on the brane configurations, various gauge algebras can be realized. For instance, a stack of N coincident D7-branes ($[1,0]$-branes) supports an $SU(N)$ gauge groups. Hence a basis of seven branes is sufficent to generate all ADE groups [52]. The study of (p,q)-strings and branes by so-called string junctions [53, 54, 55] is one way to describe non-perturbative type IIB theory. However, we follow a geometric approach to explore the profile of varing axio-dilaton τ induced by general seven brane configurations. This geometric description is F-theory, the main focus of this thesis.

2.2 F-theory in a nutshell

Due to the backreactions on the seven branes, the axio-dilaton τ has non-trivial profile in the normal space of the branes. This non-trivial profile connects to an elliptic fibration by interpreting the axio-dilaton of type IIB theory as the complex structure modulus of an elliptic curve. F-theory is remarked by its geometric descriptions of compactifications involving such profiles.

Recall that an elliptic curve $\mathbb{E}_\tau$, which is a complex torus with a marked point. Every complex torus can be described as

$$\mathbb{E}_\tau = \mathbb{C}/\Lambda = \{w \in \mathbb{C} : w \simeq w + (n + m\tau)\}\,, \qquad n, m \in \mathbb{Z}, \qquad \tau = \tau_1 + i\tau_2 \in \mathbb{H}\,, \quad (2.2.1)$$

where $\mathbb{H}$ is the complex upper half-plane. The shape of lattice is invariant under the

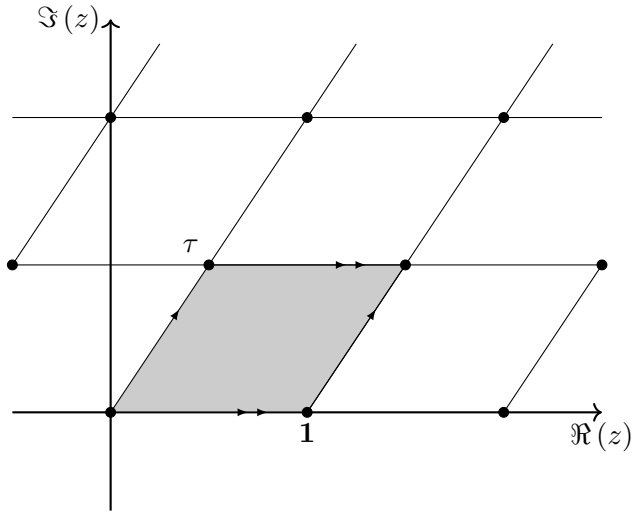

Figure 3: The lattice Λ defining a torus, it is obtained from identification $z \sim z+1 \sim z+\tau$.

transformation $\tau \to \frac{a\tau+b}{c\tau+d}$ with $\left(\begin{smallmatrix} a & b \\ c & d \end{smallmatrix}\right) \in SL(2,\mathbb{Z})$. This inspires us to identify type IIB supergravity field τ with the complex structure of the torus. Thus the varying of τ under the monodromy $SL(2,\mathbb{Z})$ is encoded in the geometry of elliptic curve $\mathbb{E}_\tau$, and it is natural to consider an elliptic fibration $\mathbb{E}_\tau \hookrightarrow Y_{n+1} \to B_n$. Note that the elliptic curve fiber $\mathbb{E}_\tau$

In particular, the lattice spanning vectors can be related to the two non-trivial cycles on the torus. The value of τ can be related to the ratio of the length of the two cycles, and thus determine the shape of the torus. An infinite value of τ is geometrically interpreted as shrinking the size of one of the cycles to zero, namley, the torus becomes singular. On the other hand, in the type IIB decription, the axio-dilaton field function 2.1.9 indicates that this infinity corresponds to the limit $z \to z_0$. Therefore, the singular torus occurs at the postion where seven branes locate. From the compactification perspective, type IIB compactified on B_n is corresponding to an F-theory compactification as a fibration X_{n+1}, the elliptic fiber becomes singular at certain codimension one locus $\Delta \in B_n$ as depicted below. Furthermore, supersymmetry preserving requires that the fibration must

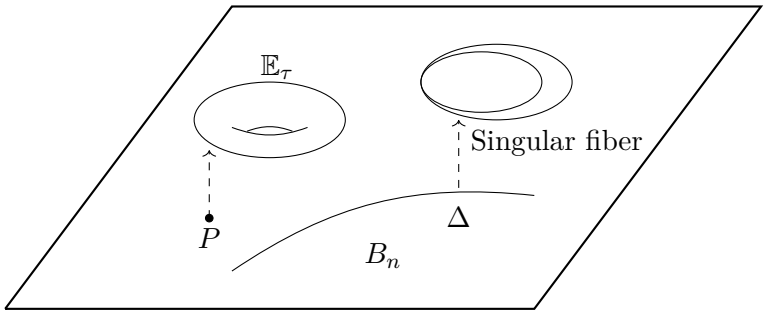

Figure 4: The elliptic fibration Y_{n+1} of F-theory, where singular fiber appears along certain base locus $\Delta \in B_n$.

be Calabi-Yau. We will see momentarily that the type of singularity over Δ encodes the gauge dynamics on the D7-branes in question.

The Weiestrass form It is commonly to apply the so-called Weierstrass form to represent an elliptic curve, which is described by the vanishing locus of the polynomial

$$P_W := y^2 - (x^3 + fxz^4 + gz^6)\,, \tag{2.2.2}$$

where $[x, y, z]$ are homogeneous coordinates of the weighted projective space $\mathbb{P}_{231}$. Globally, f,g are sections of line bundles on the base B_n, such that they determine the shape of the elliptic curve. The vanishing of the discriminant $\Delta := 4f^3 + 27g^2$ is tied to the

degenerating of the fiber

$$f \in \mathcal{O}(-4K_{B_n}), \quad g \in \mathcal{O}(-6K_{B_n}), \quad \Delta \in \mathcal{O}(-12K_{B_n}) \tag{2.2.3}$$

On the local patch $z = 1$, where the point $[1 : 1 : 0]$ lies at infinity, the real parts of the vanishing locus can be ploted as below The singularity type has been classfied

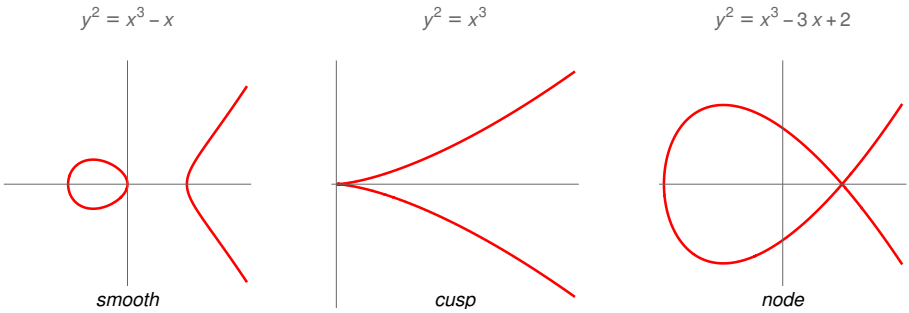

Figure 5: A smooth elliptic curve (a), and two types of singular curve (b) and (c).

systematically by Kodaira [56] by the vanishing order of f, g and Δ. Below we list the Kodaira classification inspired by [57] of singularities as well as their associated gauge groups:

ord (f)	ord (g)	ord (Δ)	singularity	nonabelian symmetry algebra
≥ 0	≥ 0	0	none	none
0	0	$n \geq 2$	A_{n-1}	$\mathfrak{su}(n)$ or $\mathfrak{sp}(\lfloor n/2 \rfloor)$
≥ 1	1	2	none	none
1	≥ 2	3	A_1	$\mathfrak{su}(2)$
≥ 2	2	4	A_2	$\mathfrak{su}(3)$ or $\mathfrak{su}(2)$
≥ 2	≥ 3	6	D_4	$\mathfrak{so}(8)$ or $\mathfrak{so}(7)$ or $\mathfrak{g}_2$
2	3	$n \geq 7$	D_{n-2}	$\mathfrak{so}(2n-4)$ or $\mathfrak{so}(2n-5)$
≥ 3	4	8	$\mathfrak{e}_6$	$\mathfrak{e}_6$ or $\mathfrak{f}_4$
3	≥ 5	9	$\mathfrak{e}_7$	$\mathfrak{e}_7$
≥ 4	5	10	$\mathfrak{e}_8$	$\mathfrak{e}_8$
≥ 4	≥ 6	≥ 12	does not occur in F-theory	

Table 2: Kodaira's classification of singular fibers and gauge groups.

Therefore, the framework of F-theory provide an one-to-one correspondence between seven brane configurations with backreactions in the type IIB supergravity decription and Cal-

abi–Yau elliptic fibration. The geometry of F-theory compactifications allows us to read off physics concerned objects in type IIB, for instance, the non-abelian gauge group G_i specified by stack of coincident seven branes are translated into the singularity occurance at certain codimension one locus Σ_i of the base B_n. The origin of abelian symmetry like $U(1)$ can be traced back to the existence of extra rational sections other than the zero section $[1:1:0]$ in the fibration. We consider the appearance of multi-sections when the discrete symmetry is involved.

Over special loci $C_{i,j} = \Sigma_i \cap \Sigma_j$, the singularity becomes more severe due to the increasing of vanishing orders $(\mathrm{ord}(f), \mathrm{ord}(g), \mathrm{ord}(\Delta))$. We expect the occurance of matter charged under both gauge group G_i and G_j and relates to the bifundamental representation of the group $G_i \times G_j$. Let us assume that the discriminant divisor is of the form $\Sigma = \Sigma_0 \cup \Sigma_1$ with only one non-abelian gauge algebra along a smooth divisor Σ_1, but the model is otherwise maximally generic. The possible enhancement types of the Weierstrass model in codimension two and the associated matter representations have been classified in [58, 57] for all Weierstrass models.

We advance to seek more realizations of ingredients in the realistic model building. Chirality in 4D F-theory compactification can be computed by introducing a G_4-flux [36, 37, 38, 39, 40, 41, 42]. Namely, the chiral index can computed by:

$$\chi(\mathbf{R}) = \int_{S(\mathbf{R})} G_4 \tag{2.2.4}$$

where $S(R)$ is the fibration over the codimension two matter curve $C_{\mathbf{R}} \in B_n$. Moreover, the exact value of chiral and anti-chiral multiplets are counted by the sheaf cohomologies of $L_{\mathbf{R}}$ specified by the internal C_3 profile in the dual M-theory geometry. We have $h^0(C_{\mathbf{R}}, L_{\mathbf{R}})$ massless chiral and $h^1(C_{\mathbf{R}}, L_{\mathbf{R}})$ massless anti-chiral superfields in representation $\mathbf{R}$ on $C_{\mathbf{R}}$. We address more in the following chapters when visit the realizations of different model buildings.

Part III

F-theory Realization of the exact Chiral MSSM

CHAPTER 3: A Model with $SU(3) \times SU(2) \times U(1) \times \mathbb{Z}_2$ Symmetry

After the pedagogical introductions of the previous chapters, we would like to use F-theory to construct 4D $\mathcal{N} = 1$ SUGRA theories with the Standard Model gauge group, three chiral generations, and matter parity in order to forbid all dimension four baryon and lepton number violating operators. The underlying geometries are derived by constructing smooth genus-one fibered Calabi–Yau fourfolds using toric tops that have a Jacobian fibration with rank one Mordell–Weil group and $SU(3) \times SU(2)$ singularities. The necessary gauge backgrounds on the smooth fourfolds are shown to be fully compatible with the quantization condition, including positive integer D3-tadpoles. This construction realizes for the first time a consistent UV completion of an MSSM-like model with matter parity in F-theory. Moreover our construction is general enough to also exhibit other relevant $\mathbb{Z}_2$ charge extensions of the MSSM such as lepton and baryon parity. Such models however are rendered inconsistent by non-integer fluxes, which are necessary for producing the exact MSSM chiral spectrum. These inconsistencies turn out to be intimately related to field theory considerations regarding a UV-embedding of the $\mathbb{Z}_2$ into a $U(1)$ and the resulting discrete anomalies.

3.1 Introduction

One of the major goals of string theory is to provide a possible framework to UV complete the Standard Model of particle physics together with gravity. The web of string theories, connected by various dualities, exhibits a rich landscape of possibilities, and each corner provides an interesting starting point towards this goal, coming with its own benefits and challenges. In particular, F-theory [27] provides a very flexible tool to cover the to date largest set of consistent vacua [28, 29, 30, 31] from string theory by using a non-peturbative extension of Type IIB strings (see [33, 34, 35, 26] for some reviews).

This flexibility lies in the systematic engineering of gauge theories coupled to gravity using powerful tools of algebraic geometry, that combines the strength of various perturbative

string theories. In its early days, F-theory has been employed to engineer the whole Standard Model through a unified gauge group $SU(5)$ on a single divisor [59, 60, 61], which then has to be broken to the Minimal Supersymmetric Standard Model (MSSM) by a flux in the hypercharge Cartan subgroup [62]. The localization of the $SU(5)$ made a simple local treatment of the compactification space possible, although it was required to enhance these models by additional Abelian symmetries to control proton decay and Yukawa textures [63]. The global realization of Abelian gauge symmetries and its connection to the Mordell–Weil group of the fibration, although already pointed out earlier [64], was only further explored later on in [65, 66, 67]. These developments kicked off the construction of globally consistent realizations of GUTs together with $U(1)$ symmetries [68, 38, 69, 39, 70, 71, 72]. Nevertheless, these construction were still relying on a GUT breaking mechanism via hypercharge flux [73] which is often technically hard to implement or might lead to vector-like exotics [74] when global Wilson lines are used.

However, the newly gained insights into Abelian symmetries made the direct engineering of the MSSM another valid option [75, 76, 40, 42]. But similar as in the GUT picture, the MSSM gauge group per se is not enough to forbid various dangerous proton decay inducing operators and must be considered incomplete. One possibility is to extend the symmetries by another gauged $U(1)$ [76, 42], however, one is then faced with the issue of how to lift the additional massless photon from the spectrum. Alternatively, one can add a discrete symmetry, which from the effective field theory perspective is rather minimally invasive and unproblematic, due to the lack of strong anomalies. However this is not true anymore when coupled to (quantum) gravity, as here black hole arguments [77, 78] suggest an inconsistency of every symmetry that does not have a gauged origin. Hence, if we couple gravity to the MSSM, we can only add very specific discrete symmetries that allow a gauging. One of the mildest additions to the MSSM that forbids baryon and lepton number violating operators at the renormalizable level which is also known to be (discrete) anomaly free [79] is matter parity. Therefore, a valid quest is to explore

F-theory constructions of such models.

This article is structured as follows: In Section 3.2 we review the need for additional discrete symmetries in the MSSM and their field theory constraints from anomaly considerations. In Section 3.3 we present an F-theory model with matter parity, together with the relevant computational details regarding the geometry and G_4-fluxes. We then demonstrate that these rather formal techniques, when applied to the most simplistic fibrations over the base $B = \mathbb{P}^3$, can produce a number of different, consistent configurations that has the exact chiral MSSM spectrum. Along the way, we highlight the subtle interplay between discrete gauge anomalies in the field theory and intersection number arithmetic of the geometry. In Section 3.4 we construct another fibration in which we will look for other parity assignments, and confront these with discrete anomaly cancellation conditions. Section 3.5 summarizes the results and gives an outlook onto possible future directions.

3.2 Prelude: R-parity violation in the MSSM

In this section we provide a short summary of R-parity violating operators in the MSSM and their tension with experimental bounds. These operators have also appeared in earlier F-theory constructions that directly engineer the MSSM [75, 76, 40, 42]. We review possible $\mathbb{Z}_2$ symmetries that can forbid these operators.

At the renormalizable level, the superpotential of the MSSM can be written as

$$\begin{aligned}\mathcal{W}_{\text{MSSM}} = & Y^u_{i,j} Q \overline{u} H_u + Y^d_{i,j} Q \overline{d} H_d + Y^e_{i,j} \overline{e} L H_d + \mu H_u H_d \\ & + \beta_i L_i H_u + \lambda_{i,j,k} \overline{e} L L + \lambda'_{i,j,k} Q \overline{d} L + \lambda''_{i,j,k} \overline{u}\overline{d}\overline{d}\,.\end{aligned} \tag{3.2.1}$$

The couplings in the second row violate baryon and lepton number conservation and are severely constrained by experimental bounds. These usually come from proton or lepton decays mediated by massive superpartners. The strongest bounds are related to products

of the above couplings and less strong for the single ones. Roughly, they are as follows:

$$\begin{aligned} \lambda'' &< 10^{-(2-6)} \left(\frac{\widetilde{m}}{100\text{GeV}}\right), \qquad & |\lambda\lambda''| &< 10^{-(3-19)} \left(\frac{\widetilde{m}}{100\text{GeV}}\right)^2, \\ \lambda' &< 0.01 \left(\frac{\widetilde{m}}{100\text{GeV}}\right), & |\lambda'\lambda''| &< 10^{-27} \left(\frac{\widetilde{m}}{100\text{GeV}}\right)^2, \\ \lambda &< 0.01 \left(\frac{\widetilde{m}}{100\text{GeV}}\right), \end{aligned} \tag{3.2.2}$$

where $\widetilde{m}$ are the masses of the decay mediating superpartners generated upon SUSY breakdown (see [80, 81] and references therein). These couplings can effectively be forbidden by imposing a discrete symmetry on the MSSM which in the simplest case is a $\mathbb{Z}_2$. Differing by the discrete charge assignments of MSSM superfields, the phenomenologically most relevant cases are matter, lepton and baryon parity, as summarized in Table 3.

G_{SM} Rep	Matter
$(\mathbf{3},\mathbf{2})_{\frac{1}{6}}$	Q
$(\overline{\mathbf{3}},\mathbf{1})_{-\frac{2}{3}}$	$\overline{u}$
$(\overline{\mathbf{3}},\mathbf{1})_{\frac{1}{3}}$	$\overline{d}$
$(\mathbf{1},\mathbf{2})_{\pm\frac{1}{2}}$	L, H_d, H_u
$(\mathbf{1},\mathbf{1})_1$	e

	Q	$\overline{u}$	$\overline{d}$	L	$\overline{e}$	H_d	H_u
$\mathbb{Z}_2^{M_1}$	+	-	-	+	-	-	-
$\mathbb{Z}_2^{M_2}$	-	-	-	-	-	+	+
$\mathbb{Z}_2^{L}$	+	+	+	-	-	+	+
$\mathbb{Z}_2^{B}$	+	-	-	-	+	-	-

Table 3: Summary of gauge quantum numbers of chiral MSSM superfields. The left table shows the gauged quantum numbers, while the table on the right shows the $\mathbb{Z}_2$ charge assignments for matter parities $Z_2^{M_1}$, $Z_2^{M_2}$, lepton parity $\mathbb{Z}_2^L$ and bayron parity $\mathbb{Z}_2^B$.

For each charge assignment we summarize the field theoretically forbidden tree level couplings in Table 4.

Both matter parities can forbid all unwanted baryon and lepton number violating couplings while lepton and baryon parity can only forbid their respective ones.

Two comments concerning the discrete charge assignments are in order. First we note that the two matter parities are field theoretically equivalent by mixing the $U(1)_Y$ charge

	Coupling	$\mathbb{Z}_2^{M_1}$	$\mathbb{Z}_2^{M_2}$	$\mathbb{Z}_2^{L}$	$\mathbb{Z}_2^{B}$
Yukawa-Couplings	$Q\overline{u}H_u$	✓	✓	✓	✓
	$Q\overline{d}H_d$	✓	✓	✓	✓
	$\overline{e}LH_d$	✓	✓	✓	✓
μ-term	H_uH_d	✓	✓	✓	✓
B-& L-Violation	LH_u	X	X	X	✓
	$Q\overline{d}L$	X	X	X	✓
	$\overline{e}LL$	X	X	X	✓
	$\overline{u}\overline{d}\overline{d}$	X	X	✓	X

Table 4: Summary of allowed and forbidden tree level couplings under different $\mathbb{Z}_2$ symmetry charge assignments. While the first four terms are required to be present the later four should better be forbidden.

with the $\mathbb{Z}_2$. Explicitly, we have

$$\mathbb{Z}_2^{M_1} = \mathbb{Z}_2^{M_2} + 6\,U(1)_Y \mod 2\,. \tag{3.2.3}$$

As all $SU(3)$ triplets have hypercharges that are multiples of $1/3$, the above redefinition is trivial for them. Meanwhile, $SU(2)$ doublets as well as the bifundamental states have hypercharge $1/2$ or $1/6$, which leads to a sign flip upon performing the rotation 3.2.3. Second we note that matter parity is clearly superior to the other $\mathbb{Z}_2$ charge assignments when it comes to the problematic tree level couplings. However, in SUSY breaking schemes where the sfermion masses are large, the other charge assignments might still be phenomenologically interesting. In such cases certain individual couplings might still be within their mild experimental bounds and thus acceptable. Only the products in 3.2.2 with the λ'' coupling are strongly constrained and those are still forbidden for both parities.

$$\mathbb{Z}_2 - G^2 : \sum_{\mathbf{R}_G} Q_{\mathbb{Z}_2}(\mathbf{R})\, C_G^{(2)}(\mathbf{R}) = m\,, \quad m \in \mathbb{Z}\,, \tag{3.2.4}$$

where G is the non-Abelian gauge group.[1]

3.3 F-theory construction of 4d MSSM vacua with matter parity

In this section, we will present the details of an F-theory compactification which realizes a three-family MSSM vacuum with an additional $\mathbb{Z}_2$ symmetry that is identified with the matter parity $\mathbb{Z}_2^{M_2}$. The necessary ingredients, which we will now discuss in the same order, are

1. the generic fiber structure that realizes the Abelian part of the gauge symmetry,
2. codimension one singularities (with resolution) corresponding to the non-Abelian gauge algebra,
3. matter representations associated with codimension two fiber components and G_4-fluxes,
4. specification of the base and fibration and consistent three-family configurations.

By keeping the base generic for the first three points, we will have the capabilities to analyze a large number of concrete models for the last point.

3.3.1 Toric hypersurface with two bisection classes

With our phenomenological motivations, we seek to realize an F-theory model whose Abelian gauge sector is $U(1) \times \mathbb{Z}_2$. As studied in [82], a straightforward fiber type that does the job is described in terms of one of the 16 reflexive 2D polygons. Labelled as F_2 in [82], the generic fiber $\mathfrak{f}$ of this geometry is a bi-quadric curve, given as the vanishing of

[1] There are also mixed Abelian discrete symmetries, that are less conclusive due to ambiguities in the charge normalization [79].

the polynomial

$$p_{F_2} = (b_1\, y^2 + b_2\, s\, y + b_3\, s^2)\, x^2 + (b_5\, y^2 + b_6\, s\, y + b_7\, s^2)\, x\, t + (b_8\, y^2 + b_9\, s\, y + b_{10}\, s^2)\, t^2 \tag{3.3.1}$$

inside the surface $\mathbb{P}^1 \times \mathbb{P}^1$ with homogeneous coordinates $([x : t], [y : s])$. By promoting the coefficients b_i to functions over a complex threefold base B, we obtain a genus-one fibered fourfold $Y \subset \mathcal{A}$. Here, $\mathcal{A}$ is the ambient space obtained by fibering $\mathbb{P}^1 \times \mathbb{P}^1$ over the same base B. The full configuration is summarized via the commutative diagram:

$$\begin{array}{ccccc} \mathfrak{f} & \hookrightarrow & \mathbb{P}^1 \times \mathbb{P}^1 & \hookrightarrow & \mathcal{A} \\ & \searrow & & \nearrow & \downarrow \\ & & Y & \xrightarrow[\pi]{} & B \end{array} \,. \tag{3.3.2}$$

The ambient space fibration is specified by two line bundles with divisor classes S_7 and S_9 over the base. They determine the relative "twisting" of the fiber coordinates over the base via the linear equivalence relations

$$[x] = [t] - \overline{K}_B + S_9\,, \quad [y] = [s] - \overline{K}_B + S_7\,, \tag{3.3.3}$$

where $\overline{K}_B$ is the anti-canonical class of the base. For Y to be Calabi–Yau, the coefficients b_i of the polynomial 3.3.1 have to be sections with the following divisor classes:

$$\begin{array}{lll} [b_1] = 3\,\overline{K}_B - S_7 - S_9\,, & [b_2] = 2\,\overline{K}_B - S_9\,, & [b_3] = \overline{K}_B + S_7 - S_9\,, \\ [b_5] = 2\,\overline{K}_B - S_7\,, & [b_6] = \overline{K}_B\,, & [b_7] = S_7\,, \\ [b_8] = \overline{K}_B + S_9 - S_7\,, & [b_9] = S_9\,, & [b_{10}] = S_7 + S_9 - \overline{K}_B\,. \end{array} \tag{3.3.4}$$

The genus-one fibration Y has no rational section, but two independent bisection classes 3.3.3, corresponding to the two hyperplanes of the fiber ambient space $\mathbb{P}^1 \times \mathbb{P}^1$ (modulo vertical divisors). They have been shown to give rise to a $U(1) \times \mathbb{Z}_2$ symmetry in F-

theory [82, 83]. A multisection of a genus-one fibration is just as good as a section of an elliptic fibration when it comes to identifying the Kaluza–Klein (KK) $U(1)$ in the dual M-theory compactification [84]. However, in the absence of a section, new subtleties arise in the additional possibilities that an n-section can intersect codimension two fiber components. As has been extensively studied in [85, 86, 87, 88, 89], one can understand these intersection numbers as the mod n charge of the matter states under a discrete $\mathbb{Z}_n$ symmetry, which in the M-theory phase is mixed with the KK-$U(1)$ to give rise to the massless Abelian vector field dual to the n-section class.

For the model 3.3.1, we pick the divisor class

$$D_{\mathbb{Z}_2} := [x] \tag{3.3.5}$$

to be the one dual to the massless vector of the KK/$\mathbb{Z}_2$ combination. Then the other bisection class, $[y] = [s]$ mod D_B, gives rise to another massless vector that uplifts to a genuine massless $U(1)$ gauge field in F-theory. To be precise, this $U(1)$ is dual to a divisor class that is "orthogonal" to $D_{\mathbb{Z}_2}$, which is

$$D_{U(1)} = [y] - [x] + \frac{1}{2}(\overline{K}_B + S_7 - S_9)\,. \tag{3.3.6}$$

This modified divisor can be understood as a generalized Shioda map for genus-one fibrations with more than one independent multisection class [83].

As extensively studied in [82], this bisection geometry can be obtained through a complex structure deformation of an elliptic fibration with Mordell–Weil rank two, which in F-theory gives rise to a $U(1)^2$ gauge group. The associated conifold transition corresponds in field theory to the Higgsing of one of these $U(1)$ factors to a $\mathbb{Z}_2$ by giving vev to a singlet of charge $(0, 2)$. Therefore, we see explicitly that the $\mathbb{Z}_2$ symmetry we construct via F-theory has a gauged origin, and hence should have a consistent quantum gravity embedding.

3.3.2 Non-Abelian symmetries with matter parity via tops

We include non-Abelian $SU(3) \times SU(2)$ gauge symmetries using the methods of tops [90, 91]. There are four possibilities for each of the $SU(3)$ and $SU(2)$ tops, cf. appendix In the following, we will focus on a combination of $SU(3)$ top 3 and $SU(2)$ top 1. The toric description modifies the ambient space $\mathcal{A}$ to include additional toric divisors $\{f_i\}_{i=0,1,2}$ and $\{e_j\}_{j=0,1}$, which themselves are fibered over codimension one loci $\{w_3\}$ resp. $\{w_2\}$ inside the base B. Their restriction, or intersection, with the likewise modified hypersurface $\hat{Y} \equiv Y_{31}$ are now the exceptional, or "Cartan" divisors that resolve the $SU(3)$ resp. $SU(2)$ singularities over respective codimension one loci on B. The $\mathbb{P}^1$ fibers of these divisors intersect in the affine Dynkin diagrams of the corresponding Lie algebra.

Explicitly, the modified hypersurface equation is given by the vanishing of a polynomial p_{31}, which is a specialization of the polynomial 3.3.1 with coefficients

$$\begin{aligned} &b_1 = d_1\, e_0\, f_1, \quad b_2 = d_2\, e_0\, f_0\, f_1, \quad b_3 = d_3\, e_0\, f_0^2\, f_1, \quad b_5 = d_5\, f_1\, f_2, \\ &b_6 = d_6, \quad b_7 = d_7\, f_0, \quad b_8 = d_8\, e_1\, f_1\, f_2^2, \quad b_9 = d_9\, e_1\, f_2, \quad b_{10} = d_{10}\, e_1\, f_0\, f_2\,. \end{aligned} \tag{3.3.7}$$

The functions d_i are again sections of line bundles over the base, whose divisor classes are related to those without the top 3.3.4 via

$$\begin{aligned} &[d_1] = [b_1] - W_2\,, \quad [d_2] = [b_2] - W_2 - W_3\,, \quad [d_3] = [b_3] - W_2 - 2\,W_3\,, \\ &[d_5] = [b_5]\,, \qquad [d_6] = [b_6]\,, \qquad [d_7] = [b_7] - W_3\,, \\ &[d_8] = [b_8]\,, \qquad [d_9] = [b_9]\,, \qquad [d_{10}] = [b_{10}] - W_3\,, \end{aligned} \tag{3.3.8}$$

where we have denoted the classes of $\{w_{2/3}\}$ by $W_{2/3}$. Furthermore, we shall denote the classes of the exceptional divisors by F_i resp. E_j. Though these are strictly speaking classes on the ambient space $\mathcal{A}$, we will abusively use the same notation for their restrictions to Y_{31}.

Through the toric construction, we can straightforwardly determine the linear equivalence

relations (LIN) between the divisors and the Stanley–Reisner ideal (SRI), that is, the set of divisors whose intersection product is trivial in the Chow ring. For Y_{31}, these are

$$\begin{aligned} \text{LIN} = \{&[x] = [t] + E_1 + F_2 - \overline{K}_B + S_9,\, W_2 = E_0 + E_1\,, \\ &[s] = [y] + F_1 + F_2 + \overline{K}_B - S_7,\, W_3 = f_0 + f_1 + f_2\}\,, \\ \text{SRI} = \{&xt, xe_1, xf_2, ys, yf_0, te_0, e_0f_2, tf_1, sf_1, sf_2\}\,. \end{aligned} \tag{3.3.9}$$

In the presence of codimension one reducible fibers, the divisors dual to the KK/$\mathbb{Z}_2$ and the $U(1)$ vector field needs to be refined, in order for these to be "orthogonal" to each other and to the Cartan $U(1)$s of the non-Abelian symmetries. Geometrically, this is necessary because the bisections will intersect the fibers of the exceptional divisors non-trivially. For example, while the bisection $[x]$ intersects only the affine node (the fiber component of E_0) of the $SU(2)$, it intersects the $SU(3)$ divisors non-trivially, namely each of the fibers of F_0 and F_1 once. Physically, it would mean that the W-bosons of $SU(3)$ were charged non-trivially under the $\mathbb{Z}_2$, which is of course unacceptable. However, much like in the case of $U(1)$s, we can add a linear combination of the Cartan divisors to the (bi-)section to correct the intersection numbers [86, 87, 41, 92]. For the case at hand, it can be checked that the correct $\mathbb{Z}_2$ is given by the divisor

$$D_{\mathbb{Z}_2} = [x] + \frac{1}{3}(2\,F_1 + F_2)\,. \tag{3.3.10}$$

Similarly, the modified $U(1)$ generator that is orthogonal to the Cartans as well a the $\mathbb{Z}_2$ is

$$D_{U(1)} = [x] - [y] - \frac{1}{2}\,E_1 - \left(\frac{1}{3}\,F_1 + \frac{2}{3}\,F_2\right) - \frac{1}{3}\,W_3 + \frac{1}{2}\,\overline{K}_B + \frac{1}{2}\,S_7 - \frac{1}{2}\,S_9\,. \tag{3.3.11}$$

Note that we have also flipped the sign of the bisections compared to 3.3.6, so that it matches the hypercharge $U(1)_Y$ of the MSSM.

The global gauge group structure

Let us briefly discuss the global group structure of this model. Though our fourfold Y_{31} is not elliptically fibered, we can apply the same intersection number argument employed in [93] to determine the constraints on the charges and non-Abelian representations of matter states arising from M2-branes wrapping fibral curves Γ. Essentially, one employs the fact that multisections as integer divisor classes have integer intersection number with any fiber component. This in turns means that the Abelian charges—given by intersection numbers of Γ with the divisors 3.3.10 and 3.3.11—differ by an integer from the specific fractional linear combinations of the non-Abelian weights—given by the fraction linear combination of exceptional divisors in 3.3.10 and 3.3.11. For the $U(1)$, the fractional contributions from the exceptional divisors of both $SU(3)$ and $SU(2)$ are exactly those compatible with the $\mathbb{Z}_6$ quotient of the continuous part of the gauge algebra [93], namely charge $1/2$ mod $\mathbb{Z}$ for doublets, $2/3$ mod $\mathbb{Z}$ for triplets, and $1/6$ mod $\mathbb{Z}$ for bifundamentals.

For the discrete symmetry, note that triplets will generically have charges quantized in $1/3$ with respect to the divisor in 3.3.10. Because the generic fiber still has intersection 2 with $D_{\mathbb{Z}_2}$, we can still only interpret the charge under $D_{\mathbb{Z}_2}$ modulo 2. Thus, naively, we would expect that the discrete symmetry is enhanced to a $\mathbb{Z}_6$ by the presence of the non-Abelian symmetries. But not all charges of the $\mathbb{Z}_6$ can appear! First, it is clear that $SU(2)$ matter will only be charged under a $\mathbb{Z}_2$ subgroup, because their intersection numbers with $D_{\mathbb{Z}_2}$ are integer. Furthermore, by the analogous argument as in [93], one can construct an order three central element of $SU(3) \times \mathbb{Z}_6$ which acts trivially on any matter states. Essentially, it follows because $(D_{\mathbb{Z}_2} - 1/3(2F_1 + F_2)) \cdot \Gamma = [x] \cdot \Gamma \in \mathbb{Z}$. Since $\mathbb{Z}_6 = \mathbb{Z}_2 \times \mathbb{Z}_3$ has a unique order three subgroup, we conclude that the only non-trivially acting part is the $\mathbb{Z}_2$. To infer the charges under it, we can simply multiply all intersection numbers with $D_{\mathbb{Z}_2}$ with three and then take the result modulo 2. In order to differentiate it more easily from the $U(1)$ charges, we will denote even/odd charges by

+/−. To summarize, the global gauge group of the F-theory model on Y_{31} is

$$\frac{SU(3) \times SU(2) \times U(1)}{\mathbb{Z}_6} \times \mathbb{Z}_2 \,. \tag{3.3.12}$$

Note that it was already anticipated before in [85] that, by engineering a non-Abelian symmetry algebra $\mathfrak{g}$ inside an n-section fibration, the discrete symmetry can be potentially enhanced to $\mathbb{Z}_{n\times r}$, where r is the order of the center $Z(\mathfrak{g})$. In general, $\mathbb{Z}_{n\times r} \neq \mathbb{Z}_n \times \mathbb{Z}_r$ (namely, whenever n and r are *not* coprime), and the enhancement can be physical. However, due to the mechanism that leads to such an enhancement—namely, the divisor associate with the discrete symmetry is shifted by the Cartan divisors—the resulting global gauge group necessarily has to be non-trivial. For example, there is an $SU(2)$ top constructed over the F_2 polygon that has an enhancement, such that the gauge group is $[SU(2) \times \mathbb{Z}_4]/\mathbb{Z}_2$ (we have omitted the $U(1)$, which itself has a non-trivial gauge group structure associated with the $SU(2)$, see Table 17). We will leave a detailed derivation and classification along the lines of [93] for future work.

3.3.3 Matter surfaces, fluxes and the chiral spectrum

To specify the chiral spectrum of the F-theory compactification, we need two geometric ingredients, namely the surfaces on which the matter states are localized, and the description of the G_4-flux in terms of their dual four cycle classes. Based on the techniques first developed in [43, 37] and further advanced in [39, 40, 41, 42, 46], we perform a completely base independent analysis of fluxes and chiralities, which then can be straightforwardly applied to specific fibrations.

Matter surfaces and their homology classes

Through the mapping to its Jacobian [82], we can straightforwardly determine the codimension two loci where the fiber singularities of Y_{31} enhance. These are of them form

$\{w_i\} \cap \{g_{\mathbf{R}}\}$ for some polynomials $g_{\mathbf{R}}$:

$$
\begin{aligned}
g_{\mathbf{2}_1} &= d_{10}d_6^2 d_8 - d_{10}d_5 d_6 d_9 - d_6 d_7 d_8 d_9 + d_5 d_7 d_9^2 + w_3\left(d_{10}^2 d_5^2 - 2d_{10}d_5 + d_7^2 d_8^2\right), \\
g_{\mathbf{2}_2} &= d_1 d_3 d_6^2 - d_1 d_2 d_6 d_7 + d_1^2 d_7^2 + w_3\left(d_2^2 d_5 d_7 - d_2 d_3 d_5 d_6 - 2d_1 d_3 d_5 d_7 + d_3^2 d_5^2 w_3\right), \\
g_{\mathbf{3}_1} &= d_1\,, \\
g_{\mathbf{3}_2} &= d_{10}d_6 - d_7 d_9\,, \\
g_{\mathbf{3}_3} &= d_3 d_6^2 - d_2 d_6 d_7 + d_1 d_7^2\,, \\
g_{\mathbf{3}_4} &= d_6^2 d_8 - d_5 d_6 d_9 + d_1 d_9^2 w_2\,.
\end{aligned}
\tag{3.3.13}
$$

Furthermore, there are two charged singlets with $U(1)$ charge 1, but differ in their $\mathbb{Z}_2$ charge, which are localized over curves given by complicated ideals $I_{+/-}$.

There is also an uncharged singlet with negative $\mathbb{Z}_2$ parity [82]. These matter states have the same quantum numbers as right-handed neutrinos. Correspondingly, they interact with Higgs and lepton doublets via perturbatively realized Yukawa couplings in the F-theory geometry. The presence of such massless states in the effective field theory not only depends on the flux, but also on the complex structure moduli [45, 46]. However, because it is a real representation, there cannot be any net chirality associated with these matter states. Geometrically, this is reflected in the fact that the components of the I_2 fiber associated with this matter are exchanged via monodromy. Consistently, the transversality conditions 3.3.15 imply that the intersection product between the flux and this singlet's matter surface is 0. Hence, we will disregard this representation for the rest of this paper, since we are mainly interested in the chiral spectrum.

Over the codimension two loci $C_{\mathbf{R}} = \{w_i\} \cap \{g_{\mathbf{R}}\}$, the reducible fibers contain localized $\mathbb{P}^1$ components, giving rise to matter states in the representation $\mathbf{R}$ in F-theory. By fibering one such $\mathbb{P}^1$ over the curve on the base, one obtains a four-cycle $\gamma_{\mathbf{R}}$, a so-called matter surface associated with a weight $\mathbf{w}$ of a representation $\mathbf{R}$ (or its conjugate). To

determine the homology classes of these matter surfaces, we use prime ideals techniques and algorithms detailed in [42], utilizing the computer algebra program `Singular` [94]. The specific states, whose matter surfaces we determine this way, are listed in Table 5. Their corresponding matter surface classes are collected in the appendix, cf. Table 12.

rep	$U(1) \times \mathbb{Z}_2$	Cartan charges	parent exceptional	base locus	$\mathbb{Z}_2^{M_2}$ Rep.
$\mathbf{2}_1$	$\left(\frac{1}{2}, -\right)$	$(0, 0 \,\vert\, 1)$	E_0	$\{w_2\} \cap \{g_{\mathbf{2}_1}\}$	L
$\mathbf{2}_2$	$\left(\frac{1}{2}, +\right)$	$(0, 0 \,\vert\, -1)$	E_1	$\{w_2\} \cap \{g_{\mathbf{2}_2}\}$	Higgs
$\overline{\mathbf{3}}_1$	$\left(-\frac{2}{3}, -\right)$	$(0, 1 \,\vert\, 0)$	F_0	$\{w_3\} \cap \{g_{\mathbf{3}_1}\}$	$\bar{d}$
$\mathbf{3}_2$	$\left(\frac{2}{3}, +\right)$	$(-1, 1 \,\vert\, 0)$	F_1	$\{w_2\} \cap \{g_{\mathbf{3}_2}\}$	exotic
$\overline{\mathbf{3}}_3$	$\left(\frac{1}{3}, -\right)$	$(1, -1 \,\vert\, 0)$	F_2	$\{w_3\} \cap \{g_{\mathbf{3}_3}\}$	$\bar{u}$
$\overline{\mathbf{3}}_4$	$\left(\frac{1}{3}, +\right)$	$(0, 1 \,\vert\, 0)$	F_0	$\{w_3\} \cap \{g_{\mathbf{3}_4}\}$	exotic
$(\overline{\mathbf{3}}, \mathbf{2})$	$\left(-\frac{1}{6}, -\right)$	$(0, 1 \,\vert\, -1)$	E_1, F_0	$\{w_2\} \cap \{w_3\}$	Q
$\mathbf{1}_1$	$(1, -)$	$(0, 0 \,\vert\, 0)$	n.a.	$V(I_{(1,-)})$	E
$\overline{\mathbf{1}}_2$	$(-1, +)$	$(0, 0 \,\vert\, 0)$	n.a.	$V(I_{(1,+)})$	exotic
$\mathbf{1}_3$	$(0, -)$	$(0, 0 \,\vert\, 0)$	n.a.	$V(I_{(0,-)})$	exotic (ν_R)

Table 5: States and charges associated with the matter surfaces. The polynomials g_i defining the matter curves in the base are in equation 3.3.13. We have included the identification with the MSSM spectrum, where the $\mathbb{Z}_2$ is identified with matter parity.

Note that the only bifundamental matter states we have in this model have odd $\mathbb{Z}_2$ charge. Therefore, this toric model Y_{31} only allows for an identification of the geometrically realized $\mathbb{Z}_2$ with the second matter parity $\mathbb{Z}_2^{M_2}$ listed in Table 3. We will see in the next section other geometries whose corresponding F-theory model may realize the other parities.

Vertical fluxes from matter surfaces

We now turn to the computation of G_4-fluxes. In practice, these are expressed through their Poincaré-dual four cycle classes (also denoted by G_4), such that the integral giving the chiral index can also be computed via intersection product:

$$\chi(\mathbf{R}) = \int_{\gamma_{\mathbf{R}}} G_4 = G_4 \cdot [\gamma_{\mathbf{R}}] \tag{3.3.14}$$

Not all four cycles give rise to consistent fluxes. As is well known by now, the fluxes have to satisfy the so-called transversality conditions [95] in order to uplift from M- to F-theory. These conditions have been generalized in [41] to genus-one fibrations:

$$G_4 \cdot D_B^{(1)} \cdot D_B^{(2)} = 0\,, \quad G_4 \cdot D_B \cdot [x] = 0 \tag{3.3.15}$$

for some vertical divisors $D_B^{(i)}$. In addition, the flux must not break the non-Abelian symmetries, which requires

$$G_4 \cdot \mathrm{Ex} \cdot D_B = 0\,, \tag{3.3.16}$$

where $\mathrm{Ex} \in \{E_1, F_1, F_2\}$ are the Cartan divisors.

For a fibration over a base threefold B, we can use the quotient ring description to determine a basis of vertical fluxes [42]. For generic choices of fibration and base, i.e., such that no further singularity enhancements are induced whose resolution would introduce further divisors, the space of vertical fluxes is spanned by $U(1)$-fluxes of the form $D_{U(1)} \cdot F$, where $F \in \pi^*(H^{1,1}(B))$, and five non-$U(1)$-fluxes. In this paper, we follow the method of [46] and express the non-$U(1)$-fluxes through so-called matter surfaces fluxes. At this point, there is no technical advantage for this procedure, and we could also use the flux basis provided by the algorithm of [42] to compute the chiralities. However, hoping that in future works we will have the computational power to also determine the vector-like

spectrum with the methods of [46], we will collect the necessary input in the Appendix A.2. For now, we content ourselves with a basis for vertical fluxes in terms of matter surfaces.

As the name suggests, the matter surface fluxes are constructed using the matter surfaces $[S_{\mathbf{R}}]$. By construction, these surfaces are orthogonal to any curve in the base:

$$[S_{\mathbf{R}}] \cdot D_B^{(1)} \cdot D_B^{(2)} = 0\,, \tag{3.3.17}$$

thus automatically satisfying the first of the transversality conditions 3.3.15. To satisfy the other as well as the gauge symmetry condition 3.3.16, we can add correction terms of the form $\mathrm{Ex}_i \cdot D_B + D_B^{(a)} \cdot D_B^{(b)}$ to $[S_{\mathbf{R}}]$. Note that these correction terms will not spoil the condition 3.3.17. Denoting such corrected matter surfaces by $A(\mathbf{R})$, we can choose a basis of five of them such that together with the $U(1)$-fluxes, they span the full space of vertical fluxes. Here, we will use the fluxes associated with $\mathbf{2}_2, \mathbf{3}_2, \overline{\mathbf{3}}_4, (\overline{\mathbf{3}}, \mathbf{2}), \overline{\mathbf{1}}_2$, which are:

$$\begin{aligned}
A(\mathbf{2}_2) &= [S_{\mathbf{2}_2}] + E_1 \cdot (W_2 + W_3 - 3\,\overline{K}_B + S_9)\,,\\
A(\mathbf{3}_2) &= [S_{\mathbf{3}_2}] + \frac{1}{3}\,(-F_1 + F_2) \cdot (S_7 + S_9 - W_3) - \frac{1}{3}\,W_3 \cdot [g_{\mathbf{3}_2}]\,,\\
A(\mathbf{3}_4) &= [S_{\overline{\mathbf{3}}_4}] + \frac{1}{3}\,(F_1 + 2\,F_2) \cdot (3\,\overline{K}_B - S_7 + S_9) - \frac{2}{3}\,W_3 \cdot [g_{\mathbf{3}_4}]\,,\\
A((\mathbf{3}, \mathbf{2})) &= [S_{(\overline{\mathbf{3}}, \mathbf{2})}] + \frac{1}{3}\,(F_1 + 2\,F_2) \cdot W_2 - \frac{1}{2}\,E_1 \cdot W_3 - \frac{1}{6}\,W_2 \cdot W_3\,,\\
A(\overline{\mathbf{1}}_2) &= [S_{\overline{\mathbf{1}}_2}]\,.
\end{aligned} \tag{3.3.18}$$

Including the $U(1)$-flux, we parametrize the most generic vertical G_4 in this model as

$$G_4 = a_1 A(\mathbf{2}_2) + a_2 A(\mathbf{3}_2) + a_3 A(\mathbf{3}_4) + a_4 A((\mathbf{3}, \mathbf{2})) + a_5 A(\overline{\mathbf{1}}_2) + D_{U(1)} \wedge F\,. \tag{3.3.19}$$

The chiral indices of matter representations can be straightforwardly computed in the quotient ring description of the vertical cohomology ring. Instead, one can also use the

more geometric picture laid out in [45, 46] and relate the chiralities to the homology classes of the Yukawa points. Their rather uninspiring explicit expressions are presented in the appendix, Formula A.2.3. As a consistency check, it is straightforward to verify that all 4D continuous gauge anomalies induced by the chiral spectrum are indeed canceled. It would be interesting to reproduce this result also in the weakly coupled type IIB limit of this model, along the lines of [96].

3.3.4 Concrete three family models

We are now in a position to scan for configurations that admit a three family flux solution. Recall that because the bifundamental states in this geometry have odd $\mathbb{Z}_2$ charge, the only phenomenological parity extension that is compatible is the matter parity $\mathbb{Z}_2^{M_2}$. Then, consistency with the observed spectrum (cf. table 3) requires to have the following chiral indices of the matter representations:

$\mathbf{R}$	$\mathbf{2}_1$	$\mathbf{2}_2$	$\overline{\mathbf{3}}_1$	$\mathbf{3}_2$	$\overline{\mathbf{3}}_3$	$\overline{\mathbf{3}}_4$	$(\overline{\mathbf{3}},\mathbf{2})$	$\mathbf{1}_{(1,+)}$	$\mathbf{1}_{(1,-)}$
χ	-3	0	3	0	3	0	-3	0	3

(3.3.20)

In addition to these chiral indices, we have to ensure the vanishing of the flux-induced D-term of the $U(1)$,

$$\xi \sim G_4 \wedge D_{U(1)} \wedge J_B \,, \tag{3.3.21}$$

where J_B is the Kähler form of the base. Note that this expression can be easily computed when we express G_4 in terms of the matter surface fluxes 3.3.18, because the $U(1)$ generator $D_{U(1)}$ is orthogonal to all the correction terms. Hence, the D-term is just a linear combination of the matter curves times the base's Kähler form, where the coefficients are

the $U(1)$ charges. For the explicit flux parametrization 3.3.19, this yields

$$\xi \sim J_B \cdot \left(\frac{a_1}{2} C_{\mathbf{2}_2} + \frac{2\,a_2}{3} C_{\mathbf{3}_2} + \frac{a_3}{3} C_{\mathbf{3}_2} - \frac{a_4}{6} W_2\, W_3 - a_5\, C_{\mathbf{1}_2} + \underbrace{\left(\frac{1}{2} W_2 + \frac{2}{3} W_3 - 2\,\overline{K}_B \right)}_{=\pi_*(D_{U(1)} \cdot D_{U(1)})} F \right) . \tag{3.3.22}$$

To find explicit models with this chiral spectrum, we need to specify the base B, the fibration structure in terms of the classes $S_{7/9}$, the choices for the non-Abelian divisors $W_{2/3}$, and the explicit flux which induces the correct chiralities. To make our lives as easy as possible, we will restrict ourselves to the simplest possible base, $B = \mathbb{P}^3$. As we shall see, this choice admits multiple solution and is hence by no means too restrictive.

Realistic chiral models over the base $\mathbb{P}^3$

For this simple choice of the base, the only independent divisor class is the hyperplane class H. Parametrizing the divisors in terms of H,

$$\overline{K}_B = 4H\ , \quad W_2 = n_2 H\ , \quad W_3 = n_3 H\ , \quad S_7 = s_7 H\ , \quad S_9 = s_9 H. \tag{3.3.23}$$

the integers n_i, s_j have to be such that the classes 3.3.8 of the coefficients d_i as well as $W_{2,3}$ are non-negative. On this specific base, the generic vertical flux 3.3.19 is parametrized by the five coefficients a_i of the matter surfaces fluxes and the $U(1)$-flux $D_{U(1)} \wedge (\lambda\, H)$. We collect these numbers in the flux vector $\mathcal{F} = (a_1, a_2, a_3, a_4, a_5, \lambda)$. We can now scan over all possible fibrations over $B = \mathbb{P}^3$ for flux solutions that generate the spectrum 3.3.20 as well as a vanishing D-term 3.3.22 (for $B = \mathbb{P}^3$, the Kähler form is simply $J_B \sim H$). In Table 6, we list the five configurations satisfying these requirements.

A few comments about these results are in order. First, we emphasize that the search procedure is based on the base *independent* flux 3.3.19 and chirality computation. This way, we do not have to first construct the full fibration and then construct the fluxes, which, as demonstrated in [42], can be very inefficient (largely due to the technical issues

	(n_2, n_3, s_7, s_9)	flux $\mathcal{F} =$	$(a_1,$	$a_2,$	$a_3,$	$a_4,$	$a_4,$	$\lambda)$	n_{D3}
$\mathbb{Z}_2^{M_2}$	$(1,3,7,3)$		$(0,$	$\frac{7}{4},$	$-\frac{3}{4},$	$-2,$	$\frac{3}{4},$	$-\frac{3}{2})$	33
	$(3,1,5,1)$		$(0,$	$-\frac{5}{12},$	$-\frac{1}{12},$	$-\frac{2}{3},$	$\frac{1}{12},$	$-\frac{1}{2})$	43
	$(1,2,5,3)$		$(\frac{7}{48},$	$\frac{1}{6},$	$-\frac{1}{48},$	$-\frac{5}{6},$	$\frac{1}{48},$	$\frac{5}{24})$	38
	$(2,1,5,2)$		$(\frac{1}{12},$	$\frac{7}{24},$	$-\frac{1}{48},$	$-\frac{5}{6},$	$\frac{1}{48},$	$\frac{5}{24})$	44
	$(3,1,5,2)$		$(\frac{7}{96},$	$\frac{7}{16},$	$-\frac{1}{32},$	$-\frac{5}{6},$	$\frac{1}{32},$	$\frac{5}{16})$	39

Table 6: The summary of geometric and flux data that lead to three chiral generations in the $\mathbb{Z}_2^{M_2}$ matter parity assignment. The first two configurations each contain a redundant flux parameter; we chose to eliminate this redundancy by setting $a_1 = 0$. For completeness, we have also included the D3-tadpole.

of triangulating the polytope of the toric ambient space). In particular, as our results in Table 6 show, the gauge divisors $W_{2,3}$ are never both toric (i.e., have the divisor class H) in fibrations with three generation flux configurations. Realizing such fibrations explicitly would of course be a good consistency check, but very ineffective for the purpose of scanning a large number of different models. We content ourselves with the verification that these choices of classes generically do not induce any additional non-abelian gauge divisors or any factorization of the generically present matter curves. Second, we point out that first two solutions in Table 6 are at the boundary of the allowed region for (n_2, n_3, s_7, s_9), i.e., at these points, some of the coefficients d_i become constant. Concretely, in the two cases here, it is d_8. When this happens, also the chosen flux basis 3.3.19 becomes linearly dependent, meaning that one parameter becomes redundant.[2] For concreteness, we set $a_1 = 0$ in these cases. Third, note that in all these cases, the D3-tadpole (see below) is positive, which is required for a stable vacuum. Moreover, the fact that all of them are integer is a necessary condition that fluxes are properly quantized. In the following, we will provide further arguments for the correct flux quantization in our realizations.

[2]In some cases it can happen, that some constant d_i lead to an enhanced Mordell–Weil group, induced by a multi-section that can become rational. We checked that this jump does not happen in the $[d_8] = 0$ case.

3.3.5 Flux quantization and discrete anomalies

The condition for flux quantizaion reads [97]:

$$G_4 + \frac{1}{2}c_2(Y) \in H^4(\mathbb{Z}, Y)\,, \tag{3.3.24}$$

where $c_2(Y)$ is the second Chern class of the fourfold. In practice, verifying this condition explicitly is extremely challenging, and we will not attempt it here. However, we will perform several non-trivial sanity checks, which in particular involves the relationship of the quantization condition to the gauge anomalies of the $\mathbb{Z}_2$.

D3-tadpole and intersection numbers

One important quantity which has to be integer for a properly quantized flux is the D3-tadpole [98],

$$n_3 = \frac{\chi}{24} - \frac{1}{2}\int_Y G_4 \wedge G_4\,. \tag{3.3.25}$$

Here, χ is the Euler characteristic of the fourfold Y, which can be computed as the integral of the fourth Chern class of Y over Y. For toric fibrations, one can compute the Chern classes via adjunction for any base B (see [82, 41, 42] for examples). As we already mentioned above, it turns out that the tadpole is always integer for all three generation flux configurations (cf. table 6).

Furthermore, given the integrality condition 3.3.24, we necessarily need to have

$$\left(G_4 + \frac{1}{2}c_2(Y)\right) \cdot D_1 \cdot D_2 \in \mathbb{Z} \tag{3.3.26}$$

for any two integer divisor classes D_1, D_2. In practice, we test this condition with D_i being the restrictions of one of the toric divisors from the ambient space. On the hypersurface, these give rise to the Cartan divisors and the four bisections and are thus manifestly integer classes. In the above models with three family spectra, all these intersection numbers are

integer, thus further supporting the claim that the flux is properly quantized.

Geometric incarnation of discrete anomaly cancellation

One particularly fascinating aspect of the quantization condition is its relationship to the cancellation of discrete anomalies 3.2.4. Recall that for the case at hand, we are only interested in the $\mathbb{Z}_2 - G^2$ anomaly. For $G = SU(2)$, it receives contributions from doublets which have odd $\mathbb{Z}_2$ charge. Within the spectrum (cf. Table 5) of F-theory on Y_{31}, these are the bifundamentals $(\mathbf{3}, \mathbf{2})$ and the doublets $\mathbf{2}_2$. Therefore, the geometric version of the $\mathbb{Z}_2 - SU(2)^2$ anomaly cancellation condition is

$$\mathcal{A}_{\mathbb{Z}_2 - SU(2)^2} = 3 \cdot \chi((\mathbf{3}, \mathbf{2})) + \chi(\mathbf{2}_2) = G_4 \cdot \Big(3\,[S_{(\mathbf{3},\mathbf{2})}] + [S_{\mathbf{2}_2}]\Big) \in 2\,\mathbb{Z}\,. \tag{3.3.27}$$

Inserting the matter surface classes and using the transversality 3.3.15 and gauge symmetry 3.3.16 constraints of G_4, this expression simplifies to

$$\mathcal{A}_{\mathbb{Z}_2 - SU(2)^2} = G_4 \cdot (2\,[y]\,[e_0] - 4\,E_1\,F_1)\ . \tag{3.3.28}$$

Thus, the anomaly is canceled if and only if

$$\mathcal{A}_{\mathbb{Z}_2 - SU(2)^2} \in 2\,\mathbb{Z} \iff \frac{1}{2}\mathcal{A}_{\mathbb{Z}_2 - SU(2)^2} = G_4 \cdot ([y]\,[e_0] - 2\,E_1\,F_1) \in \mathbb{Z}\,. \tag{3.3.29}$$

While this expression depends on the flux and has a priori no reason to be integer, we note that the four cycle class in parenthesis is manifestly integer. Thus, as long as the flux is properly quantized 3.3.24, one necessarily has to have

$$\Big(G_4 + \frac{1}{2}c_2(Y_{31})\Big) \cdot ([y]\,[e_0] - 2\,E_1\,F_1) \in \mathbb{Z}\,. \tag{3.3.30}$$

Hence, to guarantee 3.3.29, it suffices to show that

$$\frac{1}{2}c_2(Y_{31}) \cdot ([y]\,[e_0] - 2\,E_1\,F_1) \in \mathbb{Z}\,. \tag{3.3.31}$$

The same method has been used in [88] to proof that an F-theory model with $SU(5)\times\mathbb{Z}_2$ has no $\mathbb{Z}_2$ anomaly. There, to show that the equivalent version of 3.3.31 held for *any* choice of base and fibration, it was crucial to know how the fluxes and chiralities matched across the conifold transition which unhiggsed the $\mathbb{Z}_2$ into a $U(1)$. Doing the same for our model here is beyond the scope of this paper. However, we can simply evalute 3.3.31 for every explicit choices of base and fibration structure, in particular on which we found three generation configurations. And indeed, it turns out that in all fibrations over $\mathbb{P}^3$, the $\mathbb{Z}_2 - SU(2)^2$ anomaly 3.3.29 is canceled due to 3.3.31.

Likewise, the $\mathbb{Z}_2 - SU(3)^2$ anomaly is

$$\mathcal{A}_{\mathbb{Z}_2-SU(3)^2} = \chi(\mathbf{3}_1) + \chi(\mathbf{3}_3) = G_4 \cdot ([S_{\mathbf{3}_1}] + [S_{\mathbf{3}_3}]) = G_4 \cdot (2\,F_1\,F_2) \overset{!}{\in} 2\,\mathbb{Z}\,. \tag{3.3.32}$$

Proceeding analogously as above, this condition is equivalent to

$$\frac{1}{2} c_2(Y_{31}) \cdot F_1\,F_2 \in \mathbb{Z}\,, \tag{3.3.33}$$

which we can explicitly verify to be true in all cases with $B = \mathbb{P}^3$.

3.4 Other $\mathbb{Z}_2$ symmetries assignments

In this section we want to consider other $\mathbb{Z}_2$ charge assignments that can be of phenomenological relevance. These include the other matter parity assignment $\mathbb{Z}_2^{M_1}$ as well as lepton and baryon parity, as discussed in Table 3. In order to realize them, we consider a different top combination, but perform exactly the same steps that were presented in the previous section. Hence, we will be brief about the details in this section.

3.4.1 Summary of geometric data

The top combination that we are considering is $SU(2)$ top 1 and $SU(3)$ top 2, as given in Appendix A.3. The toric data of the model is summarized in Table 7.

top vertices	$SU(2):\quad e_0:(0,0,1)\,,\quad e_1:(1,0,1)\,,$ $SU(3):\quad f_0:(0,0,-1)\,,\quad f_1:(0,1,-1)\,,\quad f_2:(-1,1,-1)$
$b_1=e_0f_1f_2^2d_1$	$b_3=e_0f_0f_2d_3$ $\quad b_6=d_6$ $\quad b_8=e_1f_1d_8$ $\quad b_{10}=e_1f_0^2f_1d_{10}$ $b_2=e_0f_2d_2$ $\quad b_5=f_1f_2d_5$ $\quad b_7=f_0d_7$ $\quad b_9=e_1f_0f_1d_9$
SRI:	$\{xt, xe_1, xf_1, ys, yf_0, te_0, tf_2, sf_2, e_1f_2, sf_1\}\,.$
$D_{U(1)}=$	$[x]-[y]-\frac{1}{2}E_1-(\frac{1}{3}F_1+\frac{2}{3}F_2)-\frac{1}{3}W_3+\frac{1}{2}\overline{K}_B+\frac{1}{2}S_7-\frac{1}{2}S_9\,,$
$D_{\mathbb{Z}_2}=$	$x+\frac{2}{3}(F_1+2F_2)\,.$
$[d_1]=3\overline{K}_B-S_7-S_9-W_2$	$[d_5]=2\overline{K}_B-S_7$ $\quad [d_8]=\overline{K}_B+S_9-S_7$
$[d_2]=2\overline{K}_B-S_9-W_2$	$[d_6]=\overline{K}_B$ $\quad [d_9]=S_9-W_3$
$[d_3]=\overline{K}_B+S_7-S_9-W_3-W_2$	$[d_7]=S_7-W_3$ $\quad [d_{10}]=S_9+S_7-\overline{K}_B-2W_3$

Table 7: Geometric data for the hypersurface specialization of the second top.

The matter loci can easily be determined by the information of the two tops given in Appendix A.3 including the additional bifundamental representation at $W_2=W_3=0$ as summarized in Table 8. The spectrum is very similar as before but includes a $\mathbb{Z}_2$-even charged bifundamental.

This allows for a straightforward identification of the geometric $\mathbb{Z}_2$ with the other three parities listed in Table 3.

The matter homology classes of the curves in terms of ambient divisors is given in Table 13 of Appendix A.1 which can be used to obtain the five independent matter surface fluxes:

$$\begin{aligned}
A(\mathbf{2}_2) &= [S_{\mathbf{2}_2}]-\frac{1}{2}E_1\cdot(-2W_2-W_3+6\overline{K}_B-2S_9)\,,\\
A(\overline{\mathbf{3}}_2) &= [S_{\mathbf{3}_2}]-\frac{1}{3}(2F_1+F_2)\cdot(2\overline{K}_B-W_2-W_3+S_7-S_9)+\frac{1}{3}C_{\mathbf{3}_2}\,,\\
A(\mathbf{3}_4) &= [S_{\mathbf{3}_4}]+\frac{1}{3}(2F_1+F_2)\cdot(-W_2+5\overline{K}_B-S_7-S_9)-\frac{1}{3}C_{\mathbf{3}_4}\,,\\
A((\mathbf{3},\mathbf{2}) &= [S_{(\mathbf{3},\mathbf{2})}]+\frac{1}{3}(-F_1+F_2)\cdot W_2+\frac{1}{2}E_1\cdot W_3-\frac{1}{3}W_2\cdot W_3\,,\\
A(\overline{\mathbf{1}}_2) &= [S_{\overline{\mathbf{1}}_2}]\,,
\end{aligned}\tag{3.4.1}$$

where $C_{\mathbf{R}}$ denotes the classes of the associated matter curves. These admit the following

Label	$G_{\rm SM} \times \mathbb{Z}_2$ Rep.	$\mathbb{Z}_2^{M_1}$	$\mathbb{Z}_2^{L}$	$\mathbb{Z}_2^{B}$
$\mathbf{2}_1$	$(\mathbf{1},\mathbf{2})_{(-\frac{1}{2},-)}$	H_d, H_u	L	L
$\mathbf{2}_2$	$(\mathbf{1},\mathbf{2})_{(-\frac{1}{2},+)}$	L	H_d, H_u	$-$
$\overline{\mathbf{3}}_1$	$(\overline{\mathbf{3}},\mathbf{1})_{(-\frac{2}{3},-)}$	$\overline{u}$	$-$	$\overline{u}$
$\overline{\mathbf{3}}_2$	$(\overline{\mathbf{3}},\mathbf{1})_{(-\frac{2}{3},+)}$	$-$	$\overline{u}$	$-$
$\mathbf{3}_3$	$(\mathbf{3},\mathbf{1})_{(-\frac{1}{3},-)}$	$\overline{d}$	$-$	$\overline{d}$
$\mathbf{3}_4$	$(\mathbf{3},\mathbf{1})_{(-\frac{1}{3},+)}$	$-$	$\overline{d}$	$-$
$(\overline{\mathbf{3}},\mathbf{2})$	$(\overline{\mathbf{3}},\mathbf{2})_{(-\frac{1}{6},+)}$	Q	Q	Q
$\mathbf{1}_1$	$(\mathbf{1},\mathbf{1})_{(1,-)}$	$\overline{e}$	$\overline{e}$	$-$
$\mathbf{1}_2$	$(\mathbf{1},\mathbf{1})_{(-1,+)}$	$-$	$-$	$\overline{e}$

Table 8: Matter curves and their charges as given for the second top combination. MSSM field identifications under various $\mathbb{Z}_2$ symmetries are given in the last three columns. For each identification we assign the chirality three to MSSM fields whereas states marked with a "$-$" must be non-chiral.

algebraic equivalence relations between the above flux basis and other vertical 4-cycles:

$$\begin{aligned} A(\mathbf{2}_2) - A((\mathbf{3},\mathbf{2})) - 2D_{U(1)}\cdot W_2 + A(\mathbf{2}_1) &= 0\,, \\ A((\overline{\mathbf{3}},\mathbf{2})) - A(\overline{\mathbf{3}}_2) + D_{U(1)}\cdot W_3 - A(\overline{\mathbf{3}}_1) &= 0\,, \\ A(\mathbf{3}_4) + A((\mathbf{3},\mathbf{2})) - D_{U(1)}\cdot W_3 + A(\mathbf{3}_3) &= 0\,, \\ A((\mathbf{3},\mathbf{2})) + A(\mathbf{1}_2) + D_{U(1)}\cdot(-6\overline{K}_B + 2W_2 + 3W_3) - A(\mathbf{1}_1) &= 0\,. \end{aligned} \tag{3.4.2}$$

The G_4-flux in the above basis is then given by

$$G_4 = a_1 A(\mathbf{2}_2) + a_2 A(\mathbf{3}_2) + a_3 A(\mathbf{3}_4) + a_4 A((\overline{\mathbf{3}},\mathbf{2})) + a_5 A(\overline{\mathbf{1}}_2) + D_{U(1)}\wedge F\,. \tag{3.4.3}$$

3.4.2 Three family searches and discrete anomalies

For concrete three family realizations, we again pick the base to be $\mathbb{P}^3$. In this model, we now have the possibility to assign different physical interpretations to the $\mathbb{Z}_2$. In each fibration parametrized by (n_2, n_3, s_7, s_9), we search for flux configurations $(a_1, a_2, a_3, a_4, a_5, \lambda)$ compatible with one of the three possible identifications listed in Table 8. In all of them, we again impose the vanishing of the fluxed induced D-term of the $U(1)$. Those solutions that also have a positive integer D3-tadpole are listed in Table 9.

	(n_2, n_3, s_7, s_9)	$(a_1,$	$a_2,$	$a_3,$	$a_4,$	$a_5,$	$\lambda)$	n_{D3}
$\mathbb{Z}_2^{M_1}$	(1,3,7,4)	$(0,$	$-\frac{7}{4},$	$\frac{3}{4},$	$2,$	$\frac{3}{4},$	$-\frac{3}{2})$	33
	(3,1,5,4)	$(0,$	$-\frac{5}{12},$	$\frac{1}{12},$	$\frac{2}{3},$	$\frac{1}{12},$	$-\frac{1}{2})$	43
	(1,2,5,4)	$(\frac{7}{48},$	$-\frac{1}{6},$	$\frac{1}{48},$	$-\frac{11}{16},$	$\frac{1}{48},$	$-\frac{1}{12})$	38
	(2,1,5,4)	$(\frac{1}{12},$	$-\frac{7}{24},$	$\frac{1}{48},$	$\frac{3}{4},$	$\frac{1}{48},$	$-\frac{1}{8})$	44
	(3,1,5,3)	$(\frac{7}{96},$	$-\frac{7}{16},$	$\frac{1}{32},$	$-\frac{73}{96},$	$\frac{1}{32},$	$-\frac{1}{8})$	39
$\mathbb{Z}_2^{L}$	(1,2,4,4)	$(0,$	$\frac{5}{16},$	$-\frac{5}{96},$	$\frac{15}{32},$	$\frac{1}{6},$	$-\frac{73}{48})$	43
	(1,2,5,3)	$(0,$	$\frac{1}{12},$	$-\frac{1}{12},$	$\frac{1}{2},$	$0,$	$0)$	42
	(1,2,5,5)	$(0,$	$\frac{1}{4},$	$-\frac{1}{4},$	$\frac{1}{2},$	$0,$	$0)$	40
	(3,2,5,3)	$(0,$	$\frac{1}{4},$	$-\frac{1}{4},$	$\frac{1}{6},$	$0,$	$0)$	32
	(1,2,6,4)	$(\frac{41}{384},$	$\frac{7}{32},$	$-\frac{61}{384},$	$\frac{175}{384},$	$-\frac{23}{384},$	$\frac{23}{96})$	39
$\mathbb{Z}_2^{B}$	(3,2,5,4)	$(0,$	$0,$	$-\frac{1}{3},$	$\frac{1}{3},$	$-\frac{1}{6},$	$\frac{5}{3})$	34
	(1,2,5,4)	$(-\frac{1}{12},$	$-\frac{1}{3},$	$-\frac{1}{12},$	$\frac{3}{4},$	$-\frac{1}{12},$	$\frac{4}{3})$	38

Table 9: The summary of geometric and flux quanta that lead the three chiral generations for the three discrete symmetry assignments of the second top combination.

First we note that the solutions we obtain for the second matter parity assignment have a very similar structure compared to the models we obtained in the previous section (cf. Table 6), including the same number of D3-branes. This points towards an equivalence between the two fibrations defined via the two different top combinations.[3] A more general analysis of this equivalence including the necessary redefinitions of the abelian symmetry

[3]The classes of the sections of the two tops can be related by a change $d_1 \leftrightarrow d_8, d_9 \leftrightarrow d_2, d_{10} \leftrightarrow d_3$.

generators is left for future research. Secondly it is important to emphasize that only the flux configurations for matter parity fulfill the G_4-flux integrality condition

$$(G_4 + \frac{1}{2}c_2(Y)) \cdot D_1 \cdot D_2 \in \mathbb{Z}\,, \tag{3.4.4}$$

whereas the lepton and baryon parity assignments do not. Again, we can nicely relate this rather obscure geometric property directly to the cancellation of $\mathbb{Z}_2$ anomalies.

Namely, these are

$$\begin{aligned} \mathcal{A}_{Z_2-SU(2)^2} &= \chi(\mathbf{2}_1) = G_4 \cdot ([S_{\mathbf{2}_1}]) = -2\,[y]\,E_0 \in 2\mathbb{Z} \\ \mathcal{A}_{Z_2-SU(3)^2} &= \chi(\mathbf{3}_1) + \chi(\mathbf{3}_3) = G_4 \cdot (-[S_{\overline{\mathbf{3}}_1}] + [S_{\mathbf{3}_3}]) = 2\,F_1\,F_2 \in 2\mathbb{Z}\,. \end{aligned} \tag{3.4.5}$$

Like in the previous section, the quantization condition translates these conditions into a question about integrality of the intersection numbers

$$\frac{1}{2}c_2(Y_{32}) \cdot \begin{cases} [y]\,E_0 \\ F_1\,F_2 \end{cases}\,, \tag{3.4.6}$$

which both turn out to be indeed integral for all the fibrations we scanned over. However, we also know that only the matter parity $\mathbb{Z}_2^{M_1}$ assignment of the chiralities is anomaly free, whereas the lepton and baryon parity assignments are not with the spectrum in 8. Since the flux configurations are chosen to reproduce these chiral spectra, we arrive at the same conclusion—but based on field theoretic anomaly considerations—that the flux solutions for these two assignments in Table 9 cannot be properly quantized.

3.5 Summary and Conclusion

In this chapter we have engineered globally consistent four dimensional MSSM-like particle physics models with three chiral generations that admit $\mathbb{Z}_2$ quantum numbers under the matter parity extension of the Standard Model gauge group. Our compactifiations are genus-one fibered fourfolds with G_4-flux over a simple $\mathbb{P}^3$ base space that pass all

necessary consistency conditions: The G_4-flux is properly quantized, and the D3-tadpole is canceled with a positive and integral number of D3-branes. For this explicit construction we employed toric geometry to engineer the resolved fourfold which allows the direct computation of all (discrete) gauged quantum numbers. In addition, the fact that the internal space is smooth allows us to easily handle the gauge background, giving us the power to scan systematically for configurations leading to three chiral generations. These constructions are flexible enough to also allow, at least in principle, for other $\mathbb{Z}_2$ symmetries, such as lepton and baryon parity, by choosing different flux configurations. These models however suffer from non-properly quantized G_4-fluxes, even though they give three chiral families and a positive integer number of D3-branes. We have shown that this is not just a coincidence, but actually intimately related to the fact that lepton and baryon parities are not free of discrete anomalies with just the MSSM spectrum.

However several interesting questions remain. First it would be exciting to investigate the interplay between fluxes and discrete anomalies further. For example, an analysis similar to [87, 41] of the conifold transition that unhiggses the $\mathbb{Z}_2$ into a $U(1)$ could allow us to proof the cancellation of discrete anomalies for *generic* fibrations. Moreover we have left out possible Abelian-$\mathbb{Z}_2$ anomalies as they are hard to investigate in the field theory due to an ambiguous $U(1)$ charge normalization [79]. However, since in F-theory there is a natural charge quantization inherited from the Mordell–Weil lattice [93], one might hope that a more geometric treatment of this issue is possible. Further important steps towards more realistic phenomenology is to understand the full vector-like sector and to decouple possible (vector-like) exotics while keeping one pair of Higgs doublets light. This would also allow us to determine the presence of right-handed neutrinos, whose representation is, at least in principle, realized explicitly in the geometry. Due to recent progress [45, 46] this goal seems to be in reach. However, applying the methods presented there to a complex configuration of matter curves, such as we have in our models, are not feasible with the given algorithms and computing power today. But even without exotics, this

model might still suffer from higher dimensional operators in the effective action such as

$$\mathcal{W} \ni \kappa^1 QQQL + \kappa^2 \overline{u}\overline{u}\overline{d}E\,, \tag{3.5.1}$$

whose coefficients are strongly constrained by proton decay but can not be forbidden with matter parity alone. Hence one might want to construct higher order discrete symmetries, ideally the $\mathbb{Z}_6$ proton hexality [99] which forbids also other dangerous higher dimensional operators, and is anomaly free. The classification or construction of higher order (possibly non-Abelian [100, 101, 102]) discrete symmetries base-independently beyond $\mathbb{Z}_4$ [103, 104] are unknown yet (see, however, [105] for some recent examples over specific bases) and, hence, a topic of great interest. Once such a classification is available, we hope that a generalization of our work can realize the chiral MSSM with such a discrete symmetry extension.

This chapter is based on the paper [32]. In this chapter we present $\mathcal{O}(10^{15})$ string compactifications with the exact chiral spectrum of the Standard Model of particle physics. This ensemble of globally consistent F-theory compactifications automatically realizes gauge coupling unification. Utilizing the power of algebraic geometry, all global consistency conditions can be reduced to a single criterion on the base of the underlying elliptically fibered Calabi–Yau fourfolds. For toric bases, this criterion only depends on an associated polytope and is satisfied for at least $\mathcal{O}(10^{15})$ bases, each of which defines a distinct compactification.

4.1 MSSM model buildings in F-theory constructions

As a theory of quantum gravity that naturally gives rise to rich gauge sectors at low energies, string theory is a leading candidate for a unified theory. Achieving unification is an ambitious goal that requires accounting for all aspects of our physical world, which includes not only a rich cosmological history, but also the detailed structure of the Standard Model of particle physics.

In this paper we present an explicit construction that guarantees the existence of $\mathcal{O}(10^{15})$ fully consistent string compactifications which realize the exact chiral particle spectrum of the minimally supersymmetric Standard Model (MSSM). This construction is performed in the framework of F-theory [27], a strongly coupled generalization of type IIB superstring theory. It captures the non-perturbative back-reactions of 7-branes onto the compactification space B_3 in terms of an elliptically fibered Calabi–Yau fourfold $\pi : Y_4 \to B_3$ over it. Gauge symmetries, charged matter, and Yukawa couplings are then encoded beautifully by Y_4's singularity structures in codimensions one, two, and three, respectively.[1]

In the present work, we consider a class of elliptically fibered Calabi–Yau fourfolds giving rise to precisely the three-generation MSSM spectrum provided certain geometric condi-

[1] We refer the interested reader to [26] and references therein for recent reviews on F-theory.

tions on the base of the fibration are satisfied. We perform a concrete analysis, finding $\mathcal{O}(10^{15})$ such bases. All these models come equipped with moduli-dependent quark and lepton Yukawa couplings, as well as gauge coupling unification at the compactification scale.

The existence of a very large number of Standard Model realizations in string theory could perhaps be anticipated within the set of an even larger number of string compactifications (see, e.g., [106]) that form the so-called string landscape. Indeed, though Standard Model realizations within the landscape could potentially be scarce [107], recent works hint towards an astronomical number of them [108]. Our construction *explicitly* demonstrates this possibility, increasing the number of concretely known, global Standard Model compactifications in string theory by about ten orders of magnitude.

There are also explicit constructions of the Standard Model in other corners of string theory. Some of the early examples of globally consistent intersecting brane models [23] in type II compactifications (see also [24] and references therein) were strongly constrained by global consistency conditions such as tadpole cancellation. In the heterotic string, the typical difficulties of constructions like [109, 110] arise from having a stable hidden bundle and the existence of Yukawa couplings. These issues are solved elegantly in F-theory through the geometrization of non-perturbative stringy effects: (almost all[2]) global conditions analogous to tadpole cancellation or bundle stability are automatically taken care of by having a compact, elliptic Calabi–Yau fourfold Y_4, and the presence or absence of Yukawa couplings can be easily read off from codimension three singularities of Y_4.

Despite these advantages, only a handful [40, 44] of F-theory compactifications that realize the exact chiral spectrum of the MSSM are currently known, due to focusing on a very simple base, $B_3 = \mathbb{P}^3$. This limitation will be avoided in the current work by instead studying smooth toric varieties, which provide a much larger class [30] of geometries. To

[2]In F-theory, D3-tadpole cancellation requires extra care, and will be a major theme in our constructions.

take advantage of this large ensemble, we first construct a class of elliptic fibrations (based on the class $\mathbb{P}_{F_{11}}$ in [82]) that can be consistently fibered over all such toric threefolds.

Every such fibration realizes the precise Standard Model gauge group $[SU(3) \times SU(2) \times U(1)]/\mathbb{Z}_6$ as well as its matter representations and Yukawa couplings [82, 40, 93]. Moreover, all models exhibit gauge coupling unification at the compactification scale, compatible with the existence of a complex structure deformation to a geometry realizing the Pati–Salam model with unified gauge coupling [82, 40].

Furthermore, for each compatible B_3 there exists a G_4-flux that induces three families of chiral fermions. These models have a particularly pleasant feature: all global consistency conditions on the flux (including quantization and D3-tadpole cancellation) can be reduced to a single criterion on the intersection number $\overline{K}_B^3$ of the anti-canonical class $\overline{K}_B$ of the base B_3. For toric threefolds which have a description in terms of a reflexive polytope Δ, $\overline{K}_B^3$ depends only on the point configuration of Δ and not its triangulation. On the other hand, for a single polytope there can be multiple different toric threefolds associated with the different fine regular star triangulations (FRSTs) of Δ, the number of which grows exponentially with the number of lattice points in the polytope [30]. Putting together these different components, we find that the number $N_{\text{SM}}^{\text{toric}}$ of globally consistent three-family Standard Models in our construction is

$$7.6 \times 10^{13} \lesssim N_{\text{SM}}^{\text{toric}} \lesssim 1.6 \times 10^{16}. \tag{4.1.1}$$

We emphasize that this number is construction dependent; F-theory could realize more Standard Models.

The detailed derivation of this count first requires the construction in section 4.2 of a class of elliptic fibrations with a flux inducing three chiral families. All flux consistency conditions reduce to a single criterion on the base B_3. To count how many B_3 satisfy this criterion, we discuss the methods to construct FRSTs of 3D polytopes in section

4.3, which ultimately lead us to $\mathcal{O}(10^{15})$ possibilities. We close in section 4.4 with some geometric and physical comments, as well as future directions.

4.2 Universally Consistent Fibrations with Three Families

The class of elliptic fibrations we are interested is based on an elliptic curve that is a specialized cubic inside $\mathbb{P}^2$ with homogeneous coordinates $[u : v : w]$, given by the vanishing of the polynomial

$$P := s_1 u^3 + s_2 u^2 v + s_3 u v^2 + s_5 u^2 w + s_6 u v w + s_9 v w^2. \tag{4.2.1}$$

By promoting the coefficients s_i to rational functions over a Kähler threefold B_3, one obtains a singular, elliptically fibered fourfold $\pi : Y_4^{(s)} \to B_3$. For $Y_4^{(s)}$ to be Calabi–Yau, the functions s_i have to be holomorphic sections of line bundles on B_3 with first Chern classes $[s_i] \in H^{1,1}(B_3, \mathbb{Z})$ given by [82, 40]:

$$\begin{aligned} &[s_1] = 3\,\overline{K}_B - \mathcal{S}_7 - \mathcal{S}_9\,, \quad [s_2] = 2\,\overline{K}_B - \mathcal{S}_9\,, \quad [s_6] = \overline{K}_B\,, \\ &[s_3] = \overline{K}_B + \mathcal{S}_7 - \mathcal{S}_9\,, \qquad [s_5] = 2\,\overline{K}_B - \mathcal{S}_7\,, \quad [s_9] = \mathcal{S}_9\,, \end{aligned} \tag{4.2.2}$$

where $\overline{K}_B \equiv c_1(B_3)$ is the anti-canonical class of B_3. The classes $\mathcal{S}_{7,9} \in H^{1,1}(B_3, \mathbb{Z})$ parametrize different fibrations over the same base, on which $\{s_i = 0\}$ define effective divisors.

When all s_i are generic, (that is, irreducible and $s_i \neq s_j$ for $i \neq j$), F-theory compactified on $Y_4^{(s)}$ has the gauge symmetry $[SU(3) \times SU(2) \times U(1)]/\mathbb{Z}_6$ [82, 93]. The global gauge group structure is reflected in the precise agreement between the geometrically realized matter representations and those of the Standard Model:

$$(\mathbf{3}, \mathbf{2})_{\frac{1}{6}}\,, \;\; (\mathbf{1}, \mathbf{2})_{-\frac{1}{2}}\,, \;\; (\overline{\mathbf{3}}, \mathbf{1})_{-\frac{2}{3}}\,, \;\; (\overline{\mathbf{3}}, \mathbf{1})_{\frac{1}{3}}\,, \;\; (\mathbf{1}, \mathbf{1})_{1}\,. \tag{4.2.3}$$

These data can be extracted via the M-/F-theory duality from an explicit resolution Y_4

of $Y_4^{(s)}$, which preserves the Calabi–Yau structure.

A chiral spectrum in F-theory requires a non-zero flux $G_4 \in H^{2,2}(Y_4)$, which must also be specified. For the relevant subspace of so-called primary vertical G_4-fluxes, there is by now a large arsenal of computational methods [41, 42] (see also [39, 40, 96]) that allows us to determine *base-independently* the most general flux on Y_4.

For physical consistency, this G_4-flux has to satisfy certain conditions. The first condition is a proper quantization [95, 111]:

$$G_4 + \frac{1}{2}\, c_2(Y_4) \in H^{2,2}(Y_4, \mathbb{Z})\,, \tag{4.2.4}$$

where $c_2(Y_4)$ is the second Chern class of Y_4. Heuristically, this condition ensures that the notion of fermions (that requires a flux-dependent spin structure on subspaces of Y_4) is well-defined. Since explicitly verifying this condition for concrete geometries is difficult, we will content ourselves with the usual necessary consistency checks [112, 39, 40, 42, 44]. The second consistency condition is a D3-tadpole satisfying [98],

$$n_{\text{D3}} = \frac{\chi(Y_4)}{24} - \frac{1}{2}\int_{Y_4} G_4 \wedge G_4 \overset{!}{\in} \mathbb{Z}_{\geq 0}\,. \tag{4.2.5}$$

While integrality follows as a consequence of the quantization condition 3.3.24, positivity aids in ensuring the stability of the compactification.

We must also impose phenomenological constraints on the flux. A massless electroweak hypercharge $U(1)_Y$ is guaranteed if the D-terms vanish [113, 114]:

$$\forall \eta \in H^{1,1}(B_3): \quad \int_{Y_4} G_4 \wedge \sigma \wedge \pi^*\eta \overset{!}{=} 0. \tag{4.2.6}$$

Here, σ is the $(1,1)$-form Poincaré-dual to the so-called *Shioda-divisor* associated with

the $U(1)$ [115]. A three-family chiral Standard Model requires that [59],

$$\chi(\mathbf{R}) = \int_{\gamma_{\mathbf{R}}} G_4 \stackrel{!}{=} 3\,, \tag{4.2.7}$$

for all representations $\mathbf{R}$ in 4.2.3. The geometric data $c_2(Y_4)$, $\chi(Y_4)$, and the matter surfaces $\gamma_{\mathbf{R}}$ were computed in [82, 40]. In the supplemental material, we provide the explicit expression of the generic vertical flux in the resolution Y_4 presented in [82], and explain in detail how the above conditions can be checked using well-studied topological methods.

We now present our main result, on how these consistency conditions can be satisfied for a large ensemble of explicit geometries. For that, we first consider the generic flux configuration on (smooth) fibrations Y_4 with $\mathcal{S}_{7,9} = \overline{K}_B$, which simplifies the expressions for the topological quantities 4.2.5–4.2.7. In fact, one can show that all consistency conditions are reduced to a *single* criterion on B_3 from the D3-tadpole:

$$n_{\mathrm{D3}} = 12 + \frac{5}{8}\,\overline{K}_B^3 - \frac{45}{2\,\overline{K}_B^3} \stackrel{!}{\in} \mathbb{Z}_{\geq 0}\,, \tag{4.2.8}$$

where $\overline{K}_B^3$ denotes the triple self-intersection number of the anti-canonical class $\overline{K}_B$ of the base. This dramatic simplification only requires $\overline{K}_B^3$ of appropriate value and a base that allows irreducible and distinct s_i, all of which are sections of the anti-canonical class.

In summary, we have constructed a class of elliptically fibered Calabi–Yau fourfolds which gives rise in F-theory to the Standard Model gauge group and matter representations with three chiral generations. The only consistency requirement that guarantees flux quantization and D3-tadpole cancellation is that the base B_3 of the fibration is a smooth Kähler threefold with non-rigid irreducible anti-canonical divisors that satisfy 4.2.8. In fact, some basic arithmetic shows that the only values $\overline{K}_B^3$ can take such that $n_{\mathrm{D3}} \in \mathbb{Z}_{\geq 0}$

are

$$\overline{K}_B^3 \in \{2, 6, 10, 18, 30, 90\}\,. \tag{4.2.9}$$

4.3 Counting Standard Model Geometries

Any smooth threefold B_3 with non-rigid anti-canonical divisors satisfying 4.2.9 realizes a globally consistent three-family MSSM in F-theory. A subset of such spaces, which can be enumerated combinatorially, is the set of weak Fano toric threefolds encoded by 3D reflexive polytopes Δ. While there are "only" 4319 such polytopes [2], each Δ can specify inequivalent manifolds B_3 through different *fine-regular-star triangulations* (FRSTs) of the polytope, whose numbers can be very large [30].

What makes this ensemble particularly attractive for our purpose is the fact that the intersection number $\overline{K}_B^3$ is determined solely by the polytope Δ, and is completely triangulation-independent. Therefore any B_3 associated to an FRST of Δ gives rise to a consistent chiral three-generation MSSM by our construction, provided that the triangulation-independent constraint on $\overline{K}_B^3$ is satisfied. In fact, there is a set S with 708 polytopes that satisfy 4.2.9. By our construction we immediately have

$$N_{\rm SM}^{\rm toric} = \sum_{\Delta \in S} N_{\rm FRST}(\Delta)\,, \tag{4.3.1}$$

where $N_{\rm FRST}(\Delta)$ is the number of FRSTs of Δ.

Hence, the problem of counting the number of consistent F-theory models that admit the chiral MSSM spectrum by our construction reduces to counting FRSTs of reflexive polytopes.

Since $N_{\rm FRST}(\Delta)$ grows exponentially with the number of lattice points in Δ, the set of consistent threefolds B_3 is dominated by triangulations of the largest polytope [30], labelled Δ_8 in the list of [2]. The FRSTs of this polytope (with $\overline{K}_B^3 = 6$ and 39 lattice

points) cannot be all constructed explicitly using the standard computer programs such as `SageMath` [116]. To enumerate them, we therefore follow the strategy put forward in [30] to provide bounds on $N_{\text{FRST}}(\Delta_8)$.

The idea is to reduce the complexity by first counting the number of *fine-regular triangulations* (FRTs) of each *facet* of a polytope Δ. Since the facets are two dimensional polytopes, it is possible to brute-force the combinatorics of FRTs for (almost[3]) all polytopes' facets. By virtue of the reflexivity of Δ, any combination of FRTs of all its facets yields fine star triangulation of Δ.

The drawback of this approach is that the triangulation of Δ_8 obtained this way is not guaranteed to be regular. To tackle this issue, we randomly pick 1.3×10^4 samples out of $\mathcal{O}(10^9)$ fine-star triangulations constructed by gluing together FRTs of the facets Δ_8. Out of these samples, we find roughly $\frac{2}{3}$ to be also regular triangulations. Combining the factor $\frac{2}{3}$ with the bounds of *fine-star triangulations* (FSTs) for Δ_8 [30], we then obtain $2.6 \times 10^{13} \leq N_{\text{FRST}}(\Delta_8) \leq 1.6 \times 10^{16}$.

For the other polytopes in S (i.e., those leading to threefolds satisfying 4.2.9) we can either compute all FRSTs, or we can resort to a similar estimation as with Δ_8 if the polytope is too large to brute-force all FRSTs. We find that these other polytopes sum up to "only" $\sim 5 \times 10^{13}$ FRSTs, which confirms the dominance of Δ_8. In total, we therefore expect the number of consistent three-family F-theory Standard Models in our construction over toric threefold bases to be

$$7.6 \times 10^{13} \lesssim N_{\text{SM}}^{\text{toric}} \lesssim 1.6 \times 10^{16}\,.$$

[3]For facets with more than 15 lattice points, brute-forcing FRTs also becomes computationally too costly. For these facets, we use different methods outlined in [30] to obtain lower and upper bounds for the number of FRTs.

4.4 Discussion and Outlook

We have presented a construction that ensures the existence of $\mathcal{O}(10^{15})$ explicit, globally consistent string compactifications having the exact chiral spectrum of the Standard Model within the framework of F-theory. To our knowledge, this is the largest such ensemble in the literature, outnumbering existing results by about 10 orders of magnitude. The models arise by varying the base of one "universal" class of elliptic fibrations introduced in [82, 40]. We have only focused on the set of toric bases, which already produces around a quadrillion examples. However, we expect that the ensemble of Standard Models arising from our construction is of orders of magnitude larger than this, as might be shown, for instance, by including non-toric bases.

All these models have in common that the Higgs and lepton doublets are localized on the same matter curve. As such, this curve must have non-zero genus to allow for the existence of vector-like pairs [45]. Given the homology class of the doublet curve [40] and our restriction $\mathcal{S}_{7,9} = \overline{K}_B$, the genus in question is indeed $g = 1 + 9/2\overline{K}_B^3 > 0$, since $\overline{K}_B^3 \geq 2$ by 4.2.9. It would be very interesting, albeit extremely difficult with current methods, to study the precise complex structure dependence of the number of Higgs doublets and other charged vector-like pairs in this ensemble.

Furthermore, since our models have no additional (possibly massive) abelian gauge symmetries, all Yukawa couplings relevant for the Standard Model are automatically realized perturbatively, as can be shown by an explicit study of codimension three singularities [82]. However, this in turn also implies that certain proton decay operators compatible with the Standard Model gauge group will in general be present [40]. We expect that in some corners of the moduli space, which incidentally could also support high-scale SUSY breaking, these operators can be suppressed. Another avenue could be to instead focus on "F-theory Standard Models" that have additional ($U(1)$ [76, 42] or R-parity [44]) selection rules, and estimate their numbers in the toric base landscape. We leave this for future

work.

One interesting aspect of our ensemble is gauge coupling unification without a manifest GUT-origin at the compactification scale. It can be easily read off geometrically from the divisors on B_3, which the 7-branes supporting the gauge symmetries in the type IIB picture wrap. Due to our restriction $\mathcal{S}_{7,9} = \overline{K}_B$, both $SU(3)$ and $SU(2)$ gauge symmetries are realized on anti-canonical divisors $\{s_9 = 0\}$ and $\{s_3 = 0\}$ with class $\overline{K}_B$.[4] Therefore, the gauge couplings are $g^2_{3,2} = 2/\mathrm{vol}(\overline{K}_B)$ [113, 117].[5] The $U(1)_Y$ coupling is the inverse volume of the so-called height-pairing divisor $b \subset B_3$ [67], which has been computed in [82, 22] and reduces to $b = 5\overline{K}_B/6$ in our ensemble. Therefore, we have the standard MSSM gauge coupling unification,

$$g_3^2 = g_2^2 = \frac{5}{3}\, g_Y^2 = \frac{2}{\mathrm{vol}(\overline{K}_B)}\,, \tag{4.4.1}$$

which for our models is achieved at the compactification scale. While this scale as well as the actual values of the couplings will depend on the details of moduli stabilization, the relationship 4.4.1 is independent of Kähler moduli. It would be interesting to see if this relationship originates from an honest geometric realization of a GUT-structure. Given the known connection of our ensemble to a Pati–Salam $[SU(4) \times SU(2)^2]/\mathbb{Z}_2$ model [82, 40], we expect an underlying $SO(10)$.

Our results may provide phenomenological motivation for the study of new moduli stabilization scenarios. Specifically, though gauge coupling unification is automatic in our ensemble, it is natural to ask whether the correct value $\alpha_{\mathrm{GUT}} \simeq .03$ can be obtained in canonical moduli stabilization schemes. For instance, the KKLT and Large Volume scenarios assume that cycles are at sufficiently large volume to safely ignore string worldsheet

[4] Note that because $\overline{K}_B$ is not rigid, its deformation moduli give rise to non-chiral charged matter at the compactification scale. They have to stabilized suitably at low energies.

[5] The factor of 2 arises because in F-theory, the normalization dictated by geometry is one where the Cartan generators satisfy $\mathrm{tr}_{\mathrm{fund}}(T_i\, T_j) = C_{ij}$ with C the Cartan matrix. On the other hand, the particle physics convention necessary to determine the coupling is $\mathrm{tr}_{\mathrm{fund}}(T_i\, T_j) = \frac{\delta_{ij}}{2}$.

instanton corrections to the Kähler potential. This is essential because it is not known how to systematically compute and control all instanton contributions in $\mathcal{N} = 1$ backgrounds. A necessary condition for safely ignoring these corrections is to have $\text{vol}(C) > 1$ (in string units) for all curves $C \subset B_3$. This condition defines a stretched out subset of the Kähler cone [118], where it was also shown that the Kähler cones become increasingly narrow for increasing $h^{1,1}$. In effect, this forces toric divisors to be increasingly large in order to safely ignore worldsheet instantons, leading to smaller gauge couplings, because on toric B_3 the class $\overline{K}_B$ is the sum of all toric divisors. Brief calculations suggest that the correct α_{GUT} cannot be obtained in this controlled regime, in which case realistic models in our scenario are not consistent with the KKLT or Large Volume scenarios. Firmly concluding this requires a more detailed study, but we emphasize that it would not rule out our models, and instead motivate the study of new moduli stabilization scenarios that allow for the observed value of gauge couplings.

Our compactifications also exhibit D3-branes. These sectors generically give rise to $U(1)$ gauge theories that could be cosmologically relevant as dark photons. Each has its own open string moduli, the position of the D3-brane, which are massless at tree level but may be stabilized by non-perturbative effects due to their appearance in instanton prefactors [119]. However, since all but one of the toric divisors are rigid in the geometries we study, it is likely that there are many instanton corrections to the superpotential. Each instanton acts with an attractive force on the D3-brane, pulling it toward the associated divisor, but the existence of many such contributions would provide competing forces that stabilize the D3-brane away from each toric divisor. In particular, due to these competing effects we see a priori no reason that the D3-branes should be stabilized anywhere near the $SU(3)$ or $SU(2)$ 7-branes, in which case jointly charged matter in the form of 3-7 strings decouple from the spectrum. Such a scenario gives rise to numerous dark photon sectors that have cosmological effects only through kinetic mixing with the visible sector and with one another. It would be interesting to study these sectors further, in light of

current and future dark photon experiments.

We note that gravity cannot be decoupled in our ensemble since the Standard Model gauge divisors are in the anti-canonical class, yielding a non-trivial interplay between gravity and the visible sector. This interplay arises due to the details of our construction and could lead to other interesting interactions between particle physics and cosmology. At the level of toric geometry, the models of our ensemble differ from one another by how the facets are triangulated. This does not affect the structure of the anti-canonical divisors that realize $SU(3)$ and $SU(2)$, and thus the particle physics spectrum is insensitive to details of the triangulation; it is, after all, what gives rise to the large number of Standard Models in our construction. The triangulation is critical, however, for moduli stabilization. For instance, the classical Kähler potential on Kähler moduli is determined by triangulation-dependent topological intersections. This affects numerous aspects of the cosmology of these models, including inflation.

This visible sector universality in the midst of cosmological diversity might lead one to question the extent to which these should be counted as truly different models. Though a natural question, it has a clear answer: since the geometries are different they lead to distinct four-dimensional effective theories below the Kaluza–Klein scale, each of which could give rise to numerous metastable vacua. Instead, our view is that the universal structure in the visible sector provides some evidence for a long-held hope in the string landscape, that, despite large numbers of vacua, there could exist semi-universal features that lead to meaningful statistical predictions.

Part IV

Towards Complete Matter Spectra in 4d F-theory

Motivated by engineering vector-like (Higgs) pairs in the spectrum of 4d F-theory compactifications, we combine machine learning and algebraic geometry techniques to analyze line bundle cohomologies on families of holomorphic curves. To quantify jumps of these cohomologies, we first generate 1.8 million pairs of line bundles and curves embedded in dP_3, for which we compute the cohomologies. A white-box machine learning approach trained on this data provides intuition for jumps due to curve splittings, which we use to construct additional vector-like Higgs-pairs in an F-Theory toy model. We also find that, in order to explain quantitatively the full dataset, further tools from algebraic geometry, in particular Brill–Noether theory, are required. Using these ingredients, we introduce a diagrammatic way to express cohomology jumps across the parameter space of each family of matter curves, which reflects a stratification of the F-theory complex structure moduli space in terms of the vector-like spectrum. Furthermore, these insights provide an algorithmically efficient way to estimate the possible cohomology dimensions across the entire parameter space.

5.1 Introduction

The spectrum of light chiral particles is a defining feature of any four dimensional quantum field theory. Their precise number affects aspects such as the moduli space of vacua, or the behavior of the theory under RG flow. Moreover, they are also of paramount importance to phenomenology, in particular when it comes to models of beyond-the-Standard-Model physics. Therefore, to be able to draw formal and phenomenological lessons from string theory about 4d field theories, one needs efficient methods to compute the spectrum in compactification scenarios.

From an effective field theory perspective, the chiral excess $\chi(\mathbf{R})$ — the difference between chiral and anti-chiral modes of the same matter representation $\mathbf{R}$ — is a discrete parameter, whereas the individual number of light (anti-)chiral modes depend on contin-

uous mass parameters. In string theory, this is reflected by the fact that $\chi(\mathbf{R})$ is typically a topologically protected quantity, whereas the (perturbative) mass parameters[1] are captured by continuous deformations, or *moduli*, which for certain values can lead to a pair of chiral and anti-chiral modes — a *vector-like pair* — to become massless.

In many string compactification scenarios, we know in principle what the relevant computations are: massless fields are zero modes of some differential operators on the internal space, and therefore counted by appropriate sheaf cohomologies. However, oftentimes these computations are so complicated that in practice, they can only be carried out explicitly for toy models, or for specialized values of the deformation parameters. On the other hand, an exact understanding of how the cohomologies depend on these parameters is necessary for a complete description of the physical interpretation. The moduli dependence and the possibility of jumps in the massless spectrum have been first discussed in the context of heterotic string theory in [120, 121, 122, 123, 110, 124]. More recently, the complex structure moduli dependence of the cohomology dimensions has been studied in [125, 126] and [127] in the context of instanton and perturbative superpotential terms, respectively.

In comparison, an analogous analysis in the context of F-theory compactifications [27] is largely missing and has only been discussed in part in [128]. The main reason is because, unlike the chiral spectrum which is accessible via intersection theory [59, 129, 130, 131, 43, 37, 132, 38, 39, 40, 41, 42, 44, 32], the vector-like spectrum in F-theory depends on a gauge background, which is encoded in mathematically rather intricate objects such as the intermediate Jacobian and Deligne cohomology [133, 134, 135, 136]. Recent progress [45, 46] has made the spectrum computationally more accessible. Namely, for a four-dimensional $\mathcal{N} = 1$ F-theory compactifications on an elliptically fibered Calabi–Yau fourfold $\pi : Y_4 \to B_3$ with a given gauge background, the massless spectrum of chiral particles in representation $\mathbf{R}$ can be counted by certain line bundle cohomologies

[1] In this work we will neglect moduli stabilization, flux-induced superpotentials and non-perturbative effects.

$h^i(C_{\mathbf{R}}, \mathcal{L}_{\mathbf{R}}), i = 0, 1$ on complex curves $C_{\mathbf{R}} \subset B_3$ — the matter curves — in the base. Given a compact model with a fixed gauge background, $C_{\mathbf{R}}$ and $\mathcal{L}_{\mathbf{R}}$ are specified by global data in terms of polynomials on B_3 , whose coefficients are (parts of) the complex structure parameters of Y_4. In this case, one can model the line bundle as a coherent sheaf on B_3, whose cohomology computation can be systematized in a computer algebra system [47]. While this algorithm can be applied to a broad class of global F-theory models, the calculations for almost all phenomenologically interesting examples overburden even super-computers specifically designed for such tasks. The reason is that here, and in fact in many cohomology computations using commutative algebra or computational algebraic geometry, we need to compute Groebner Bases, whose computational complexity scales extremely poorly.

The introduction of ideas from *Big Data* and *machine learning* (ML) to string phenomenology [137, 138, 139, 140] provides new perspectives; see [141] for an introduction and comprehensive overview. One advantage that a trained algorithm provides is that it recognizes more subtle patterns without the need of a complete, "microscopic" understanding of the task. In particular, recent studies suggest that supervised learning can be used to predict line bundle cohomologies in string compactifications [139, 142, 143]. One may be tempted to apply these techniques, which are mostly motivated by heterotic compactifications, directly to the F-theory. However, there is a significant difference in the way the line bundle data are specified in global heterotic vs. F-theory models. In heterotic examples, the line bundles are typically given in a "canonical" way, namely as an element of the Picard group $\mathrm{Pic}(X)$ of the underlying manifold X. This was used, e.g., in [144, 145] to derive formulae for line bundle cohomologies in terms of topological indices.

However, in the F-theory setting, there is no straightforward fashion to extract even the structure of the Picard group of $C_{\mathbf{R}}$, given its polynomial description. Likewise, because the same data specifies $\mathcal{L}_{\mathbf{R}}$ essentially as a sum of points p_i on B_3 that also lie on $C_{\mathbf{R}}$,

it is by no means obvious if, say, $p_1 - p_2$ is trivial or not on $C_{\mathbf{R}}$. What makes the situation particularly challenging is that, by varying the complex structure parameters, the structure of $\mathrm{Pic}(C_{\mathbf{R}})$ as well as the points specifying $\mathcal{L}_{\mathbf{R}}$ will change. Together with the fact that we simply do not have a large data set of non-trivial F-theory examples, it is a priori unclear whether we could train an algorithm that reliably predicts the cohomologies for realistic models with arbitrary complex parameters.

Instead, we will use machine learning techniques on less complex examples to gain some intuition for circumstances under which line bundle cohomologies *jump*. Physically, this is already interesting as such a jump can engineer one or possibly more massless vector-like pairs in situations where one generically expects none. Even if the trained algorithm does not perform perfectly, understanding its strategy can provide a guiding principle for the behavior of the vector-like spectrum in non-trivial examples. For this reason, we focus on white-box machine learning techniques, in particular on decision trees.

To fully understand the results of the machine learning, we further employ "formal" techniques from algebraic geometry, in the form of *Brill–Noether theory*. This allows to identify "microscopically" the sources for jumps in cohomology, either from the curve $C_{\mathbf{R}}$ or the line bundle $\mathcal{L}_{\mathbf{R}}$ becoming non-generic. With these insights, we provide an algorithmic way to estimate the admissible numbers of vector-like pairs over the entire parameter space of a matter curve in a global F-theory model with given gauge background. Furthermore, our analysis also reveals a convenient diagrammatic way to encode the *stratification* on the parameter space induced by the number of vector-like pairs. We believe that this is progress towards understanding the full complex structure dependence of the vector-like spectrum in global F-theory models.

The paper is organized as follows. In 5.2 we discuss our machine learning approach. Using the exact methods implemented in [146], we generate a database [147] of cohomologies of pullback line bundles on hypersurface curves in dP_3. Interpreting these results with decision trees, we find that curve splittings typically lead to jumps in the vector-like

spectrum. In 5.3, we demonstrate that such curve splittings provide a practial way to engineer jumps in a global F-theory GUT-model. To investigate the origin of these jumps, we turn in 5.4 to algebraic and analytic techniques. We find a unified perspective on jumps due to curve splittings and non-generic line bundles described by Brill–Noether theory, and introduce a diagrammatic way to illustrate the natural stratification of the complex structure parameter space in terms of the vector-like spectrum. In 5.5, we present a refined analysis of jumps due to curve splittings. This rests on a procedure to count the global sections by gluing "local contributions" along intersections of curve components, which leads to two interesting results: First, we are able to formulate sufficient conditions for jumps of vector-like spectra. Second, we can propose an algorithmic h^0 estimate, which relies mostly on topological data, and hence provides a quick, approximative scan of the vector-like spectrum over the entire parameter space of a matter curve. In contrast to currently existing exact methods, such as [146], our implementation [148] has a much lower demand of computational resources and run times.

5.2 Machine learning

5.2.1 Introduction to Decision Trees

We are interested in tuning complex structure moduli to engineer jumps in the dimensions of sheaf cohomologies over complex curves. It is a priori not clear how to efficiently identify these subloci in complex structure moduli space. In order to state (at least) necessary conditions for jumps to occur, we address the problem using ML. Since we are interested in interpreting the results of the ML algorithm, we resort to white-box models, in particular to binary decision trees.

In more detail, we use binary decision trees as classifiers in supervised machine learning, following the notation and conventions of [141]. Supervised learning means that we have a set of inputs x_i^μ (called features) together with associated labels[2] y_i, where $i = 1, \ldots, N$

[2]In general, there could be more than one label for each feature vector; however, for the cases studied in this paper, the label corresponds to a class the input belongs to, labeled by an integer.

counts the feature-label-pairs, and $\mu = 1, \ldots, F$ counts the F features of each input. This set of feature-label combinations is now divided into a train set and a test set (typically around 90 percent of the pairs are assigned to the train set and 10 percent to the test set). Using the train set, an algorithm is trained to learn a map from the features to the labels. The training consists of adjusting parameters of the algorithm to optimize the map. This is typically done by minimizing the loss, which is a measure for how well the algorithm reproduces the labels. Once training ends, the algorithm is tested on the test set. This is necessary in order to see how well it performs on (hitherto unseen) data. If the test set have been chosen generically enough, performance on the test set will serve as an indicator for how well the trained algorithm will perform.

After this general discussion, let us describe these steps in the context of binary decision trees. Trees are data structures that appear abundantly in computer science. They can be thought of as acyclic, directed, connected graphs with a unique root vertex (in trees, vertices are called nodes). In binary trees, each node has either zero or exactly two vertices, each of which is connected to a unique node. These two subnodes are called child nodes, and the original node is called parent node. A node with no children is called a leaf node.

A decision tree expects numerical features $x_i^{(0)}$. It then introduces boolean splitting criteria of the type $x_i^{(0)} \leq \kappa_i$ for some constant $\kappa_i \in \mathbb{R}$. All data that satisfy this criterion are assigned to one child node, while data that does not satisfy the criterion is assigned to the other child node. The tree is now built recursively by splitting each child node according to some other feature $x_j^{(0)} \leq \kappa_j$, etc. This procedure segments feature space (which is in our case $\mathbb{R}^N$) along hyperplanes $x_i = \kappa_i$ with the goal to find regions such that all inputs in that region belong to the same class.

At each node, it is checked how many of the data carry which label. For single membership classification problems, which is what we will be using, the labels are just the different classes which the input feature vector belongs to. A typical loss function is the Gini

impurity of a node, which measures how "impure" the data at that node actually is, i.e., how many features with different classes are in the region in feature space corresponding to this node. Denoting the set of features in the region of node a by N_a, we find for K classes the fraction of elements that belong to a class $y_k \in K$ via

$$p_{a,k} = \frac{1}{|N_a|} \sum_{i \in N_a} \delta_{i,k} \,. \tag{5.2.1}$$

The Gini impurity G_a at node a can then be written as

$$G_a = \sum_{k=1}^{K} p_{a,k}(1 - p_{a,k}) \,. \tag{5.2.2}$$

In particular, if all elements of N_a belong to the same class, $G_a = 0$. In such a case, the node is turned into a leaf, since no further splits are necessary.

The decision tree is now trained by starting from the root node and trying to split by any of the F features. For κ_i, one tries all[3] intermediate values between consecutive values of feature i. The solution that leads to the lowest Gini impurity at the child nodes is accepted, and the procedure is repeated for the two child nodes and the remaining features, etc.

In cases where the map from the input to the labels is not one-to-many, one can eventually reach a perfect classification, if need be with a single element in each region. Typically, this is undesired and hence one stops splitting a node if there are less than some fixed number of elements in its corresponding region. Turning this around, if the minimal number at which a node is split is set to 2, and if the tree does not find a solution where all leaves have Gini impurity zero, this means that the map defined by the input-label-pairs is many-to-one, i.e., even all features combined are not sufficient to distinguish between the class labels.

[3] In case of many different values for a feature, this might be unfeasible, in which case a number of equally spaced values are tried for κ_i.

5.2.2 Divisors and line bundles on dP_3

While in the general F-theoretic setup, matters curves $C_{\mathbf{R}}$ are a priori defined on a threefold $\mathcal{B}_3$, in most models there is a distinguished surface $S \subset \mathcal{B}_3$ that is wrapped by the 7-branes supporting a non-abelian gauge theory, in which the matter curve sits. A part of the complex structure moduli then parametrizes deformations of the curve inside S, which will in general affect the vector-like spectrum. These deformations can be described by pulling back all defining polynomials on $\mathcal{B}_3$ onto S, and then simply consider the coefficients of these in terms of the homogeneous coordinates on S.

For our data collection, we will mimic such a "pulled back" description by focusing on curves embedded inside the del Pezzo surface dP_3. One advantage of this choice is that dP_3 has a toric description in terms of a reflexive polygon, which simplifies many computations. Another one is that it fits the setup for section 5.3, where we consider an F-theory toy model with non-abelian gauge degrees of freedom localized precisely on a dP_3 surface.

To set the notation, we denote the toric coordinates of dP_3 by $x_i, i = 1, ..., 6$. They are graded by homogeneous scalings with associated divisor classes, which are summarized in the following table:

	x_1	x_2	x_3	x_4	x_5	x_6
H	1			1	1	
E_1	-1	1		-1		
E_2	-1		1		-1	
E_3				-1	-1	1

(5.2.3)

The columns give the divisor classes of the coordinate's vanishing loci. E.g., $[\{x_1\}] = H - E_1 - E_2$. The Stanley–Reisner ideal is

$$I_{\text{SR}} = \langle x_3x_6, x_2x_6, x_1x_6, x_4x_5, x_2x_5, x_1x_5, x_3x_4, x_1x_4, x_2x_3 \rangle \,, \tag{5.2.4}$$

and the anti-canonical class is $-K_{dP_3} = \sum_i [\{x_i\}] = 3H - E_1 - E_2 - E_3$. The independent intersection numbers are

$$H^2 = 1\,, \quad E_i \cdot E_j = -\delta_{ij}\,, \quad H \cdot E_i = 0\,. \tag{5.2.5}$$

In order to simplify the notation, we introduce the short-hand notation $(a; b, c, d)$ with $a, b, c, d \in \mathbb{Z}$ for a divisor $D = aH + bE_1 + cE_2 + dE_3$.

We then define curves C inside dP_3 via $C = \{P = 0\} \equiv V(P)$ with

$$P = \sum_i c_i m_i(x_1, \ldots, x_6)\,, \tag{5.2.6}$$

where m_is are monomials of appropriate multi-degree under the grading in 5.2.3. Importantly, the coefficients c_i parametrize the shape of the curve and thus model (parts of) the complex structure parameters of a global F-theory compactification. The (arithmetic) genus of the curve depends only on the divisor class $[C]$ of the curve (equivalently, the multi-degree of the monomials in P) and is given via adjunction formula as

$$g = 1 + \frac{1}{2}[C] \cdot ([C] + K)\,. \tag{5.2.7}$$

Next, we also need to specify a line bundle $\mathcal{L}$ on C. Again, instead of focusing on the most general setup, where $\mathcal{L}$ is directly specified by a set of points on C, we consider the slightly simpler cases where $\mathcal{L}$ is a pullback of a line bundle $L = \mathcal{O}_{dP_3}(D)$ on dP_3:

$$\mathcal{L} = \mathcal{O}_{dP_3}(D)|_{dP_3}\,. \tag{5.2.8}$$

One can think of the points then as the (weighted) intersections $\{a_i\, p_i\}$ between C and a generic representative in the class D. Note that in this case, another representative of D, intersecting C at $\{b_j\, p'_j\}$, necessarily must give the same divisor on C, i.e., $\{a_i\, p_i\} \sim \{b_j\, p'_j\}$ are linearly equivalent on C. However, in general we cannot say anything about linear

equivalences among any two of the points. Therefore, we expect, and also will find, that even for pullback line bundles, there can be special divisor alignments, i.e., p_1 and p_2, say, move into special positions, when we deform C, thus leading to jumps in the cohomology.

5.2.3 Generating the data set

We generate training data by picking 6 different curve classes $[C]$ with genus $1 \leq g \leq 6$. For each class we consider several line bundles L on dP_3 and compute (using techniques from [47]) the cohomologies $h^i(C(\mathbf{c}), L|_{C(\mathbf{c})})$, where we vary the curve $C(\mathbf{c})$ by considering all possible combinations of $c_i \in \{0, 1\}, i = 1, \ldots, d$ for the coefficients.[4] This way, we calculate cohomologies of L pulled back to $2^d - 1$ genus g curves in the class $[C]$. While this seems to be a very limited choice, it nevertheless reveals enough structures to correlate jumps in cohomology with degenerations of the geometry. On the other hand, it also introduces some bias in the data. For example, a common way the curve degenerates is if all monomials in the defining polynomial share a common variable; this happens frequently if many c_i are set to 0. However, for certain polynomials, restricting $c_i \in \{0, 1\}$ misses out possible factorizations, where factors are not just a single variable. We will see later that we can easily generalize the interpretation based on our data with algebraic methods to these cases as well.

For this data set, we then compute/collect the following features for each choice of line bundle L on each curve C with coefficients c_i:

1. The coefficients c_i that define the curve.

2. The genus of the curve.

3. The number of global sections of the line bundle.[5]

4. Are the curves smooth?

[4] We exclude the case where all $c_i = 0$.

[5] The dimension of $H^1(C, L)$ can then be computed from the index which is topological and does not depend on c_i.

5. The number of components the curve splits into.

6. Are the splits smooth?

7. Are the splits reduced?

8. The genera of the split components.

9. The intersection numbers among the split components.

Note that all of this data is numerical (the true/false features are encoded as 1/0). We aggregate the features above into a single feature called the *split type*. We want to consider two curves as identical if their features F4-F9 are identical (up to relabeling the individual components). In order to check this, we would in principle have to check all permutations of all split components and see whether any of them have the same data. Since this becomes prohibitively expensive, we perform the following necessary checks:

- Are the data F4 and F5 identical for the two curves?
- Are the data F6-F8 identical as sets for the two curves? This can be checked by ordering the tuples and comparing them, which is much faster than checking actual permutations.
- Is the determinant of the intersection matrix in F9 identical for the two curves? Note that the determinant is permutation invariant. However, at that point we do not check whether the permutations that make all sets match are actually the same.

Curves which are identical under these checks are assigned the same integer that encodes the split type.

Equipped with this data, we generate four different data sets which we use to train the decision trees and compare the results. In the first, we use the coefficients c_i as features and assign a label of 0 if the cohomology dimension of $H^0(C(\mathbf{c}), \mathcal{L})$ has the generic (i.e.,

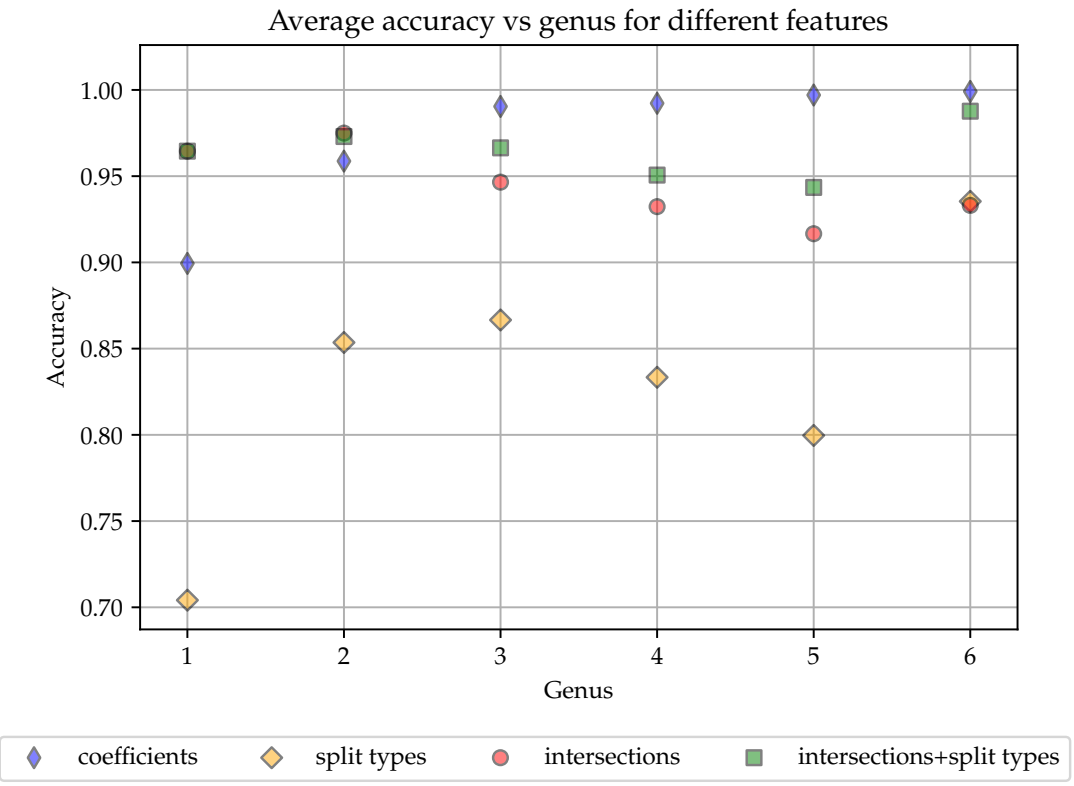

Figure 6: Average accuracy on the test set as a function of the genera of the curves for different features.

the lowest) value and a label of 1 if there is a jump. Note that at this point, we only classify the curve according to whether a jump occurs, but not according to how large the jump is. For the second data set, we use the same labels, while the features are taken to be the topological intersection numbers between the curve components and the line bundle divisors. For the third data set we use the split type as explained above. Finally, for the fourth data set, we use both the split type and the topological intersection numbers between the curve components and the line bundle divisor as features. In addition, we perform a train:test split of 90:10 for all four data sets.

5.2.4 Decision Trees to learn cohomology jumps

Training the decision trees only takes a few seconds on a modern desktop computer. We train a separate decision tree for each line bundle and each of the four data sets. It is instructive to compare the performance of all four training sets on both the train and the test set.

The results for the accuracy of the trained trees on the test set are summarized in Figure 6. One notices that the accuracy of all data sets improves with the genus of the curve. This is due to the fact that the size of the data set grows with the genus: While the genus 0 curve we are considering has only 7 coefficients c_i and hence only $2^7 - 1 = 128$ data points per line bundle, the genus 6 curve has $2^{18} - 1 = 262143$ data points.

For the blue data points, which uses the coefficients c_i as labels, we find that the decision tree performs best. This is to be expected, since these are the finest feature set, i.e., the one with the most information, out of the four feature sets we studied. Indeed, the trees reach an accuracy of essentially 1 as soon as the training set becomes large enough (there are 3685 points in the training set for genus 3). For the other three data sets, we see that they perform worse, but still reaches high accuracies. Using just the split type as a feature, for the larger genus cases where enough data is available, we reach accuracies around 80 to 85 percent. Using the intersection numbers, accuracies around 94 percent are obtained. Lastly, combining the split type and the intersection numbers, improves the results obtained when either is used individually, to an accuracy of around 97 percent. This means that the two features contain different types of information which the three can use in order to improve its prediction when given access to both.

One can learn more information about the data by also analyzing the performance on the training set, as explained in Section 5.2.1. Indeed, we find that, when not imposing constraints on the tree, the accuracy on the train set when using the coefficients as features is always 100 percent. This is not surprising, since the coefficients uniquely identify each

case and hence the tree can learn a sequence of splits that puts each data point in the correct leaf node (if necessary, this leaf might only contain this single data point). For the other data sets, we find that the performance on the test set is already below 100 percent. Hence, the features are not enough to decide whether a jump in cohomology occurs, not even in principle.

Let us illustrate this by looking at the decision tree trained on the full data set for a genus three curve $D_C = (4; -1, -1, -1)$ inside dP_3 with line bundle $D_L = (1, 2, -2, -1)$, cf. Section B.2.1. We give the full decision tree in Figure 7. Looking at the root node, we see that for this bundle, there are 4095 different data points ("samples"). Out of these, 1791 exhibit a cohomology jump for this line bundle, while 2304 do not. The tree assigns a class label to this (non-leaf) node based on the majority, which is "no jump". However, there are almost as many data points with a jump as there are data points without, which is why the uncertainty is high. This is encoded in the light blue color: the more certain a node predicts no jump, the darker blue it is colored. Similarly, the more certain there is a jump, the darker orange it is.

Recall that integers labelling the split type (based on the features F4-F9) are by construction small if the number of components the curve splits into is small. Hence, small split types correspond to irreducible curves, or curves with only few split components. We expect such curves being close to generic (in a sense that will be made mathematically more precise in Section 5.4), hence the cohomologies should also take generic values.

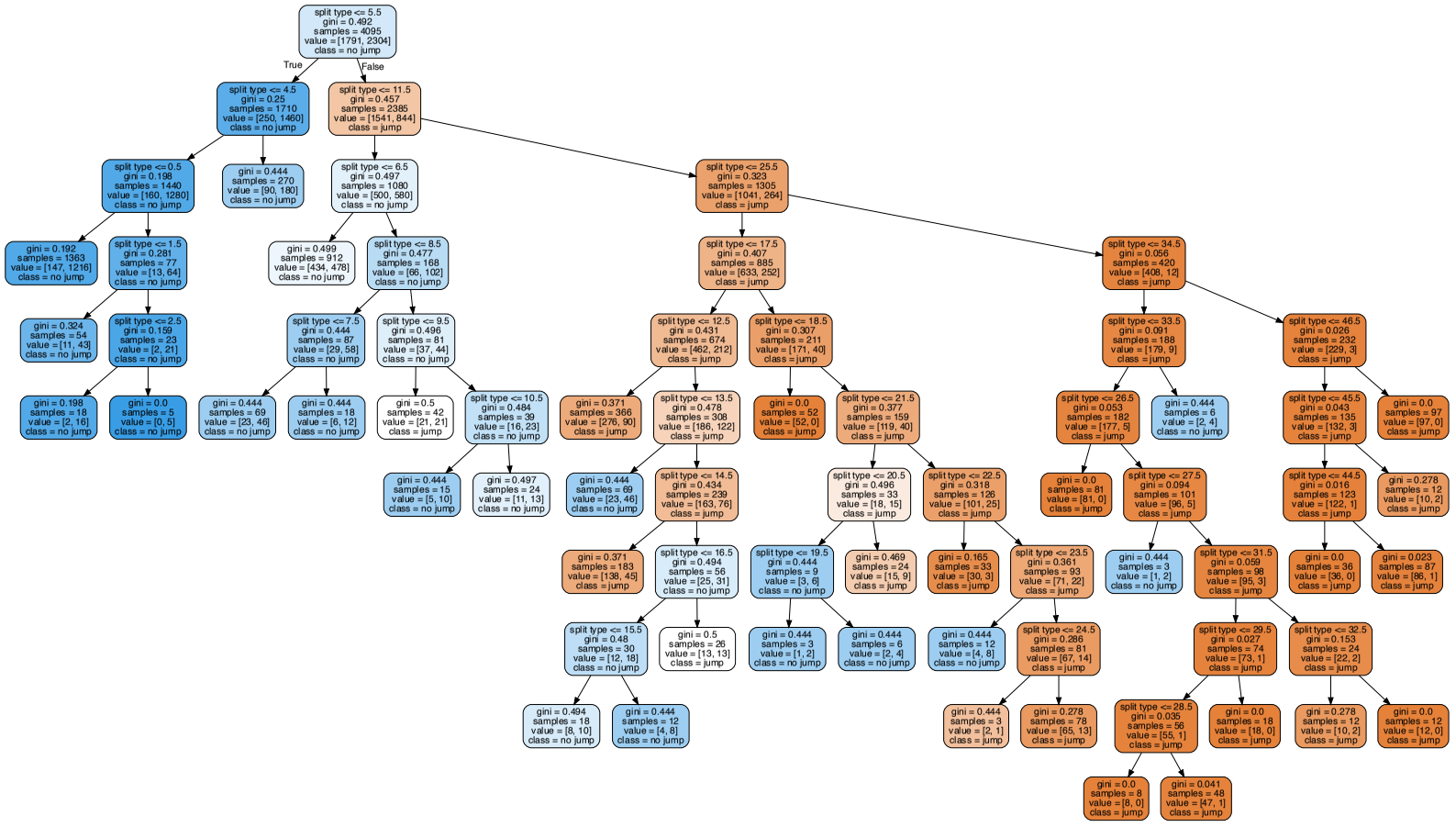

Figure 7: Trained decision tree that classifies the presence of cohomology jumps based on split types for the genus three curve example.

Indeed, we observe that the first split is performed according to whether or not the split type is smaller than 5.5. This first split already gives a good indicator in the sense that out of the 1710 training data points that have a split type of 5 or smaller, 85 percent actually do not have a jump in their cohomologies. This also illustrates that decision trees can be used for feature selection: important features that are good indicators for the classes tend to be used for splitting higher up in the tree, while more unimportant features are used further down the tree (or not at all, if they do not have any predictive power for the class membership). Now, in our case, we only have a single feature, but it is a composite feature of several quantities. The fact that the first split does not occur around the median (which would be 27) but at much smaller value indicates that the number of split components is a good criterion to distinguish jumps.

While the split types are integers, the tree always chooses half-integer decision boundaries. The reason is that the tree does not know that the feature only takes integer values. Hence, splitting in the middle between the feature values that appear in the train set will allow the most slack in either direction when the tree is presented with unseen data.

By focusing on the leaf nodes, we can also see that the tree is not classifying the data perfectly, not even the training data. Indeed, many nodes have a non-zero Gini impurity, i.e., both curves with and without jumps share the same split type associated with this leaf node. Looking for example at the bottom right leaf node, we see that three curves have the same split type (with value 48). However, two of these have a jump while one does not. This means that the topological data F4-F9 used to construct the split type is not enough to decide whether or not a cohomology jump occurs.

5.2.5 Interpretation of results

Jumps from curve splittings

We have seen that the decision tree trained on a combination of split types and intersection numbers performs very well. Moreover, the tree trained with just the split types splits

on small split types first. This suggests that there is a tight correlation between changes in the topology of the curve and jumps in the line bundle cohomology. In particular, the data set has an abundance of cases with jumps where the curve C splits off one or more rigid components: For 78 (about 95%) of the 82 pairs of geometries D_C and line bundles D_L considered in our database, we find that we can split off a rigid component E, i.e., $C \to \tilde{C} \cup E$, such that

$$h^0_{\min}(\tilde{C} \cup E, L|_{\tilde{C}\cup E}) > h^0_{\min}(C, L|_C)\,. \tag{5.2.9}$$

Put differently, for almost all pairs (D_C, D_L) in our database, there exists a rigid divisor such that splitting off this rigid divisor from the curve C leads to a jump in the number of global sections on that curve. At the same time, for a given combination (D_C, D_L), we observe a jump of $h^0_{\min}$ only for a subset of all possible splits $C \to \tilde{C} \cup E$, suggesting that E and D_L must have some correlation in order for the cohomology to enhance. We list the details of these splittings and jumps in B.2.1.

It is obvious that the jumps stemming from rigid component splittings can be associated with the curve C becoming non-generic. While per se not unexpected, the machine learning process reveals — without explicitly "knowing" algebraic geometry — these features.

It is important in this context to address the bias in the data coming from considering only values of $\{0, 1\}$ for the coefficients. Namely, within the data, we only observe jumps associated with splittings of rigid components. Naively, one might conclude that rigidity of a split component is a necessary condition. However, as we already stressed in the beginning of 5.2.3, setting enough coefficients to 0 usually factors out one of the homogeneous coordinates x_i. The corresponding curve splitting then always involves the toric divisor $V(x_i)$ which on a dP_3 is rigid for any $i = 1, ..., 6$. Therefore, the strong correlation between a rigid component and a jump is likely due to the bias in the data.

Indeed, we will find in sections 5.4 and 5.5 with insights from algebraic geometry, that

the main source for cohomology jumps in cases of curve splittings is actually insensitive to components being rigid. We will also supplement a concrete example in 5.4.1 where we find a jump from non-rigid curve splittings. Furthermore, we will combine these arguments with the intuition about curve splittings we gained through the data to phrase a sufficient condition for a jump in cohomology to occur in terms of topological data only. We will discuss this idea in 5.5.

Unpredicted jumps

The fact that the decision tree cannot predict all jumps hints towards sources for additional sections (and hence cohomology jumps) beyond curve splitting. Within the data set, we observe that in rare occasions, the curve remains smooth despite a deformation which induces a jump.

For illustration purposes, consider again the genus three curve with the line bundle discussed above. Generically, this genus 3 curve is cut out by the polynomial

$$\begin{aligned} P(\mathbf{c}) = {} & c_1 x_1^3 x_2^3 x_3^2 x_4 + c_2 x_1^2 x_2^3 x_3 x_4^2 x_6 + c_3 x_1 x_2^3 x_4^3 x_6^2 + c_4 x_1^3 x_2^2 x_3^3 x_5 + c_5 x_1^2 x_2^2 x_3^2 x_4 x_5 x_6 \\ & + c_6 x_1 x_2^2 x_3 x_4^2 x_5 x_6^2 + c_7 x_2^2 x_4^3 x_5 x_6^3 + c_8 x_1^2 x_2 x_3^3 x_5^2 x_6 + c_9 x_1 x_2 x_3^2 x_4 x_5^2 x_6^2 \\ & + c_{10} x_2 x_3 x_4^2 x_5^2 x_6^3 + c_{11} x_1 x_3^3 x_5^3 x_6^2 + c_{12} x_3^2 x_4 x_5^3 x_6^3 \,. \end{aligned} \tag{5.2.10}$$

The pullback of $\mathcal{O}_{dP_3}(D_L)$ onto C defines a line bundle $\mathcal{L}$ of degree $d = 3$. By Riemann–Roch we have $\chi(\mathcal{L}) = h^0 - h^1 = 1$.

In our database, we have computed the number of global sections for this line bundle for coefficient choices $\mathbf{c} \in \{0,1\}^{12} - \mathbf{0}$. For these 4095 curves, we find

- $h^0 = 1$: 2304 (56.3%) ,
- $h^0 = 2$: 1664 (40.6%) ,
- $h^0 = 3$: 127 (3.1%) .

Our database indicates that a jump to $h^0 = 3$ occurs whenever $c_1 = c_2 = c_3 = c_{11} = c_{12} = 0$. This corresponds to a splitting

$$C = V(x_2) \cup V(x_5) \cup V(P|_{c_1=c_2=c_3=c_{11}=c_{12}=0}) \,. \tag{5.2.11}$$

The majority of the cases with $h^0 = 2$ are where either $V(x_2)$ or $V(x_5)$ splits off, each being a rigid $\mathbb{P}^1$. This is in line with the above observation. However, we also have instances (about 9% of all curves with $h^0 = 2$) where the curve remains smooth and irreducible. Despite having $h^0 = 2$, the split type features cannot distinguish these cases from the generic setup with $h^0 = 1$, thus leading to an imperfect performance of the decision tree.

While we will come back to a detailed discussion of this phenomenon and the associated algebraic description in terms of Brill–Noether theory in 5.4.2, it is evident that these cases of jumps are associated to the line bundle $\mathcal{L}$ on C becoming non-generic. Moreover, we also observe that such Brill–Noether-type jumps can sometimes produce values of h^0 that cannot be obtained by splittings off rigid curve components. This becomes particularly important in F-theory models, as we will discuss now.

5.3 Application: F-theory model building

In the previous section, we have used machine learning techniques to gain some intuition on how line bundle cohomologies jump under complex structure deformations. While we will discuss the underlying "precise" description of these various sources of jumps in the next section, we would like to show that these "rules of thumb" inferred from the withe-box machine learning results can be applied directly in string phenomenology. To this end, we consider an F-theory toy model and exemplify how curve splittings help "controlling" the number of vector-like pairs.[6]

[6]For the purpose of this work, and in particular this section, we will only focus on the matter curves and their embeddings into the "GUT"-surface that supports the non-abelian gauge symmetry. We refer the interested reader to recent reviews [26, 149] for detailed introduction to F-theory.

Let us first summarize the relevant features of the model, whose explicit construction is detailed in [47]. The model has an $SU(5)$ gauge symmetry localized on a dP_3 surface inside the compact base threefold $\mathcal{B}_3$, which itself is a smooth hypersurface inside a toric variety. There are matter states in the representations $\mathbf{10}_1$, $\mathbf{5}_3$ and $\mathbf{5}_{-2}$, where the subscript denote the charges under an additional $U(1)$ gauge symmetry. Each representation $\mathbf{R}$ resides on a curve $C_{\mathbf{R}}$ inside the dP_3 surface. One can find a globally consistent vertical G_4-flux configuration that induces the chiral spectrum

$$\chi(\mathbf{10}_1) = 3\,, \quad \chi(\mathbf{5}_3) = 15\,, \quad \chi(\mathbf{5}_{-2}) = -18\,. \tag{5.3.1}$$

In the following, we will analyze in detail the vector-like spectrum in this setup.

Geometry of curves

In the global geometry, the matter curves $C_{\mathbf{R}}$ are complete intersections involving the dP_3 surface and another divisor on the base $\mathcal{B}_3$. As discussed in [47], a generic choice of the complex structure parameters for the elliptic fourfold also induces a generic curve $C_{\mathbf{R}}$ on dP_3. In other words, we can parametrize them in terms of global sections of $\mathcal{O}_{dP_3}([C_{\mathbf{R}}])$, where $[C_{\mathbf{R}}]$ denotes the divisor class of the curve inside dP_3.

Furthermore, the data defining the zero mode spectrum in a global F-theory model can be extracted from the G_4-configuration and packaged into a line bundle (or, more generally, a coherent sheaf) for each curve $C_{\mathbf{R}}$ [45, 46]. For the case at hand, the flux inducing the chiral spectrum 5.3.1 induces line bundles which are pullbacks of various bundles on dP_3 to the curves [47].

Using the same notation as in the previous section[7], the curves with their genus and their

[7] Divisor classes $aH + bE_1 + cE_2 + dE_3$ are denoted by $(a; b, c, d)$.

corresponding zero-modes counting bundles are:

curve	class	genus	bundle	h^i
$C_{\mathbf{10}_1}$	$(4;-1,-1,-2)$	2	$\mathcal{O}_{dP_3}(1;-1,-1,1)$	$(3,0)$
$C_{\mathbf{5}_3}$	$(10;-3,-3,-4)$	24	$\mathcal{O}_{dP_3}(5;-4,-4,3)$	$(15+n,n)$
$C_{\mathbf{5}_{-2}}$	$(17;-5,-5,-7)$	79	$\mathcal{O}_{dP_3}(6;0,0,-6)$	$(7,25)$

(5.3.2)

Note that the cohomologies on $C_{\mathbf{10}_1}$ and $C_{\mathbf{5}_{-2}}$ are fixed by the exactness of the corresponding Koszul resolutions, and hence there are no complex-structure-dependent jumps possible.[8] For the representation $\mathbf{5}_3$, no such arguments apply, and thus we expect the number n of light vector-like pairs to vary.

The curve $C_{\mathbf{5}_3} = \{a_{3,2} = 0\}$ is the vanishing locus of a polynomial with class (10; -3, -3, -4), whose explicit expression in the parametrization of the toric dP_3 coordinates x_i are given in appendix B.1, cf. B.1.60. With the curve having genus 24, it would be almost impossible to perform a scan by varying all the complex structure parameters (B.1.60 has 44 coefficients), as we did previously for the low genus cases. However, the intuition we gained from the low genus examples will help us to "control" n — that is, to efficiently find suitable geometries realizing the desired vector-like spectrum.

5.3.1 Engineering jumps in cohomology

What we have learned from the machine learning results is that the line bundle cohomology is more likely to jump if the curve in question is reducible. Though we have already emphasized that rigidity of the components is not necessary, the abundance of toric coordinates makes it handy to factor out various different curves which in this case happen to be rigid. For the purpose of finding *a* concrete realization of a particular jump in the vector-like spectrum, these rigid factors turn out to be sufficient.

[8] This can change if we modify the flux by, e.g., horizontal pieces. However, for the purpose of this work, we focus on jumps induced by geometric changes.

We thus modify the coefficients of the defining polynomial $a_{3,2}$ in B.1.60 such that individual toric coordinates x_i of dP_3 factor out. Of course, not every such factorization will lead to a jump: the rigid component must in some way receive a "non-trivial contribution", i.e., intersection, from the divisor D_L defining the line bundle. The intuitions we gained from the previous section is that a *negative* intersection of D_L with $V(x_i)$ will lead to a jump. It is then intuitive to assume that the more rigid components splits off, the higher the jumps tend to be. With this intuition, we now proceed to engineer step-wise jumps of the vector-like spectrum.

Using the linear relations 5.2.3 and intersection numbers 5.2.5, we easily verify the divisor defining the line bundle, $D_L = 5H - 4E_1 - 4E_2 + 3E_3$, has only negative intersections with $[x_1]$ and $[x_6]$. Inspecting B.1.60, one finds that if we set

$$c_{40} = c_{41} = c_{42} = c_{43} = c_{44} = 0\,, \tag{5.3.3}$$

the polynomial factors as $a_{3,2} = x_6\, R_2$, where R_2 is an irreducible polynomial in the class $(10; -3, -3, -5)$. And indeed, a computer-assisted computation with methods from [47] reveals that for this curve $C_2 = \{x_6\, R_2 = 0\}$, we have

$$h^i(C_2, \mathcal{O}_{dP_3}(5; -4, -4, 3)|_{C_2}) = (17, 2)\,, \tag{5.3.4}$$

We can factor out another factor x_6 from R_2 by setting

$$c_{34} = c_{35} = c_{36} = c_{37} = c_{38} = c_{39} = c_{40} = c_{41} = c_{42} = c_{43} = c_{44} = 0\,, \tag{5.3.5}$$

yielding $C_{\mathbf{5}_3} \to C_3 = \{x_6^2\, R_3 = 0\}$, with R_3 an irreducible polynomial of class (10; -3, -3, -6). In this case, we find a jump by three,

$$h^i(C_3, \mathcal{O}_{dP_3}((5; -4, -4, 3)|_{C_3}) = (18, 3)\,. \tag{5.3.6}$$

To achieve a jump by four, we factorize $C_{\mathbf{5}_3} \to C_4 = \{x_1\, x_6\, R_4 = 0\}$, with $[R_4] = (9; -2, -2, -5)$, with the following choice of complex structure:

$$c_1 = c_2 = c_3 = c_4 = c_5 = c_{40} = c_{41} = c_{42} = c_{43} = c_{44} = 0\,. \tag{5.3.7}$$

Then we find

$$h^i(C_4, \mathcal{O}_{dP_3}((5; -4, -4, 3)|_{C_4}) = (19, 4)\,. \tag{5.3.8}$$

Lastly, we also easily construct a model with five vector-like pairs, by setting

$$\begin{aligned} &c_1 = c_2 = c_3 = c_4 = c_5 = c_{34} = c_{35} = c_{36} = c_{37} = 0 \\ &c_{38} = c_{39} = c_{40} = c_{41} = c_{42} = c_{43} = c_{44} = 0\,. \end{aligned} \tag{5.3.9}$$

On this sublocus in complex structure moduli space, the matter curve factorizes as $C_{\mathbf{5}_3} \to C_5 = \{x_1\, x_6^2\, R_5 = 0\}$, with $[R_5] = (9; -2, -2, -6)$. In this case we have

$$h^i(C_5, \mathcal{O}_{dP_3}((5; -4, -4, 3)|_{C_5}) = (20, 5)\,. \tag{5.3.10}$$

5.3.2 Single vector-like pair from Brill–Noether theory

The above examples demonstrate how the machine learning intuition led us to a step-wise increase in the number of vector-like pairs by suitable tuning of the complex structure parameters. These jumps occur because the matter curve in question splits into several components. However, such splittings induce a jump from zero vector-like pairs to at least two (or three, or four, or five). If we are interested in models with a single vector-like pair — such as for the Higgs field in MSSM realizations — then we need to look for other effects than curve splitting.

As we have seen earlier, such effects are related to the cases not predicted by the trained

decision tree. Here, the jumps in cohomology are not due to the curve becoming non-generic, but rather the line bundle. In fact, Brill–Noether theory (to be discussed in the next section, see also B.1.1) tells us that for the matter curve $C_{\mathbf{5}_3}$ of genus 24, we expect that a scenario with a single vector-like pair — i.e., one having $h^i = (16, 1)$ — to occur on a subvariety of dimension $\rho = g - h^0 \cdot h^1 = 8$ of the space $\mathrm{Jac}(C_{\mathbf{5}_3})$ which parametrizes the line bundles on $C_{\mathbf{5}_3}$. Note that the same formula would yield $\rho = -10$ for jumps by two, and hence no such jumps can occur *for a generic* $C_{\mathbf{5}_3}$. This agrees with the above instances, as each of those requires the curve to become non-generic.

Because of this, engineering the jump by 1 becomes more challenging, and in particular requires additional tools from algebraic geometry. We defer the details of the relevant computations to B.1 and simply remark here that the necessary tuning is

$$\begin{aligned} &c_1 = c_2 = c_3 = c_4 = c_5 = c_7 = c_8 = c_9 = c_{10} = c_{35} = c_{36} = c_{37} = c_{38} = 1\,, \\ &c_{40} = c_{41} = c_{42} = c_{43} = c_{44} = 1, \quad c_{11} = c_{34} = -1, \quad c_6 = c_{39} = 2\,. \end{aligned} \tag{5.3.11}$$

One can easily verify that the polynomial $a_{3,2}$ in B.1.60 does not factorize in this case, and that the curve $C_{\mathbf{5}_3}$ remains smooth. Therefore, the enhancement in cohomology in this case is indeed of Brill–Noether type.

5.4 Cohomology jumps throughout the moduli space

To put the intuition we gained from machine learning onto more solid grounds, we now apply tools from algebraic geometry to develop a more complete, "microscopic" understanding for the various sources of jumps we encountered in our data. As we will see, the resulting insights lead to a diagrammatic representation of a *stratification* of the complex structure moduli space of F-theory compactifications induced by vector-like spectra.

As we have alluded to in 5.2, based on our database we can essentially distinguish two types of jumps:

1. Jumps due to a non-generic line bundle.

2. Jumps due to a non-generic curve.

This shows that our samplings are very atypical. Namely, true jump loci have lower dimensionality than the full set of parameters. Therefore, jump loci form sets of measure 0 and should never be encountered by a genuinely random sample.

It is central to our discussion that algebraic geomemtry can bound from below the 'size' of such jump loci. In particular, this is true for jumps due to non-generic line bundles. Such jumps have been analyzed since 1874 in the context of *Brill–Noether theory*[9] [150]. Given a generic curve C_g of genus g and an integer d, Brill–Noether theory provides an integer $\rho(r, g, d)$ which measures how likely it is that a line bundle $\mathcal{L}_d$ of degree d on C_g has $r + 1$ independent non-trivial global sections, i.e., has $h^0(C_g, \mathcal{L}_d) = r + 1$.

To formulate this more precisely, first recall that the Jacobian $\mathrm{Jac}(C_g)$ of the curve C_g is isomorphic to $\mathbb{C}^g/\Lambda$ where Λ is the full-dimensional period lattice of C_g. By the Abel–Jacobi map, equivalence classes of line bundles of degree d form a copy of the Jacobian $\mathrm{Jac}(C_g)$. Let us focus on the subset of the Jacobian formed by all equivalence classes of line bundles of degree d which admit exactly $r + 1$ global sections. Then a lower bound on the dimension of this space is given by the integer

$$\rho(r, g, d) = g - (r + 1) \cdot (r + 1 - (d - g + 1)) \equiv g - n^0 \cdot n^1 \,. \tag{5.4.1}$$

In the last equality we use the intuitive notation $n^0 = r + 1$. Furthermore, we have used that by the Riemann–Roch theorem, $n^1 \equiv n^0 - (d - g + 1)$ is equal to $h^1(C_g, \mathcal{L}_d)$ if $h^0(C_g, \mathcal{L}_d) = n^0$. Further details on Brill–Noether theory can be found in appendix B.1.1, and a more complete presentation is given in [151, 152].

An important result follows from [153]: If the curve is generic, then lines bundles of degree d only admit numbers $r + 1$ of global sections for which $\rho(r, g, d)$ is non-negative. Put

[9] The physics community may find it entertaining to learn that this theory is named after Max Noether, the father of Emmy Noether.

differently, there are no line bundles on generic curves with $r+1$ global sections with $\rho(r,g,d)<0$. Furthermore, the value of ρ gives a very clear notion of the likelihood to have $r+1$ sections in terms of a dimension on the "moduli" space of line bundles.

Let us demonstrate this for a line bundle $\mathcal{L}$ of degree $d=2$ on a curve C_g of genus $g=3$. By general theory, the number of section of this line bundle cannot exceed its degree. Hence, it has 0, 1 or 2 sections. With this information, let us compute $\rho(r,d,g)$:

r	h^i	$\rho(r,d,g)$
-1	$(0,0)$	3
0	$(1,1)$	2
1	$(2,2)$	-1

(5.4.2)

From this we learn, that most line bundles $\mathcal{L}$ of degree $d=2$ on a genus $g=3$ curve C_3 satisfy $h^0\left(C_3,\mathcal{L}\right)=0$. Since for these bundles ρ matches the dimension of the Jacobian of C_3, we can say that these line bundles are associated to generic points of the Jacobian. Furthermore, we learn that there are line bundles with $h^0\left(C_3,\mathcal{L}\right)=1$. However, these are special in the sense that they are associated to a codimension-1 locus in the Jacobian $\mathrm{Jac}(C_3)$.

Finally, $\rho=-1$ for $r=1$ begs for an explanation. This explanation follows from work of Griffiths and Harris [153]:

$$\text{On } \textbf{generic} \text{ curves, } \dim(G_d^{r+1})=\rho\left(r,d,g\right).$$

So in particular, on generic curves it holds $G_d^{r+1}=\emptyset$ if and only if $\rho\left(r,d,g\right)<0$. Consequently, we conclude from B.1.14, that on generic genus $g=3$ curve, there is no line bundle $\mathcal{L}$ of degree 2 such that $h^0(C_3,\mathcal{L})=2$.

Note however, that this does not rule out the possibility that non-generic curves may host such line bundles. In the case at hand, it follows from the theorem of Clifford [153]

that hyperelliptic curves H_3 of genus $g = 3$ admit line bundles $\mathcal{L}$ of degree $d = 2$ and $h^0(H_3, \mathcal{L}) = 2$. Note that hyperelliptic curves of genus $g > 2$ are non-generic. Hence, this points us to jumps of the vector-like spectrum, which originate from non-generic deformations of the curve.

Let us give another such example, which illustrates a jump on a singular curve. To this end, let us consider a line bundle $\mathcal{L}$ of degree $d = 5$ on a genus $g = 2$ curve. Then $\chi(\mathcal{L}) = 4$ and $h^0(C_2, \mathcal{L}) \in \{4, 5\}$. Let us compute $\rho(r, d, g)$ for these two values of global sections:

r	$h^i(C_2, \mathcal{L})$	$\rho(r, d, g)$
3	(4,0)	2
4	(5,1)	-3

(5.4.3)

Thus, on a smooth curve of genus $g = 2$, any line bundle of degree $d = 5$ has 4 global sections. Even more, since the degree d is in the stable range, we find 4 global sections for this line bundle on every smooth curve of genus $g = 2$ — generic or not. Hence, 5 sections can only be realized on a singular curve.

This can be achieved by choosing the curve parameters (which model the complex structure moduli of global F-theory models) such that the curve becomes reducible, and factors into various components which intersect transversely in a number of points. A way to construct global sections on such curves is then as follows: First, consider each component individually and identify which sections they support. Then, by demanding that these sections agree at the intersection points, we glue these local sections to global sections. We will return to this gluing procedure in more detail in 5.5.

In this section, we will take a closer look at the interplay of jumps that occur due to non-genericity both of the line bundle and the curve. In particular, since in global F-theory models, both the bundle and the curve depend on the complex structure parameters of the elliptic fibration in the same fashion (namely through the coefficients of its defin-

ing polynomials), they should be treated on the same footing, which we can summarize diagrammatically. The following analysis requires, at a technical level, a working understanding of the Koszul resolution of a pullback bundle, its associated long exact sequence in sheaf cohomology, inferring the maps in this long exact sequence from Čech ochomology as well as a basic understanding of on-reduced curves. For convenience of the reader, further details are provided in B.1.

5.4.1 Jumps from curve splittings

We first analyze examples with jumps from curve splittings. We will see that rigidity of the components that split off play no role in the section counting. The reason why we found in earlier chapters that rigid divisors split off is due to our special choice of setting all coefficients in the polynomial that specify the curve in dP_3 to either zero or one.

Example: one additional section

Setup Let us return to the example of a line bundle on a genus 2 curve discussed above. In more detail, the curve and line bundle are given by

$$D_C = (4; -1, -2, -1)\,, \qquad D_L = (3; -3, -1, -2)\,. \tag{5.4.4}$$

The curve $C(\mathbf{c}) = V(P(\mathbf{c}))$ is defined by a polynomial $P(\mathbf{c}) \in H^0(dP_3, \mathcal{O}_{dP3}(D_C)) \cong \mathbb{C}^{10}$ with

$$\begin{aligned} P(\mathbf{c}) = {} & c_1 x_1^3 x_2^3 x_3 x_4 + c_2 x_1^2 x_2^3 x_4^2 x_6 + c_3 x_1^3 x_2^2 x_3^2 x_5 + c_4 x_1^2 x_2^2 x_3 x_4 x_5 x_6 + c_5 x_1 x_2^2 x_4^2 x_5 x_6^2 \\ & + c_6 x_1^2 x_2 x_3^2 x_5^2 x_6 + c_7 x_1 x_2 x_3 x_4 x_5^2 x_6^2 + c_8 x_2 x_4^2 x_5^2 x_6^3 + c_9 x_1 x_3^2 x_5^3 x_6^2 + c_{10} x_3 x_4 x_5^3 x_6^3\,, \end{aligned} \tag{5.4.5}$$

where the coefficients $\mathbf{c} \in \mathbb{C}^{10}$ form the parameter space of this genus $g = 2$ setup. The line bundle $\mathcal{L}(\mathbf{c}) = \mathcal{O}_{dP3}(D_L)|_{C(\mathbf{c})}$ satisfies $\deg(\mathcal{L}(\mathbf{c})) = 5$. Hence, on smooth curves, the

theorem of Riemann–Roch tells us

$$\chi(\mathcal{L}(\mathbf{c})) = \deg(\mathcal{L}(\mathbf{c})) - g + 1 = 5 - 2 + 1 = 4\,. \tag{5.4.6}$$

Moreover, since $\deg(\mathcal{L}(\mathbf{c})) = 5 > 2g-2$, we know that for smooth curves $h^1(C(\mathbf{c}), \mathcal{L}(\mathbf{c})) = 0$. Hence, $h^0(\mathcal{L}(\mathbf{c})) = 5$ is only possible on non-smooth curves.

Comparison with database In our database, we have considered choices of parameters $\mathbf{c} \in \{-1, 0, 1\}^{10} - \mathbf{0}$. On about 96% of these 59048 curves, $\mathcal{L}(\mathbf{c})$ has 4 sections. This fits with the above picture, that generically we expect 4 sections. However, we also find 2186 curves for which $\mathcal{L}(\mathbf{c})$ has 5 sections. Those curves satisfy $c_3 = c_6 = c_9 = 0$, which means that $C(\mathbf{c}) = V(x_4) \cup B$, where

$$\begin{aligned} B = V(&c_1 x_1^3 x_2^3 x_3 + c_2 x_1^2 x_2^3 x_4 x_6 + c_4 x_1^2 x_2^2 x_3 x_5 x_6 + c_5 x_1 x_2^2 x_4 x_5 x_6^2 \\ &+ c_7 x_1 x_2 x_3 x_5^2 x_6^2 + c_8 x_2 x_4 x_5^2 x_6^3 + c_{10} x_3 x_5^3 x_6^3) \end{aligned} \tag{5.4.7}$$

is a genus-0 curve with $V(x_4) \cdot B = 3$. We will now argue that $\mathcal{L}(\mathbf{c})$ admits 5 sections if and only if $C(\mathbf{c})$ decomposes in this way.

Classification of jump geometries To this end, we consider the Koszul resolution

$$0 \to \mathcal{O}_{dP_3}(D_L - D_C) \xrightarrow{\alpha} \mathcal{O}_{dP_3}(D_L) \to \mathcal{L}(\mathbf{c}) \to 0\,. \tag{5.4.8}$$

Its associated long exact sequence in sheaf cohomology takes the form

$$\begin{array}{l} 0 \longrightarrow 0 \longrightarrow H^0(dP_3, D_L) \cong \mathbb{C}^1 \longrightarrow H^0(C(\mathbf{c}), \mathcal{L}(\mathbf{c})) \\ \quad \hookrightarrow H^1(dP_3, D_L - D_C) \cong \mathbb{C}^4 \xrightarrow{\varphi} H^1(dP_3, D_L) \cong \mathbb{C}^1 \longrightarrow H^1(C(\mathbf{c}), \mathcal{L}(\mathbf{c})) \\ \quad\quad \hookrightarrow 0 \longrightarrow 0 \longrightarrow 0 \longrightarrow 0 \end{array} \tag{5.4.9}$$

The exactness of this sequence implies that

$$h^0(C(\mathbf{c}), \mathcal{L}(\mathbf{c})) = 5 - \dim\left(\mathrm{im}\varphi\right) = 5 - \mathrm{rk}\left(M_\varphi\right) \ , \tag{5.4.10}$$

where $M_\varphi = (c_3, c_6, c_9, 0)$. We explain the construction of the mapping matrix M_φ in more detail in B.1.

Obviously, M_φ has rank 1 iff $(c_3, c_6, c_9) \neq \mathbf{0}$ and its rank vanishes iff $(c_3, c_6, c_9) = \mathbf{0}$. This immediately leads to the following classification of curve geometries:

$\mathrm{rk}\left(M_\varphi\right)$	explicit condition	curve splitting
1	$(c_3, c_6, c_9) \neq \mathbf{0}$	C
0	$(c_3, c_6, c_9) = \mathbf{0}$	$V(x_4) \cup B$

(5.4.11)

showing that we obtain one additional vector-like pair if and only if the curve factors as $V(x_4) \cup B$. We illustrate this result in the following diagram:

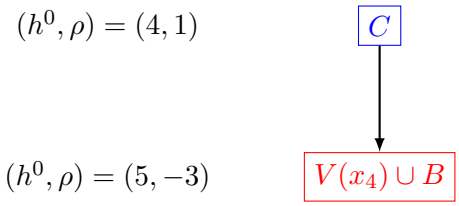

(5.4.12)

In this diagram, the a^{th} node represents a family $\mathcal{F}_a$ of curves, for which we give the generic element in this family.

For example, the family $\mathcal{F}_1$ of curves at the first node is defined by the nonvanishing condition $(c_3, c_6, c_9) \neq \mathbf{0}$ and has the curve C as its generic element, which is a smooth, irreducible curve of genus $g = 2$. Note that (non-generic) members of $\mathcal{F}_1$ can also be singular curves with several components. For example, the curve $V(x_1^3 x_2^2 x_3^2 x_5)$ is defined by the condition that all c_i but c_3 vanish. This curve is clearly singular and has several connected components. Recall that $\mathcal{F}_1$ is the family of curves on which the line bundle

in question admits four global sections. Hence, the statement is that even on such a very singular curve, the bundle in question admits exactly four sections.

This feature changes exactly on the family of curves $\mathcal{F}_2$, which are defined by $(c_3, c_6, c_9) \equiv \mathbf{0}$. Its generic element is a curve of the form $V(x_4) \cup B$, where B is a smooth genus $g = 0$ curve touching $V(x_4)$ in 3 distinct points. We can also view $\mathcal{F}_1 = \{\mathbf{c} \,|\, (c_3, c_6, c_9) \neq 0\}$ and $\mathcal{F}_2 = \{\mathbf{c} \,|\, (c_3, c_6, c_9) = 0\}$ as subspaces of the parameter space $\mathbb{C}^{10} \ni \mathbf{c}$. In this case it is trivial to see that

$$\mathcal{F}_1 \cap \mathcal{F}_2 = \emptyset\,, \qquad \mathcal{F}_2 \subset \overline{\mathcal{F}_1}\,, \tag{5.4.13}$$

where $\overline{\mathcal{F}_1}$ the closure with respect to the standard topology on $\mathbb{C}^{10}$. We will come back to this property shortly.

An h^0-gap

Whilst factoring-off curve components typically increases the number of global sections, this effect need not necessarily generate exactly one additional section, as we have already seen above. Rather, it can force multiple additional sections to appear simultaneously. An example of this sort is

$$D_C = (3; -1, -1, -1)\,, \qquad D_L = (1; -1, -3, -1)\,. \tag{5.4.14}$$

In this case, $C(\mathbf{c}) = V(P(\mathbf{c}))$ is a genus 1 curve defined by

$$\begin{aligned} P(\mathbf{c}) = {} & c_1 x_1^2 x_2^2 x_3 x_4 + c_2 x_1^2 x_2 x_3^2 x_5 + c_3 x_1 x_2^2 x_4^2 x_6 + c_4 x_1 x_2 x_3 x_4 x_5 x_6 \\ & + c_5 x_1 x_3^2 x_5^2 x_6 + c_6 x_2 x_4^2 x_5 x_6^2 + c_7 x_3 x_4 x_5^2 x_6^2\,. \end{aligned} \tag{5.4.15}$$

Moreover, $\mathcal{L}$ is a line bundle of degree $d = -2$. Hence, its degree is in the stable regime and on any smooth curve we find $h^0(C, \mathcal{L}) = 0$. Still, as demonstrated in 5.4.1, non-smooth curves can admit higher numbers of global sections. Here, we will argue, that

even on singular curve, the pullback line bundle $\mathcal{L}$ can never have exactly one section.

To see this, let us look at the long exact sequence in sheaf cohomology associated to the Koszul resolution of the setup:

$$\begin{array}{c} 0 \longrightarrow 0 \longrightarrow 0 \longrightarrow H^0\left(D_C, \mathcal{L}\right) \\ \hookrightarrow H^1\left(dP_3, D_L - D_C\right) \cong \mathbb{C}^3 \xrightarrow{\varphi} H^1\left(dP_3, D_L\right) \cong \mathbb{C}^5 \longrightarrow H^1\left(C, \mathcal{L}\right) \\ \hookrightarrow 0 \longrightarrow 0 \longrightarrow 0 \longrightarrow 0 \end{array} \tag{5.4.16}$$

The exactness of this sequence implies $h^0(C, \mathcal{L}) = 3 - \dim\left(\mathrm{im}\varphi\right) = 3 - \mathrm{rk}\left(M_\varphi\right)$ with

$$M_\varphi = \begin{pmatrix} c_6 & 0 & 0 \\ c_7 & c_6 & 0 \\ c_3 & 0 & 0 \\ c_1 & 0 & c_3 \\ c_4 & c_3 & c_6 \end{pmatrix}. \tag{5.4.17}$$

Consequently, the statement that on the curves in class D_C the pullback of D_L never has exactly one section is equivalent to saying that M_φ never has rank 2. We see this by studying the four non-trivial and independent 3×3-minors of M_φ:

$$m_1 = c_6^2 c_3\,, \qquad m_2 = c_6^3 \qquad m_3 = c_3^3\,, \qquad m_4 = c_6 c_4 c_3 - c_7 c_3^2 - c_6^2 c_1\,. \tag{5.4.18}$$

Now, $\mathrm{rk}(M_\varphi) < 3$ requires $m_1 = m_2 = m_3 = m_4 = 0$. This is equivalent to $c_3 = c_6 = 0$ and

$$M_\varphi|_{c_3 = c_6 = 0} = \begin{pmatrix} 0 & 0 & 0 \\ c_7 & 0 & 0 \\ 0 & 0 & 0 \\ c_1 & 0 & 0 \\ c_4 & 0 & 0 \end{pmatrix}, \tag{5.4.19}$$

which can have at most rank 1. More generally, we can classify the rank of M_φ and

thereby summarize the curve geometry as follows:

$\mathrm{rk}(M_\varphi)$	explicit condition $(\mathcal{F}_i)$	splitting of curve
3	$c_3, c_6 \neq 0$	C
1	$c_3 = c_6 = 0$	$E_2 \cup B$
0	$c_1 = c_3 = c_4 = c_6 = c_7 = 0$	$E_6 \cup E_4 \cup E_2^{(2)} \cup A$

(5.4.20)

Observe again that within the parameter space of $\mathbf{c}$, we have

$$\mathcal{F}_i \cap \mathcal{F}_j = \emptyset\,, \quad \overline{\mathcal{F}_1} \supset \mathcal{F}_2\,, \quad \overline{\mathcal{F}_2} \supset \mathcal{F}_3\,. \tag{5.4.21}$$

The corresponding diagram is

$\mathcal{F}_1 : (h^0, \rho) = (0, 1)$

$\mathcal{F}_2 : (h^0, \rho) = (2, -7)$

$\mathcal{F}_3 : (h^0, \rho) = (3, -14)$

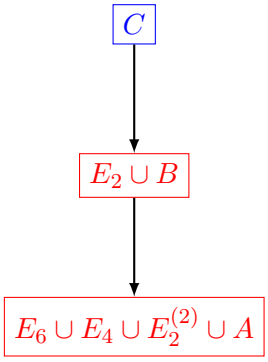

(5.4.22)

Jump from non-rigid curve splitting

We now address the bias in our data, and provide a concrete example of jumps from curve splitting where none of the components are rigid. To this end, we consider $D_C = (2; -1, -1, 0)$ and $D_L = (-2, 0, 4, 0)$. This curve is thus given by

$$P = c_1 x_4 x_5 x_6^2 + c_2 x_1 x_3 x_5 x_6 + c_3 x_1 x_2 x_4 x_6 + c_4 x_1^2 x_2 x_3\,. \tag{5.4.23}$$

For generic coefficients c_i, the curve C is a smooth curve of genus $g = 0$ and $\mathcal{L}$ has degree $d = 0$. Hence we conclude $h^0(C, \mathcal{L}) = 1$.

To understand jumps at special coefficients, we employ the Koszul resolution and find $h^0\left(C(\mathbf{c}), \mathcal{L}(\mathbf{c})\right) = 7 - \mathrm{rk}(M)$ where

$$M = \begin{pmatrix} 0 & 0 & 0 & c_1 & 0 & c_3 & 0 \\ c_4 & 0 & 0 & 0 & c_1 & c_2 & c_3 \\ c_3 & 0 & 0 & 0 & 0 & c_1 & 0 \\ 0 & c_1 & 0 & c_2 & c_3 & c_4 & 0 \\ 0 & 0 & c_1 & c_3 & 0 & 0 & 0 \\ 0 & 0 & 0 & 0 & c_2 & 0 & c_4 \end{pmatrix}. \tag{5.4.24}$$

The rank drops of this matrix include both cases of rigid and non-rigid splittings. Explicitly, let us set $A_i = V(x_i)$, which are rigid components. Moreover, we also have the following possible genus $g = 0$ components which are non-rigid:

$$\begin{aligned} D_1 &= V(c_2x_3x_5x_6 + c_3x_2x_4x_6 + c_4x_1x_2x_3)\,, \\ D_2 &= V(c_3x_4x_6 + c_4x_1x_3)\,, \\ D_3 &= V(c_4x_1x_2 + c_2x_5x_6)\,, \\ D_4 &= V(c_2x_1x_3 + c_1x_4x_6)\,, \\ D_5 &= V(c_3x_1x_2 + c_1x_5x_6)\,. \end{aligned} \tag{5.4.25}$$

With these, we can then summarize the rank drops as follows:

rk(M)	explicit condition	curve splitting
6	generic	C
5	$c_1 = 0$	$A_1 \cup D_1$
5	$c_1 c_4 = c_2 c_3$	$D_2 \cup D_3$
3	$c_1 = c_3 = 0$	$A_1 \cup A_3 \cup D_3$

(5.4.26)

The corresponding diagram is of the form

$\mathcal{F}_1 : (h^0, \rho) = (1, 0)$

$\mathcal{F}_2 : (h^0, \rho) = (2, -2)$

$\mathcal{F}_4 : (h^0, \rho) = (4, -12)$

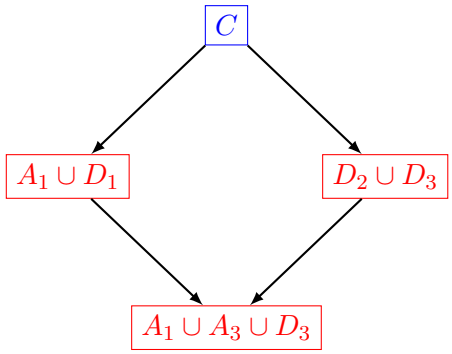

(5.4.27)

Similar to our discussion in 5.4.1, there is a gap at $h^0 = 3$. Crucially, since D_2 and D_3 are non-rigid, the deformation $C \to D_2 \cup D_3$ provides an explicit example of a jump associated to curve splitting with no rigid components.

5.4.2 Jumps from non-generic line bundles

We now turn to jumps due to special alignments of the points that define a line bundle divisor. These phenomena are described by Brill–Noether theory.

Additional section due to special divisors

Let us consider the pair

$$D_C = (4; -1, -1, -1)\,, \qquad D_L = (1; 2, -2, -1)\,. \tag{5.4.28}$$

This genus $g = 3$ curve $C(\mathbf{c}) = V(P(\mathbf{c}))$ is defined by

$$\begin{aligned} P(\mathbf{c}) = {} & c_1 x_1^3 x_2^3 x_3^2 x_4 + c_2 x_1^2 x_2^3 x_3 x_4^2 x_6 + c_3 x_1 x_2^3 x_4^3 x_6^2 + c_4 x_1^3 x_2^2 x_3^3 x_5 + c_5 x_1^2 x_2^2 x_3^2 x_4 x_5 x_6 \\ & + c_6 x_1 x_2^2 x_3 x_4^2 x_5 x_6^2 + c_7 x_2^2 x_4^3 x_5 x_6^3 + c_8 x_1^2 x_2 x_3^3 x_5^2 x_6 + c_9 x_1 x_2 x_3^2 x_4 x_5^2 x_6^2 \\ & + c_{10} x_2 x_3 x_4^2 x_5^2 x_6^3 + c_{11} x_1 x_3^3 x_5^3 x_6^2 + c_{12} x_3^2 x_4 x_5^3 x_6^3 \,. \end{aligned} \tag{5.4.29}$$

Brill–Noether theory implies

curve	g	$\mathcal{L}$	χ	d	BN-theory		
					h^0	h^1	ρ
$C = V(P)$	3	$\mathcal{O}_{dP3}(D_L)\|_C$	1	3	1	0	3
					2	1	1
					3	2	-3

(5.4.30)

Hence, a jump on the generic curve — a Brill–Noether jump — to $h^0(C(\mathbf{c}), \mathcal{L}(\mathbf{c})) = 2$ is possible. To explicitly construct such curves, we again inspect the long exact sequence, associated to the Koszul resolution of $\mathcal{L}(\mathbf{c})$, which is given by

$$\begin{array}{l} 0 \longrightarrow 0 \longrightarrow 0 \longrightarrow H^0\left(D_C, \mathcal{L}\right) \hookrightarrow \\ \quad H^1\left(dP_3, D_L - D_C\right) \cong \mathbb{C}^3 \xrightarrow{\varphi} H^1\left(dP_3, D_L\right) \cong \mathbb{C}^2 \longrightarrow H^1\left(C, \mathcal{L}\right) \hookrightarrow \\ \qquad 0 \longrightarrow 0 \longrightarrow 0 \longrightarrow 0 \,. \end{array} \tag{5.4.31}$$

From the exactness of this sequence, we learn that $h^0(C(\mathbf{c}), \mathcal{L}(\mathbf{c})) = 3 - \mathrm{rk}\left(M_\varphi\right)$ with

$$M_\varphi = \begin{pmatrix} c_3 & c_2 & c_1 \\ 0 & c_{12} & c_{11} \end{pmatrix} . \tag{5.4.32}$$

We set $\mathbb{P}^1_a = V(x_2)$, $\mathbb{P}^1_b = V(x_5)$. Then the possible h^0 jumps are classified as

$\mathrm{rk}(M_\varphi)$	explicit condition	curve splitting
2	$(c_3c_{11}, c_3c_{12}, c_2c_{11} - c_1c_{12}) \neq \mathbf{0}$	C^1
1	$c_3 = 0,\ c_2c_{11} - c_1c_{12} = 0$	C^2
1	$c_1 = c_2 = c_3 = 0$	$B_2 \cup \mathbb{P}^1_b$
1	$c_{11} = c_{12} = 0$	$\mathbb{P}^1_a \cup B_1$
0	$c_1 = c_2 = c_3 = c_{11} = c_{12} = 0$	$\mathbb{P}^1_a \cup A \cup \mathbb{P}^1_b$

(5.4.33)

The corresponding diagram is of the form

$\mathcal{F}_1 : (h^0, \rho) = (1, 3)$

$\mathcal{F}_2 : (h^0, \rho) = (2, 1)$

$\mathcal{F}_3 : (h^0, \rho) = (3, -3)$

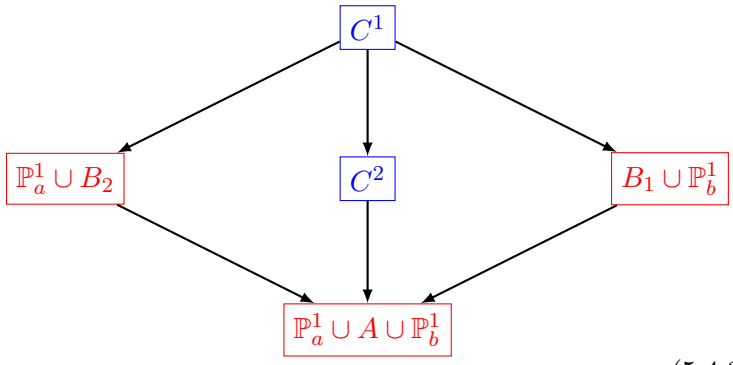

(5.4.34)

The change of coefficients

$$\mathbf{c} = (1,1,1,1,1,1,1,1,1,1,1,1) \quad \rightarrow \quad \mathbf{c} = (1,1,0,1,1,1,1,1,1,1,1,1) \tag{5.4.35}$$

leads to a transition $C^1 \rightarrow C^2$ of smooth, irreducible curves. Since the topology of the curve does not change for this choice of parameters, such a transition cannot be detected from the topological data which we used for our machine learning. Therefore, such transitions are the major source of error in our decision trees.

On smooth curves C^i, the nature of the jump $C^1 \rightarrow C^2$ can be analyzed by using Serre

duality:

$$\begin{aligned} h^1\left(C, \mathcal{O}_C\left(D_L|_C\right)\right) > 0 \quad &\Leftrightarrow \quad h^0\left(C, \mathcal{O}_C\left(K_C - D_L|_C\right)\right) > 0 \\ &\Leftrightarrow \quad K_C - D_L|_C \text{ effective} \\ &\Leftrightarrow \quad \exists p \in C\colon K_C - p \sim D_L|_C \ . \end{aligned} \tag{5.4.36}$$

Hence, the origin of this jump is that K_C and the line bundle divisor differ, modulo linear equivalence, only by a point on C. Such a divisor is known as a *special divisor*. Loosely speaking, we may thus say that the origin of this one additional sections is that the points, which define the line bundle on the curve, move into a special alignment.

Note that also in this case, the diagram 5.4.34 encodes a hierarchy $\overline{\mathcal{F}_1} \supset \mathcal{F}_2$, $\overline{\mathcal{F}_2} \supset \mathcal{F}_3$. This is a generic feature of the parameter space and reflects a *stratification* induced by the vector-like spectrum.

5.4.3 h^0-stratification of the parameter space

A stratification of a topological space X is a decomposition $X = \bigcup_i \mathcal{F}_i$ into locally closed subspaces $\mathcal{F}_i$ such that

1. $\mathcal{F}_i \cap \mathcal{F}_j = \emptyset$ if $i \neq j$,
2. if $\mathcal{F}_i \cap \overline{\mathcal{F}_j} \neq \emptyset$, then $\mathcal{F}_i \subset \overline{\mathcal{F}_j}$.

Intuitively speaking, a feature associated to a subspace $\mathcal{F}_i$ — a so-called stratum — becomes "less likely" with increasing codimension of $\mathcal{F}_i$, and being contained in (the closure of) a higher dimensional stratum $\mathcal{F}_j$ implies a "specialization" of the feature when going from $\mathcal{F}_i$ to $\mathcal{F}_j$ with $j > i$. The second defining property has a convenient diagrammatic representation: Let the strata $\mathcal{F}_i$ form vertices of a graph, then there is a directed edge going from j to i if $\mathcal{F}_i \subset \overline{\mathcal{F}_j}$. This is precisely the structure of the diagrams 5.4.12, 5.4.22, 5.4.27, and 5.4.34. Here, the stratified X is the parameter space $\{\mathbf{c}\}$ associated with a pair (D_C, D_L), and the strata are defined by the value of $h^0(C(\mathbf{c}), \mathcal{L}(\mathbf{c}))$

in the notation of the previous subsections. Hence, we call these diagrams h^0-*stratification*, or in short, stratification diagrams.

Note that Brill–Noether theory basically provides an analog description of the moduli space of line bundles / divisors on a smooth curve. In particular, it provides lower bounds on the dimension of the strata in terms of ρ. For F-theory models, where also deformations of the curve's topology become relevant, we see that the stratification by h^0 can be extended to the enlarged moduli space.

We observe that in this generalized setting, a stratum associated to a certain value of h^0 can consist of several disjoint subfamilies of different dimensions. In the example 5.4.34, the stratum $\mathcal{F}_2$ associated with $h^0 = 2$ decomposes as $\mathcal{F}_2 = \mathcal{F}_2^{(a)} \cup \mathcal{F}_2^{(s)} \cup \mathcal{F}_2^{(b)}$ with

$$\begin{aligned}
\mathcal{F}_2^{(a)} &= \{\mathbf{c} \,|\, c_{11} = c_{12} = 0\,, c_1 \neq 0, c_2 \neq 0, c_3 \neq 0\}\,, \\
\mathcal{F}_2^{(b)} &= \{\mathbf{c} \,|\, c_1 = c_2 = c_3 = 0, c_{11} \neq 0 \neq c_{12}\}\,, \\
\mathcal{F}_2^{(s)} &= \{\mathbf{c} \,|\, c_3 = 0 = c_2 c_{11} - c_1 c_{12}\,, c_1 \neq 0 \neq c_2\,, c_{11} \neq 0 \neq c_{12}\}\,.
\end{aligned} \tag{5.4.37}$$

It is easy to see that each of these components also satisfies the axioms for strata (since they satisfy $\mathcal{F}_2^{(x)} \cap \overline{\mathcal{F}}_2^{(y)} = \emptyset$ for $x \neq y$). Furthermore, their closure contains the common stratum $\mathcal{F}_3 = \{\mathbf{c} \,|\, c_1 = ... = c_{12} = 0\}$ of higher codimension with $h^0 = 3$, as can be seen from the arrows connecting the three subfamilies of the stratum $\mathcal{F}_2$ to $\mathcal{F}_3$ in 5.4.34.

In general, a stratification diagram can be roughly divided into three regions. At low values of h^0, jumps typically occur for divisor alignment, i.e., are allowed by Brill–Noether theory on a smooth curve. To get to high h^0, i.e., many vector-like pairs, the curve typically needs to factorize into many components. In the middle regime, we can have a mixture, meaning in particular that a jump occurs due to divisor alignment on a split component.

To illustrate such a "typical" case, consider

$$D_C = (5; -1, -1, -2)\,, \qquad D_L = (1; 1, -4, 1)\,. \tag{5.4.38}$$

This genus $g = 5$ curve is given by $C(\mathbf{c}) = V(P(\mathbf{c}))$ with

$$\begin{aligned} P := {} & c_1 x_1^3 x_2^4 x_3^2 x_4^2 + c_2 x_1^2 x_2^4 x_3 x_4^3 x_6 + c_3 x_1 x_2^4 x_4^4 x_6^2 + c_4 x_1^3 x_2^3 x_3^3 x_4 x_5 + c_5 x_1^2 x_2^3 x_3^2 x_4^2 x_5 x_6 \\ & + c_6 x_1 x_2^3 x_3 x_4^3 x_5 x_6^2 + c_7 x_2^3 x_4^4 x_5 x_6^3 + c_8 x_1^3 x_2^2 x_3^4 x_5^2 + c_9 x_1^2 x_2^2 x_3^3 x_4 x_5^2 x_6 \\ & + c_{10} x_1 x_2^2 x_3^2 x_4^2 x_5^2 x_6^2 + c_{11} x_2^2 x_3 x_4^3 x_5^2 x_6^3 + c_{12} x_1^2 x_2 x_3^4 x_5^3 x_6 + c_{13} x_1 x_2 x_3^3 x_4 x_5^3 x_6^2 \\ & + c_{14} x_2 x_3^2 x_4^2 x_5^3 x_6^3 + c_{15} x_1 x_3^4 x_5^4 x_6^2 + c_{16} x_3^3 x_4 x_5^4 x_6^3\,. \end{aligned} \tag{5.4.39}$$

From Brill–Noether theory, we then find

curve	g	$\mathcal{L}$	χ	d	BN-theory		
					h^0	h^1	ρ
$C = V(P)$	5	$\mathcal{O}_{dP3}(D_L)\vert_C$	0	4	0	0	5
					1	1	4
					2	2	1

(5.4.40)

The stratification of curve geometries follows from the long exact sequence

$$\begin{array}{ccccccc} 0 & \longrightarrow & 0 & \longrightarrow & 0 & \longrightarrow & H^0\left(C(\mathbf{c}), \mathcal{L}(\mathbf{c})\right) \\ \hookrightarrow H^1\left(dP_3, D_L - D_C\right) \cong \mathbb{C}^7 & \xrightarrow{\varphi} & H^1\left(dP_3, D_L\right) \cong \mathbb{C}^7 & \longrightarrow & H^1\left(C(\mathbf{c}), \mathcal{L}(\mathbf{c})\right) & & \\ \hookrightarrow 0 & \longrightarrow & 0 & \longrightarrow & 0 & \longrightarrow & 0 \end{array} \tag{5.4.41}$$

Consequently $h^0\left(C(\mathbf{c}), \mathcal{L}(\mathbf{c})\right) = 7 - \mathrm{rk}(M_\varphi)$ and we find

$$M_\varphi = \begin{pmatrix} c_{15} & c_{11} & c_7 & 0 & 0 & 0 & 0 \\ 0 & c_{10} & c_6 & c_3 & c_{11} & c_7 & 0 \\ c_{12} & c_6 & c_3 & 0 & c_7 & 0 & 0 \\ 0 & c_5 & c_2 & 0 & c_6 & c_3 & c_7 \\ c_8 & c_2 & 0 & 0 & c_3 & 0 & 0 \\ 0 & c_{14} & c_{11} & c_7 & 0 & 0 & 0 \\ 0 & c_1 & 0 & 0 & c_2 & 0 & c_3 \end{pmatrix} . \tag{5.4.42}$$

We list the curve strata in 10 and display the corresponding stratification diagram in 8.

Of particular interest is the transition $A_3 \cup D_1 \to A_3 \cup D_2$. The former curve admits 3, the latter 4 sections. This change in the number of sections is due to a Brill–Noether jump on the curve components D_i:

curve	class	genus	d	h^0	h^1	ρ
D_i	$(5,-1,-2,-2)$	4	0	0	3	4
				1	4	0

Hence, provided that the line bundle divisor is chosen such that $K_{D_i} - D_L|_{D_i}$ is effective, we find an additional section on D_i, due to a Brill–Noether effect. More explicitly, in the case at hand this condition states that the line bundle divisor is linearly equivalent to the trivial divisor, i.e. $D_L|_{D_i} \sim \emptyset$. This condition is satisfied on D_2 but not on D_1. For this reason we find one additional section on $A_3 \cup D_2$.

5.5 Local to global section counting

In this section, we provide an in-depth analysis of the procedure of gluing local sections on reducible curves. As a result, we can place a lower bound on the number of global sections. We find sufficient topological conditions for a jump of h^0 to occur. This further

$\mathrm{rk}(M_\varphi)$	explicit condition	curve splitting
7	$\det(M_\varphi) \neq 0$	C^0
6	$\det(M_\varphi) = 0$	C_1^1
5	$c_3c_7c_{12} = c_{15}c_3^2 + c_8c_7^2, \quad c_{11}c_3^2 = c_3c_6c_7 - c_2c_7^2$ $c_1c_7^3 + c_{10}c_3^2c_7 = c_{14}c_3^3 + c_3c_5c_7^2$	C_1^2
4	$c_3 = c_7 = 0$	$A_3 \cup D_1$
3	$c_3 = c_7 = 0 \quad c_{11}c_8 = c_{15}c_2 \quad c_{11}c_{12} = c_{15}c_6$ $c_{11}c_2c_5 = c_{14}c_2^2 + c_1c_{11}c_6 \quad c_{10}c_{11}c_2 = c_1c_{11}^2 + c_{14}c_2c_6$	$A_3 \cup D_2$
3	$c_3 = c_7 = c_8 = c_{12} = c_{15} = 0$	$A_3 \cup A_4 \cup D_3$
2	$c_2 = c_3 = c_6 = c_7 = c_{11} = 0$	$A_3^{(2)} \cup D_4$
1	$c_1 = c_2 = c_3 = c_5 = c_6 = c_7 = c_{10} = c_{11} = c_{14} = 0$	$A_3^{(3)} \cup A_5 \cup D_5$
1	$c_2 = c_3 = c_6 = c_7 = c_8 = c_{11} = c_{12} = c_{15} = 0$	$A_3^{(2)} \cup A_4 \cup D_6$
0	$c_1 = c_2 = c_3 = c_5 = c_6 = c_7 = 0$ $c_8 = c_{10} = c_{11} = c_{12} = c_{14} = c_{15} = 0$	$A_3^{(3)} \cup A_4 \cup A_5 \cup D_7$

Table 10: The curve strata for $D_C = (5; -1, -1, -2)$ and $D_L = (1; 1, -4, 1)$.

allows us to formulate an algorithm to estimate the possible numbers of vector-like pairs on the moduli space of F-theory compactifications.

5.5.1 Gluing local sections to global sections

Trivial boundary conditions

Let us start by looking at a simple example. To this end, we go back to the geometry discussed in 5.4.1, i.e.

$$D_C = (3; -1, -1, -1)\,, \qquad D_L = (1; -1, -3, -1)\,. \tag{5.5.1}$$

Recall that in this case, $C(\mathbf{c}) = V(P(\mathbf{c}))$ is a genus 1 curve defined by

$$\begin{aligned} P(\mathbf{c}) = {} & c_1x_1^2x_2^2x_3x_4 + c_2x_1^2x_2x_3^2x_5 + c_3x_1x_2^2x_4^2x_6 + c_4x_1x_2x_3x_4x_5x_6 \\ & + c_5x_1x_3^2x_5^2x_6 + c_6x_2x_4^2x_5x_6^2 + c_7x_3x_4x_5^2x_6^2\,. \end{aligned} \tag{5.5.2}$$

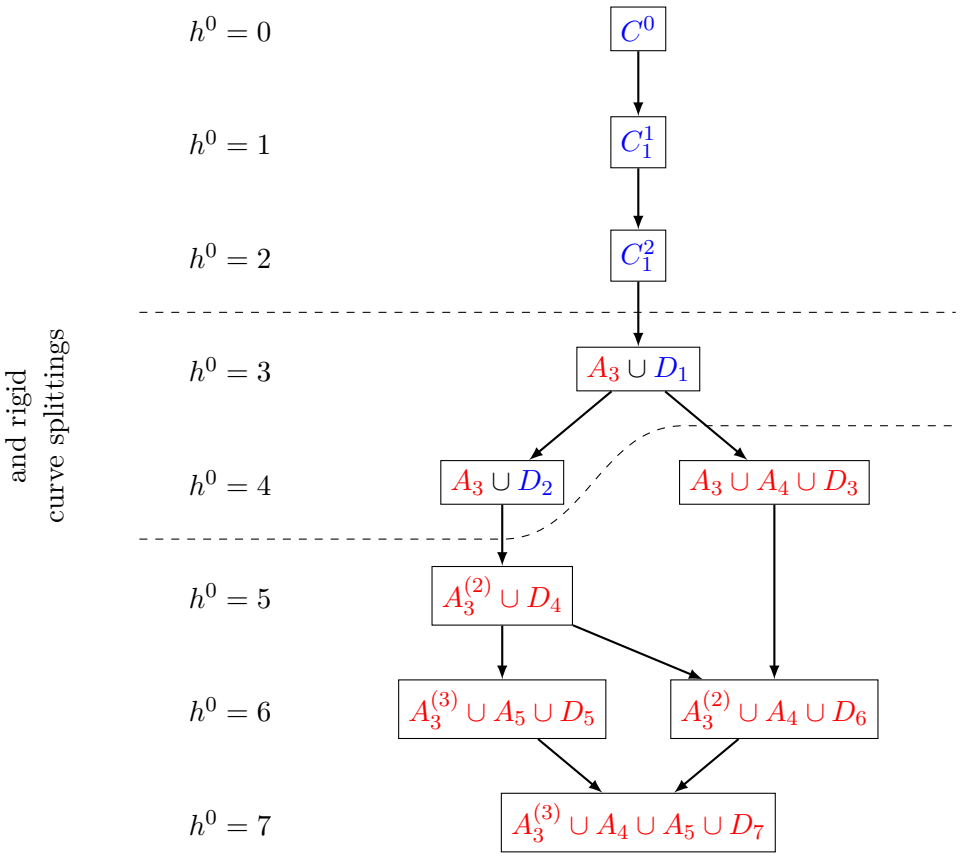

Figure 8: The stratification diagram for $D_C = (5; -1, -1, -2)$, $D_L = (1; 1, -4, 1)$.

We found that for $c_1 = c_3 = c_4 = c_6 = c_7 = 0$ we have 3 global sections. Furthermore, we have already seen that for this choice of parameters, the curve has 4 components

$$C(\mathbf{c}) = E_6 \cup E_4 \cup E_2^{(2)} \cup A\,. \tag{5.5.3}$$

These components have the following properties:

curve component	equation	class	g	d	$h^0(C_i, D_L)$
A	$V(c_2x_1x_2 + c_5x_5x_6)$	$(1;0,-1,0)$	0	-2	0
E_4	$V(x_1)$	$(1;-1,-1,0)$	0	-3	0
E_6	$V(x_5)$	$(1;0,-1,-1)$	0	-3	0
$E_2^{(2)}$	$V(x_3^2)$	$(0;0,2,0)$	-2	6	9

(5.5.4)

In the last column we give the number of sections of the restriction of the bundle $\mathcal{O}_{dP_3}(D_L)$ to these curve components. We will refer to these sections in the following as the *local sections*.

We display this geometry in 9. Our task is to glue the *local sections* to global sections on the curve $C = E_6 \cup E_4 \cup E_2^{(2)} \cup A$. To this end, we work out the sections explicitly and then subject them to boundary conditions at the intersection points of the different curve components.

For the components A, E_4 and E_6 we already know that the only allowed local section vanishes identically. On $E_2^{(2)}$ however, the situation is a bit more involved since $E_2^{(2)}$ is a non-reduced curve. As a set, $E_2^{(2)}$ is the locus $V(x_3)$. Using the scaling relations of dP_3, we can then set $x_2 = x_4 = x_6 = 1$ and thereby identify (x_1, x_5) as coordinates of $E_2^{(2)}$. Note, however, that since $E_2^{(2)}$ is a non-reduced curve, the polynomial x_3 is a non-trivial function on this curve component. These observations allow us to conclude

$$H^0\left(E_2^{(2)}, \mathcal{O}_{dP_3}(D_L)|_{E_2^{(2)}}\right) \cong P_3(x_1, x_5) \oplus x_3 \cdot P_4(x_1, x_5)\,, \tag{5.5.5}$$

where $P_i(x_1, x_5)$ is the space of polynomials of degree i in x_1 and x_5. Upon homogenization

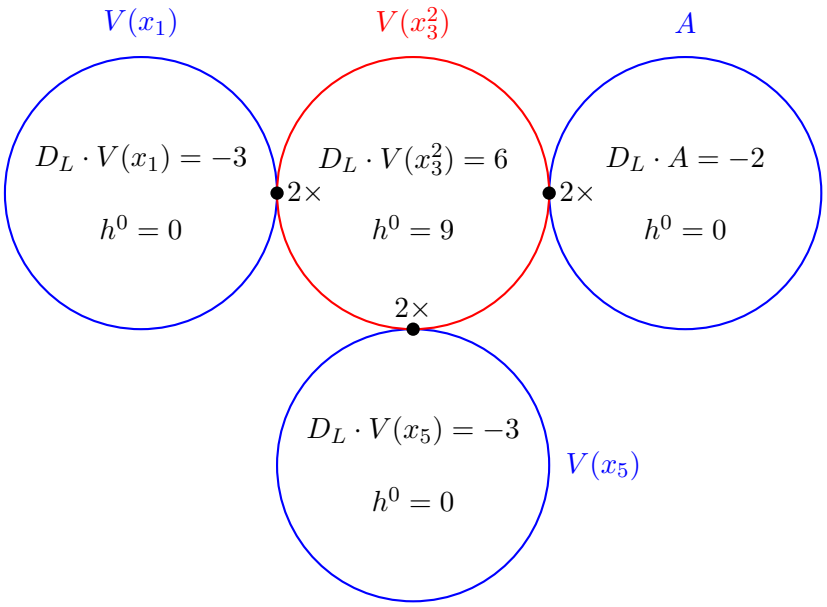

Figure 9: The 9 local sections on A lead to $9 - 3 \times 2 = 3$ global sections.

with x_2, x_4, x_6, we can then write

$$H^0\left(E_2^{(2)}, \mathcal{O}_{dP_3}(D_L)|_{E_2^{(2)}}\right) \cong \mathrm{Span}_{\mathbb{C}}\left\{\frac{x_5^3}{x_2^3x_4^2}, \frac{x_1x_5^2}{x_2^2x_4^2x_6}, \frac{x_1^2x_5}{x_2x_4^2x_6^2}, \frac{x_1^3}{x_4^2x_6^3}\right\} \\ \oplus\, x_3 \cdot \mathrm{Span}_{\mathbb{C}}\left\{\frac{x_5^4}{x_2^4x_4^3}, \frac{x_5^3x_1}{x_2^3x_4^3x_6}, \frac{x_1^2x_5^2}{x_2^2x_4^3x_6^2}, \frac{x_1^3x_5}{x_2x_4^3x_6^3}, \frac{x_1^4}{x_4^3x_6^4}\right\}. \tag{5.5.6}$$

From this, we learn that the only sections on $V(x_3^2)$, which vanish at $V(x_1)$, $V(x_5)$ and $V(c_2x_1x_2 + c_5x_5x_6)$, are linear combinations of the following three sections:

$$s_1 = c_5\frac{x_1x_5^2}{x_2^2x_4^2x_6} + c_2\frac{x_1^2x_5}{x_2x_4^2x_6^2} = \frac{x_1x_5\left(c_2x_1x_2 + c_5x_5x_6\right)}{x_2^2x_4^2x_6^2}, \tag{5.5.7}$$

$$s_2 = c_5\frac{x_5^3x_1}{x_2^3x_4^3x_6} + c_2\frac{x_1^2x_5^2}{x_2^2x_4^3x_6^2} = \frac{x_1x_5^2\left(c_2x_1x_2 + c_5x_5x_6\right)}{x_2^3x_4^3x_6^2}, \tag{5.5.8}$$

$$s_3 = c_5\frac{x_1^2x_5^2}{x_2^2x_4^3x_6^2} + c_2\frac{x_1^3x_5}{x_2x_4^3x_6^3} = \frac{x_1^2x_5\left(c_2x_1x_2 + c_5x_5x_6\right)}{x_2^2x_4^3x_6^3}. \tag{5.5.9}$$

Consequently, by extending these sections by zero outside of $V(x_3^2)$, we obtain 3 global sections.

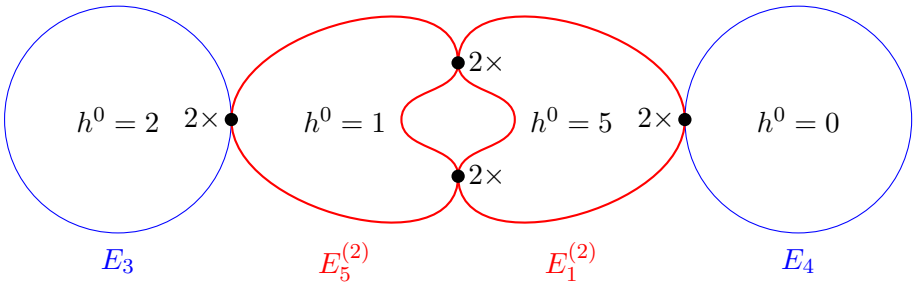

Figure 10: A non-trivial gluing example which gives no global sections.

Non-trivial boundary conditions

Let us consider $D_C = (3, -1, -1, -1)$ and $D_L = (5; -4, -4, 3)$. We pick special values for the parameters such that $C = V(x_1 x_2^2 x_4^2 x_6)$. The curve thus factors into four components, as displayed in 10. These components have the following properties:

curve	class	eqn.	d	g	h^0	basis of sections
E_3	$(0; 0, 0, 1)$	$V(x_6)$	1	0	2	$\frac{x_4}{x_3^3}, \frac{x_5}{x_2 x_3^2}$
$E_5^{(2)}$	$(2; -2, 0, -2)$	$V(x_4^2)$	-2	-2	1	$\frac{x_4}{x_3^3}$
$E_1^{(2)}$	$(0; 2, 0, 0)$	$V(x_2^2)$	2	-2	5	$\frac{x_1}{x_3^2 x_6}, \frac{x_4}{x_3^3}, \frac{x_2 x_4^2}{x_3^4 x_5}, \frac{x_2 x_1 x_4}{x_3^3 x_5 x_6}, \frac{x_2 x_1^2}{x_3^2 x_5 x_6^2}$
E_4	$(1; -1, -1, 0)$	$V(x_1)$	-3	0	0	0

(5.5.10)

We have also listed bases for the sections on the individual curve components. By starting in E_3, we see that there is a unique section which extends to $E_5^{(2)}$ and then to $E_1^{(2)}$ – this section is $\frac{x_4}{x_3^3}$. However, this section fails to vanish on $V(x_1)$. Consequently, this geometry only admits the global section which is identically zero.

From trivial to non-trivial boundary conditions

We have seen an interesting geometric transition when we discussed $D_C = (5, -1, -1, -2)$ and $D_L = (1; 1, -4, 1)$ in 5.4.3. Namely, the transition

$$A_3 \cup D_1 \to A_3 \cup D_2 \tag{5.5.11}$$

enforces a Brill–Noether jump on D_2. Whilst D_1 only supports the trivial section, D_2 supports a one-dimensional space of non-trivial sections. As a consequence, $A_3 \cup D_2$ admits one additional section as compared to $A_3 \cup D_1$. Let us investigate this finding in more detail. We depict this geometry in 11 and recall the following information:

curve	class	degree	genus	h^0
A_3	$(0;0,1,0)$	4	0	5
D_1	$(5,-1,-2,-2)$	0	4	0
D_2	$(5,-1,-2,-2)$	0	4	1

To simplify our analysis, let us work with a particular class of curves D_1 and D_2, for which the transition $D_1 \to D_2$ is particularly simple:

$$\begin{aligned} D_1 = V\Big(& c_{12}x_1^2x_2x_3^3x_5^3x_6 + c_{13}x_1x_2x_3^2x_4x_5^3x_6^2 + c_{16}x_3^2x_4x_5^4x_6^3 + c_4x_1^3x_2^3x_3^2x_4x_5 \\ & + c_9x_1^2x_2^2x_3^2x_4x_5^2x_6 + x_1^3x_2^4x_3x_4^2 + x_1^3x_2^2x_3^3x_5^2 + x_1^2x_2^4x_4^3x_6 \\ & - x_1^2x_2^3x_3x_4^2x_5x_6 - x_1x_2^2x_3x_4^2x_5^2x_6^2 - x_1x_3^3x_5^4x_6^2 - x_2^2x_4^3x_5^2x_6^3 \\ & + x_2x_3x_4^2x_5^3x_6^3\Big)\,, \\ D_2 = {} & D_1|_{c_{12}=0}\,. \end{aligned} \tag{5.5.12}$$

Next, we turn to the sections on $A_3 \cong \mathbb{P}^1$. We note that the homogeneous coordinates are $[x_1 : x_5]$. Hence, the line bundle sections at hand are of the form ($\lambda = x_2x_6^{-1}$):

$$H^0\left(A_3, \mathcal{L}|_{A_3}\right) = \frac{1}{x_4^3} \cdot \mathrm{Span}_{\mathbb{C}}\left\{x_1^4 \cdot \lambda^2,\ x_1^3x_5 \cdot \lambda, x_1^2x_5^2,\ x_1x_5^3 \cdot \lambda^{-1},\ x_5^4 \cdot \lambda^{-2}\right\}. \tag{5.5.13}$$

At $x_3 = 0$, we may set $x_2 = x_4 = x_6 = 1$ by the scaling relations of dP_3. In terms of these inhomogeneous coordinates, we find

$$A_3 \cap D_i = V(x_3, x_1 - x_5) \cup V(x_3, x_1 + x_5)\,. \tag{5.5.14}$$

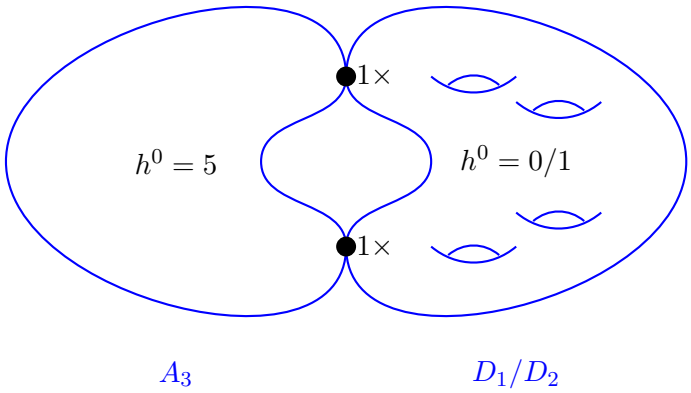

Figure 11: A Brill–Noether jump $D_1 \to D_2$ generates one additional global section.

That all said, we can discuss the global sections on $A_3 \cup D_1$ and $A_3 \cup D_2$:

- On D_1, the only supported section vanishes identically. Hence, we may only consider sections on A_3, which vanish at $A_3 \cap D_1$. It is not too hard to see that the space of these sections is generated by

$$s_1 = -x_1^4 + x_5^4\,, \qquad s_2 = -x_1^3 x_5 + x_1 x_5^3\,, \qquad s_3 = -x_1^4 + x_1^2 x_5^2\,. \tag{5.5.15}$$

- On D_2 however, the line bundle divisor is special. In fact, since it is a divisor of degree zero, this divisor must be the trivial divisor. Consequently, the sections on D_2 are the constant ones. It is not too hard to see that the sections on A_3, which have value 1 at the intersection points $A_3 \cap D_2$, are generated by

$$t_1 = x_1^4\,, \qquad t_2 = t_1 + s_1\,, \qquad t_3 = t_1 + s_2\,, \qquad t_4 = t_1 + s_3\,. \tag{5.5.16}$$

This explains the one additional section on $A_3 \cap D_2$ as opposed to $A_3 \cap D_1$.

Overcounting boundary conditions

As a final example, let us look at $D_C = (4; -1, -1, -1)$ and $D_L = (1, 1, -3, 0)$. Let us deform the curve C such that it is given by

$$P = x_1 \cdot Q\,, \qquad Q = x_1^2 x_2^2 x_3^3 x_5 + x_2^3 x_4^3 x_6^2 + x_3^3 x_5^3 x_6^2\,. \tag{5.5.17}$$

We display this curve geometry in 12. The two curve components have the following properties:

component	equation	class	g	d	h^0
C_1	$V(x_1)$	$(1; -1, -1, 0)$	0	-1	0
C_2	$V(Q)$	$(3; 0, 0, -1)$	1	3	3

Up to canonical isomorphism (induced from the connection homomorphism), we find a basis of the sections on C_2 as

$$\mathcal{B} = \left\{ \frac{1}{x_2 x_3^3 x_4^2 x_6}, \frac{x_5}{x_2^2 x_3^2 x_4^3 x_6}, \frac{x_1}{x_2 x_3^2 x_4^3 x_6^2} \right\}. \tag{5.5.18}$$

From this we can see that the third section automatically vanishes at the intersection $C_1 \cap C_2$, whilst the other two sections do not vanish there. Consequently, and in agreement with the computational results by *gap*, we find $h^0\left(C_1 \cup C_2, \mathcal{L}\right) = 1$.

Importantly, a naive guess cannot predict this number. In this case, we would have counted as follows: 3 sections on C_2 subject to vanishing conditions at the 3 intersection points $C_1 \cap C_2$ should leave us only with the trivial section. Hence, in this example, a naive counting fails. Such phenomena were originally studied more generally in [154, 155] — see also [156] for a more modern exposition of the material.

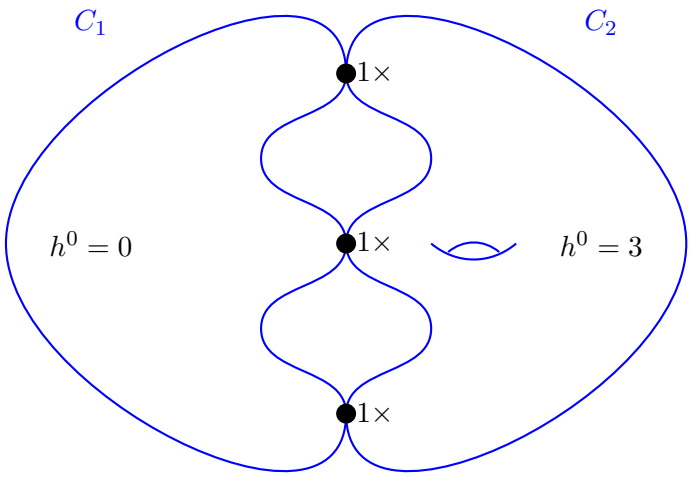

Figure 12: Naively, we expect $3 - 3 = 0$ global sections. However, one section on C_2 automatically vanishes at $C_1 \cap C_2$, leading to $h^0(C_1 \cup C_2, \mathcal{L}) = 1$.

5.5.2 Sufficient jump condition and algorithmic section estimate

As demonstrated in the previous section, gluing local sections to global sections is a non-trivial task. The exact details depend, among other things, on the relative position of the line bundle divisor and the intersection points of the curve components: the results change when some of these intersection points coincide and when the bundle divisor is special on some curve components.

In the following, we will propose a counting mechanism with the following key properties:

- It relies mostly on topological data.
- It provides a lower bound on the number of global sections.

Of course, such a simplified counting procedure will fail to predict intricate geometries as discussed in [154, 155, 156]. Still, it has two distinct advantages. First, since it relies mostly on topological data, it is very fast. Given a curve C and a line bundle $\mathcal{L}$ on C, we

can apply the strategy to place a lower bound on $h^0\left(C(\mathbf{c}), \mathcal{L}(\mathbf{c})\right)$ for many different choices of parameters $\mathbf{c}$ of C. The collection of these lower bounds can then serve as an estimate of the vector-like spectrum of $(C, \mathcal{L})$ over the parameter space. Note that obtaining such an estimate is unfeasible with existing exact algorithms, e.g., those implemented in [146], since these algorithms require extensive computational resources and often take a long time to finish. The second advantage results from the fact that our counting procedure systematically underestimates the actual number of global sections. Therefore, it allows us to formulate sufficient conditions for a jump in the vector-like spectrum to happen.

Counting procedure

Let us consider a curve C with

$$C = \bigcup_{i=1}^{N} C_i \,, \tag{5.5.19}$$

i.e., C has N components C_i. For our counting procedure to be as simple and reliable as possible, let us avoid setups of the type discussed in 5.5.1 and 5.5.1. Hence, let us consider a line bundle $\mathcal{L}$ on C such that neighboring curve components do not support non-trivial sections simultaneously. Put different, we only consider setups where for all curve components C_i the following holds true:

$$h^0\left(C_i, \mathcal{L}|_{C_i}\right) > 0 \quad \Rightarrow \quad h^0\left(C_j, \mathcal{L}|_{C_j}\right) = 0 \quad \forall\, C_j \text{ with } C_i \cap C_j \neq \emptyset \,. \tag{5.5.20}$$

Let us denote by b_i the number of intersection points of C_i with the other curve components. Generically, we then impose b_i conditions on the "local" sections in $H^0(C_i, \mathcal{L}|_{C_i})$. Consequently,

$$n_i(C_i) = \begin{cases} h^0(C_i, \mathcal{L}|_{C_i}) - b_i & \text{if } h^0(C_i, \mathcal{L}|_{C_i}) \geq b_i \\ 0 & \text{else} \end{cases} \tag{5.5.21}$$

is a lower bound to the number of sections on C_i which satisfy the gluing boundary conditions. The sum of these contributions over all curve components places a lower bound on $h^0(C, \mathcal{L})$:

$$\sum_{i=1}^{N} n_i(C_i) \leq h^0(C, \mathcal{L})\,. \tag{5.5.22}$$

We expect that equality holds in generic situations and that only fairly tuned geometries, in the spirit of [154, 155, 156], will lead to a proper inequality.

As simple demonstration, let us apply this procedure to the geometry discussed in 5.5.1: 5.5.1:

component C_i	$h^0(C_i, \mathcal{L}\|_{C_i})$	b_i	n_i
$V(x_1)$	0	2	0
$V(x_3^2)$	9	6	3
$V(x_5)$	0	2	0
A	0	2	0

Indeed, $\sum_{i=1}^{3} n_i = 3$ in agreement with our discussion in 5.4.1. However, if we apply this counting to $A_3 \cup D_2$, as discussed in 5.5.1, then we find the inequality

$$n_1 + n_2 = (5-2) + 0 = 3 < 4 = h^0(A_3 \cup D_2, \mathcal{L})\,. \tag{5.5.23}$$

This shows that, if we are interested in the exact number rather than a lower bound, we should restrict our counting procedure to curve geometries where neighboring curve components do not support non-trivial sections simultaneously. Furthermore, the geometry studied in 5.5.1 shows that even under this assumption, there are exceptions to this counting procedure. In this case, this can be attributed to a special alignment of the line bundle divisor and the intersection points, such that one of the sections automatically satisfies all of the boundary conditions.

Accuracy on our database

Let us now apply this counting procedure to our database [147] to obtain an estimate of how often the inequality is satisfied. To this end, we need to identify the number of local sections, which can be challenging for complicated curve geometries and could call for an application of, e.g., the exact methods implemented in [146]. However, given the vast number of curve components in our database, we find it more appealing to focus on those curves for which we can identify the number of local sections quicker. To this end, we focus on the following two types of curves:

- Smooth curves:

  We consider the line bundle degree $d = \deg(\mathcal{L}|_{C_i})$. Provided that $d < 0$, we know that $\mathcal{L}|_{C_i}$ does not admit non-trivial sections. Conversely, if $d > 2g(C_i) - 2$, then it follows from application of the Kodaira vanishing theorem, that $h^0(C_i, \mathcal{L}|_{C_i}) = d - g + 1$. If none of these conditions is satisfied, we discard the curve for this test.

- Non-split curves:

  For these curves, we can simply read off the number of local sections from our database.

Based on these local section counts, we have then applied the counting procedure presented in 5.5.2. Recall that a large number of curves in our database do neither consist of smooth curve components nor are non-split. Furthermore, recall that we subject the curve geometry to the condition that neighboring components do not support non-trivial sections simultaneously. Let us emphasize that the latter is a simplifying assumption to simplify our counting procedure. Whilst we leave extensions in this direction to future work, we can still apply our (restricted) counting procedure to roughly 60% of the cases in our database. For these, we predict the correct number of global sections with an accuracy of more than 99%, i.e. our counting procedure works remarkably well. We list the detailed results in B.2.2.

Sufficient conditions for jumps in cohomology

These insights of gluing local sections to form global sections, imply sufficient conditions for jumps in cohomology. First, we have the following

Lemma 5.5.1. *Let S be a smooth surface, $\mathcal{L} \in \mathrm{Pic}(S)$ a line bundle, and $|C|$ a linear system of curves on S. Consider a special member $C_1 \cup C_2$ such that the curves C_1, C_2 meeting transversely in $C_1 \cdot C_2 > 0$ distinct points. Let $N_1 = h^0(C_1, \mathcal{L}|_{C_1})$ and $N_2 = h^0(C_2, \mathcal{L}|_{C_2})$. Then*

$$h^0\left(C_1 \cup C_2, \mathcal{L}\right) \geq N_1 + N_2 - C_1 \cdot C_2\,. \tag{5.5.24}$$

Proof We consider the short exact sequence $0 \to \mathcal{L}|_{C_1 \cup C_2} \to \mathcal{L}|_{C_1 \sqcup C_2} \to \mathcal{L}|_{C_1 \cap C_2} \to 0$. The associated long exact sequence in sheaf cohomology begins with

$$0 \to h^0\left(C_1 \cup C_2, \mathcal{L}|_{C_1 \cup C_2}\right) \to h^0\left(C_1 \sqcup C_2, \mathcal{L}|_{C_1 \sqcup C_2}\right) \to h^0\left(C_1 \cap C_2, \mathcal{L}|_{C_1 \cap C_2}\right) \to \dots \tag{5.5.25}$$

Now, since $h^0(C_1 \sqcup C_2, \mathcal{L}|_{C_1 \sqcup C_2}) = N_1 + N_2$ and $h^0(C_1 \cap C_2, \mathcal{L}|_{C_1 \cap C_2}) = C_1 \cdot C_2$, the statement follows. □

We can use this result, together with the insights on gluing local sections to global sections, to derive the following

Corollary 5.5.2. *Let S be a smooth surface, $\mathcal{L} \in \mathrm{Pic}(S)$ a line bundle, and $|C|$ a linear system of curves on S with smooth general member C and special member $C_1 \cup C_2$ where C_1, C_2 are smooth curves of genera g_1, g_2 meeting transversely in $C_1 \cdot C_2 > 0$ distinct points. We assume $h^1(C, \mathcal{L}|_C) = 0$, $\deg\left(\mathcal{L}|_{C_2}\right) > 2g_2 - 2$ and $\deg\left(\mathcal{L}|_{C_1}\right) < \min\{0, g_1 - 1\}$. Then*

$$h^0\left(C_1 \cup C_2, \mathcal{L}\right) - h^0\left(C, \mathcal{L}\right) \geq g_1 - 1 - \deg\left(\mathcal{L}|_{C_1}\right)\,. \tag{5.5.26}$$

Proof Since $\deg\left(\mathcal{L}|_{C_1}\right) < 0$, there are no sections on C_1. Hence, from 5.5.1 we obtain the inequality

$$h^0\left(C_1 \cup C_2, \mathcal{L}\right) \geq h^0\left(C_2, \mathcal{L}|_{C_2}\right) - C_1 \cdot C_2\,. \tag{5.5.27}$$

Note that $g_C = g_1 + g_2 + C_1 \cdot C_2 - 1$. Consequently, since $\deg\left(\mathcal{L}|_{C_2}\right) > 2g_2 - 2$, we can write

$$\begin{aligned} h^0(C_2, \mathcal{L}|_{C_2}) &= \deg\left(\mathcal{L}|_{C_2}\right) - g_2 + 1 \\ &= \deg\left(\mathcal{L}|_{C_2}\right) - (g_C - g_1 - C_1 \cdot C_2 + 1) + 1 \\ &= \left(\deg\left(\mathcal{L}|_C\right) - g_C + 1\right) + C_1 \cdot C_2 + g_1 - 1 - \deg\left(\mathcal{L}|_{C_1}\right) \\ &= h^0(C, \mathcal{L}|_C) + C_1 \cdot C_2 + g_1 - 1 - \deg\left(\mathcal{L}|_{C_1}\right)\,. \end{aligned} \tag{5.5.28}$$

Hence, we conclude

$$\begin{aligned} & h^0(C_1 \cup C_2, \mathcal{L}) \geq h^0\left(C_2, \mathcal{L}|_{C_2}\right) - C_1 \cdot C_2 = h^0(C, \mathcal{L}|_C) + g_1 - 1 - \deg\left(\mathcal{L}|_{C_1}\right)\,, \\ \Leftrightarrow \quad & h^0(C_1 \cup C_2, \mathcal{L}) - h^0(C, \mathcal{L}|_C) \geq g_1 - 1 - \deg\left(\mathcal{L}|_{C_1}\right)\,. \end{aligned} \tag{5.5.29}$$

Finally, since we assume $\deg\left(\mathcal{L}|_{C_1}\right) < \min\{0, g_1 - 1\}$, the number of additional sections on $C_1 \cup C_2$ is bounded from below by the positive integer $g_1 - \deg\left(\mathcal{L}|_{C_1}\right) - 1$. □

We expect that equality holds in generic situations and that only special setups in the spirit of [154, 155] lead to a proper inequality. Still, our result is powerful enough to give a sufficient condition for a jump. Let us demonstrate this in the geometries discussed in 5.3.1. Recall that we are looking at $S = dP_3$ and

$$D_C = (10; -3, -3, -4)\,, \qquad D_L = (5; -4, -4, 3)\,. \tag{5.5.30}$$

We found that on the genus $g = 24$ curve C it holds $h^1(C, \mathcal{L}|_C) = 0$. Moreover, let

us consider the splitting $C \to C_1 \cup C_2$ where $C_1 = V(x_6)$. These two curves have the following properties:

curve	class	degree	genus	h^0
C_1	(0;0,0,1)	-3	0	0
C_2	(10;-3,-3,-5)	41	20	22

(5.5.31)

From this we see that 5.5.2 applies to this geometry and implies

$$h^0\left(C_1 \cup C_2, \mathcal{L}\right) - h^0\left(C, \mathcal{L}\right) \geq g_1 - 1 - \deg\left(\mathcal{L}|_{C_1}\right) = 0 - 1 - (-3) = 2\,, \tag{5.5.32}$$

This is in agreement with our discussion in 5.3.1.

In many string theory constructions, it is important to engineer exactly one additional vector-like pair. This is particularly true when generating exactly one Higgs pair in MSSM constructions. It is intuitive, that such a minimal change in the vector-like spectrum, requires only mild changes in the geometry. As long as 5.5.2 applies, a necessary condition for such a mild change is to merely split off either a $\mathbb{P}^1$ or a torus — $g_1 \geq 2$ implies $h^0\left(C_1 \cup C_2, \mathcal{L}\right) - h^0\left(C, \mathcal{L}\right) \geq 2$.

More generally, it is of interest to identify the allowed numbers of global sections on a given curve. Therefore, we will now describe an estimate for these values, which is based on the counting procedure presented in 5.5.2, 5.5.1 and 5.5.2.

Algorithmic spectrum estimates

We can use our results to formulate an algorithmic estimate for the vector-like spectrum over the parameter space of a given setup (D_C, D_L) in a global model. For the time being, our algorithm is focused on the case of a curve in dP_3 defined by $\{P = 0\}$ and pullback line bundles on these curves. We have implemented this algorithm in the package *H0Approximator* [148] as part of [146]. Our algorithm proceeds as follows:

1. Input: Curve class D_C and line bundle class D_L

2. Identify all combinations of toric $\mathbb{P}^1$s that can be split off from the curve D_C.

3. Identify the *generic* number of sections of D_L on each curve component.

4. Use the counting procedure presented in 5.5.2 as well as 5.5.1 and 5.5.2 to place a lower bound on the number of global sections.

$\Rightarrow$ The collection of all these global section estimates forms an estimate for h^0 of D_L on the parameter space of the curve D_C.

Let us emphasize a couple of important points of this counting procedure. First, in the second step we do not apply exact methods, such as [146], to find the exact number of local sections. Rather, we identify the generic number of sections, by which we mean $h^0(C, \mathcal{L}) = \chi(\mathcal{L})$ if $\chi(\mathcal{L}) \geq 0$ and $h^0(C, \mathcal{L}) = 0$ otherwise. The advantage of this is, that the chiral index can be obtained from topology only. Hence, the number of global sections can be estimated very quickly. Furthermore, this strategy does not violate our *lower bound philosophy*, since the generic number of sections is never larger than the actual number of sections. Consequently, this strategy allows us to quickly identify a lower bound to the actual number of global sections.

Secondly, let us point out that one disadvantage of our approach of *generic local sections* is that we are unable to identify Brill–Noether jumps on the curve components in this way. However, since such a quick spectrum estimate over the entire parameter space of the curve is currently unfeasible or impossible to obtain with the fully accurate methods, we accept this minor drawback.

Finally, note that upon splitting off $\mathbb{P}^1$s from the curve, the curve could (accidentally) factor further. Computing these further factorizations requires a primary ideal decomposition of the corresponding principal ideal. Currently, this is the most time consuming operation in our algorithm. We reserve optimizations for future work.

This algorithm correctly predicts all the possible values of h^0 for 67 of the 83 pairs (D_C, D_L) in our database [147]. Only for one pair (D_C, D_L), our prediction misses more than 2 values of the exact spectrum. Given the simplicity of our approximation, which means that we cannot detect intricate Brill–Noether jumps and effects discussed in [154, 155], we consider this a very positive result. We list the details in B.2.2.

Let us complete this section by applying our procedure to estimate the vector-like spectrum of the F-theory setup discussed in 5.3. Recall that in this case we are looking at $D_C = (10; -3, -3, -4)$, i.e., a complicated genus 24 curve. The line bundle in this case is $D_L = (5; -4, -4, 3)$. Even though this geometry is fairly involved, our approximator can estimate the spectrum in a couple of minutes[10]. Hence, we have identified 26 curve splittings into irreducible components, for which our counting procedure can estimate the spectrum. Based on this, we expect $h^0 \in \{15, 17, 18, 19, 20, 21\}$. As we know from our analysis in 5.3, indeed $15 \leq h^0 \leq 21$ and $h^0 = 16$ is only possible by a Brill–Noether jump. The latter cannot be predicted by this method. More information on this implementation can be found in [146].

5.6 Conclusion and Outlook

Motivated by a better understanding of the exact massless spectra of 4d F-theory compactifications, we have analyzed in this work families of curves $C(\mathbf{c})$ in a complex surface and line bundles $\mathcal{L}(\mathbf{c})$ on these. Our focus has been on the interplay between changes in the cohomology $h^0(C(\mathbf{c}), \mathcal{L})$ and variations of the parameters $\mathbf{c}$, which play the role of complex structure moduli in the context of global F-theory models. To gain insights on how these two are related, we have used two approaches.

To begin with, we first used ideas from Big data and machine learning to gain some intuitions, based on computationally simpler examples, under what circumstances the cohomology may jump, leading to additional vector-like pairs in the F-theory interpreta-

[10] In this case, this long run time is mostly attributed to the primary decomposition, which we perform to check irreducibility of the curve components.

tion. To this end we have generated, in 5.2, a database [147] of cohomologies for pairs $(C(\mathbf{c}), \mathcal{L}(\mathbf{c}))$ by varying the parameters $\mathbf{c}$, where the curves are of genus $1 \leq g \leq 6$, and the line bundles were pullback bundles from a dP_3 surface. For these less complex examples, the cohomologies can be computed using the computer implementations in [146]. We then use supervised learning on decision trees to predict jumps in the value of h^0. Using different features for training, we find that, while not performing perfectly, topological criteria are surprisingly well-suited (reaching about 95% accuracy) for distinguishing cases with generic vs. enhanced h^0. In particular, the algorithm learns from the data a strong correlation between jumps and curves $C(\mathbf{c})$ which split into various components. This intuition can be applied, without any detailed understanding of the origin of the jumps, directly to find complex structure tunings targeted at generating additional vector-like pairs in F-theory model building. We demonstrate this in 5.3 with an F-theory toy model containing a curve of genus 24, for which a scan over the relevant parameter space would be computationally infeasible. Nevertheless, we found that we can use curve splittings alone to easily engineer 2 to 5 additional vector-like pairs. This highlights the effectiveness of the machine learning approach to learn certain features from simpler examples, and without any previous knowledge. However, we also saw there that by curve splitting alone, a spectrum with just one vector-like pair is impossible to achieve.

To overcome this obstacle, we have employed well-known techniques in algebraic geometry, such as the Koszul resolution and Čech cohomology, which also helps to explain our findings from the machine learning approach in more detail. We conclude that deformations of the parameters $\mathbf{c}$ leading to a jump in cohomology can be largely classified as either the curve $C(\mathbf{c})$ or the line bundle $\mathcal{L}(\mathbf{c})$ becoming non-generic. While the former comes from curve splittings and is thus topological[11], the latter is due to special alignments of the points on $C(\mathbf{c})$ defining $\mathcal{L}(\mathbf{c})$, and not visible just from topological criteria. The fact that the learner performed so well with the topological criteria is due to a bias in the

[11] More generally, a curve can also remain smooth while being non-generic, e.g., if it becomes hyperelliptic. Such transitions are of non-topological nature, and therefore more subtle to detect. We have neglected them for simplicity in our discussions.

dataset, which contains only a small number of instances with non-generic line bundles. Such jumps can never be predicted by the learner based just on split type and intersection numbers. However, as we discussed in 5.4, we find in general "equally likely" jumps due to non-generic line bundles. The likeliness can be quantified by comparing the dimension of the corresponding subspace of the parameter space on which the jumps occur, which for non-generic line bundles is the subject of *Brill–Noether* theory. This is generalized in the F-theoretic setup, where complex structure deformations affect genericity of the curve and line bundle democratically. This leads to a *stratification* of the parameter space by the values of h^0. That is, the complex structure moduli space of global F-theory models decomposes into disjoint subspaces labelled by the vector-like spectrum. The relationship between the strata can be represented by a Hasse-type diagram, which we term h^0*-stratification diagrams*.

The connection between decision trees and the stratification diagrams, which are also Hasse diagrams, is rather intriguing. While they bear some resemblance with decision trees, a key difference is that, unlike in decision trees, nodes can have more than one *incoming* edge. It would be interesting to investigate whether other graph-based machine learning techniques, such as Graph NNs, can be used to train algorithms that can predict the presence of jumps more accurately than the decision trees. Furthermore, recall that global F-theory models typically contain more than one matter curve. The complex structures of these curves are determined by the global moduli of the elliptic fibration, and it is in general not possible to tune the complex structures of all of these curves independently. Therefore, it would be important to extend our analysis to a simultaneous h^0-stratification of the moduli space by all the matter curves in a global F-theory model.

In 5.5, we then investigated the "microscopic" origins of jumps due to curve-splittings. It follows a simple counting procedure of local sections on individual curve components, which we then glue to global contributions to h^0 on the whole curve. The boundary conditions are imposed by the intersection patterns of the components, these can lead

to a net-increase of global sections on the reducible curve compared to the generic case. We have used this understanding to formulate sufficient conditions for a jump in the vector-like spectrum to occur as a result of a curve splitting. These criteria are purely topological, and combine the gluing arguments with vanishing theorems on individual components. Let us stress that this in general provides only a lower bound for h^0 for the split curve, because it does not take into account alignments of the intersection points of the components and divisors on the individual components. It will be interesting to investigate, if these bounds can be further improved by topological considerations.

Despite these simplifications, we found these criteria extremely useful to provide a rough estimate of the possible spectrum of h^0 on the moduli space of F-theory compactifications, and implemented the algorithm in [148]. To fully appreciate this implementation, let us mention that to the best knowledge of the authors, the exact algorithms implemented in[157, 158, 146] do not allow for a parametric cohomology computation. Rather, they will focus on one particular point in the complex structure moduli space and provide the exact answer at this very point. Since each of these computations requires huge amounts of computational resources and runtime, it is impractical to repeat such computations for many points in the complex structure moduli space. In contrast, the new algorithm yields an approximate, but oftentimes sufficiently accurate, estimate — even for complicated examples such as the genus 24 curve discussed in 5.3 — within minutes. We leave generalizations of this counting algorithm, as well as extensions to other toric surfaces, for future work.

Another limitation of our approach is that we have only considered pullback line bundles so far. However, as already alluded to in the introduction, vector-like spectra in F-theory are oftentimes encoded in line bundles described by a formal weighted sum of points. Such a description is computationally harder for two main reasons. First, it takes much longer to compute line bundle cohomologies of non-pullback bundles with the technologies of [146]. This makes it more challenging to generate a sufficiently large database to apply

ideas from Big data and machine learning. The second obstacle is the parametrization of the line bundles. Namely, distinct point configuration can encode equivalent line bundles if their difference is the divisor of a meromorphic function. To have a better handle on tracking how these equivalences change with complex structure deformations, we need a better understanding of meromorphic functions on higher genus curves. The crucial tool in this direction is the *Abel–Jacobi map*, which also plays a similar role in the hyperelliptic curve cryptography. It would be interesting to see to what extent machine learning ideas can be beneficial here.

A related issue arises for *fractional bundles* or *root bundles*. These appear frequently in explicit global F-theory constructions that engineer a three-generation Standard-Model-like particle physics sector [43, 40, 42, 44, 32]. The constraint to have chiral indices with $|\chi| = 3$ in these models lead to line bundles $\mathcal{L}$ on curves C which satisfy $\mathcal{L}^{\otimes n} = L|_C$, where L is a line bundle on the base $\mathcal{B}_3$ of the elliptic fibration. In case $n = 2$ and $L = K_{\mathcal{B}_3}$ is the canonical bundle of the base, the bundle $\mathcal{L}$ can be understood as the pullback of the spin bundle of $\mathcal{B}_3$ to C. However, for general F-theory constructions, also 3rd and higher roots of bundles $\mathcal{L} \neq K_{\mathcal{B}_3}$ appear. An understanding of which line bundles $\mathcal{L}$ on C satisfy such an equation again requires a detailed understanding of which points — in this case the intersection points of C with the divisor on $\mathcal{B}_3$ dual to L — on the curve define equivalent divisors. We expect that this will also be intimately related to satisfying the quantization condition [97] for the gauge flux background.

Finally, it is important to point out that the complex structure parameters of the elliptic fibration are not the only parameters of the physical theory. Rather, a large part of this parameter space which we have not touched upon is in the parametrization of all possible gauge backgrounds. This includes in particular backgrounds with so-called *non-vertical* G_4-flux [159, 160], for which explicit construction methods in global models are largely unknown. While these typically do not contribute to the chiral index, it is not clear at the moment if they could modify the flux-induced line bundles on the matter curves. However,

since non-vertical fluxes contribute prominently to a superpotential for the moduli, their presence will dynamically select points in the moduli space that can be a vacuum for the theory, thus have a very different, but direct influence on the vector-like spectrum. We will therefore need a much better handle on these gauge backgrounds first before we can develop a full understanding for the space of 4d F-theory vacua.

CHAPTER 6: Root bundles in F-Theory and Limit root applications in F-theory

Motivated by the appearance of fractional powers of line bundles in studies of vector-like spectra in 4d F-theory compactifications, we analyze the structure and origin of these bundles. Fractional powers of line bundles are also known as root bundles and can be thought of as generalizations of spin bundles. We explain how these root bundles are linked to inequivalent F-theory gauge potentials of a G_4-flux.

While this observation is interesting in its own right, it is particularly valuable for F-theory Standard Model constructions. In aiming for MSSMs, it is desired to argue for the absence of vector-like exotics. We work out the root bundle constraints on all matter curves in the largest class of currently-known F-theory Standard Model constructions without chiral exotics and gauge coupling unification. On each matter curve, we conduct a systematic "bottom"-analysis of all solutions to the root bundle constraints and all spin bundles. Thereby, we derive a lower bound for the number of combinations of root bundles and spin bundles whose cohomologies satisfy the physical demand of absence of vector-like pairs.

On a technical level, this systematic study is achieved by a well-known diagrammatic description of root bundles on nodal curves. We extend this description by a counting procedure, which determines the cohomologies of so-called limit root bundles on full blow-ups of nodal curves. By use of deformation theory, these results constrain the vector-like spectra on the smooth matter curves in the actual F-theory geometry.

6.1 Introduction

String theory elegantly couples gauge dynamics to gravity. This makes string theory a leading candidate for a unified theory of quantum gravity. As such, it must account for all aspects of our physical reality, especially the low energy particle physics that we observe. As a first order approximation, one desires an explicit demonstration in which one can actually obtain the particle spectrum of the Standard Model from string theory.

In the past decades, enormous efforts have been undertaken to achieve this goal. Many of these models concentrated on perturbative corners of string theory, such as the $E_8 \times E_8$ heterotic string [13, 161, 109, 110, 124, 162, 163, 108] or intersecting branes models in type II [17, 18, 19, 20, 21, 22, 23] (see also [24] and references therein). These perturbative models were among the first compactifications from which the Standard Model gauge sector emerged with its chiral or, in the case of [110, 124], even the vector-like spectrum. Unfortunately, these constructions are limited due to their perturbative nature in the string coupling, and they typically suffer from chiral and vector-like exotic matter. Among these perturbative models, the first globally consistent MSSM constructions are [110, 124] (see [164, 165] for more details on the subtle global conditions for slope-stability of vector bundles).

The non-perturbative effects in string theory are elegantly described by F-theory [27, 166, 167]. As a non-perturbative extension of type IIB string theory, the framework of F-theory describes the gauge dynamics on 7-branes *including* their back-reactions (to all orders in the string coupling) onto the compactification geometry B_n. These back-reactions are encoded in the geometry of an elliptically fibered Calabi-Yau space $\pi\colon Y_{n+1} \twoheadrightarrow B_n$. By studying this space Y_{n+1} with well-established tools of algebraic geometry, one can then ensure the global consistency conditions of the physics in $10-2n$ non-compact dimensions.

An important characteristic of 4d $\mathcal{N} = 1$ F theory compactifications (i.e., $n = 3$), which must match the particle physics that we observe, is the chiral fermionic spectrum. In F-theory, this spectrum is uniquely fixed by a background gauge flux, which in turn is most conveniently specified by the internal C_3 profile in the dual M-theory geometry. The chiral spectrum then only depends on the flux $G_4 = dC_3 \in H^{(2,2)}(Y_4)$. By now, there exists an extensive toolbox for creating and enumerating the so-called primary vertical subspace of G_4 configurations [131, 37, 38, 39, 40, 41, 42]. The application of these tools led to the construction of globally consistent chiral F-theory models [43, 40, 42, 44], which recently culminated in the largest class of explicit string vacua that realize the Standard

Model gauge group with their exact chiral spectrum and gauge coupling unification [32].

However, these methods are insufficient to determine the exact vector-like spectrum of the chiral zero modes (i.e., not just the difference between chiral and anti-chiral fields). This is because the zero modes depend not only on the flux G_4, but also on the flat directions of the potential C_3. The complete information is encoded in the so-called *Deligne cohomology*. In[45, 46, 47], methods for determining the exact vector-like spectra were put forward. This approach exploits the fact that (a subset of) the Deligne cohomology can be parameterized by Chow classes. By use of this parameterization, one can extract line bundles $L_{\mathbf{R}}$ that are defined on curves $C_{\mathbf{R}}$ in B_3. In the dual IIB picture, this can be interpreted as localization of gauge flux on matter curves, which lifts some vector-like pairs on these curves. Explicitly, the zero modes are counted by the sheaf cohomologies of $L_{\mathbf{R}}$ and we have $h^0(C_{\mathbf{R}}, L_{\mathbf{R}})$ massless chiral and $h^1(C_{\mathbf{R}}, L_{\mathbf{R}})$ massless anti-chiral superfields in representation $\mathbf{R}$ on $C_{\mathbf{R}}$.

Although this procedure works in theory for any compactification, technical limitations arise in practical applications. Intuitively, one may think of the technical difficulties as reflections of the delicate complex structure dependence of the line bundles cohomologies. Even state-of-the-art algorithms such as [168, 157, 169] (see also [46, 47]) on supercomputers specifically designed for such computations (such as `Plesken` at *Siegen University*), can oftentimes not perform the necessary operations in realistic compactification geometries. For instance, the models studied in [45, 46, 47] focused on computationally simple geometries as a result. While this led to a proof of principle, these models have unrealistically large numbers of chiral fermions. Therefore — even though it is expected — it remains an open question whether or not F-theory compactifications can actually realize effective theories that resemble the matter spectra of the Standard Model.

Recently, [48] the complex structure dependence of line bundle cohomologies was investigated . This analysis was inspired from the F-theory GUT models discussed in [47] and focused on simple geometries, in which the algorithms in [168] could generate a

large data set [147]. This data was analyzed by use of data science techniques, in particular decision trees. A theoretical understanding of this data was achieved by supplementing the data science results by Brill-Noether theory [150] (see [156] for a modern exposition and [128] for an earlier application of Brill-Noether theory in F-theory). These insights led to a quantitative study of jumps of charged matter vector pairs as a function of the complex structure parameters of the matter curves.

Results In globally consistent F-theory constructions with the exact chiral spectra of the Standard Model and gauge coupling unification [32], the vector-like spectra on the low-genus matter curves are encoded in cohomologies of a line bundle, which are identified with a fractional power of the canonical bundle. On high-genus curves, these fractional powers of the canonical bundle are further modified by contributions from Yukawa points.

In order to make sense of these fractional powers, we study the G_4-flux in more detail. The models in [32] consider a background G_4-flux, which not only leads to the exact chiral spectra but also satisfies global consistency conditions, such as the D3-tadpole cancelation and masslessness of the $U(1)$-gauge boson. We lift this very background G_4-flux to a gauge potential in the *Deligne cohomology* to identify the line bundles $L_{\mathbf{R}}$. This process requires an understanding of the intermediate Jacobian $J^2(Y_4)$, which labels inequivalent gauge backgrounds. A naive analysis, which does not properly take the intermediate Jacobian into account, leads to the fractional line bundle powers mentioned above. In past works [45, 46, 47], such scenarios were avoided as it is not immediately clear how to interpret these fractional expressions. However, since these expressions appear ubiquitously in compact models with realistic chiral indices, this work analyzes the origin and meaning of these bundles in detail.

The objects we are therefore interested in are fractional powers of line bundles, also known as root bundles. They may be thought of as generalizations of spin bundles. Similar to spin bundles, root bundles are far from unique. The mathematics of root bundles indicates that we should think of the different root bundles as being induced from inequivalent gauge

potentials for a given G_4-flux. While [45, 46, 47] has already anticipated that inequivalent gauge potentials for a given G_4-flux lead to different vector-like spectra, the root bundle interpretation allows one to test this expectation.

In general, not all root bundles on the matter curves are induced from F-theory gauge potentials in the Deligne cohomology $H^4_D(\widehat{Y}_4, \mathbb{Z}(2))$. This mirrors the expectation that only some of the spin bundles on the matter curves are consistent with the F-theory geometry $\widehat{Y}_4$. This raises the interesting and important question of identifying which roots and spin bundles are induced top-down. While this work does not answer this question, we hope that it initiates and facilitates this analysis by providing a systematic approach to all root bundles and spin bundles on the matter curves. In particular, we identify pairs of root bundles and spin bundles such that their tensor product is a line bundle whose cohomologies satisfy the physical demand of the presence/absence of vector-like pairs.

On a technical level, this requires a sufficient understanding of root bundles and their cohomologies on a matter curve $C_{\mathbf{R}}$. We gain this control from a deformation $C_{\mathbf{R}} \to C^{\bullet}_{\mathbf{R}}$ into a nodal curve. On the latter, root bundles are described in a diagrammatic way by so-called *limit roots* [170]. We extend these ideas to a counting procedure for the global sections of limit roots, which we use to infer the cohomologies of root bundles on $C_{\mathbf{R}}$. This approach is demonstrated in the largest class of currently-known constructions of globally consistent F-theory Standard Models without chiral exotics and gauge coupling unification [32]. In one particular such geometry, we derive a lower bound to the number of pairs of root bundles and spin bundles whose tensor product is a line bundle without vector-like exotics.

Outline In 6.2, we recall zero mode counting in F-theory and the appearance of fractional line bundle powers. We explain that these fractional powers of line bundles, also known as root bundles, relate to inequivalent gauge potentials in F-theory. These ideas are subsequently applied to the largest currently-known family of globally consistent F-theory Standard Model constructions without chiral exotics and gauge coupling unification [32].

We explain how the background G_4-flux, which satisfies global consistency conditions such as the cancellation of the D3-tadpole and the masslessness of the $U(1)$-gauge boson, induces root bundles on the matter curves. Details of this derivation are summarized in C.2. This derivation heavily relies on a detailed understanding of the elliptically fibered 4-fold F-theory geometry $\widehat{Y}_4$, including intersection numbers in the fiber over the Yukawa points. We supplement the earlier works [82, 40, 32] with a complete list of all fiber intersection numbers in C.1.

In 6.3 we first summarize well-known results about root bundles before we describe the limit root constructions, which were originally introduced in [170]. We extend the limit root constructions by a counting procedure for the global sections of limit roots on full blow-ups of nodal curves. In fortunate instances, this even provides a means to explore *Brill-Noether theory* of *limit roots*, which we demonstrate in an example inspired from [171].

Finally, we apply these ideas to globally consistent constructions of F-theory Standard Models without chiral exotics and gauge coupling unification [32] in 6.4. In an explicit base space geometry, we deform the matter curves to nodal curves, construct limit roots on these nodal curves, identify the number of global sections of these limit roots and finally use deformation theory to relate these counts to the cohomologies of root bundles in the actual F-theory geometry. Thereby, we explicitly prove the existence of root bundle solutions without vector-like pairs. Technical details of the specific base geometry and the limit root constructions are summarized in C.2.4.

6.2 Root bundles in F-theory

6.2.1 The appearance of root bundles

Zero mode counting in F-theory We consider an F-theory compactification to four dimensions given by a singular, elliptically fibered 4-fold $\pi\colon Y_4 \twoheadrightarrow B_3$. We assume that this fibration has a section $s \cong B_3$ and admits a smooth, flat, crepant resolution $\widehat{\pi}\colon \widehat{Y_4} \twoheadrightarrow$

B_3. In such a compactification, the flux $G_4 \in H^{(2,2)}(\widehat{Y}_4)$ is subject to the quantization condition [97]

$$G_4 + \frac{1}{2}c_2(T_{\widehat{Y}_4}) \in H^{(2,2)}_{\mathbb{Z}}(\widehat{Y}_4) = H^{(2,2)}(\widehat{Y}_4) \cap H^4(\widehat{Y}_4, \mathbb{Z})\,. \tag{6.2.1}$$

For simplicity, we focus on compactifications with even $c_2(T_{\widehat{Y}_4})$, which holds true for F-theory compactifications on an elliptically fibered smooth Calabi-Yau 4-fold with globally defined Weierstrass model [111].[1] Under the simplifying assumption that $c_2(T_{\widehat{Y}_4})$ is even, 6.2.1 requires that $G_4 \in H^{(2,2)}_{\mathbb{Z}}(\widehat{Y}_4)$. We will show an example of this and the following root bundle analysis in the largest currently-known class of F-theory Standard Model constructions with gauge coupling unification and no chiral exotics [32] in 6.2.2.

Over the codimension-2 matter curves $C_{\mathbf{R}} \subseteq B_3$, the reducible fibers of $\widehat{Y}_4$ contain a chain of $\mathbb{P}^1$s. A state with weight $\mathbf{w}$ in the representation $\mathbf{R}$ corresponds to a linear combination of these $\mathbb{P}^1$'s. By fibering this linear combination over the matter curve $C_{\mathbf{R}}$, one obtains the matter surface $S_{\mathbf{R}}$.[2] The chiral index of the massless matter localized on the matter curve $C_{\mathbf{R}} \subseteq B_3$ is then specified by [59, 172, 173, 174, 130, 36, 129] [43, 37, 112] as

$$\chi\,(\mathbf{R}) = \int\limits_{S_{\mathbf{R}}} G_4\,. \tag{6.2.2}$$

The vector-like spectrum induced by a G_4-flux has been analyzed in [45, 46, 47]. We employ the short exact sequence

$$0 \to J^2(\widehat{Y}_4) \hookrightarrow \iota H^4_D(\widehat{Y}_4, \mathbb{Z}(2)) \to \widehat{c}H^{(2,2)}_{\mathbb{Z}}(\widehat{Y}_4) \to 0\,, \tag{6.2.3}$$

where there exists a surjection $\widehat{c}$ that maps the gauge potential $A \in H^4_D(\widehat{Y}_4, \mathbb{Z}(2))$ as an element of the Deligne cohomology group to its G_4-flux. The Deligne cohomology classes

[1] For zero mode counting of half-integer quantized G_4-fluxes, see e.g. [45].

[2] In general, a G_4-flux can induce different chiral indices and vector-like spectra on the different weight states. In such instances, it makes sense to keep track of $\mathbf{w}$ and write $S^{\mathbf{w}}_{\mathbf{R}}$. However, in anticipation of [32], we focus on gauge invariant G_4-fluxes, which induce the same chiral index and vector-like spectra for all weight states.

encode the full gauge background data. Therefore, they parallel the internal 3-form potentials C_3 in the dual M-theory picture in which $G_4 = dC_3$. As long as $C_3' - C_3$ is a closed 3-form, C_3' has the same field strength G_4 as C_3. In F-theory, such closed 3-form potentials are encoded by the intermediate Jacobian. Put differently, two inequivalent $A', A \in H_D^4(\widehat{Y}_4, \mathbb{Z}(2))$ with $\widehat{c}(A') = \widehat{c}(A) = G_4$ differ by $A' - A = \iota(B)$, where $B \in J^2(\widehat{Y}_4)$ is an element of the intermediate Jacobian corresponding to a closed M-theory 3-form potential.[3]

The Deligne cohomology group $H_D^4(\widehat{Y}_4, \mathbb{Z}(2))$ is hard to handle in explicit computations. However, we can parametrize (at least a subset of) $H_D^4(\widehat{Y}_4, \mathbb{Z}(2))$ by the Chow group $\mathrm{CH}^2(\widehat{Y}_4, \mathbb{Z})$. This is summarized in the commutative diagram[4]

$$\begin{array}{ccccccccc} 0 & \longrightarrow & \mathrm{CH}^2_{\mathrm{hom}}(\widehat{Y}_4, \mathbb{Z}) & \longrightarrow & \mathrm{CH}^2(\widehat{Y}_4, \mathbb{Z}) & \xrightarrow{\gamma} & H^{(2,2)}_{\mathrm{alg}}(\widehat{Y}_4) & \longrightarrow & 0 \\ & & \downarrow & & \downarrow \widehat{\gamma} & & \downarrow & & \\ 0 & \longrightarrow & J^2(\widehat{Y}_4) & \longrightarrow & H_D^4(\widehat{Y}_4, \mathbb{Z}(2)) & \xrightarrow{\widehat{c}} & H^{(2,2)}_{\mathbb{Z}}(\widehat{Y}_4) & \longrightarrow & 0 \end{array} \tag{6.2.4}$$

Unless stated differently, the symbol $\mathcal{A}$ is reserved for an element $\mathcal{A} \in \mathrm{CH}^2(\widehat{Y}_4, \mathbb{Z})$, by which we specify an F-theory gauge potential $A = \widehat{\gamma}(\mathcal{A})$.

In order to count the zero modes in representation $\mathbf{R}$ in the presence of such a gauge potential $\widehat{\gamma}(\mathcal{A}) \in H_D^4(\widehat{Y}_4, \mathbb{Z}(2))$, we consider the matter surface $S_{\mathbf{R}}$ with

$$\iota_{S_{\mathbf{R}}} \colon S_{\mathbf{R}} \hookrightarrow \widehat{Y}_4 \,, \qquad \pi_{S_{\mathbf{R}}} \colon S_{\mathbf{R}} \twoheadrightarrow C_{\mathbf{R}} \,. \tag{6.2.5}$$

The cylinder map, which sends $\mathcal{A} \in \mathrm{CH}^2(\widehat{Y}_4, \mathbb{Z})$ to a class $D_R(\mathcal{A}) \in \mathrm{Pic}\,(C_{\mathbf{R}})$, is the restriction to S_R followed by integration over the fibers to C_R:

$$D_{\mathbf{R}}\,(\mathcal{A}) = \pi_{S_{\mathbf{R}}*}\left(\iota^*_{S_{\mathbf{R}}}\,(\mathcal{A})\right) \in \mathrm{Pic}\,(C_{\mathbf{R}})\ . \tag{6.2.6}$$

[3] Equivalently, different gauge potentials in $H_D^4(\widehat{Y}_4, \mathbb{Z}(2))$ differ by their Wilson lines [175, 176].
[4] For more details, see [45] and references therein.

The matter spectrum is then determined in terms of sheaf cohomology groups:

$$\begin{aligned} h^0\left(C_{\mathbf{R}}, L_{\mathbf{R}}\left(\mathcal{A}\right)\right) &\quad\leftrightarrow\quad \text{chiral zero modes}\,, \\ h^1\left(C_{\mathbf{R}}, L_{\mathbf{R}}\left(\mathcal{A}\right)\right) &\quad\leftrightarrow\quad \text{anti-chiral zero modes}\,, \end{aligned} \tag{6.2.7}$$

where

$$L_{\mathbf{R}}\left(\mathcal{A}\right) = \mathcal{O}_{C_{\mathbf{R}}}\left(D_{\mathbf{R}}\left(\mathcal{A}\right)\right) \otimes_{\mathcal{O}_{C_{\mathbf{R}}}} \mathcal{O}_{C_{\mathbf{R}}}^{\text{spin}}\,, \tag{6.2.8}$$

with $\mathcal{O}_{C_{\mathbf{R}}}^{\text{spin}}$ an appropriate spin bundle on $C_{\mathbf{R}}$. This is a refinement of 6.2.2, since Riemann-Roch gives

$$\chi(\mathbf{R}) = h^0\left(C_{\mathbf{R}}, L_{\mathbf{R}}\left(\mathcal{A}\right)\right) - h^1\left(C_{\mathbf{R}}, L_{\mathbf{R}}\left(\mathcal{A}\right)\right) = \chi\left(L_{\mathbf{R}}(\mathcal{A})\right) = deg\left(D_{\mathbf{R}}(\mathcal{A})\right) = \int_{S_{\mathbf{R}}} G_4. \tag{6.2.9}$$

Roots of F-theory gauge potentials For an F-theory model, we need an F-theory gauge potential, i.e. a class in the Deligne cohomology group $H_D^4(\widehat{Y}_4, \mathbb{Z}(2))$. This will be specified as $\widehat{\gamma}(\mathcal{A})$ for some "potential" $\mathcal{A} \in \mathrm{CH}^2(\widehat{Y}_4, \mathbb{Z})$. We find that the geometry determines a class $\widehat{\gamma}(\mathcal{A}') \in H_D^4(\widehat{Y}_4, \mathbb{Z}(2))$ and an integer $\xi \in \mathbb{Z}_{>0}$ such that $\mathcal{A}$ is subject to the two constraints:

$$\gamma(\mathcal{A}) = G_4\,, \qquad \xi \cdot \widehat{\gamma}(\mathcal{A}) \sim \widehat{\gamma}(\mathcal{A}')\,. \tag{6.2.10}$$

The condition $\gamma(\mathcal{A}) = G_4$ immediately follows from 6.2.4 and it means that $\widehat{\gamma}(\mathcal{A})$ is an F-theory gauge potential for the given G_4-flux. We will illustrate with several examples below that the absence of chiral exotics in the F-theory Standard Models boils down to the second constraint. It is important to notice that the gauge potential $\mathcal{A}$ specified by the two conditions in 6.2.10 is in general not unique. It is difficult to say much about solutions in the Chow group itself, but going to the bottom row in 6.2.4, we see that the collection of all ξ-th roots of $\widehat{\gamma}(\mathcal{A}')$ (if non empty) is a coset of the group of all ξ-th roots of 0. In particular, the number of solutions is $\xi^{2\cdot\dim_{\mathbb{C}}\left(J^2(\widehat{Y}_4)\right)}$.

All these solutions lead to the same chiral spectrum 6.2.2, since they all have the same degree when restricted to the curves $C_{\mathbf{R}}$, hence the same index. However, they could differ in their actual spectrum 6.2.7. This extra flexibility is the key tool that we intend to use to produce a desirable spectrum such as the MSSM.

Roots on the matter curves In theory, we could simply analyze the algebraic cycles $\mathcal{A}$ which satisfy 6.2.10. However, as we will demonstrate momentarily, we can explicitly construct $\mathcal{A}' \in \mathrm{CH}^2(\widehat{Y}_4, \mathbb{Z})$. Therefore, we have a sufficient level of arithmetic control over $\widehat{\gamma}(\mathcal{A}')$ and it is natural to ask how the induced divisors $D_{\mathbf{R}}(\mathcal{A}')$ and $D_{\mathbf{R}}(\mathcal{A})$ are related. The map $D_{\mathbf{R}} \colon \mathrm{CH}^2(\widehat{Y}_4, \mathbb{Z}) \to \mathrm{CH}^1(C_{\mathbf{R}}, \mathbb{Z}) \cong \mathrm{Pic}(C_{\mathbf{R}})$, as defined in 6.2.6, factors through $\widehat{\gamma}$ and a group homomorphism

$$H^4_D(\widehat{Y}_4, \mathbb{Z}(2)) \to \mathrm{Pic}(C_{\mathbf{R}})\,. \tag{6.2.11}$$

Thus, it follows that

$$\xi \cdot D_{\mathbf{R}}(\mathcal{A}) \sim D_{\mathbf{R}}(\mathcal{A}') \in \mathrm{Pic}(C_{\mathbf{R}})\,. \tag{6.2.12}$$

This means that the F-theory gauge potential $A = \widehat{\gamma}(\mathcal{A})$ induces *a* divisor $D_{\mathbf{R}}(\mathcal{A})$, whose ξ-th multiple is linearly equivalent to the divisor $D_{\mathbf{R}}(\mathcal{A}')$ that is induced by the F-theory gauge potential $A' = \widehat{\gamma}(\mathcal{A}') \in H^4_D(\widehat{Y}_4, \mathbb{Z}(2))$. Such a divisor $D_{\mathbf{R}}(\mathcal{A})$ is termed a ξ-th root of $D_{\mathbf{R}}(\mathcal{A}')$.

In general, ξ-th roots of $D_{\mathbf{R}}(\mathcal{A}')$ do not exist. When they do, they are not unique. This is particularly well known for the case $\xi = 2$ and $D_{\mathbf{R}}(\mathcal{A}') = K_{\mathbf{R}}$, where the 2nd roots of the canonical bundle are the spin structures on $C_{\mathbf{R}}$. If $C_{\mathbf{R}}$ is a curve of genus g, then it admits 2^{2g} spin structures (see e.g. [177, 178]). This easily extends to $\xi > 2$ and $D_{\mathbf{R}}(\mathcal{A}') \neq K_{\mathbf{R}}$. While we will provide more details on root bundles in 6.3.1, it suffices to state here that ξ-th roots of $D_{\mathbf{R}}(\mathcal{A}')$ do exist if and only if ξ divides $\deg(D_{\mathbf{R}}(\mathcal{A}'))$. So on a genus g curve, there exist ξ^{2g} ξ-th roots of $D_{\mathbf{R}}(\mathcal{A}')$.

In general, it cannot be expected that ξ-th roots of $D_{\mathbf{R}}(\mathcal{A}') \in \mathrm{Pic}(C_{\mathbf{R}})$ and ξ-th roots of $A' = \widehat{\gamma}(\mathcal{A}') \in H^4_D(\widehat{Y}_4, \mathbb{Z}(2))$ are one-to-one. Rather, only a subset of the ξ-th roots of $D_{\mathbf{R}}(\mathcal{A}')$ will be realized from F-theory gauge potentials in $H^4_D(\widehat{Y}_4, \mathbb{Z}(2))$. In this sense, the root bundle constraint in 6.2.12 is necessary but not sufficient to conclude that the divisor $D_{\mathbf{R}}(\mathcal{A})$ stems from an F-theory gauge potential.

It is an interesting question to investigate which roots of $D_{\mathbf{R}}(\mathcal{A}') \in \mathrm{Pic}(C_{\mathbf{R}})$ are induced from F-theory gauge potentials. While this work does not answer this question, we hope to initiate and facilitate this study by providing a systematic approach to all ξ-th roots of $D_{\mathbf{R}}(\mathcal{A}')$. In particular, we will provide a counting procedure, which allows one to infer the cohomologies of some of these root bundles. This allows one to search for roots which satisfy the physical demand of the presence/absence of vector-like pairs.

Before we show an example of these notions in the F-theory Standard Models [32], let us briefly comment on spin bundles $\mathcal{O}^{\mathrm{spin}}_{C_{\mathbf{R}}}$. Recall that Freed-Witten anomaly cancelation requires spin^c-structures on $D7$-branes in perturbative IIB-compactifications [179]. As explained in [60], this extends to the demand of spin^c-structures on gauge surfaces $S \subset B_3$ in F-theory compactifications. Then, a choice of spin^c-structure on $N_{C_{\mathbf{R}}|S}$ induces a unique spin^c-structure on $C_{\mathbf{R}}$ [180]. Therefore, the question of which spin^c-structures are realized from the F-theory geometry $\widehat{Y}_4$ arises. While this is a fascinating question, we will not answer it in this work. Rather, we will systematically study all ξ-th roots of $D_{\mathbf{R}}(\mathcal{A}')$ and all spin bundles on $C_{\mathbf{R}}$. Our goal is to identify combinations of root and spin bundles such that their tensor product is a line bundle whose cohomologies satisfy the physical demand of presence/absence of vector-like pairs.

6.2.2 Root bundles in F-theory Standard Models

We will now exhibit an example of the root bundle analysis in the largest class of currently-known globally consistent F-theory Standard Model constructions that support gauge coupling unification and avoid chiral exotics [32]. Earlier geometric details can be found in the works [82, 40]. For convenience, we briefly summarize the geometry before we

discuss the G_4-flux and its lifts.

The analysis of the induced line bundles, i.e., evaluating 6.2.6, is both tedious and lengthy. It makes use of the intersection numbers in the fibers over the matter curves and Yukawa points. As an extension of the past works on this class of F-theory geometries, we list exhaustive details of the fiber geometry in C.1. The necessary intersection computations are detailed in C.2. The latter includes a section on topological intersection numbers of non-complete intersections, which we determine rigorously from the Euler characteristic of the structure sheaf of the intersection variety.

The resolved elliptic fibration $\widehat{\mathbf{Y}}_\mathbf{4}$

4-fold geometry For a base 3-fold B_3, the resolved elliptic fibration $\widehat{Y}_4$ is a hypersurface in the space $X_5 = B_3 \times \mathbb{P}_{F_{11}}$. The fiber ambient space $\mathbb{P}_{F_{11}}$ is the toric surface with the following toric diagram. In the accompanying table, we indicate its $\mathbb{Z}^6$-graded Cox ring:

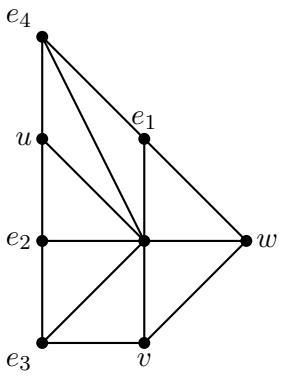

	u	v	w	e_1	e_2	e_3	e_4
H	1	1	1				
E_1	-1		-1	1			
E_2	-1	-1			1		
E_3		-1			-1	1	
E_4	-1			-1			1

(6.2.13)

Equivalently, the Stanley-Reisner ideal of $\mathbb{P}_{F_{11}}$ is given by

$$I_{\mathrm{SR}}\left(\mathbb{P}_{F_{11}}\right) = \langle e_4 w, e_4 e_2, e_4 e_3, e_4 v, e_1 u, e_1 e_2, e_1 e_3, e_1 v, wu, we_2, we_3, ve_2, uv, e_3 u\rangle\,. \quad (6.2.14)$$

Consider sections $s_i \in H^0(B_3, \overline{K}_{B_3})$. Then, in the space X_5, the resolved 4-fold $\widehat{Y}_4$ is the hypersurface $V(p_{F_{11}})$ with

$$\begin{aligned} p_{F_{11}} = s_1 e_1^2 e_2^2 e_3 e_4^4 u^3 + s_2 e_1 e_2^2 e_3^2 e_4^2 u^2 v + s_3 e_2^2 e_3^3 u v^2 + s_5 e_1^2 e_2 e_4^3 u^2 w \\ + s_6 e_1 e_2 e_3 e_4 u v w + s_9 e_1 v w^2 \,. \end{aligned} \tag{6.2.15}$$

It is instructive to note that

$$\left\{ e_1^2 e_2^2 e_3 e_4^4 u^3, e_1 e_2^2 e_3^2 e_4^2 u^2 v, e_2^2 e_3^3 u v^2, e_1^2 e_2 e_4^3 u^2 w, e_1 e_2 e_3 e_4 u v w, e_1 v w^2 \right\} \tag{6.2.16}$$

is a basis of $H^0\left(\mathbb{P}_{F_{11}}, \overline{K}_{\mathbb{P}_{F_{11}}}\right)$. Since $X_5 = B_3 \times \mathbb{P}_{F_{11}}$ and $s_i \in H^0(B_3, \overline{K}_{B_3})$, it follows from the Künneth-formula that $p_{F_{11}}$ is a section of $\overline{K}_{X_5}$. Consequently, $\widehat{Y}_4$ is a smooth elliptically fibered Calabi-Yau 4-fold.

Gauge group, matter curves and Yukawa points Over $V(s_3) = \{s_3 = 0\} \subset B_3$, the fibration $\widehat{Y}_4$ admits an $SU(2)$ gauge enhancement. Similarly, there is an $SU(3)$ enhancement over $V(s_9)$. The fibration $\widehat{\pi}\colon \widehat{Y}_4 \twoheadrightarrow B_3$ admits two independent sections $s_0 = V(v)$ and $s_1 = V(e_4)$. We call $s_0 = V(v)$ the zero section and employ the Shioda map to associate a $U(1)$-gauge symmetry to s_1. Consequently, $\widehat{Y}_4$ admits an $SU(3) \times SU(2) \times U(1)$ gauge symmetry with zero section $s_0 = V(v)$.

We label the matter curves by the representations of $SU(3) \times SU(2) \times U(1)$ in which the zero modes, localized on these curves, transform:

$$C_{(\mathbf{3},\mathbf{2})_{1/6}} = V(s_3, s_9)\,, \qquad C_{(\mathbf{1},\mathbf{2})_{-1/2}} = V\left(s_3, s_2 s_5^2 + s_1(s_1 s_9 - s_5 s_6)\right)\,, \tag{6.2.17}$$

$$C_{(\overline{\mathbf{3}},\mathbf{1})_{-2/3}} = V(s_5, s_9)\,, \qquad C_{(\overline{\mathbf{3}},\mathbf{1})_{1/3}} = V\left(s_9, s_3 s_5^2 + s_6(s_1 s_6 - s_2 s_5)\right)\,, \tag{6.2.18}$$

$$C_{(\mathbf{1},\mathbf{1})_1} = V(s_1, s_5)\,. \tag{6.2.19}$$

These curves intersect in the Yukawa loci

$$Y_1 = V(s_3, s_5, s_9)\,, \qquad Y_2 = V(s_3, s_9, s_2 s_5 - s_1 s_6)\,, \qquad Y_3 = V(s_3, s_6, s_9)\,, \tag{6.2.20}$$

$$Y_4 = V(s_1, s_3, s_5)\,, \qquad Y_5 = V(s_9, s_5, s_6^2)\,, \qquad Y_6 = V(s_1, s_5, s_9)\,. \tag{6.2.21}$$

We represent the intersections among the matter curves including the physically relevant self-intersections as follows:

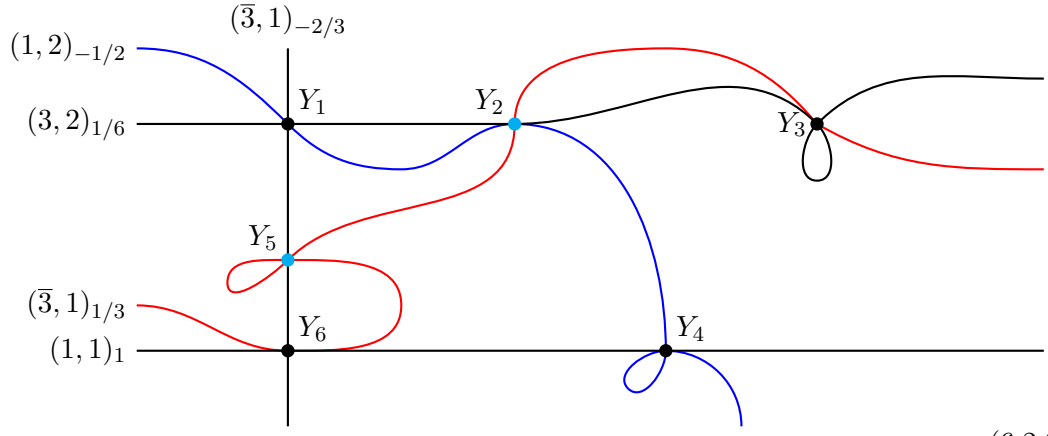

(6.2.22)

The topological intersection number is $\overline{K}^3_{B_3}$ at Y_1, Y_3, Y_4, Y_6 and $2\cdot\overline{K}^3_{B_3}$ at Y_2, Y_5.

G_4-flux

Let us identify the root bundles whose sections count the localized zero modes in the presence of the (candidate) G_4-flux introduced in [32]. This flux is a *base dependent* linear combination of the $U(1)$-flux $\omega\wedge\sigma$, where σ is the Shioda $(1,1)$-form associated to the divisor $s_1 = V(e_4)$, and of the matter surface flux $G_4^{(\mathbf{3},\mathbf{2})_{1/6}}$ on the curve $C_{(\mathbf{3},\mathbf{2})_{1/6}}$:

$$G_4(a,\omega) = a\cdot G_4^{(\mathbf{3},\mathbf{2})_{1/6}} + \omega\wedge\sigma \in H^{(2,2)}_{\text{alg}}(\widehat{Y}_4)\,. \tag{6.2.23}$$

The parameters $a\in\mathbb{Q}$ and $\omega\in\pi^*\left(H^{(1,1)}(B_3)\right)$ are subjected to flux quantization, D_3-tadpole cancelation, masslessness of the $U(1)$-gauge boson, and exactly three chiral families on all matter curves. These conditions are solved by

$$\omega = \frac{3}{\overline{K}^3_{B_3}}\cdot\overline{K}_{B_3}\,, \qquad a = \frac{15}{\overline{K}^3_{B_3}}\,. \tag{6.2.24}$$

Explicitly, the resulting flux candidate can be expressed as (see C.2.1 for details)

$$G_4 = \frac{-3}{\overline{K}_B^3}\cdot\Big(5[e_1]\wedge[e_4] \\ + \widehat{\pi}^*\left(\overline{K}_B\right)\wedge\left(-3[e_1]-2[e_2]-6[e_4]+\widehat{\pi}^*\left(\overline{K}_B\right)-4\,[u]+[v]\right)\Big)\Big|_{\widehat{Y}_4}\,. \tag{6.2.25}$$

In this expression, $[e_1]=\gamma(V(e_1))\in H^{(1,1)}_{\text{alg}}(X_5)$ is the image of the divisor $V(e_1)\subseteq X_5$ under the cycle map γ. Also, we use the projection map $\widehat{\pi}\colon \widehat{Y}_4 \twoheadrightarrow B_3$. This G_4-flux candidate cancels the D3-tadpole and ensures the masslessness of a $U(1)$-gauge boson.

We must verify that the G_4-flux candidate in 6.2.25 satisfies the flux quantization $G_4+\frac{1}{2}c_2(T_{\widehat{Y}_4})\in H^{(2,2)}_{\mathbb{Z}}(\widehat{Y}_4)$[97]. As a necessary check, in [32], the integrals of $G_4+\frac{1}{2}c_2(T_{\widehat{Y}_4})$ over all matter surfaces $S_{\mathbf{R}}$ and complete intersections of toric divisors were worked out. By employing the results in [111, 181], these were found to be integral. A sufficient check for 6.2.25 to be properly quantized is computationally very demanding and currently beyond our arithmetic abilities. Therefore, the authors of [32] proceeded under the assumption that this candidate G_4-flux is properly quantized. We will also follow this line of thought.

Furthermore, we slightly extend this result. Namely, we integrate only $c_2(T_{\widehat{Y}_4})$ over the matter surfaces and over the complete intersections of toric divisors. By the reduction technique in [42], we can relate these integrals to intersection numbers in the base $\mathcal{B}_3$. An explicit computation reveals that the only quantities which are not manifestly even are

$$\int_{B_3} c_2(B)\wedge\overline{K}_B\,, \qquad \int_{B_3}\alpha\wedge(c_2(B_3)+\overline{K}_B^2)\ \text{ for all }\ \alpha\in H^{1,1}(B_3,\mathbb{Z})\,, \tag{6.2.26}$$

where $c_2(B_3)$ is the second Chern class of B_3. For smooth 3-folds B_3 that appear as a base of a smooth elliptic Calabi–Yau 4-fold, it is known [111] that $c_2(B_3)+\overline{K}_B^2$ is an *even* class. Furthermore, [181] states that $\int_{B_3}c_2(B_3)\cdot\overline{K}_B=24$ is *even* as well. It thus follows that $c_2(T_{\widehat{Y}_4})$ passes the necessary conditions for being even. Likewise, we can integrate the G_4-flux candidate 6.2.25 over the matter surfaces and over the complete intersections

of toric divisors. All of those are found to be integral. Since a sufficient check is currently beyond our arithmetic abilities, we proceed under the assumption that $c_2(T_{\widehat{Y}_4})$ is even and that the G_4-flux candidate 6.2.25 is integral.

It should be mentioned that the G_4-flux (candidate) 6.2.25 was chosen so that the F-theory Standard Model vacua are stable, that is the D3-tadpole can be canceled. This requires

$$n_{D3} = \frac{\chi\left(T_{\widehat{Y}_4}\right)}{24} - \frac{1}{2}\int\limits_{\widehat{Y}_4} G_4 \wedge G_4 \overset{!}{\in} \mathbb{Z}_{\geq 0}\,. \tag{6.2.27}$$

Moreover, the masslessness condition for the $U(1)$-gauge boson was enforced:

$$\forall \eta \in H^{1,1}(B_3): \quad \int_{Y_4} G_4 \wedge \sigma \wedge \pi^*\eta \overset{!}{=} 0\,. \tag{6.2.28}$$

Here, σ is the $(1,1)$-form that relates to the so-called *Shioda-divisor* associated with the $U(1)$ [115, 66].

Zero modes and root bundles

We now discuss the zero modes in the presence of the flux in 6.2.25. As explained in 6.2.1, we thus look for a lift to $H^4_D(\widehat{Y}_4, \mathbb{Z}(2))$ in the diagram 6.2.4. For computational simplicity, we aim to parametrize such a lift as $A = \widehat{\gamma}(\mathcal{A})$ with $\mathcal{A} \in \mathrm{CH}^2(\widehat{Y}_4, \mathbb{Z})$. To describe a candidate, we recall that the cycle map $\gamma\colon \mathrm{CH}^2(\widehat{Y}_4, \mathbb{Z}) \to H^{2,2}_{\mathrm{alg}}(\widehat{Y}_4)$ is a ring homomorphism in which the intersection product in $\mathrm{CH}^*(X_5, \mathbb{Z})$ is compatible with the cup product in $H^*(X_5, \mathbb{C})$. By De Rham's theorem and the Hodge decomposition, it follows that

$$H^{2k}(X_5, \mathbb{C}) \cong H^{2k}_{DR}(X_5, \mathbb{C}) = \bigoplus_{p+q=2k} H^{p,q}(X_5)\,. \tag{6.2.29}$$

The cup product in $H^*(X_5, \mathbb{C})$ respects the grading, and restricts to the wedge product of (p,q)-forms. For any two divisors $V(r)$ and $V(s)$ on X_5, it therefore follows that

$\gamma(V(r,s)) = \gamma(V(r)\cdot V(s)) = [r]\wedge[s]$. This also shows that $[r]\wedge[s] \in H^{2,2}_{\text{alg}}(\widehat{Y}_4)$ is in the image of γ. With this in mind, it is natural to consider

$$\begin{aligned}\mathcal{A}' = -3\cdot\Big(&5V(e_1,e_4) - 3V(e_1,t_1) - 2V(e_2,t_2) - 6V(e_4,t_3)\\ &+V(t_4,t_5) - 4V(t_6,u) + V(t_6,v)\Big)\Big|_{\widehat{Y}_4} \in \mathrm{CH}^2(\widehat{Y}_4,\mathbb{Z})\,,\end{aligned} \tag{6.2.30}$$

where $t_i \in H^0(X_5, \alpha^*(\overline{K}_B))$ and $\alpha\colon X_5 = B_3\times\mathbb{P}_{F_{11}} \twoheadrightarrow B_3$. Note that $\gamma(\mathcal{A}') = \overline{K}_B^3\cdot G_4$. Therefore, the gauge potential $A' = \widehat{\gamma}(\mathcal{A}')$ would induce chiral exotics unless we "divide" it by $\xi = \overline{K}_B^3$. Hence, we are led to consider gauge potentials $A = \widehat{\gamma}(\mathcal{A}) \in H^4_D(\widehat{Y}_4, \mathbb{Z}(2))$ with

$$\gamma(\mathcal{A}) = G_4\,, \qquad \xi\cdot\widehat{\gamma}(\mathcal{A}) \sim \widehat{\gamma}(\mathcal{A}')\,. \tag{6.2.31}$$

Hence, we can infer that the line bundles induced from $A = \widehat{\gamma}(\mathcal{A})$ are $\overline{K}^3_{B_3}$-th roots of the ones induced from $A' = \widehat{\gamma}(\mathcal{A}')$. We can explicitly compute the latter from 6.2.30 and 6.2.6. As an example, let us consider the curve $C_{(\mathbf{3},\mathbf{2})_{1/6}}$. For this curve, we find (details in C.2)

$$D_{(\mathbf{3},\mathbf{2})_{1/6}}(\mathcal{A}') = 3\cdot V(t,s_3,s_9) = 3\cdot\overline{K}_B\Big|_{C_{(\mathbf{3},\mathbf{2})_{1/6}}}\,, \qquad t\in H^0(B_3,\overline{K}_B)\,, \tag{6.2.32}$$

where the last equality follows from the adjunction formula. From this, we conclude that $D_{(\mathbf{3},\mathbf{2})_{1/6}}(\mathcal{A})$ satisfies

$$\xi\cdot D_{(\mathbf{3},\mathbf{2})_{1/6}}(\mathcal{A}) = \overline{K}_B^3\cdot D_{(\mathbf{3},\mathbf{2})_{1/6}}(\mathcal{A}) \sim D_{(\mathbf{3},\mathbf{2})_{1/6}}(\mathcal{A}') = 3\cdot\overline{K}_B\Big|_{C_{(\mathbf{3},\mathbf{2})_{1/6}}}\,. \tag{6.2.33}$$

The zero modes in the representation $(\mathbf{3},\mathbf{2})_{1/6}$ are counted by the tensor product of the line bundle associated with $D_{(\mathbf{3},\mathbf{2})_{1/6}}(\mathcal{A})$ and a spin bundle. Let us emphasize again that we wish to provide a systematic study of all ξ-th roots of $D_{(\mathbf{3},\mathbf{2})_{1/6}}(\mathcal{A}')$ and all the spin

bundles on $C_{(\mathbf{3},\mathbf{2})_{1/6}}$. To this end, recall the defining property of spin bundles on $C_{(\mathbf{3},\mathbf{2})_{1/6}}$:

$$2 \cdot D^{\text{spin}}_{(\mathbf{3},\mathbf{2})_{1/6}} \sim K_{(\mathbf{3},\mathbf{2})_{1/6}} \sim \overline{K}_B\Big|_{C_{(\mathbf{3},\mathbf{2})_{1/6}}} . \tag{6.2.34}$$

Consequently, we notice

$$\begin{aligned} 2\overline{K}_B^3 \cdot \left(D_{(\mathbf{3},\mathbf{2})_{1/6}}(\mathcal{A}) + D^{\text{spin}}_{(\mathbf{3},\mathbf{2})_{1/6}}\right) &\sim 2 \cdot \left(\overline{K}_B^3 \cdot D_{(\mathbf{3},\mathbf{2})_{1/6}}(\mathcal{A})\right) + \overline{K}_B^3 \cdot \left(2 \cdot D^{\text{spin}}_{(\mathbf{3},\mathbf{2})_{1/6}}\right) \\ &\sim \left(6 + \overline{K}_B^3\right) \cdot \overline{K}_B\Big|_{C_{(\mathbf{3},\mathbf{2})_{1/6}}} . \end{aligned} \tag{6.2.35}$$

Expressed in line bundles, we thus conclude that[5]

$$P^{\otimes 2\overline{K}_B^3}_{(\mathbf{3},\mathbf{2})_{1/6}} \sim \left(\overline{K}_B\Big|_{C_{(\mathbf{3},\mathbf{2})_{1/6}}}\right)^{\otimes\left(6+\overline{K}_B^3\right)} \sim K^{\otimes\left(6+\overline{K}_B^3\right)}_{(\mathbf{3},\mathbf{2})_{1/6}} . \tag{6.2.36}$$

By repeating this computation for the other matter curves, one finds the following root bundle constraints:

curve	root bundle constraint
$C_{(\mathbf{3},\mathbf{2})_{1/6}} = V(s_3, s_9)$	$P^{\otimes 2\overline{K}_B^3}_{(\mathbf{3},\mathbf{2})_{1/6}} = K^{\otimes\left(6+\overline{K}_B^3\right)}_{(\mathbf{3},\mathbf{2})_{1/6}}$
$C_{(\mathbf{1},\mathbf{2})_{-1/2}} = V(s_3, P_H)$	$P^{\otimes 2\overline{K}_B^3}_{(\mathbf{1},\mathbf{2})_{-1/2}} = K^{\otimes\left(4+\overline{K}_B^3\right)}_{(\mathbf{1},\mathbf{2})_{-1/2}} \otimes \mathcal{O}_{C_{(\mathbf{1},\mathbf{2})_{-1/2}}}(-30 \cdot Y_1)$
$C_{(\overline{\mathbf{3}},\mathbf{1})_{-2/3}} = V(s_5, s_9)$	$P^{\otimes 2\overline{K}_B^3}_{(\overline{\mathbf{3}},\mathbf{1})_{-2/3}} = K^{\otimes\left(6+\overline{K}_B^3\right)}_{(\overline{\mathbf{3}},\mathbf{1})_{-2/3}}$
$C_{(\overline{\mathbf{3}},\mathbf{1})_{1/3}} = V(s_9, P_R)$	$P^{\otimes 2\overline{K}_B^3}_{(\overline{\mathbf{3}},\mathbf{1})_{1/3}} = K^{\otimes\left(4+\overline{K}_B^3\right)}_{(\overline{\mathbf{3}},\mathbf{1})_{1/3}} \otimes \mathcal{O}_{C_{(\overline{\mathbf{3}},\mathbf{1})_{1/3}}}(-30 \cdot Y_3)$
$C_{(\mathbf{1},\mathbf{1})_1} = V(s_1, s_5)$	$P^{\otimes 2\overline{K}_B^3}_{(\mathbf{1},\mathbf{1})_1} = K^{\otimes\left(6+\overline{K}_B^3\right)}_{(\mathbf{1},\mathbf{1})_1}$

(6.2.37)

In this table, we use $P_H = s_2 s_5^2 + s_1(s_1 s_9 - s_5 s_6)$ and $P_R = s_3 s_5^2 + s_6(s_1 s_6 - s_2 s_5)$. Note that the line bundles on the Higgs curve $C_{(\mathbf{1},\mathbf{2})_{-1/2}}$ and the curve $C_{(\overline{\mathbf{3}},\mathbf{1})_{1/3}}$ depend on the Yukawa points $Y_1 = V(s_3, s_5, s_9)$ and $Y_3 = V(s_3, s_6, s_9)$ (see C.2 for details). It must also

[5]Inspired by greek word for root, P refers to root bundles throughout this article.

be noted that for two divisors D and E,

$$D \sim E \qquad \Rightarrow \qquad n \cdot D \sim n \cdot E \,. \tag{6.2.38}$$

The converse is not true. This is why we do not cancel common factors. Finally, let us point out that the toric base spaces for these F-theory Standard Model constructions must satisfy $\overline{K}_B^3 \in \{6, 10, 18, 30\}$ [32]. We provide an explicit list of the root bundles constraints for these values of $\overline{K}_B^3$ in C.2.3.

6.3 Root bundles from limit roots

In the previous section, we explained that root bundles feature prominently in vector-like spectra in F-theory. For the largest currently-known class of globally consistent F-theory Standard Model constructions without chiral exotics and gauge coupling unification [32], we have worked out these bundle expressions explicitly and summarized them in C.2.3. In aiming for MSSM constructions, i.e., vacua without vector-like exotics, the cohomologies of root bundles beg to be investigated. Therefore, our goal is to construct roots whose number of global sections is exactly the amount required by the physical considerations.

Before we exhibit an example of this in 6.4, we first summarize well-known facts about root bundles in general. In particular, we outline an argument for the existence of such bundles on smooth, irreducible curves. From this argument, it can be extrapolated that explicit constructions of root bundles on smooth, irreducible curves – not to mention an explicit count of their sections – are very challenging at best. Fortunately, we can employ deformation theory to simplify the task. Namely, it is possible to relate root bundles on smooth, irreducible curves to so-called limit roots on nodal curves. This follows from the detailed study in [170]. For convenience to the reader, we summarize the essential steps in these limit root constructions before we extend these ideas. Namely, we provide a simple counting procedure for the global sections of many limit root bundles. Our analysis in 6.4 will employ exactly this counting strategy in order to gain insights into the vector-like

spectra of F-theory Standard Models.

6.3.1 Root bundles

Let us look at root bundles on a smooth, complete Riemann surface (or curve) C of genus g. We focus on a line bundle $L \in \mathrm{Pic}(C)$ and an integer n with $n \geq 2$, and $n|\deg(L)$. We first recall the following definition.

Definition 6.3.1 (n-th root bundle)**.** An *n-th root bundle of L* is a line bundle P such that $P^n \cong L$. Collectively, we denote the n-th roots of P by $\mathrm{Roots}(n, L)$

Equivalently, in the language of divisors, an n-th root D of a divisor $\widetilde{D}$ is a divisor such that $nD \sim \widetilde{D}$. The first important result about root bundles concerns their existence. While this seems to be a well-known fact, we were surprised to notice that well-established references, such as [182, 183, 152], do not give an explicit proof. Not only does the proof nicely illustrates the challenge in constructing root bundles on high genus curves, it also allows us to easily understand why there are n^{2g} root bundles and why their differences are torsion divisors. For all these reasons, let us give a proof for the existence of root bundles on smooth, complete Riemann surfaces.

Proposition 6.3.2. *Let $n \in \mathbb{Z}$ with $n \geq 2$. For every $L \in \mathrm{Pic}(C)$, there exists an n-th root bundle P of L if and only if $n|\deg(L)$.*

Proof. For the forward direction, if there exists an n-th root bundle P such that $P^n \cong L$, then $n \deg(P) = \deg(L)$ and $n| \deg(L)$. Conversely, suppose that $n|\deg(L)$. Recall that $J(C)$ is a complex torus of the form V/Λ, where V is a vector space of dimension g, and Λ is a discrete subgroup of V of rank $2g$. Denote the n-fold tensor product of line bundles by $[n] : P \mapsto nP$.

First, we will describe some properties of the map $[n] : J(C) \to J(C)$. Observe that its

kernel is given by

$$\ker([n]) = \{P \in V/\Lambda : nP + \Lambda = \Lambda\} = ((1/n)\Lambda)/\Lambda \cong \Lambda/n\Lambda \cong (\mathbb{Z}/n\mathbb{Z})^{2g}\,, \tag{6.3.1}$$

because Λ is a discrete subgroup of rank $2g$. Hence, $\ker([n]) = [n]^{-1}(0)$ is finite, and has dimension 0. Since $J(C)$ is a complete variety, its image $[n](J(C))$ is a closed subvariety. For any $a \in [n](J(C))$, the translation map

$$t_a : [n]^{-1}(0) \to [n]^{-1}(a), \quad x \mapsto x + a\,, \tag{6.3.2}$$

is an isomorphism. It follows from the dimension formula that

$$0 = \dim[n]^{-1}(0) = \dim[n]^{-1}(a) \geq \dim(J(C)) - \dim[n](J(C)) \geq 0\,. \tag{6.3.3}$$

Hence, $[n] : J(C) \to J(C)$ is surjective.

Now, consider the following commutative diagram, where deg is the degree map, and $(\times n)$ is the multiplication of integers by n.

$$\begin{array}{ccccccccc} 0 & \longrightarrow & J(C) & \longrightarrow & \mathrm{Pic}(C) & \xrightarrow{\deg} & \mathbb{Z} & \longrightarrow & 0 \\ & & \downarrow{\scriptstyle [n]} & & \downarrow{\scriptstyle [n]} & & \downarrow{\scriptstyle \times n} & & \\ 0 & \longrightarrow & J(C) & \longrightarrow & \mathrm{Pic}(C) & \xrightarrow{\deg} & \mathbb{Z} & \longrightarrow & 0 \end{array} \tag{6.3.4}$$

Applying the Snake Lemma yields an exact sequence of the cokernels of the vertical maps, i.e.

$$0 = J(C)/[n](J(C)) \to \mathrm{Pic}(C)/[n](\mathrm{Pic}(C)) \xrightarrow{\cong} \mathbb{Z}/n\mathbb{Z} \to 0\,, \tag{6.3.5}$$

where the isomorphism is provided by the degree map. Since $n|\deg(L)$, we have that $L \in [n](\mathrm{Pic}(C))$. So, there exists $P \in \mathrm{Pic}(C)$ such that $P^n \cong L$, i.e. an n-th root

bundle. □

There are two important lessons that we can learn from this proposition. First, there are n^{2g} n-th root bundles P of L. This is because 6.3.2 is an isomorphism, and so,

$$t_{\deg(L)} : (\mathbb{Z}/n\mathbb{Z})^{2g} \cong \ker([n]) = [n]^{-1}(0) \to [n]^{-1}(\deg(L)) = \text{Roots}(n, L)\,, \tag{6.3.6}$$

is an isomorphism as well. If $L = K_C$, then the n-th roots are called *n-spin bundles* [184].

The second lesson concerns the difference between two root bundles. Any two n-th root bundles differ by an n-torsion line bundle, i.e. a line bundle $M \in J(C)$ such that $M^n \cong \mathcal{O}_C$.

The Jacobian and the linear equivalence of divisors is well-understood for elliptic curves E (see [182, 183, 152] for background). This allows us to exhibit examples of the above notions fairly explicitly. First, recall that $E \cong J(E) \cong \mathbb{C}/\Lambda$ and $\Lambda = \mathbb{Z} \oplus \mathbb{Z} \cdot \tau$, where $\tau \in \mathbb{C}$ is the complex structure modulus of the elliptic curve. We denote $D \in \text{Div}(E)$ by

$$D = \sum_{i=1}^{n} n_i \cdot (p_i)\,, \qquad n_i \in \mathbb{Z}, \quad p_i \in E\,, \tag{6.3.7}$$

i.e. we place the points $p_i \in E$ in round brackets for notational clarity. Note that $\deg(D) = \sum_{i=1}^{n} n_i$ and that a zero degree divisor satisfies

$$D \sim 0 \quad \Leftrightarrow \quad \left(\sum_{i=1}^{n} n_i \cdot p_i\right) \in \Lambda\,. \tag{6.3.8}$$

From this, we can work out the divisor classes of the 2-torsion divisors in $J(E)$:

$$D_1 = [0]\,, \qquad D_2 = \left[-1 \cdot (0) + 1 \cdot \left(\frac{1}{2}\right)\right]\,, \tag{6.3.9}$$

$$D_3 = \left[-1 \cdot (0) + 1 \cdot \left(\frac{\tau}{2}\right)\right]\,, \qquad D_4 = \left[-1 \cdot (0) + 1 \cdot \left(\frac{1+\tau}{2}\right)\right]\,. \tag{6.3.10}$$

It follows $\ker([2]) \cong (\mathbb{Z}/2\mathbb{Z})^2$, which we can intuitively collect in the following picture:

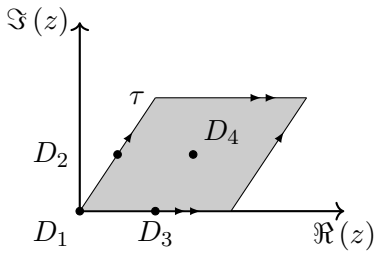

(6.3.11)

Note that $\{D_1, D_2, D_3, D_4\}$ are exactly the four spin structures on E.

In making contact with our physics applications, we should next investigate the sheaf cohomologies of root bundles. Generally speaking, this is a very challenging task. However, on elliptic curves, the situation simplifies and we can achieve a complete classification. Recall that any line bundle $L \in \mathrm{Pic}(E)$ with $\deg(L) \neq 0$ is in the Kodaira stable regime, i.e. we can infer its cohomologies from its degree. For $\deg(L) = 0$ we have

$$h^0(E, L) = 1 \quad \Leftrightarrow \quad L \cong \mathcal{O}_E \,. \tag{6.3.12}$$

Therefore, it merely remains to study the cohomologies of roots P of a line bundle $L \in \mathrm{Pic}(E)$ with $\deg(L) = 0$. This is achieved by the following proposition.

Proposition 6.3.3. *Let $L \in \mathrm{Pic}(E)$ with $\deg(L) = 0$ and consider an integer n with $n \geq 2$. Then,*

1. *$L \cong \mathcal{O}_E$: Exactly one n-th root P of L has $h^0(E, P) = 1$, and the remaining n-th roots Q have $h^0(E, Q) = 0$.*

2. *$L \ncong \mathcal{O}_E$: All n-th roots P of L have $h^0(E, P) = 0$.*

Proof. 1. Since $\mathcal{O}_E$ is an n-th root of itself, there is one n-th root $P = \mathcal{O}_E$ with $h^0(E, P) = 1$. Any other n-th root Q differs from P by a non-trivial n-torsion line

bundle. As such, Q is non-trivial and has $h^0(E, Q) = 0$.

2. L is non-trivial. Hence, all n-th roots P are non-trivial and have $h^0(E, P) = 0$. □

For example, among the 9 3rd roots P of a line bundle $L \in \mathrm{Pic}(E)$ with $\deg(L) = 0$, at least 8 have $h^0(E, P) = 0$. We will make use of this simple result in 6.4.2.

6.3.2 Deformation theory and global sections

For applications in F-theory, we wish to generalize 6.3.3 to matter curves $C_{\mathbf{R}}$ with $g > 1$. Unfortunately on such curves, it is very hard to tell if a divisor is linearly equivalent to zero. This is due to the current lack of practical understanding of the Abel-Jacobi map $\mathrm{Div}_0(C_{\mathbf{R}}) \to J(C_{\mathbf{R}})$, whose kernel is exactly given by the (classes of) trivial divisors. This in turn makes it very challenging to identify n-torsion bundles, which forms a measure-0 subset of the Jacobian $J(C_{\mathbf{R}})$. Consequently, it becomes almost impossible to explicitly identify a single n-th root bundle P of a line bundle L on $C_{\mathbf{R}}$.

To overcome this hurdle, we wonder if it is possible to simplify the matter curves $C_{\mathbf{R}}$. However, recall that the geometry of the matter curves is dictated by that of the elliptic fibration $\widehat{\pi}\colon \widehat{Y}_4 \twoheadrightarrow B_3$. Therefore, even though special, non-generic elliptic fibrations $\widehat{Y}_4$ may contain matter curves $C_{\mathbf{R}}$ with simple geometries, it can be expected that such fibrations lead to physically unwanted gauge enhancements.

Therefore, in order to remain on physically solid grounds, we stick to the geometry of the matter curves $C_{\mathbf{R}}$ as enforced by the generic fibration $\widehat{Y}_4$. In this situation, there is still a way to improve our situation. Namely, suppose that $\varphi\colon C_{\mathbf{R}}^{\mathrm{simple}} \to C_{\mathbf{R}}$ is a deformation of a curve $C_{\mathbf{R}}^{\mathrm{simple}}$, whose simple geometry allows easy access to root bundles and their cohomologies, into the actual physical matter curve $C_{\mathbf{R}} \subset \widehat{Y}_4$. Then, we can wonder if the root bundles $P_{\mathbf{R}}^{\mathrm{simple}}$ on $C_{\mathbf{R}}^{\mathrm{simple}}$ approximate the roots $P_{\mathbf{R}}$ on $C_{\mathbf{R}}$.

In general, this sort of question leads to a deep discussion of deformation theory (see e.g. [185, 186] for a modern exposition). In this work, we will not attempt to give a complete

answer. Rather, we make a special choice for $C_{\mathbf{R}}^{\text{simple}}$. Inspired by [170], we focus on curves $C_{\mathbf{R}}^{\text{simple}}$ with singularities, which locally look like $\{x \cdot y = 0\}$, i.e. are nodes. On such nodal curves $C_{\mathbf{R}}^{\bullet}$, roots $P_{\mathbf{R}}^{\bullet}$ admit a description in terms of weighted diagrams [170]. Even more, there are exactly as many roots $P_{\mathbf{R}}^{\bullet}$ as there are roots $P_{\mathbf{R}}$ and we can, at least in theory, identify them with each other by tracing them along the deformation $C_{\mathbf{R}}^{\bullet} \to C_{\mathbf{R}}$.

That said, the next question is in what sense we can use the roots $P_{\mathbf{R}}^{\bullet}$ on $C_{\mathbf{R}}^{\bullet}$ to approximate the cohomologies of the roots $P_{\mathbf{R}}$ on the physical matter curve $C_{\mathbf{R}}$. To this end, we first recall that refined section counting mechanisms exist for line bundles on singular curves [48]. In exactly this spirit, we are able to extend the ideas from [170]. In 6.3.3 we will argue that it is often possible to count the number of global sections of roots $P_{\mathbf{R}}^{\bullet}$ on a nodal curve $C_{\mathbf{R}}^{\bullet}$ from simple combinatorics.

It now remains to relate the cohomologies $h^i(C_{\mathbf{R}}^{\bullet}, P_{\mathbf{R}}^{\bullet})$ to $h^i(C_{\mathbf{R}}, P_{\mathbf{R}})$. Since, the chiral index is fixed from topology, it suffices to study how $h^0(C_{\mathbf{R}}^{\bullet}, P_{\mathbf{R}}^{\bullet})$ relates to $h^0(C_{\mathbf{R}}, P_{\mathbf{R}})$. Since $C_{\mathbf{R}}^{\bullet}$ is singular (and therefore non-generic) and $C_{\mathbf{R}}$ expected to be smooth, a tendency is known. This tendency goes by the name upper semi-continuity. It means that the number of global sections of $P_{\mathbf{R}}$ must not increase when traced along $C_{\mathbf{R}}^{\bullet} \to C_{\mathbf{R}}$ to the root $P_{\mathbf{R}}$, i.e.

$$h^0\left(C_{\mathbf{R}}, P_{\mathbf{R}}\right) \leq h^0\left(C_{\mathbf{R}}^{\bullet}, P_{\mathbf{R}}^{\bullet}\right) . \tag{6.3.13}$$

It is a very interesting but also very challenging question to distinguish the roots $P_{\mathbf{R}}^{\bullet}$ that lose sections along $C_{\mathbf{R}}^{\bullet} \to C_{\mathbf{R}}$ from the roots with a constant number of sections. While we hope to return to this question in the future, the physics applications in 6.4 focus on a subset of roots, which do not lose sections. Namely, if $\chi\left(P_{\mathbf{R}}^{\bullet}\right) \geq 0$ and

$$h^0\left(C_{\mathbf{R}}^{\bullet}, P_{\mathbf{R}}^{\bullet}\right) = \chi\left(P_{\mathbf{R}}^{\bullet}\right) , \tag{6.3.14}$$

then $P^\bullet_{\mathbf{R}}$ cannot lose sections, since its numbers of sections is already minimal. In particular, it then holds $h^0\left(C_{\mathbf{R}}, P_{\mathbf{R}}\right) = h^0\left(C^\bullet_{\mathbf{R}}, P^\bullet_{\mathbf{R}}\right)$.

6.3.3 Limit roots

In 6.3.2 we saw that n-th roots P of a line bundle L on a smooth curve C exist if $\deg(L)$ is divisible by n. This is not the case for reducible, nodal curves $C^\bullet$. Indeed, a root $P^\bullet$ of a line bundle $L^\bullet$ on such curves should restrict to a root on the irreducible components. However, even if n divides the degree of $L^\bullet$, it may not divide $\deg(L|_Z)$ for some irreducible component Z of $C^\bullet$. This is elegantly circumvented by passing to limit n-th root bundles P° on (partial) blow-ups C° of $C^\bullet$, as originally introduced in [170]. Just as every nodal curve $C^\bullet$ can be described through its dual graph, these limit n-th root bundles P° are determined by weighted graphs. This combinatorial data can be exploited to make the task of section-counting more tractable. For convenience to the reader, let us outline the important steps in these constructions before we explain the section counting for limit roots. For more material on limit roots, we refer the reader to [187, 188] in which the pushforwards of these limits roots along the blow-up map, and their moduli are extensively studied.

Nodal curves and blow-ups

A point is a node if it has a neighborhood where the curve locally looks like $\{xy = 0\}$ in $\mathbb{C}^2$. A *nodal curve* is a complete algebraic curve such that every point is either smooth, or a node. Let $C^\bullet$ be a connected (possibly reducible) nodal curve of arithmetic genus g. We associate to $C^\bullet$ a *dual graph* $\Pi_{C^\bullet}$ in which

1. every vertex corresponds to an irreducible component $C^\bullet_i$ of $C^\bullet$,

2. every half-edge emanating from a vertex $C^\bullet_i$ is a node on $C^\bullet_i$.

If a node lies on both $C^\bullet_i$ and $C^\bullet_j$, then the half-edges exiting from $C^\bullet_i$ and $C^\bullet_j$ join together to form an edge. For example, consider the *Holiday lights* – a nodal curve $H^\bullet$ with 11

components given by:[6]

- a rational curve Γ with genus $g(\Gamma) = 0$,
- 10 elliptic curves $E_1, \ldots, E_{10}$ with genus $g(E_i) = 1$.

Each elliptic curve intersects no other curve except Γ, hence the name *Holiday lights*. Its dual graph can be visualized as follows:

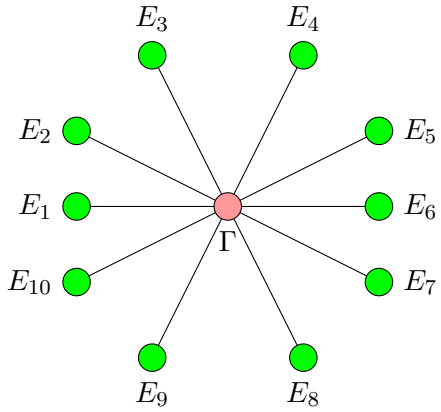

(6.3.15)

Each elliptic curve E_i is represented by a green vertex, while the rational curve Γ is represented by the pink vertex.

If $\pi : C^\circ \to C^\bullet$ is a blow-up of $C^\bullet$, then for every node $n_i \in C^\bullet$, we denote the exceptional components by

$$\pi^{-1}(n_i) = \mathcal{E}_i \cong \mathbb{P}^1 \,. \tag{6.3.16}$$

Set $C^N = \overline{C^\circ \setminus \cup_i \mathcal{E}_i}$. Then, $\pi|_{C^N} : C^N \to C^\bullet$ is the normalization of $C^\bullet$. For every node n_i, the points in $(\pi|_{C^N})^{-1}(n_i) = \mathcal{E}_i \cap C^N = \{p_i, q_i\}$ are called the *exceptional nodes*.

[6] In all base spaces B_3 of the globally consistent F-theory Standard Model constructions discussed in 6.2.2 and originally introduced in [32], the matter curves $C_{\mathbf{R}}$ are contained in K3-surfaces. Motivated from [171], it stands to wonder if the matter curves $C_{\mathbf{R}}$ admit a deformation into such a *Holiday lights*. Even more, *Holiday lights* allow easy access to Brill-Noether theory of limit roots as we will see momentarily. As such, they are very favorable nodal curves for our study. We hope to return to this question in the future.

From this point forward, we will consider blow-ups of $C^\bullet$ on the full set of nodes unless stated otherwise. We will often refer to this setup as a *full blow-up*. More general statements exist for partial blow-ups, the details of which are fully treated in [170].

Limit n-th roots and weighted graphs

Let n be a positive integer, and $L^\bullet$ be a line bundle on $C^\bullet$ so that $n|\deg(L^\bullet)$. Denote the full set of nodes by $\Delta_{C^\bullet}$.

Definition 6.3.4. A *limit n-th root* of $L^\bullet$ associated to $\Delta_{C^\bullet}$ is a triple $(C^\circ, P^\circ, \alpha)$ consisting of:

- the (full) blow-up $\pi : C^\circ \to C^\bullet$,
- a line bundle P° on C°,
- a homomorphism $\alpha : (P^\circ)^n \to \pi^*(L^\bullet)$,

satisfying the following properties:

1. $\deg(P^\circ|_{\mathcal{E}_i}) = 1$ for every exceptional component $\mathcal{E}_i$,
2. α is an isomorphism at all points of C° outside of the exceptional components.
3. for every exceptional component $\mathcal{E}_i$ of C°, the orders of vanishing of α at the exceptional nodes p_i and q_i add up to n.

We can also define limit n-th roots associated to a subset $\Delta \subseteq \Delta_{C^\bullet}$ in which the full blow-up is replaced by the partial blow-up at Δ, see [170] for details.

Limit n-th roots over $C^\bullet$ carry some combinatorial data, in the form of weighted graphs, that takes into account the combinatorial aspects of the nodal curve $C^\bullet$. Conversely, these weighted graphs allow one to construct and recover limit n-th roots. Although the correspondence between limit n-th roots and these weighted graphs are not one-to-one, it allows for a convenient parametrization of limit roots. First, let us introduce the weighted

graphs in question. Let $\widetilde{\Delta}_{C^\bullet}$ be the exceptional nodes corresponding to $\Delta_{C^\bullet}$.

Definition 6.3.5. A *weighted graph associated to a limit n-th root* $(C^\circ, P^\circ, \alpha)$ *of* $L^\bullet$ is the dual graph $\Pi_{C^\bullet}$ endowed with weights assigned by the weight function

$$w : \widetilde{\Delta}_{C^\bullet} \to \{1, \ldots, n-1\}\,, \tag{6.3.17}$$

where $w(p_i) = u_i$ and $w(q_i) = v_i$ are the orders of the vanishing of α at p_i and q_i respectively.

Such weighted graphs naturally satisfy two conditions:

1. $w(p_i) + w(q_i) = u_i + v_i = n$,
2. For every irreducible component $C_i^\bullet$ of $C^\bullet$, the sum of all weights assigned to the vertex corresponding to $C_i^\bullet$ is congruent to $\deg_{C_i^\bullet} L^\bullet \pmod n$.

We illustrate an example of a weighted graph by returning to the *Holiday lights* $H^\bullet$. We wish to find the limit 3rd roots of $K^2_{H^\bullet}$. If $C_i^\bullet$ is a component of $H^\bullet$, then set $k_i = \#C_i^\bullet \cap (\overline{H^\bullet \setminus C_i^\bullet})$. Therefore, $\deg(K_{H^\bullet}|_{C_i^\bullet}) = 2g(C_i^\bullet) - 2 + k_i$, and the multi-degree of $K_{H^\bullet}$ is

$$(\deg(K_{H^\bullet}|_\Gamma), \deg(K_{H^\bullet}|_{E_1}), .., \deg(K_{H^\bullet}|_{E_{10})}) = (8, 1, \ldots, 1)\,, \tag{6.3.18}$$

which has total degree is $2g(H^\bullet) - 2 = 18$. So, the multi-degree of $K^2_{H^\bullet}$ is $(16, 2, \ldots, 2)$. A weighted graph associated to the limit 3rd roots of $K^2_{H^\bullet}$, as well as the multi-degrees of $K^2_{H^\bullet}$, is given below. The labels inside the vertices are the multi-degrees of $K^2_{H^\bullet}$, while

the labels outside the vertices are the weights.

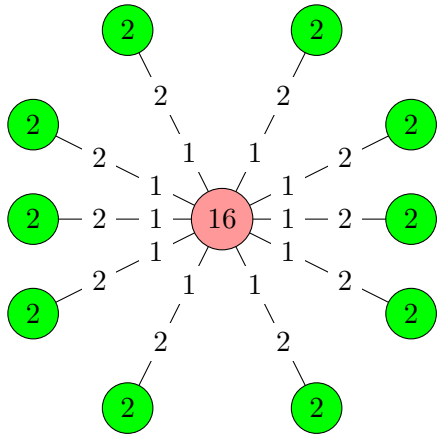

(6.3.19)

Given a weighted graph satisfying conditions A and B, we have a recipe for constructing limit n-th roots of $L^\bullet$.

Proposition 6.3.6. *Every weighted graph, whose underlying graph is $\Pi_{C^\bullet}$, and whose weight function $w : \widetilde{\Delta}_{C^\bullet} \to \{1, \ldots, n-1\}$ satisfies conditions A and B, encodes a limit n-th root $(C^\circ, P^\circ, \alpha)$ of L. Moreover, this weighted graph coincides with the weighted graph associated to $(C^\circ, P^\circ, \alpha)$ of $L^\bullet$.*

Proof. Suppose we have a weighted graph satisfying the hypothesis of the proposition, and let $\pi|_{C^N} : C^N \to C^\bullet$ be the normalization of $C^\bullet$. Thanks to condition B, the line bundle

$$(\pi|_{C^N})^*(L^\bullet)\left(-\sum_{p_i,q_i\in\widetilde{\Delta}}(u_ip_i+v_iq_i)\right) \tag{6.3.20}$$

has on each irreducible component of C^N degree divisible by n. Thus, on each irreducible component of C^N it admits an n-th root. The collection formed from an n-th root on each irreducible component is a line bundle $P^N \in \mathrm{Pic}(C^N)$. Let $\pi : C^\circ \to C^\bullet$ be the full blow-up. Over each exceptional component, glue a degree one line bundle to P^N to obtain a line bundle $P^\circ \in \mathrm{Pic}(C^\circ)$. Finally, define $\alpha : (P^\circ)^n \to \pi^*(L^\bullet)$ to be zero on the

exceptional components, and

$$\alpha|_{C^N} : (P^N)^n = (\pi|_{C^N})^*(L^\bullet)\left(-\sum_{p_i,q_i\in\widetilde{\Delta}}(u_ip_i+v_iq_i)\right) \hookrightarrow (\pi|_{C^N})^*(L^\bullet) \tag{6.3.21}$$

on C^N. Then, $(C^\circ, P^\circ, \alpha)$ is the desired limit n-th root of $L^\bullet$ associated to $\Delta_{C^\bullet}$. □

The same statements follow when $\Delta_{C^\bullet}$ is replaced by a subset Δ. In this case, the limit roots associated to Δ give rise to weighted subgraphs satisfying conditions A and B. Using the same procedure from 6.3.6, we can construct a limit root from a weighted subgraph.

Every nodal curve $C^\bullet$ and line bundle $L^\bullet$ on $C^\bullet$ has a total of $n^{b_1(\Pi_{C^\bullet})}$ weighted subgraphs satisfying conditions A and B, where

$$b_1(\Pi_{C^\bullet}) = \#\text{edges} + \#\text{connected components} - \#\text{vertices}\,, \tag{6.3.22}$$

is the first Betti number of $\Pi_{C^\bullet}$. We emphasize that this counts all of the weighted subgraphs, whose edge sets coincide with subsets of $\Delta_{C^\bullet}$. Curves, whose dual graphs are trees, will have zero b_1, and thus, will only have one weighted graph. These curves are said to be of compact type. This is certainly the case for the *Holiday lights* $H^\bullet$. Here, $b_1(\Pi_{H^\bullet}) = 0$ and the weighted graph depicted in eq. 6.3.19 is the only possible weighted graph for the 3rd limit roots of $K^2_{H^\bullet}$.

The correspondence between limit n-th roots and weighted graphs satisfying conditions A and B is not one-to-one. Indeed, the construction detailed in 6.3.6 involves a choice of a root P^N of $(\pi|_{C^N})^*(L^\bullet)(-\sum(u_ip_i+v_iq_i))$. A careful count reveals that there are n^{2g} limit n-th roots [170].

We will apply the limit root construction in 6.3.6 to describe the limit 3rd roots of $K^2_{H^\bullet}$ on the *Holiday lights* $H^\bullet$. We proceed as follows:

1. Blow-up all nodal singularities, and denote the exceptional component at the i-th

node by $\mathcal{E}_i \cong \mathbb{P}^1$. This $\mathbb{P}^1$ touches E_i at the exceptional node p_i and Γ at q_i.

2. Let H^N be the (full) normalization of $H^\bullet$, and consider the bundle

$$(\pi|_{H^N})^*(K^2_{H^\bullet}) \left(-2\sum_{i=1}^{10} p_i - \sum_{i=1}^{10} q_i \right), \tag{6.3.23}$$

which has multi-degree $(16-10, 2-2, \ldots, 2-2) = (6, 0, \ldots, 0)$. This bundle admits 3rd roots on H^N, namely $3^{2g(E_i)} = 9$ roots on each elliptic curve E_i and $3^{2g(\Gamma)} = 1$ root on Γ. Hence, there are $9^{10} = 3^{20}$ roots, and each has multi-degree $(2, 0, \ldots, 0)$.

3. Pick a 3rd root P^N, and glue to it a degree one bundle over every $\mathcal{E}_i$. The resulting *limit 3rd root* P° *of* $K^2_{H^\bullet}$ has multi-degree $(2, 0, \ldots, 0, 1, \ldots, 1)$ over H°, where

$$\deg(P^\circ|_{C_i^\bullet}) = \deg(P^N|_{C_i^\bullet}), \quad \deg(P^\circ|_{\mathcal{E}_i}) = 1. \tag{6.3.24}$$

These limit roots can be represented as follows:

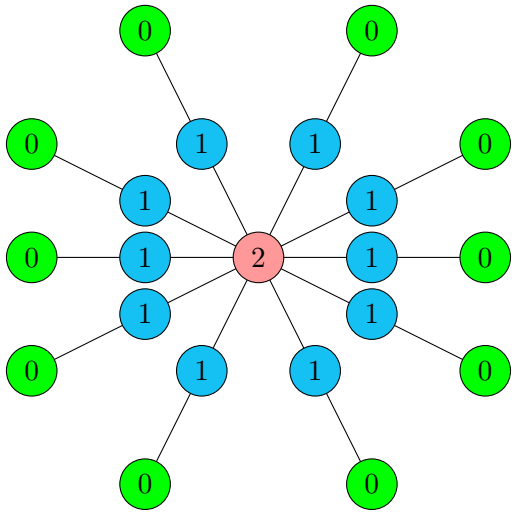

(6.3.25)

As before, the green vertices represent the elliptic curves E_i, and the pink vertex represents Γ. The blue vertices represent the exceptional component $\mathcal{E}_i$, which intersects E_i and Γ. The multi-degrees of the limit root P° is written inside the vertices. In particular, P° restricts to a degree 1 line bundle over each exceptional

component.

6.3.4 Global sections of full blow-up limit roots

Of ample importance for our analysis is the number of global sections of the limit roots. These arise from gluing sections on the irreducible components of the nodal curve across exceptional divisors, which is addressed in the next lemma.

Lemma 6.3.7. *Let p_1, p_2 be two distinct points on $\mathbb{P}^1$, and $a_1, a_2 \in \mathbb{C}$. For every $p_3 \in \mathbb{P}^1 \setminus \{p_1, p_2\}$, there exists a unique section $s \in H^0(\mathbb{P}^1, \mathcal{O}_{\mathbb{P}^1}(p_3))$ such that $s(p_1) = a_1$ and $s(p_2) = a_2$.*

Proof. Endow $\mathbb{P}^1$ with its standard open cover $\{U_0, U_1\}$. Let $z \in U_0$ and $w \in U_1$ be local coordinates so that $w = \frac{1}{z}$ in $U_0 \cap U_1$. Since PGL(2) acts transitively on $\mathbb{P}^1$, we may assume that

$$p_1 = 0, \quad p_2 = 1, \quad p_3 = \infty\,, \tag{6.3.26}$$

without loss of generality. The desired section s is given by

$$s|_{U_0}(z) = (a_2 - a_1)z + a_1\,, \quad s|_{U_1} = (a_2 - a_1) + a_1 w\,. \tag{6.3.27}$$

It remains to show uniqueness. Recall that every section $t \in \Gamma(\mathbb{P}^1, \mathcal{O}_{\mathbb{P}^1}(p_3))$ is given by two analytic functions $t_0 = t|_{U_0} \in \Gamma(U_0, \mathcal{O}_{\mathbb{P}^1}(p_3))$ and $t_1 = t|_{U_1} \in \Gamma(U_1, \mathcal{O}_{\mathbb{P}^1}(p_3))$ such that over $U_0 \cap U_1$,

$$t_0(z) = z t_1(w) = z t_1(1/z)\,. \tag{6.3.28}$$

If $t_0(z) = \sum_{k\geq 0} \alpha_k z^k$ and $t_1(w) = \sum_{k\geq 0} \beta_k w^k$, the above implies that

$$\sum_{k\geq 0} \alpha_k z^k = z\left(\sum_{k\geq 0} \beta_k w^k\right) = z\left(\sum_{k\geq 0} \beta_k z^{-k}\right) = \sum_{k\geq 0} \beta_k z^{1-k}\,. \tag{6.3.29}$$

It follows that $\alpha_k = \beta_k = 0$ for $k > 1$, which leaves $\alpha_0 = \beta_1$ and $\alpha_1 = \beta_0$. As such, every section t is given by $t_0(z) = \alpha_0 z + \alpha_1$ and $t_1 = \alpha_0 + \alpha_1 w$. If t also satisfies $t(0) = a_1$ and $t(1) = a_2$, then within the chart U_0 containing $0, 1 \in \mathbb{P}^1$,

$$a_1 = t_0(0) = \alpha_1\,, \qquad a_2 = t_0(1) = \alpha_0 + \alpha_1 = \alpha_0 + a_1\,. \tag{6.3.30}$$

Thus, $t_0(z) = (a_2 - a_1)z + a_1$ and $t_1(w) = (a_2 - a_1) + a_1 w$, which coincides with s. □

By virtue of the above lemma, there is a unique way of gluing a local section over an exceptional component to local sections over the irreducible components at each end. This leads us to the following corollary.

Corollary 6.3.8. *Let $C^\bullet$ be a connected nodal curve with irreducible components $C_i^\bullet$. Let $L^\bullet$ be a line bundle on $C^\bullet$, and n be an integer with $n \geq 2$ and $n|\deg(L^\bullet)$. For any limit n-th root $(C^\circ, P^\circ, \alpha)$ of $L^\bullet$,*

$$h^0(C^\circ, P^\circ) = \sum_{i=1}^{k} h^0(C_i^\bullet, P^\circ|_{C_i^\bullet}). \tag{6.3.31}$$

Proof. Let two irreducible components $C_i^\bullet$ and $C_j^\bullet$ intersect an exceptional component $\mathcal{E} \cong \mathbb{P}^1$ at $p_i \in C_i^\bullet$ and $p_j \in C_j^\bullet$ respectively. Set $Y = C_i^\bullet \cup \mathcal{E} \cup C_j^\bullet$. Then, we have

$$\begin{aligned} h^0(Y, P^\circ) &\geq h^0(C_i^\bullet, P^\circ|_{C_i^\bullet}) + h^0(C_j^\bullet, P^\circ|_{C_j^\bullet}) + h^0(\mathcal{E}, P^\circ|_{\mathcal{E}}) \\ &\quad - h^0(C_i^\bullet \cap \mathcal{E}, P^\circ|_{C_i^\bullet \cap \mathcal{E}}) - h^0(C_j^\bullet \cap \mathcal{E}, P^\circ|_{C_j^\bullet \cap \mathcal{E}}) \\ &\geq h^0(C_i^\bullet, P^\circ|_{C_i^\bullet}) + h^0(C_j, P^\circ|_{C_j^\bullet}) + 2 - 1 - 1 \\ &\geq h^0(C_i^\bullet, P^\circ|_{C_i^\bullet}) + h^0(C_j^\bullet, P^\circ|_{C_j^\bullet}). \end{aligned} \tag{6.3.32}$$

It remains to prove equality. Recall that the number of independent conditions met at p_i and p_j is at most 2 – the number of intersection points on $\mathcal{E}$. The previous lemma showed that there are exactly two independent conditions; one at each p_i and p_j. Thus, equality

holds. Since any two irreducible components of $C^\bullet$ either intersect a common exceptional component, or they do not in the full blow-up, the result follows. □

Let us apply these results to the *Holiday lights* $H^\bullet$, and count the global sections of the limit 3rd roots of $K^2_{H^\bullet}$. Recall that $H^\bullet$ is the union of a rational curve Γ, and 10 elliptic curves E_i. Also, the limit 3rd root P° of $K^2_{H^\bullet}$ has multi-degree $(2, 0, \ldots, 0, 1, \ldots, 1)$. Since Γ is rational, $h^0(\Gamma, P^\circ|_\Gamma) = h^0(\mathbb{P}^1, \mathcal{O}_{\mathbb{P}^1}(2)) = 3$. By the above results, we have

$$h^0(H^\circ, P^\circ) = h^0(\Gamma, P^\circ|_\Gamma) + \sum_{i=1}^{10} h^0(E_i, P^\circ|_{E_i}) = 3 + \left\{ \begin{array}{c} 0 \\ 1 \end{array} \right\} + \cdots + \left\{ \begin{array}{c} 0 \\ 1 \end{array} \right\} \tag{6.3.33}$$

The last term in the above expression means 0 or 1. This refers to the two cases described in 6.3.3 in which $P^\circ|_{E_i}$ is either non-trivial or trivial.

This example highlights the general fact that a line bundle of degree d over a smooth curve can have different h^0's. Since counting the global sections of a limit root is equivalent to counting its local sections over the smooth irreducible components, we address the effect of this phenomenon on section-counting in the following corollary.

Corollary 6.3.9. *Let $C^\bullet$ be a connected nodal curve with irreducible components $C^\bullet_1$. Let $L^\bullet$ be a line bundle on $C^\bullet$, and n be an integer with $n \geq 2$ and $n|\deg(L^\bullet)$. For any limit n-th root $(C^\circ, P^\circ, \alpha)$ of $L^\bullet$,*

$$\sum_{i=1}^{k} \min h^0(C^\bullet_i, P^\circ|_{C^\bullet_i}) \leq h^0(C^\circ, P^\circ) \leq \sum_{i=1}^{k} \max h^0(C^\bullet_i, P^\circ|_{C^\bullet_i}), \tag{6.3.34}$$

where for each i, the minimum and maximum are taken over all line bundles of degree $\deg(P^\circ|_{C^\bullet_i})$ over $C^\bullet_i$.

In the example of the *Holiday lights* $H^\bullet$,

$$\min_{P^\circ|_\Gamma \in \mathrm{Pic}^2(\Gamma)} h^0(\Gamma, P^\circ|_\Gamma) = 3, \qquad \max_{P^\circ|_\Gamma \in \mathrm{Pic}^2(\Gamma)} h^0(\Gamma, P^\circ|_\Gamma) = 3, \tag{6.3.35}$$

$$\min_{P^\circ|_{E_i}\in J(E_i)} h^0(E_i, P^\circ|_{E_i}) = 0, \quad \max_{P^\circ|_{E_i}\in J(E_i)} h^0(E_i, P^\circ|_{E_i}) = 1, \tag{6.3.36}$$

for $i = 1, ..., 10$. Hence, $3 \leq h^0(H^\circ, P^\circ) \leq 13$.

Let $\mathrm{Roots}(n, L^\bullet)^\circ$ be the set of limit n-th roots of $L^\bullet$ on $C^\bullet$. In a broader sense, we wish to understand the map,

$$h^0(C^\circ, \cdot) : \mathrm{Roots}(n, L^\bullet)^\circ \to \mathbb{N} \cup \{0\}, \quad P^\circ \mapsto h^0(C^\circ, P^\circ), \tag{6.3.37}$$

For curves of compact type, every limit root comes from one weighted graph, and is constructed over the full blow-up. In this case, the global sections of the limit root are fully determined by the local sections over the irreducible components. Hence, we can compute $|h^0(C^\circ, \cdot)^{-1}(a)|$ for every $a \in \mathbb{N} \cup \{0\}$, i.e. the number of limit n-th roots with $h^0 = a$. We illustrate this with the *Holiday lights*, which is a curve of compact type. Denote the number of elliptic curves on which $P^\circ|_{E_i}$ is non-trivial by N_i. Then, the number $N_{P^\circ}(h^0)$ of limit 3rd roots with specific h^0 are as follows:

N_i	10	9	8	7	6	5	4	3	2	1	0
$N_{P^\circ}(3)$	1	$\binom{1}{0}\cdot 8$	$\binom{2}{0}\cdot 8^2$	$\binom{3}{0}\cdot 8^3$	$\binom{4}{0}\cdot 8^4$	$\binom{5}{0}\cdot 8^5$	$\binom{6}{0}\cdot 8^6$	$\binom{7}{0}\cdot 8^7$	$\binom{8}{0}\cdot 8^8$	$\binom{9}{0}\cdot 8^9$	$\binom{10}{0}\cdot 8^{10}$
$N_{P^\circ}(4)$		1	$\binom{2}{1}\cdot 8^1$	$\binom{3}{1}\cdot 8^2$	$\binom{4}{1}\cdot 8^3$	$\binom{5}{1}\cdot 8^4$	$\binom{6}{1}\cdot 8^5$	$\binom{7}{1}\cdot 8^6$	$\binom{8}{1}\cdot 8^7$	$\binom{9}{1}\cdot 8^8$	$\binom{10}{1}\cdot 8^9$
$N_{P^\circ}(5)$			1	$\binom{3}{2}\cdot 8^1$	$\binom{4}{2}\cdot 8^2$	$\binom{5}{2}\cdot 8^3$	$\binom{6}{2}\cdot 8^4$	$\binom{7}{2}\cdot 8^5$	$\binom{8}{2}\cdot 8^6$	$\binom{9}{2}\cdot 8^7$	$\binom{10}{2}\cdot 8^8$
$N_{P^\circ}(6)$				1	$\binom{4}{3}\cdot 8^1$	$\binom{5}{3}\cdot 8^2$	$\binom{6}{3}\cdot 8^3$	$\binom{7}{3}\cdot 8^4$	$\binom{8}{3}\cdot 8^5$	$\binom{9}{3}\cdot 8^6$	$\binom{10}{3}\cdot 8^7$
$N_{P^\circ}(7)$					1	$\binom{5}{4}\cdot 8^1$	$\binom{6}{4}\cdot 8^2$	$\binom{7}{4}\cdot 8^3$	$\binom{8}{4}\cdot 8^4$	$\binom{9}{4}\cdot 8^5$	$\binom{10}{4}\cdot 8^6$
$N_{P^\circ}(8)$						1	$\binom{6}{5}\cdot 8^1$	$\binom{7}{5}\cdot 8^2$	$\binom{8}{5}\cdot 8^3$	$\binom{9}{5}\cdot 8^4$	$\binom{10}{5}\cdot 8^5$
$N_{P^\circ}(9)$							1	$\binom{7}{6}\cdot 8^1$	$\binom{8}{6}\cdot 8^2$	$\binom{9}{6}\cdot 8^3$	$\binom{10}{6}\cdot 8^4$
$N_{P^\circ}(10)$								1	$\binom{8}{7}\cdot 8^1$	$\binom{9}{7}\cdot 8^2$	$\binom{10}{7}\cdot 8^3$
$N_{P^\circ}(11)$									1	$\binom{9}{8}\cdot 8^1$	$\binom{10}{8}\cdot 8^2$
$N_{P^\circ}(12)$										1	$\binom{10}{9}\cdot 8^1$
$N_{P^\circ}(13)$											1
Factor	3^{20}	3^{18}	3^{16}	3^{14}	3^{12}	3^{10}	3^8	3^6	3^4	3^3	3^0

This table says that for $N_i = 10$, we find $N_{P^\circ}(3) = 1 \cdot 3^{20}$ limit 3rd roots P° with $h^0 = 3$. Similarly, for $N_i = 4$, we find $N_{P^\circ}(3) = \binom{6}{3} \cdot 8^3 \cdot 3^8$ limit 3rd roots P° with $h^0 = 6$. For ease of presentation, the overall factors are collected at the bottom of this table.

We would like to generalize this section-counting of limit roots for all curves, which may have multiple weighted subgraphs. Complications arise when counting the global sections of limits roots over partial blow-ups; namely, it is unclear what h^0 of a limit root is over a singular component of the curve, i.e., the component containing a singularity that has not been blown up. Although we will not discuss this direction in this paper, it presents an interesting problem which we hope to revisit in the future.

6.4 Limit root applications in F-theory

After the detailed exposition of root bundles and limit roots in the previous section, we now wish to apply these techniques to F-theory. We first outline how limit roots can be used to provide an explicit and oftentimes constructive argument for the absence of certain vector-like exotics. We demonstrate these ideas in one particular geometry among the largest class of currently-known globally consistent F-theory Standard Models without chiral exotics and gauge coupling unification [32]. We will argue that there are solutions without vector-like exotics in the representations $C_{(\mathbf{3},\mathbf{2})_{1/6}}$, $C_{(\overline{\mathbf{3}},\mathbf{1})_{-2/3}}$, $C_{(\overline{\mathbf{3}},\mathbf{1})_{1/3}}$ and $C_{(\mathbf{1},\mathbf{1})_1}$.

6.4.1 Absence of vector-like exotics

Let us look at an F-theory compactification to 4-dimensions on a space Y_4, which admits a smooth, flat, crepant resolution $\widehat{Y}_4$. As explained in 6.2.1, root bundles appear naturally in such settings when studying vector-like spectra. We found that the geometry determines a class $A' = \widehat{\gamma}(\mathcal{A}') \in H^4_D(\widehat{Y}_4, \mathbb{Z}(2))$ for some $\mathcal{A}' \in \mathrm{CH}^2(\widehat{Y}_4, \mathbb{Z})$, and an integer $\xi \in \mathbb{Z}_{>0}$ such that $\mathcal{A}$ is subject to the two constraints:

$$\gamma(\mathcal{A}) = G_4\,, \qquad \xi \cdot \widehat{\gamma}(\mathcal{A}) \sim \widehat{\gamma}(\mathcal{A}')\,. \tag{6.4.1}$$

The condition $\gamma(\mathcal{A}) = G_4$ immediately follows from 6.2.4 and it means that $A = \widehat{\gamma}(\mathcal{A})$ is an F-theory gauge potential for the given G_4-flux. The second condition ensures the absence of chiral exotics in the F-theory Standard Models [32]. It follows that the line bundle on the matter curve $C_{\mathbf{R}}$ satisfies

$$P_{\mathbf{R}} = \mathcal{O}_{C_{\mathbf{R}}}\left(D_{\mathbf{R}}(\mathcal{A})\right) \otimes_{\mathcal{O}_{C_{\mathbf{R}}}} \mathcal{O}_{C_{\mathbf{R}}}\left(D^{\text{spin}}_{C_{\mathbf{R}}}\right), \tag{6.4.2}$$

where $D_{\mathbf{R}}(\mathcal{A})$ and $D^{\text{spin}}_{C_{\mathbf{R}}}$ are solutions to the root bundle constraints

$$\xi \cdot D_{\mathbf{R}}(\mathcal{A}) \sim D_{\mathbf{R}}(\mathcal{A}'), \qquad 2 \cdot D^{\text{spin}}_{C_{\mathbf{R}}} \sim K_{\mathbf{R}}. \tag{6.4.3}$$

Recall from 6.3 that these root bundle constraints have many solutions. In general, it cannot be expected that all solutions are realized from roots in $H^4_D(\widehat{Y}_4, \mathbb{Z}(2))$ and spin^c-structures on the gauge surfaces. We reserve a detailed study of this interesting and challenging question for future works. In this article, we study all the ξ-th roots of $D_{\mathbf{R}}(\mathcal{A}')$ and all of the spin divisors $D^{\text{spin}}_{C_{\mathbf{R}}}$ systematically. Our goal is to identify roots $P_{\mathbf{R}}$ subject to the physical demand of absence/presence of vector-like pairs. In future works, we hope to identify which of these desired roots stem from F-theory gauge potentials in $H^4_D(\widehat{Y}_4, \mathbb{Z}(2))$.

At special loci of the complex structure moduli space, massive vector-like pairs can be rendered massless. Mathematically, this is reflected in the fact that deformations of a line bundle can have higher cohomologies. For example, if we assume $\chi(P_{\mathbf{R}}) \geq 0$, then we could have:

Geometry of curves $C_{\mathbf{R}}$	$(h^0(C_{\mathbf{R}}, P_{\mathbf{R}}), h^1(C_{\mathbf{R}}, P_{\mathbf{R}}))$
Generic	$(\chi(P_{\mathbf{R}}), 0)$
Less generic	$(\chi(P_{\mathbf{R}}) + 1, 1) \equiv (\chi(P_{\mathbf{R}}), 0) \oplus (1, 1)$
Even less generic	$(\chi(P_{\mathbf{R}}) + 2, 2) \equiv (\chi(P_{\mathbf{R}}), 0) \oplus (2, 2)$
$\vdots$	$\vdots$

In [48], such cohomology jumps have been analyzed in large detail. In particular, it was explained that even on generic curves, line bundles with the same chiral index need not have the same cohomologies. This classic observation goes by the name of *Brill-Noether theory* [150] (see also [128] for another application of Brill-Noether theory to F-theory). This observation in particular applies to root bundles. In 6.3.1, we have explained that of the four spin structures on an elliptic curve, one has $h^0(E, \mathcal{O}_E^{\text{spin}}) = 1$ and the other three have vanishing number of global sections. This is a special instance of the results in [177, 178], which show that all odd spin structures have odd number of zero modes, while the remaining even spin structures have even number of zero modes. Generally speaking, different roots $P_{\mathbf{R}}$ will have different numbers of zero modes.

That said, our task is to construct root bundles $P_{\mathbf{R}}$ with the cohomologies that are physically desired. For simplicity, let us assume $\chi(P_{\mathbf{R}}) \geq 0$. Inspired by physics, we should then distinguish the generic case $h^0(P_{\mathbf{R}}) = \chi(P_{\mathbf{R}})$ and the non-generic case $h^0(P_{\mathbf{R}}) > \chi(P_{\mathbf{R}})$. The former corresponds to the absence of exotic vector-like pairs, while the latter most prominently features on the Higgs curve in F-theory Standard Model constructions. In the latter case, for MSSM constructions, one wishes to achieve $h^0(P_{\mathbf{R}}) = \chi(P_{\mathbf{R}}) + 1$ so that the additional vector-like pair describes a Higgs field.

We approach the task of constructing such physically desired root bundles $P_{\mathbf{R}}$ by first considering a deformation $C_{\mathbf{R}} \to C_{\mathbf{R}}^{\bullet}$, where $C_{\mathbf{R}}^{\bullet}$ is a *nodal* curve. Therefore, $P_{\mathbf{R}} \to P_{\mathbf{R}}^{\bullet}$ becomes a root bundle on the nodal curve $C_{\mathbf{R}}^{\bullet}$. We focus on roots $P_{\mathbf{R}}^{\bullet}$, which we can describe by limit roots $P_{\mathbf{R}}^{\circ}$ on the full blow-up $C_{\mathbf{R}}^{\circ}$ of $C_{\mathbf{R}}^{\bullet}$. For those limit roots, we can

employ the technology described in 6.3 in order to identify $h^0(C^\circ_{\mathbf{R}}, P^\circ_{\mathbf{R}})$. This enables us to identify roots $P^\circ_{\mathbf{R}}$ with $h^0(C^\circ_{\mathbf{R}}, P^\circ_{\mathbf{R}}) = \chi(P^\circ) + \delta$ from simple combinatorics, where $\delta \in \mathbb{Z}_{\geq 0}$ is the physically desired offset.

The pushforward of limit roots $P^\circ_{\mathbf{R}}$ along the blow-up map $\pi\colon C^\circ_{\mathbf{R}} \to C^\bullet_{\mathbf{R}}$ preserves the number of global sections, i.e. $h^0(C^\circ_{\mathbf{R}}, P^\circ_{\mathbf{R}}) = h^0(C^\bullet_{\mathbf{R}}, P^\bullet_{\mathbf{R}})$. We have thus identified the roots on $C^\bullet$ which have the physically desirable cohomologies. In theory, we can trace those roots $P^\bullet_{\mathbf{R}}$ along the deformation $C^\bullet_{\mathbf{R}} \to C_{\mathbf{R}}$ to find roots $P_{\mathbf{R}}$ on the original curve $C_{\mathbf{R}}$. Crucially though, such a deformation can change the number of sections (see e.g. [48]). For the deformation $C^\bullet_{\mathbf{R}} \to C_{\mathbf{R}}$, which turns a nodal (i.e. singular and thus non-generic) curve into a smooth, irreducible curve, it is known that the number of sections is an upper semi-continuous function. This means that the number of sections either remains constant or decreases as we trace $P^\bullet_{\mathbf{R}}$ to $P_{\mathbf{R}}$ on $C_{\mathbf{R}}$:

$$h^0(C_{\mathbf{R}}, P_{\mathbf{R}}) \leq h^0(C^\bullet_{\mathbf{R}}, P^\bullet_{\mathbf{R}}) = \chi(P_{\mathbf{R}}) + \delta\,. \tag{6.4.4}$$

The natural question is thus to look for roots $P^\bullet_{\mathbf{R}}$ for which equality holds. This happens in the generic case, i.e. the case $\delta = 0$. This is because the number of sections is then already minimal on $C^\bullet_{\mathbf{R}}$ and thus, it must remain constant along the deformation to $C^\bullet_{\mathbf{R}}$:

$$h^0(C_{\mathbf{R}}, P_{\mathbf{R}}) = h^0(C^\bullet_{\mathbf{R}}, P^\bullet_{\mathbf{R}}) = \chi(P_{\mathbf{R}})\,. \tag{6.4.5}$$

The upshot of this strategy, which we summarize in 13, is that we can provide a lower bound to the number of roots $P_{\mathbf{R}}$ without vector-like exotics by studying the combinatorics of limit roots on the full blow-up $C^\circ_{\mathbf{R}}$ of the nodal curve $C^\bullet_{\mathbf{R}}$.[7]

In aiming for F-theory MSSMs, the non-generic case $\delta = 1$ is also fairly important for the Higgs curve. While it is not hard to construct limit roots on $C^\circ_{(\mathbf{1},\mathbf{2})_{-1/2}}$ with exactly 4 sections, the corresponding roots $P^\bullet_{(\mathbf{1},\mathbf{2})_{-1/2}}$ satisfy $h^0(C^\bullet_{(\mathbf{1},\mathbf{2})_{-1/2}}, P^\bullet_{(\mathbf{1},\mathbf{2})_{-1/2}}) = 4$, which

[7]Recall that at least one of these roots stems from an F-theory gauge potential in $\mathrm{CH}^2(\widehat{Y}_4, \mathbb{Z})$.

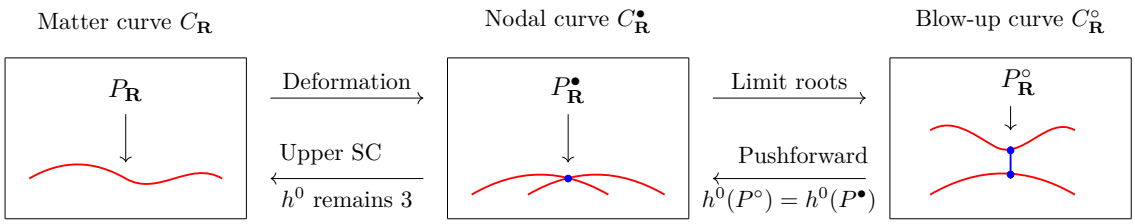

Figure 13: Roots $P_{\mathbf{R}}$ with $h^0(C_{\mathbf{R}}, P_{\mathbf{R}}) = 3$ from roots $P^{\bullet}_{\mathbf{R}}$ on a nodal curve $C^{\bullet}_{\mathbf{R}}$ and limit roots $P^{\circ}_{\mathbf{R}}$ on its blow-up $C^{\circ}_{\mathbf{R}}$.

is larger than the minimal value $\chi(P_{(\mathbf{1},\mathbf{2})_{-1/2}}) = 3$. Since the number of sections is non-minimal, we cannot conclude from upper semi-continuity that the number of sections remains constant. Rather, we expect some of those roots $P^{\bullet}_{(\mathbf{1},\mathbf{2})_{-1/2}}$ to lose a section when traced to $C_{(\mathbf{1},\mathbf{2})_{-1/2}}$. Currently, we do not know a sufficient discriminating property that allows us to identify the roots $P^{\bullet}_{(\mathbf{1},\mathbf{2})_{-1/2}}$ for which the number of sections remains constant. We reserve this interesting mathematical question for future work.

6.4.2 Application to F-theory Standard Models

We now continue the analysis initiated in 6.2.2, where we summarized the geometry of the largest currently-known class of globally consistent F-theory Standard Models without chiral exotics and gauge coupling unification [32]. The chiral index on all five matter curves

$$C_{(\mathbf{3},\mathbf{2})_{1/6}} = V(s_3, s_9)\,, \qquad C_{(\mathbf{1},\mathbf{2})_{-1/2}} = V\left(s_3, s_2 s_5^2 + s_1(s_1 s_9 - s_5 s_6)\right)\,, \tag{6.4.6}$$

$$C_{(\overline{\mathbf{3}},\mathbf{1})_{-2/3}} = V(s_5, s_9)\,, \qquad C_{(\overline{\mathbf{3}},\mathbf{1})_{1/3}} = V\left(s_9, s_3 s_5^2 + s_6(s_1 s_6 - s_2 s_5)\right)\,, \tag{6.4.7}$$

$$C_{(\mathbf{1},\mathbf{1})_1} = V(s_1, s_5)\,, \tag{6.4.8}$$

is thus exactly three. We worked out the root bundle constraints (c.f. C.2.3). In aiming for an MSSM construction, which comes with exactly one Higgs pair, the vector-like spectrum is subject to the demand $4 = h^0(C_{(\mathbf{1},\mathbf{2})_{-1/2}}, P_{(\mathbf{1},\mathbf{2})_{-1/2}})$. As explained above, since $4 = 1 + \chi(P_{(\mathbf{1},\mathbf{2})_{-1/2}})$, our current technology does not allow us to tend to this case. However, we can address the absence of vector-like exotics on the remaining matter curves

in a constructive way. That is, we can construct solutions to the constraint

$$\begin{aligned} 3 &= h^0(C_{(\mathbf{3},\mathbf{2})_{1/6}}, P_{(\mathbf{3},\mathbf{2})_{1/6}}) = h^0(C_{(\overline{\mathbf{3}},\mathbf{1})_{-2/3}}, P_{(\overline{\mathbf{3}},\mathbf{1})_{-2/3}}) \\ &= h^0(C_{(\overline{\mathbf{3}},\mathbf{1})_{1/3}}, P_{(\overline{\mathbf{3}},\mathbf{1})_{1/3}}) = h^0(C_{(\mathbf{1},\mathbf{1})_1}, P_{(\mathbf{1},\mathbf{1})_1})\,. \end{aligned} \tag{6.4.9}$$

To outline these steps, let us first look at the quark-doublet curve $C_{(\mathbf{3},\mathbf{2})_{1/6}} = V(s_3, s_9)$, where s_3, s_9 are generic sections of $\overline{K}_B$. To make our construction explicit, let us focus on base spaces B_3 with $\overline{K}_B^3 = 18$. It then follows from C.2.3 that we are trying to argue for the existence of root bundles that satisfy

$$P_{(\mathbf{3},\mathbf{2})_{1/6}}^{\otimes 36} \sim K_{(\mathbf{3},\mathbf{2})_{1/6}}^{\otimes 24}\,, \qquad h^0(C_{(\mathbf{3},\mathbf{2})_{1/6}}, P_{(\mathbf{3},\mathbf{2})_{1/6}}) = 3\,. \tag{6.4.10}$$

For this, it suffices to argue that root bundles with the following properties exist

$$P_{(\mathbf{3},\mathbf{2})_{1/6}}^{\otimes 3} \sim K_{(\mathbf{3},\mathbf{2})_{1/6}}^{\otimes 2}\,, \qquad h^0(C_{(\mathbf{3},\mathbf{2}_{1/6})}, P_{(\mathbf{3},\mathbf{2})_{1/6}}) = 3\,. \tag{6.4.11}$$

We achieve a proof of existence by studying a deformation $C_{(\mathbf{3},\mathbf{2})_{1/6}} \to C^{\bullet}_{(\mathbf{3},\mathbf{2})_{1/6}}$. Let us work with a concrete base geometry, we opt for the toric base space $B_3 = P_{39}$ with $\overline{K}_B^3 = 18$, whose details are summarized in C.2.4.

To describe the deformation $C_{(\mathbf{3},\mathbf{2})_{1/6}} \to C^{\bullet}_{(\mathbf{3},\mathbf{2})_{1/6}}$, we first notice that s_3 is a polynomial in the homogeneous coordinates $\{x_i\}_{1\leq i\leq 11}$ of P_{39}. Since s_3 is a section of $\overline{K}_{P_{39}}$, it contains the monomial $\prod_{i=1}^{11} x_i$.[8] This allows us to consider the deformation

$$V(s_3, s_9) = C_{(\mathbf{3},\mathbf{2})_{1/6}} \to C^{\bullet}_{(\mathbf{3},\mathbf{2})_{1/6}} = V\left(\prod_{i=1}^{11} x_i, s_9\right)\,. \tag{6.4.12}$$

Since we assume *generic* s_9, $C^{\bullet}_{(\mathbf{3},\mathbf{2})_{1/6}}$ is manifestly nodal in the K3-surface $V(s_9)$ and the techniques of 6.3 apply. To this end, we first identify the dual graph of $C^{\bullet}_{(\mathbf{3},\mathbf{2})_{1/6}}$, which

[8] For any toric base space B_3 with homogeneous coordinates x_i, $\prod_i x_i$ is a section of $\overline{K}_B \sim \sum_i [x_i]$.

has 17 irreducible components:

curve	equation	genus	$\deg\left(2\cdot K_{C^\bullet_{(\mathbf{3},\mathbf{2})_{1/6}}}\Big\vert_{C_i}\right)$
C_1	$V(x_1, s_9)$	1	6
C_3	$V(x_3, s_9)$	1	6
C_6	$V(x_6, s_9)$	0	12
C_{11}	$V(x_{11}, s_9)$	0	12
C_2	$V(x_2, s_9)$	0	0
$\left\{C_8^{(i)}\right\}_{1\leq i\leq 6}$	$V(x_8, x_1-\alpha_i x_3)$	0	0
$\left\{C_{10}^{(i)}\right\}_{1\leq i\leq 6}$	$V(x_{10}, x_1-\alpha_i x_3)$	0	0

(6.4.13)

For convenience, we list the degree of $2\cdot K_{C^\bullet_{(\mathbf{3},\mathbf{2})_{1/6}}}$ on all irreducible components since 6.4.11 instructs us to construct third roots of this bundle. By taking the Stanley-Reisner ideal of P_{39} into account (see C.2.4), one finds the dual graph of $C^\bullet_{(\mathbf{3},\mathbf{2})_{1/6}}$:

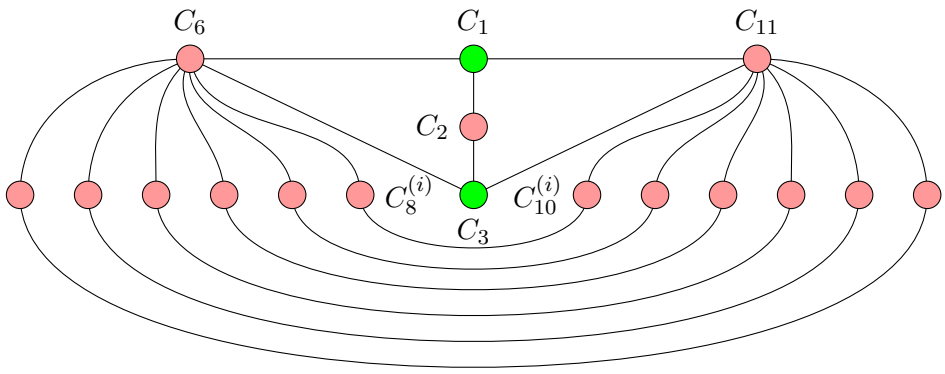

(6.4.14)

We mark the $\mathbb{P}^1$s in pink and the elliptic curves in green. This diagram is easily extended to a weighted diagram, which encodes a 3rd root of $2\cdot K_{C^\bullet_{(\mathbf{3},\mathbf{2})_{1/6}}}$. This involves placing weights $w_i\in\{1,2\}$ subject to the following two rules (cf. 6.3.3):

1. Along each edge: The sum of weights is 3.

2. At each node: The sum of weights equals the degree in 6.4.13 modulo 3.

It is readily verified that the following weighted diagram satisfies these rules:

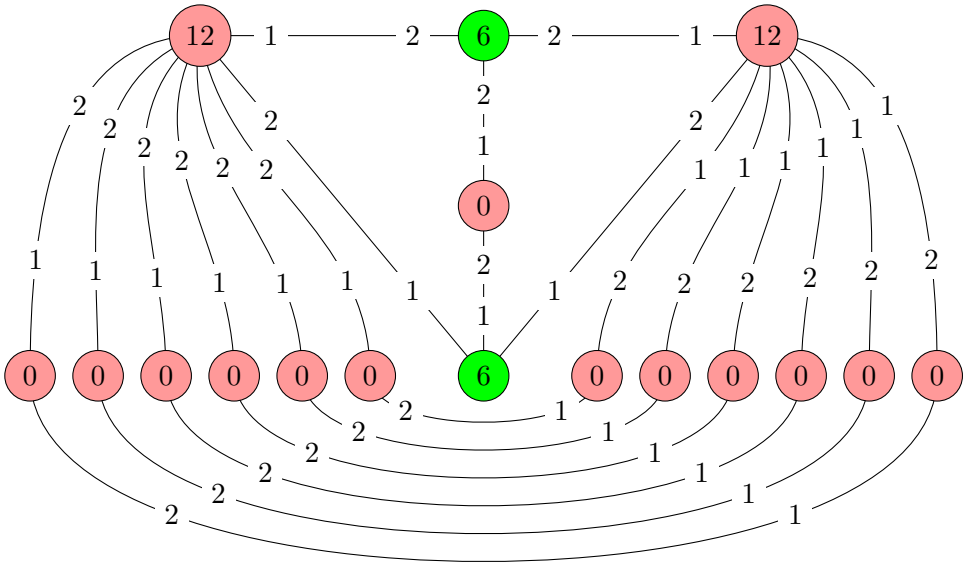

(6.4.15)

We then study the limit roots $P^{\circ}_{(\mathbf{3},\mathbf{2})_{1/6}}$ on the full blow-up $C^{\circ}_{(\mathbf{3},\mathbf{2})_{1/6}}$ of $C^{\bullet}_{(\mathbf{3},\mathbf{2})_{1/6}}$, which are

encoded by this diagram. The degree of each such limit root $P^{\circ}_{(\mathbf{3},\mathbf{2})_{1/6}}$ is as follows:

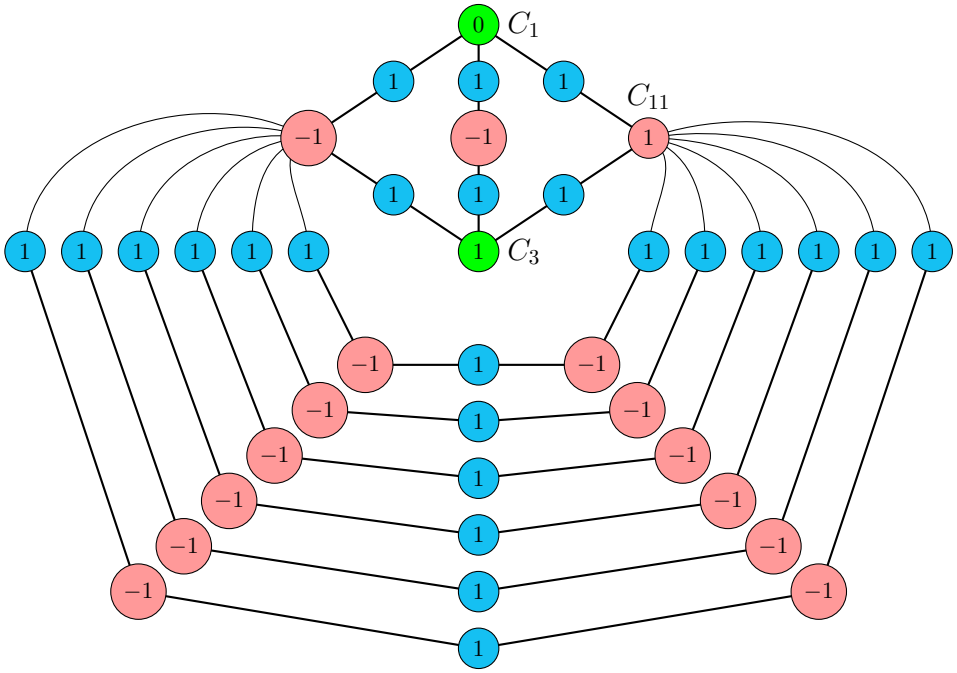

(6.4.16)

Note that we denote the blow-up $\mathbb{P}^1$s in blue and that, by construction of the limit roots, we consider a degree 1 line bundle on each of these. It follows that the (total) degree of each such limit root $P^{\circ}_{(\mathbf{3},\mathbf{2})_{1/6}}$ is 12. This is expected from 6.4.11 since it is equivalent to $\chi(P^{\circ}_{(\mathbf{3},\mathbf{2})_{1/6}}) = 3$. Here, we claim even more, namely that some of these limit roots have exactly three global sections.

To see this, recall from 6.3.4 that the number of global sections of a limit root $P^{\circ}_{(\mathbf{3},\mathbf{2})_{1/6}}$ is simply given by the sum of the sections on each irreducible component of $C^{\bullet}_{(\mathbf{3},\mathbf{2})_{1/6}}$. Hence, we have to add the number of sections on the green and pink components in 6.4.16. From the degrees, it follows that only C_1, C_3 and C_{11} support a non-zero number of sections, namely

$$h^0\left(C_1, P^{\circ}_{(\mathbf{3},\mathbf{2})_{1/6}}\right) = \left\{ \begin{array}{c} 0 \\ 1 \end{array} \right\}, \quad h^0\left(C_3, P^{\circ}_{(\mathbf{3},\mathbf{2})_{1/6}}\right) = 1\,, \quad h^0\left(C_{11}, P^{\circ}_{(\mathbf{3},\mathbf{2})_{1/6}}\right) = 2\,. \quad (6.4.17)$$

The notation for C_1 reminds us of the fact that on an elliptic curve, a line bundle with

vanishing degree can either have 0 or 1 global section. Moreover, recall from 6.3.3 that the limit roots on C_1 are actually the 3rd roots of a line bundle of vanishing degree. In anticipation of this situation, we have already given a detailed exposition of exactly those root bundles on elliptic curves in 6.3.1. In particular, it follows from 6.3.3 that at least 8 of the 9 3rd roots on C_1 satisfy $h^0(C_1, P^\circ_{(\mathbf{3},\mathbf{2})_{1/6}}) = 0$.

Note that also C_3 admits $9 = 3^{2\cdot 1}$ different roots. However, in contrast to C_1, all of these roots are in the Kodaira stable regime and have exactly one section. Therefore, we conclude that we found at least $8 \cdot 9 = 72$ limit roots $P^\circ_{(\mathbf{3},\mathbf{2})_{1/6}}$ with

$$3 = h^0\left(C^\circ_{(\mathbf{3},\mathbf{2})_{1/6}}, P^\circ_{(\mathbf{3},\mathbf{2})_{1/6}}\right) . \tag{6.4.18}$$

It therefore follows from our discussion in 6.4.1 that there are at least 72 solutions to 6.4.11 and consequently, also to 6.4.10. Let us emphasize that this analysis does not guarantee that one of these 72 solutions stems from an F-theory gauge potential in $H^4_D(\widehat{Y}_4, \mathbb{Z}(2))$. This top-down study is reserved for future work.

Along exactly the same lines, we can argue that also $C_{(\overline{\mathbf{3}},\mathbf{1})_{-2/3}} = V(s_5, s_9)$ and the singlet curve $C_{(\mathbf{1},\mathbf{1})_1} = V(s_1, s_5)$ admit at least 72 solutions to the root bundle constraints with exactly three global sections. This leaves us to discuss the vector-like spectrum on

$$C_{(\overline{\mathbf{3}},\mathbf{1})_{1/3}} = V\left(s_9, s_3 s_5^2 + s_6(s_1 s_6 - s_2 s_5)\right) . \tag{6.4.19}$$

On this curve we look for root bundles spicied in C.2.3 To this end we consider the deformation $C_{(\overline{\mathbf{3}},\mathbf{1})_{1/3}} \to C^\bullet_{(\overline{\mathbf{3}},\mathbf{1})_{1/3}}$ with

$$C^\bullet_{(\overline{\mathbf{3}},\mathbf{1})_{1/3}} = V(s_9, s_5 - s_6) \cup V(s_9, s_3 - s_6) \cup V(s_9, s_5 + s_6) \equiv Q_1 \cup Q_2 \cup Q_3 , \tag{6.4.20}$$

which is obtained from

$$s_1 \to s_6 - s_3\,, \qquad s_2 \to s_5 - \prod_{i=1}^{11} x_i\,, \qquad s_9 \to \prod_{i=1}^{11} x_i\,, \tag{6.4.21}$$

and *generic* s_3, s_5, s_6. Therefore, $C_{(\overline{\mathbf{3}},\mathbf{1})_{1/3}} \to C^{\bullet}_{(\overline{\mathbf{3}},\mathbf{1})_{1/3}}$ turns this matter curve into three nodal curves, each of which looks like the curve $C^{\bullet}_{(\mathbf{3},\mathbf{2})_{1/6}}$ that we discussed above. From this point on, we can again employ the limit root techniques. On a technical level, the only distinction to the constructions presented for $C^{\bullet}_{(\mathbf{3},\mathbf{2})_{1/6}}$ is that we have to carefully take into account the line bundle contributions from the Yukawa point Y_3. Also, the resulting weighted diagrams become very large since the nodal curve $C^{\bullet}_{(\overline{\mathbf{3}},\mathbf{1})_{1/3}}$ has 51 irreducible components. For these reasons, it suffices to state that we can argue for at least $36^2 \cdot 35^4$ solutions. Details are provided in C.2.4. We reserve a detailed top-down study of which root bundles arise from an F-theory gauge potential in $H^4_D(\widehat{Y}_4, \mathbb{Z}(2))$ for the future.

6.5 Conclusion and Outlook

This work is motivated by the frequent appearance of fractional powers of line bundles when studying vector-like spectra of globally consistent 4d F-theory Standard Models with three chiral families and gauge coupling unification [32]. In these models, the vector-like spectra on the low-genus matter curves are naively encoded in cohomologies of a line bundle that is identified with a fractional power of the canonical bundle. On high-genus curves, these fractional powers of the canonical bundle are further modified by contributions from Yukawa points. In order to understand these fractional bundles, we have analyzed their origin and nature.

First, in 6.2.1, we analyzed the origin of such fractional powers of line bundles. We recalled that the vector-like spectra are not specified by a G_4-flux, but rather by its associated gauge potential in the Deligne cohomology $H^4_D(\widehat{Y}_4, \mathbb{Z}(2))$ [45, 46, 47]. In fact, a given G_4-flux has many such gauge potentials. To see this, recall that in the dual M-theory picture, $G_4 = dC_3$, where C_3 is the internal M-theory 3-form potential. Any other 3-form

potential C_3' with closed $C_3' - C_3$ still has G_4 as its field strength. Such closed 3-form potentials are encoded by the intermediate Jacobian $J^2(\widehat{Y}_4)$ in the F-theory geometry. While it is well-defined in theory, it can be very challenging to associate even a single gauge potential in $H^4_D(\widehat{Y}_4, \mathbb{Z}(2))$ to a given G_4-flux in practice. We were able to tie the appearance of fractional powers of line bundles to exactly this challenge.

For an F-theory model, we need an F-theory gauge potential, i.e., a class in the Deligne cohomology group $A \in H^4_D(\widehat{Y}_4, \mathbb{Z})$. This will be specified as $\widehat{\gamma}(\mathcal{A})$ for some "potential" $\mathcal{A} \in \mathrm{CH}^2(\widehat{Y}_4, \mathbb{Z})$. We found that the geometry determines a class $A' = \widehat{\gamma}(\mathcal{A}') \in H^4_D(\widehat{Y}_4, \mathbb{Z}(2))$ and an integer $\xi \in \mathbb{Z}_{>0}$ such that $\mathcal{A}$ is subject to the two constraints:

$$\gamma(\mathcal{A}) = G_4\,, \qquad \xi \cdot \widehat{\gamma}(\mathcal{A}) \sim \widehat{\gamma}(\mathcal{A}')\,. \tag{6.5.1}$$

The condition $\gamma(\mathcal{A}) = G_4$ immediately follows from 6.2.4 and it means that $A = \widehat{\gamma}(\mathcal{A})$ is an F-theory gauge potential for the given G_4-flux. In the dual M-theory picture, it states that the 3-form potential C_3 satisfies $dC_3 = G_4$. We illustrated with several examples that the absence of chiral exotics in the F-theory Standard Models [32] boils down to the second constraint.

It is important to notice that the gauge potential $A = \widehat{\gamma}(\mathcal{A})$ specified by the two conditions in 6.5.1 is in general not unique. The collection of all ξ-th roots of $\widehat{\gamma}(\mathcal{A}')$ (if non-empty) is a coset of the group of all ξ-th roots of 0. In particular, the number of solutions is $\xi^{2\cdot\dim_{\mathbb{C}}\left(J^2(\widehat{Y}_4)\right)}$. All these solutions lead to the same chiral spectrum (6.2.2) since they all have the same degree when restricted to the curves $C_{\mathbf{R}}$, and hence, the same index. However, they could differ in their actual spectrum (6.2.7). This extra flexibility is the key tool that we intend to use to produce a desirable spectrum such as the MSSM.

In theory, we could proceed by studying gauge potentials $A = \widehat{\gamma}(\mathcal{A}) \in H^4_D(\widehat{Y}_4, \mathbb{Z}(2))$ subject to 6.5.1. However, in practice it seems more efficient to proceed with the algebraic cycle $\mathcal{A}'$, which we could construct explicitly in the largest currently-known class of

globally consistent F-theory Standard Models without chiral exotics and gauge coupling unification [32]. Hence, we have a sufficient level of arithmetic control over $A' = \widehat{\gamma}(\mathcal{A}')$. In particular, we can identify the $\mathbb{Z}$-Cartier divisor $D_{\mathbf{R}}(\mathcal{A}')$ induced from $\mathcal{A}'$ on the matter curve $C_{\mathbf{R}}$. It follows that

$$\xi \cdot D_{\mathbf{R}}(\mathcal{A}) \sim D_{\mathbf{R}}(\mathcal{A}')\,. \tag{6.5.2}$$

Divisors $D_{\mathbf{R}}(\mathcal{A})$, which solve this equation for given $D_{\mathbf{R}}(\mathcal{A}')$ and ξ, are called *root divisors* and their associated line bundles are *root bundles*. They exist if and only if ξ divides the degree of $D_{\mathbf{R}}(\mathcal{A}')$. Such root bundles are by no means unique. For example, spin bundles on a genus g matter curve $C_{\mathbf{R}}$ are 2nd roots of the canonical bundle $K_{\mathbf{R}}$ and there are 2^{2g} such roots. Similarly, on a genus g-curve, 6.5.2 admits ξ^{2g} solutions (if they exist).

It is well-known that not all spin bundles have the same number of global sections. Rather, roughly half of the spin bundles on a curve $C_{\mathbf{R}}$ have an odd number of global sections and the remaining ones have an even number [177, 178]. More generally, we can therefore expect that the gauge potentials $A = \widehat{\gamma}(\mathcal{A})$ subject to 6.5.1 lead to different vector-like spectra. This mirrors the physical expectation that inequivalent F-theory gauge potentials — equivalently, in the dual M-theory picture, two 3-form potentials C_3 and C_3' that differ by a closed 3-form — will in general lead to different vector-like spectra. This was anticipated e.g. in [45, 46, 47].

In general, only a subset of the root divisors in 6.5.2 are induced from F-theory gauge potentials in $H^4_D(\widehat{Y}_4, \mathbb{Z}(2))$. While this work does not answer the important question of which root divisors are induced from F-theory potentials, we hope that this work initiates and facilitates this study by providing a systematic analysis of all root bundles and spin bundles on the matter curves. Our goal in this work was to identify combinations of root bundles and spin bundles on the matter curves, such that their global sections satisfy the physical demand of the presence/absence of vector-like pairs.

While we expect that our techniques apply more generally, we have focused on the largest currently-known class of globally consistent F-theory Standard Models with realistic chiral spectra [32], which emphasizes the genuine appearance of root bundles in vector-like spectra of F-theory compactifications. It should be mentioned that the background G_4-flux in these F-theory Standard Models models does not only lead to realistic chiral spectra, but also allows cancelation of the D3-tadpole and ensures masslessness of the $U(1)$-gauge boson. We summarize the involved technical steps in the derivation of these root bundle constraints in C.2. This derivation heavily relies on a detailed understanding of the elliptically fibered 4-fold F-theory geometry $\widehat{Y}_4$, including intersection numbers in the fiber over the Yukawa points. We supplement the earlier works [82, 40, 32] by providing a complete list of all fiber intersection numbers in C.1.

Our approach to identifying root and spin bundles on the matter curves, whose cohomologies are physically desired for the presence/absence of vector-like pairs, is inspired by the work in [170], which gives a diagrammatic description of root bundles on nodal curves $C^{\bullet}_{\mathbf{R}}$. More explicitly, it relates these roots with so-called *limit roots* on (partial) blow-ups $C^{\circ}_{\mathbf{R}}$ of $C^{\bullet}_{\mathbf{R}}$. We summarized these ideas in 6.3, and then introduced counting procedures for the global sections. In order to fully appreciate this finding, recall from [48] that in general one will merely find a lower bound. The argument that we provide in this work is stronger – it provides an exact count of the global sections of limit roots on *full* blow-ups of $C^{\bullet}_{\mathbf{R}}$. This observation may be interesting in its own right since it provides a combinatoric access to Brill-Noether theory of limit roots. We demonstrated this for a nodal curve – the *Holiday lights* $H^{\bullet}$. This curve is of compact type and its only blow-up that is to be considered for the limit root is its full blow-up. Our approach then allowed us to identify exactly how many limit roots possess a certain number of global sections. It will be an interesting mathematical question to extend these ideas to partial blow-ups. We reserve this analysis for future work.

Given these insights on root bundles on nodal curves $C^{\bullet}_{\mathbf{R}}$, it remained to extract informa-

tion on root bundles on actual matter curves $C_{\mathbf{R}}$ in F-theory compactifications. As the latter are typically smooth, it is natural to wonder what we can say about (limit) roots when traced along a deformation $C_{\mathbf{R}}^{\bullet} \to C_{\mathbf{R}}$. In particular, we can wonder if there are deformations of $C_{\mathbf{R}}$ that are conducive for a more fruitful analysis. As we have already mentioned, curves of compact type, such as the *Holiday lights*, are prime candidates. The lack of cycles in their dual graph limits the number of possible weighted graphs, so much so that we have a complete understanding of the limit roots and their global sections. In contrast, the dual graphs of the deformed matter curves $C_{\mathbf{R}}^{\bullet}$ in explicit geometries are more complex in which there are multiple weighted subgraphs, and limit roots over partial blow-ups. In particular, some singularities on the curve still remain in its partial blow-up, and it is therefore far more challenging to count the sections. It would be useful to compare these two examples in more depth and to determine exactly what features of the dual graph allow for better section-counting. One obvious feature is the cyclomatic number, which happens to be the first Betti number of a graph when viewed as a 1-dimensional simplicial complex. Curves of compact type have zero cyclomatic number, and thus, are topologically simple. Subsequently, we can explore possible ways of deforming $C_{\mathbf{R}}$ to a nodal curve whose dual graph has these desirable features.

In this work, we have focused on deformations $C_{\mathbf{R}} \to C_{\mathbf{R}}^{\bullet}$ which arise naturally by modifying the defining polynomials in a concrete base geometry B_3. Most curves that we encountered in this way had planar dual graphs. Still, for the most involved matter curve discussed in this article, the dual graph is non-planar. The subject of planarity raises many interesting questions and applications in graph theory [189, 190, 191, 192, 193]. However, the geometric significance for a nodal curve to have a non-planar dual graph is not mentioned in the literature to our knowledge [194, 195]. It is possible that planarity does not play a role in the geometry of nodal curves. Indeed, the curve associated to the well-known non-planar graph $K_{3,3}$ is quite ordinary. Nevertheless, it would be useful to explore this feature as it raises the question of whether there are better ways to represent

a given dual graph.

For a physical application, we have studied vector-like spectra of F-theory Standard Models without chiral exotics in 6.4. In aiming for MSSM constructions, we should wonder what we can say about the global sections of a root $P^\bullet_{\mathbf{R}}$ as we trace it to a root $P_{\mathbf{R}}$ along a deformation $C^\bullet_{\mathbf{R}} \to C_{\mathbf{R}}$. In this work, we did not attempt to provide a complete answer to this question. Rather, we recalled that a certain behavior of the cohomologies along such a deformation is known. This is called *upper semi-continuity* and it means that the number of global sections cannot increase when tracing a root $P^\bullet_{\mathbf{R}}$ on $C^\bullet_{\mathbf{R}}$ to a root $P_{\mathbf{R}}$ on $C_{\mathbf{R}}$. Put differently,

$$h^0\left(C_{\mathbf{R}}, P_{\mathbf{R}}\right) \leq h^0\left(C^\bullet_{\mathbf{R}}, P^\bullet_{\mathbf{R}}\right) . \tag{6.5.3}$$

For F-theory MSSM constructions, it is important to understand (limit) roots on the Higgs curve with $h^0(C_{(\mathbf{1},\mathbf{2})_{-1/2}}, P_{(\mathbf{1},\mathbf{2})_{-1/2}}) = 4 = 1+\chi(P_{(\mathbf{1},\mathbf{2})_{-1/2}})$. While we can construct roots $P^\bullet_{(\mathbf{1},\mathbf{2})_{-1/2}}$ with $h^0(C^\bullet_{(\mathbf{1},\mathbf{2})_{-1/2}}, P^\bullet_{(\mathbf{1},\mathbf{2})_{-1/2}}) = 4$, upper semi-continuity does then not guarantee that $P^\bullet_{(\mathbf{1},\mathbf{2})_{-1/2}} \to P_{(\mathbf{1},\mathbf{2})_{-1/2}}$ along $C^\bullet_{(\mathbf{1},\mathbf{2})_{-1/2}} \to C_{(\mathbf{1},\mathbf{2})_{-1/2}}$ yields roots with 4 global sections. Rather, the roots could lose sections along this transition (cf. [48]). To our knowledge, a sufficient criterion that identifies the Higgs roots $P^\bullet_{(\mathbf{1},\mathbf{2})_{-1/2}}$ that do not lose sections is currently unknown. However, given the physical significance of such a condition, we hope to return to this interesting question in the future.

Even a subset of (limit) roots that do not lose sections along $C^\bullet_{\mathbf{R}} \to C_{\mathbf{R}}$ is valuable. We identified a family of such roots $P^\bullet_{\mathbf{R}}$. Namely, for a root with $h^0\left(C^\bullet_{\mathbf{R}}, P^\bullet_{\mathbf{R}}\right) = \chi(P_{\mathbf{R}}) \geq 0$, it follows from upper semi-continuity that $h^0\left(C_{\mathbf{R}}, P_{\mathbf{R}}\right) = h^0\left(C^\bullet_{\mathbf{R}}, P^\bullet_{\mathbf{R}}\right)$. Any such root thus satisfies $h^i\left(C_{\mathbf{R}}, P_{\mathbf{R}}\right) = (\chi(P_{\mathbf{R}}), 0)$, which means it describes a zero mode spectrum on $C_{\mathbf{R}}$ without vector-like pairs. For example, in the F-theory MSSM constructions, this is a desired feature for the representations $C_{(\mathbf{3},\mathbf{2})_{1/6}}$, $C_{(\overline{\mathbf{3}},\mathbf{1})_{-2/3}}$, $C_{(\overline{\mathbf{3}},\mathbf{1})_{1/3}}$, $C_{(\mathbf{1},\mathbf{1})_1}$ for which vector-like pairs are exotic, i.e. have thus far not been observed in particle accelerators.

We have applied these techniques to a particular F-theory geometry among the largest currently-known class of globally consistent F-theory Standard Model constructions without chiral exotics and gauge coupling unification [32]. To this end, we worked with the base space $B_3 = P_{39}$. This 3-fold is one of the triangulations of the 39-th polyhedron of the Kreuzer-Skarke list[2], hence the name. In this space, we have explicitly deformed the matter curves $C_{\mathbf{R}}$ to nodal curves $C^{\bullet}_{\mathbf{R}}$. On those nodal curves, we could then easily construct limit roots on the full blow-up $C^{\circ}_{\mathbf{R}}$ of $C^{\bullet}_{\mathbf{R}}$ which have exactly 3 sections. We collect details on the base space $B_3 = P_{39}$ and limit roots on the blow-up of a genus $g = 82$ matter curve in C.2.4. In future works, we hope to investigate which of these desired root bundles are realized from F-theory gauge potentials in $H^4_D(\widehat{Y}_4, \mathbb{Z}(2))$.

To fully appreciate these findings, let us point out that this task cannot be performed with state-of-the-art algorithms such as [168] unless one explicitly specifies the line bundle divisor in question. In past works [46, 47], such constructions were described. A computer model of such line bundles (by dualizing the corresponding ideal sheaf) requires Gröbner basis computations. Even by the use of state-of-the-art algorithms such as [94], the involved geometries resulted in excessively long runtimes and heavy memory consumption. By approaching root bundles from limit roots on full blow-ups, these complications are circumvented at the cost of studying deformation theory.

This work provides a constructive approach to identifying limit root bundles on full blow-ups of a nodal curve with specific number of global sections. Since our approach is completely constructive, we anticipate a computer implementation which can find all such limit roots. For this, one would work out all of the weighted diagrams associated to the dual graph of a nodal curve $C^{\bullet}_{\mathbf{R}}$, and then identify the limit roots with the desired number of global sections. In generalizing this approach even further, we anticipate a scan over many of the F-theory Standard model geometries in [32]. By employing state-of-the-art data-science and machine learning techniques, it can be expected that such a scan will lead to a more refined understanding of F-theory Standard Model constructions. We hope

to return to this fascinating question in the near future.

In the largest, currently known, class of one Quadrillion globally consistent F-theory Standard Models with gauge coupling unification and no chiral exotics, the vector-like spectra are counted by cohomologies of root bundles. In this work, we apply a previously proposed method to identify toric base 3-folds, which are promising to establish F-theory Standard Models with exactly three quark-doublets and no vector-like exotics in this representation. The base spaces in question are obtained from triangulations of 708 polytopes. By studying root bundles on the quark doublet curve $C_{(\mathbf{3},\mathbf{2})_{1/6}}$ and employing well-known results about desingularizations of toric K3-surfaces, we derive a *triangulation independent lower bound* $\check{N}_P^{(3)}$ for the number $N_P^{(3)}$ of root bundles on $C_{(\mathbf{3},\mathbf{2})_{1/6}}$ with exactly three sections. The ratio $\check{N}_P^{(3)}/N_P$, where N_P is the total number of roots on $C_{(\mathbf{3},\mathbf{2})_{1/6}}$, is largest for base spaces associated with triangulations of the 8-th 3-dimensional polytope Δ_8° in the Kreuzer-Skarke list. For each of these $\mathcal{O}(10^{15})$ 3-folds, we expect that many root bundles on $C_{(\mathbf{3},\mathbf{2})_{1/6}}$ are induced from F-theory gauge potentials and that at least every 3000th root on $C_{(\mathbf{3},\mathbf{2})_{1/6}}$ has exactly three global sections and thus no exotic vector-like quark-doublet modes.

7.1 Introduction

Like no other framework for quantum gravity, string theory encodes the consistent coupling of gauge dynamics to gravity. Therefore, it is a leading candidate for a unified theory that accounts for all aspects of the observed low energy physics. Enormous efforts have been undertaken to demonstrate the particle spectrum of the Standard Model from string theory. The earliest studies focus on the $E_8 \times E_8$ heterotic string [13, 161, 109, 110, 124, 162, 163, 108] and were later extended by intersecting branes models [17, 18, 19, 20, 21, 22, 23, 24].

While these compactifications realize the gauge sector and chiral spectrum of the Standard Model, they are limited to the perturbative regime in the string coupling. Typically, they

also suffer from vector-like exotics. The first globally consistent, perturbative MSSM constructions are [110, 124] (see [164, 165] for more details).

In string compactifications, a significant amount of information is encoded in the geometry of the compactification space. A coherent approach to analyze the relations between geometry and physics is F-theory [27, 166, 167]. It describes the gauge dynamics of 7-branes including their back-reactions *to all orders in string coupling*. In 4-dimensional compactifications, this is achieved by encoding the back-reactions in the geometry of a singular elliptically fibered Calabi-Yau 4-fold $\pi\colon Y_4 \twoheadrightarrow B_3$. The global consistency conditions of the 4-dimensional physics are enforced by studying the geometry of Y_4, e.g., by a smooth, flat, crepant resolution $\widehat{Y}_4$.

The chiral spectrum of 4d $\mathcal{N} = 1$ F-theory compactifications is determined by a background G_4-flux. This flux is specified by the internal C_3 profile of the dual M-theory compactification via $G_4 = dC_3 \in H^{2,2}(\widehat{Y}_4)$, where $H^{2,2}(\widehat{Y}_4)$ is the middle vertical fourth cohomology of $\widehat{Y}_4$. The primary vertical subspace of G_4-configurations has been studied extensively [131, 37, 38, 39, 40, 41, 42]. Applications to globally consistent chiral F-theory models [43, 40, 42, 44] have lead to the discovery of the largest, currently-known, class of one Quadrillion globally consistent F-theory Standard Models (QSMs) with gauge coupling unification and no chiral exotics [32].

The massless vector-like spectrum depends not only on G_4, but also on the C_3-flat directions. The full gauge information is encoded in *Deligne cohomology*. In [45, 46, 47], F-theory gauge potentials were parametrized by Chow classes, which in turn induce line bundles $L_{\mathbf{R}}$ on the matter curves $C_{\mathbf{R}} \subset B_3$. The (vector-like) zero modes are counted by the cohomologies of these line bundles.

In principle, this approach works for any compactification. Technical limitations arise in explicit geometries due to the intricate complex structure dependence of the cohomologies $h^i(C_{\mathbf{R}}, L_{\mathbf{R}})$ of the line bundles $L_{\mathbf{R}}$ on the matter curves $C_{\mathbf{R}}$. This dependence was

investigated for special examples of F-theory compactifications in [48]. A large data set was generated [147, 168] and investigated with data science techniques and completely understood by Brill-Noether theory [150] (cf., [156, 128]).

For the QSMs [32] another complication arises. As explained in [196], in these models the line bundles $L_{\mathbf{R}}$ are necessarily root bundles $P_{\mathbf{R}}$, which one may think of as generalizations of spin bundles. Just as spin bundles, there are typically $N_P(C_{\mathbf{R}})\mathfrak{g}1$ root bundles on $C_{\mathbf{R}}$. Some of the $N_P(C_{\mathbf{R}})$ roots stem from F-theory gauge backgrounds which induce the same chiral index but differ in their C_3-flat directions. An important task is to find the roots which are induced from F-theory gauge potentials and have cohomologies that define Minimal Supersymmetric Standard Models (MSSMs).

As a first step, a "bottom-up" analysis was conducted in [196]. This work does not identify exactly which root bundles on $C_{\mathbf{R}}$ are induced from F-theory gauge potentials in the Deligne cohomology. Rather, a systematic study of the cohomologies of all admissable root bundles on $C_{\mathbf{R}}$ has been performed. Except for the Higgs curve, the prime interest are the $N_P^{(3)}(C_{\mathbf{R}}) \leq N_P(C_{\mathbf{R}})$ roots with exactly three sections. By extending the results in [197], the authors formulated a technique to derive a lower bound $\check{N}_P^{(3)}(C_{\mathbf{R}})$ to $N_P^{(3)}(C_{\mathbf{R}})$.

The toric base spaces of the QSMs are obtained from triangulations of 708 polytopes in Kreuzer-Skarke list [2]. The goal of this letter is to explain that $\check{N}_P^{(3)}(C_{\mathbf{R}})$ *is independent of the triangulations*. We use this observation to identify promising toric 3-folds for F-Theory Standard Models without vector-like exotics on the quark-doublet curve $C_{(\mathbf{3},\mathbf{2})_{1/6}}$.

In 7.2 we recall the relation of the toric QSM base 3-folds and toric K3-surfaces. By studying limit roots on a nodal curve $C^{\bullet}_{(\mathbf{3},\mathbf{2})_{1/6}}$ and employing results of resolutions [198, 199, 200, 201, 202], we demonstrate in 7.3 that the derived lower bound $\check{N}_P^{(3)}(C_{\mathbf{R}})$ is *independent of the triangulation*. We utilize the `Gap4`-package *QSMExplorer* [168] in 7.3.3 to compute the ratio $\check{N}_P^{(3)}/N_P$ for several classes of toric QSM base 3-folds. We focus on bases, for which it can be expected that many root bundles on $C_{(\mathbf{3},\mathbf{2})_{1/6}}$ are

"top-down" determined by gauge potentials of the F-theory compactification. This points us to the 3-folds associated with the $\mathcal{O}(10^{15})$ triangulations [30] of the 8-th polytope Δ_8° in the Kreuzer-Skarke list [2]: At least every 3000-th root on $C_{(\mathbf{3},\mathbf{2})_{1/6}}$ has exactly three global sections and thus no vector-like exotics.

7.2 Genesis of 3-fold bases

Desingularizations of Calabi-Yau (CY) hypersurfaces in toric ambient space are studied in [198]. We focus on CY 2-folds, i.e. toric K3-surfaces. Those are associated to three-dimensional, reflexive lattice polytopes $\Delta \subset M_\mathbb{R}$ and their polar duals $\Delta^\circ \subset N_\mathbb{R}$, defined by $\langle \Delta, \Delta^\circ \rangle \geq -1$. Kreuzer and Skarke list all possible 3-dimensional polytopes [2]. We consider the i-th polytope Δ_i° in the Kreuzer-Skarke list as subset of $N_\mathbb{R}$.

From a polytope $\Delta \subset M_\mathbb{R}$, one can build the normal fan Σ_Δ. Its ray generators are the facet normals of Δ and the maximal cones are in one-to-one correspondence to the vertices of Δ. We give a two-dimensional example in 14. Neither the toric variety $X_\Delta \equiv X_{\Sigma_\Delta}$ nor the CY-hypersurface need be smooth. Resolutions of these CY-hypersurfaces were introduced in [198] as *maximal projective crepant partial* (MPCP) desingularizations. Equivalently, [200] refers to such desingularizations as maximal projective subdivisions of the normal fan.

To find MPCPs, we note that a refinement of the normal fan Σ_Δ by ray generators corresponding to lattice points of Δ° is crepant. We can therefore consider refinements $\Sigma(T) \to \Sigma_\Delta$ where $\Sigma(T)$ is associated to a fine, regular, star triangulation (FRST) of the lattice polytope Δ°. We recall that *star* means that every simplex in the triangulation contains the origin, *fine* ensures that every lattice point of Δ° is used as ray generator and that *regular* implies that $X_{\Sigma(T)}$ is projective. Together, this implies that $\Sigma(T)$ defines a *maximal* projective refinement of Σ_Δ. This is illustrated in 14.

In our applications to toric K3-surfaces, $X_{\Sigma(T)}$ is guaranteed to be smooth. This is because a maximal projective subdivision of Σ_Δ then constructs a 3-dimensional Gorenstein

orbifold with terminal singularities [200] which must be smooth by proposition 11.4.19 in [203] (see also [198]).

Of the 4319 polytopes in [2], 708 lead to toric 3-folds with $\overline{K}^3_{X_\Sigma(T)} \in \{6, 10, 18, 30\}$. Those are the base spaces for the Quadrillion F-theory Standard Models (QSMs) [32], in which the gauge divisors are K3-surfaces. This leads to gauge coupling unification. In the rest of this paper, we reserve the symbol $B_3(\Delta^\circ)$ for the family of all toric 3-folds obtained from FRSTs of the polytope Δ°. Our standing example will be the spaces obtained from Δ°_{52} displayed in 15.

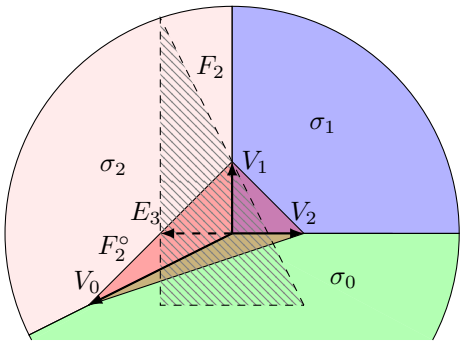

Figure 14: MPCP of $F_2^\circ = \text{Conv}(e_1, e_2, -2e_1 - e_2) \subset N_\mathbb{R}$ refines normal fan Σ_{F_2} of polytope $F_2 \subseteq M_\mathbb{R}$ by E_3.

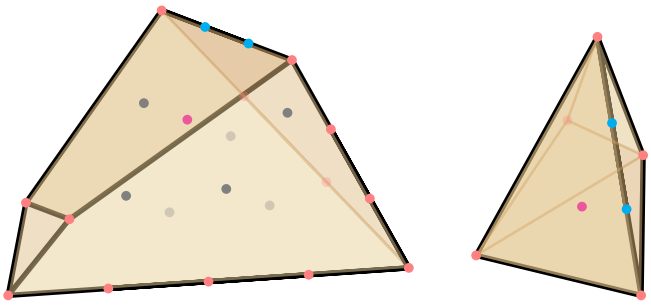

Figure 15: $\Delta^\circ_{52} \subset N_\mathbb{R}$ on the left and $\Delta_{52} \subseteq M_\mathbb{R}$ on the right [2]. The magenta point is the origin. The generic K3-surface meets trivially with gray divisors, in an irreducible curve with the pinks and in finite families of $\mathbb{P}^1$s with the cyans.

7.3 Triangulation independence

7.3.1 Dual graph

We will demonstrate that the dual graph of the nodal quark-doublet curve $C^{\bullet}_{(\mathbf{3},\mathbf{2})_{1/6}}$ introduced in [196] is identical for all 3-folds $B_3(\Delta^\circ)$ obtained from FRSTs of Δ°. Hence, this dual graph only depends on Δ°.

The homogeneous coordinates of $X_{\Sigma(T)}$ correspond to the lattice points of Δ°. A coordinate associated to a facet interior point is denoted by z_c. For a lattice point in the interior of an edge $\Theta^\circ \subset \Delta^\circ$, two facets F_1, F_2 of Δ° meet at Θ°. We notice that they are dual to vertices $m_1, m_2 \in \Delta$, and the dual edge Θ is the edge connecting m_1 and m_2. If Θ has interior points, we denote the homogeneous coordinate as y_b and otherwise by x_a. We mark these distinct types of lattice points in different colors in 15. The nodal curve $C^{\bullet}_{(\mathbf{3},\mathbf{2})_{1/6}}$ [196] is given by

$$C^{\bullet}_{(\mathbf{3},\mathbf{2})_{1/6}} = \bigcup_{a\in A} V(x_a, s_9) \cup \bigcup_{b\in B} V(y_b, s_9) \cup \bigcup_{c\in C} V(z_c, s_9)\,, \tag{7.3.1}$$

where s_9 is a generic section of $\overline{K}_{X_{\Sigma(T)}}$. The rational behind this classification is that will now explain that $V(x_a, s_9)$ *is irreducible,* $V(y_b, s_9)$ *a finite collection of* $\mathbb{P}^1$*s and* $V(z_c, s_9) = \emptyset$.

We begin with $V(z_c, s_9) = \emptyset$, which was originally proven in [198, 200] (see also [204]). Since $X_{\Sigma(T)}$ is associated to a refinement of Σ_Δ, there is a toric morphism $\varphi\colon X_{\Sigma(T)} \to X_\Delta$. By construction, this blow-down morphism is crepant and $V(z_c)$ is blown-down to a point, so that it does not intersect generic members of $|\overline{K}_{X_\Delta}|$. Since φ is crepant and birational, $V(z_c)$ does therefore not intersect generic members of $\overline{K}_{\Sigma(T)}$, i.e., $V(z_c, s_9) = \emptyset$. Hence, only the pink and cyan lattice points in 15 matter.

To see that $V(y_b, s_9)$ is reducible, we compute its self-intersection in the K3-surface $V(s_9)$. More generally, topological intersection numbers capture properties of $C^{\bullet}_{(\mathbf{3},\mathbf{2})_{1/6}}$. For ex-

ample, a curve component C_i associated to $D_i \in \mathrm{Div}_T(X_{\Sigma(T)})$ has *arithmetic* genus $g(C_i)$ with $2g(C_i) - 2 = D_i^2 \overline{K}_{X_{\Sigma(T)}}$. Similarly, the topological intersection of C_i and C_j is $D_i D_j \overline{K}_{X_{\Sigma(T)}}$. From the original work [199] (see also [201]), it follows that these intersection numbers are counted by properties of (Δ°, Δ) and are thus independent of the FRST. Let us restate this result.

Proposition 7.3.1. *Let $D_1, D_2 \in \mathrm{Div}_T(X_{\Sigma(T)})$ be two distinct divisors corresponding to lattice points $v_1, v_2 \in \Delta^\circ$. If v_1, v_2 are not contained in an edge $\Theta^\circ \subset \Delta^\circ$, then $D_1 D_2 \overline{K}_{X_{\Sigma(T)}} = 0$. Otherwise, $D_1 D_2 \overline{K}_{X_{\Sigma(T)}} = 1 + l'(\Theta)$, where $l'(\Theta)$ is the number of interior lattice points on the dual edge Θ.*

Proof. Consider a triangulation T of Δ°. Then the triple intersection among divisors D_1, D_2 and $\overline{K}_{X_{\Sigma(T)}}$ vanishes unless v_1, v_2 belong to two triangles in T, which we denote as $v_1 v_2 v_3$ and $v_1 v_2 v_4$. It follows $D_1 D_2 D_i = 0$ if $i \notin \{1, 2, 3, 4\}$ and $D_1 D_2 D_3 = D_1 D_2 D_4 = 1$. Hence

$$D_1 D_2 \overline{K}_{X_{\Sigma(T)}} = D_1 D_2 \left(D_1 + D_2 + D_3 + D_4 \right) . \tag{7.3.2}$$

The affine span of v_1, v_2, v_3 contains a facet F_3 of Δ°. The dual of F_3 is a vertex $m_3 \in \Delta$ with $\langle m_3, v_i \rangle = -1$. Let $N = \mathrm{rk}\left(\mathrm{Div}_T(X_{\Sigma(T)})\right)$, then $0 \sim \sum_{i=1}^N \langle m_3, v_i \rangle D_i$ and $D_1 + D_2 + D_3 \sim \langle m_3, v_4 \rangle D_4 + S$, where S satisfies $S D_1 D_2 = 0$. By substituting this back into 7.3.2 we find $D_1 D_2 \overline{K}_{X_{\Sigma(T)}} = 1 + \langle m_3, v_4 \rangle$. If v_1, v_2 are not contained in an edge $\Theta^\circ \subset \Delta^\circ$, then $v_4 \in F_3$, $\langle m_3, v_4 \rangle = -1$ and $D_1 D_2 \overline{K}_{X_{\Sigma(T)}} = 0$.

Conversely, if $v_1, v_2 \in \Theta^\circ \subseteq \Delta^\circ$, then $v_1 v_2 v_4$ is contained in a facet $F_4 \neq F_3$ of Δ° with dual vertex $m_4 \in \Delta$. The dual edge Θ from m_3 to m_4 only depends on v_1, v_2 but not the triangulation T. We now compare the number of interior lattice points $l'(\Theta)$ on Θ to

$$I_{12} = D_1 D_2 \overline{K}_{X_{\Sigma(T)}} = 1 + \langle m_3, v_4 \rangle . \tag{7.3.3}$$

v_1, v_2, v_4 generate $N_{\mathbb{R}}$. Therefore, $m \in M_{\mathbb{R}}$ is a lattice point iff $\langle m, v_1\rangle$, $\langle m, v_2\rangle$ and $\langle m, v_4\rangle$ are integers. Hence, lattice points on Θ are $m(k) = m_3 + \left(\frac{1+k}{I_{12}}\right) \cdot (m_4 - m_3)$, where $k \in \{-1, \ldots, I_{12}\}$. Therefore, $l'(\Theta) = I_{12} - 1$. □

We extend this to the arithmetic genera by restating another result from [199].

Corollary 7.3.2. *Let $D_1 \in \mathrm{Cl}(X_{\Sigma(T)})$ be the divisor associated to the lattice point $v_1 \in \Delta^\circ$. Then $D_1^2 \overline{K}_{X_{\Sigma(T)}}$ is independent of triangulations of Δ°. Furthermore, if v_1 is an interior point of an edge $\Theta^\circ \subset \Delta^\circ$, then $D_1^2 \overline{K}_{X_{\Sigma(T)}} = -2 - 2l'(\Theta)$.*

Proof. We consider a facet $F \subset \Delta^\circ$ with $v_1 \in F$. The dual vertex $m \in \Delta \in M_{\mathbb{R}}$ establishes $0 \sim \sum_{i=1}^{N} \langle m, v_i\rangle D_i$ and hence $D_1^2 \overline{K}_{X_{\Sigma(T)}} = \sum_{i=2}^{N} \langle m, v_i\rangle D_1 D_i \overline{K}_{X_{\Sigma(T)}}$, which is independent of FRSTs of Δ° by the preceding proposition.

Next, assume that v_1 in an interior point of an edge $\Theta^\circ \subset \Delta^\circ$ and denote its neighbors along Θ° by v_2, v_3. The associated divisors D_2, D_3 are the only divisors with non-zero $D_1 D_2 \overline{K}_{X_{\Sigma(T)}}$, $D_1 D_3 \overline{K}_{X_{\Sigma(T)}}$. Note that v_1, v_2, v_3 are contained in a facet of Δ°, whose dual vertex $m \in \Delta$ establishes $D_1 \sim -D_2 - D_3 + S$ with $D_1 S \overline{K}_{X_{\Sigma(T)}} = 0$. Hence, $D_1^2 \overline{K}_{X_{\Sigma(T)}} = -2 - 2l'(\Theta)$. □

$V(y_b, s_9)$ corresponds to $v_b \in \Theta^\circ \subset \Delta^\circ$ with $l'(\Theta) > 0$. Hence $D_b^2 \cdot \overline{K}_{X_{\Sigma(T)}} = -2(l'(\Theta) + 1) < -2$ and $V(y_b, s_9)$ is reducible into a collection of $l'(\Theta) + 1$ non-intersecting and smooth $\mathbb{P}^1$s [198, 199].

Finally, let us turn to the components $V(x_a, s_9)$. A subset of these components is associated to lattice points $v_a \in \Theta^\circ$ such that $l'(\Theta) = 0$. By the previous result, these components are irreducible and smooth. The remaining $V(x_a, s_9)$'s are associated to the vertices of Δ°. These components are smooth and irreducible by [198].

7.3.2 Computing the lower bound $\check{N}_P^{(3)}$

We have established that in every space in $B_3(\Delta^\circ)$, $C^\bullet_{(\mathbf{3},\mathbf{2})_{1/6}}$ consists of the same components C_i with the same topological properties. Therefore, the dual graph $G(C^\bullet_{(\mathbf{3},\mathbf{2})_{1/6}})$, in which components are vertices and intersections are edges, only depends on Δ°. We recall from [196], that on $C^\bullet_{(\mathbf{3},\mathbf{2})_{1/6}}$ we look for limit roots $P^\bullet_{(\mathbf{3},\mathbf{2})_{1/6}}$ with

$$\left(P^\bullet_{(\mathbf{3},\mathbf{2})_{1/6}}\right)^{\otimes 2\overline{K}^3_{X_{\Sigma(T)}}} = \left(\overline{K}_{X_{\Sigma(T)}}\Big|_{C^\bullet_{(\mathbf{3},\mathbf{2})_{1/6}}}\right)^{\otimes(6+\overline{K}^3_{X_{\Sigma(T)}})} . \tag{7.3.4}$$

Such roots are specified by weight assignments to $G(C^\bullet_{(\mathbf{3},\mathbf{2})_{1/6}})$, constrained by $(6+\overline{K}^3_{X_{\Sigma(T)}})$-times the degree of $\overline{K}_{X_{\Sigma(T)}}\big|_{C_i}$. For $V(x_a,s_9)$, $\overline{K}_{X_{\Sigma(T)}}\big|_{C_i}$ has degree $D_a\overline{K}^2_{X_{\Sigma(T)}}$. For the irreducible components of $V(y_b,s_9)$, this degree is $D_b\overline{K}^2_{X_{\Sigma(T)}}/(l'(\Theta)+1)$. Since $\overline{K}_{X_{\Sigma(T)}} = \sum_{i=1}^N D_i$, we have $D\overline{K}^2_{X_{\Sigma(T)}} = \sum_{i=1}^N DD_i\overline{K}_{X_{\Sigma(T)}}$ and by the results of [199] restated in the previous section, these degrees are FRST-invariant. Similarly, $\overline{K}^3_{X_{\Sigma(T)}}$ is FRST-invariant. Consequently, the data that specifies the limit roots on $C^\bullet_{(\mathbf{3},\mathbf{2})_{1/6}}$ depends only on Δ°. By extending the techniques of [196], we can thus compute an FRST-invariant lower bound $\check{N}_P^{(3)}$ to the number of root bundles on $C_{(\mathbf{3},\mathbf{2})_{1/6}}$ with exactly three global sections.

We illustrate our strategy with Δ°_{52} in 15. Its FRSTs give toric 3-folds with $h^{21}(\widehat{Y}_4) = 7 > 6 = g(C_{(\mathbf{3},\mathbf{2})_{1/6}})$ and $\overline{K}^3_B = 10$. The dual graph $G(C_{(\mathbf{3},\mathbf{2})_{1/6}})$ is:

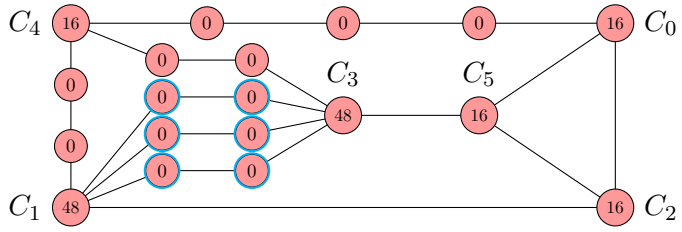

The labels inside the nodes are the degree of $16\cdot\overline{K}_{C^\bullet_{(\mathbf{3},\mathbf{2})_{1/6}}}$ on the components C_i. To find the $(2\overline{K}^3_{X_{\Sigma(T)}})$-th roots, we place weights $u_i, v_i \in \{1,2,\ldots,2\overline{K}^3_{X_{\Sigma(T)}}-1\}$ along each edge in $G(C_{(\mathbf{3},\mathbf{2})_{1/6}})$ subject to the following rules (see [197, 196] for details):

1. Along each edge, the sum of weights is $2\overline{K}^3_{X_{\Sigma(T)}}$.

2. At each node C_i, the sum of weights equals $(6+\overline{K}^3_{X_{\Sigma(T)}})$-times $D_i\overline{K}^2_{X_{\Sigma(T)}}$ modulo $2\overline{K}^3_{X_{\Sigma(T)}}$.

The number of possible weight assignments grows rapidly with the complexity of the dual graph. To speed up the counting, it is possible to replace $G(C_{(\mathbf{3},\mathbf{2})^\bullet_{1/6}})$ with a simplified graph. We remove components C_i which are connected to exactly two other components and have $D_i\overline{K}^2_{X_{\Sigma(T)}}=0$. We are thus looking at transitions:

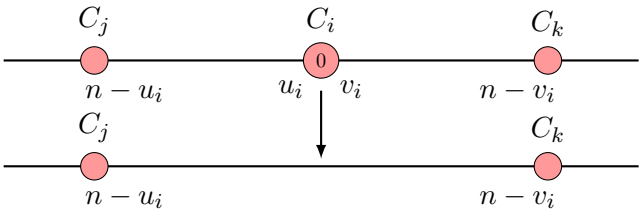

To see that this does not change the lower bound $\check{N}^{(3)}_P$, let us focus on n-th roots. Then $1\leq u_i,v_i\leq n-1$. For given u_i the weight v_i is uniquely fixed as $v_i=n-u_i$. Since, $D_i\overline{K}^2_{X_{\Sigma(T)}}=0$, the resulting root on C_i has degree -1 and supports no non-trivial sections (cf. [197, 196]). Conversely, given the diagram at the bottom, we can reconstruct the top-line by noting that $v_i=n-u_i$. For Δ°_{52}, this leads to the simplified graph:

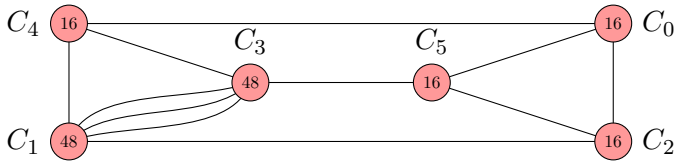

The algorithmic task of finding all weight assignments and counting the associated limit roots, can be conducted with a computer implementation. The algorithms employed are available in the `Gap4`-package *QSMExplorer*, as part of the *ToricVarieties_project* [168]. On the computer `plesken.mathematik.uni-siegen.de`, our algorithm completes for Δ°_{51} in roughly three minutes and finds $\check{N}^{(3)}_P=34.980.351$. This number is to be compared to the total number of root bundles $N_P=20^{12}$ on this $g=6$ curve. Hence, at least every 1.2×10^8-th root on $C_{(\mathbf{3},\mathbf{2})_{1/6}}$ has exactly three global sections.

7.3.3 Towards favorable F-theory base spaces

We extend this analysis to several classes $B_3(\Delta^\circ)$. Among the 708 polytopes, we focus on base spaces for which it can be expected that many roots stem from inequivalent F-theory gauge potentials in the Deligne cohomology $H^4_D(\widehat{Y}_4, \mathbb{Z}(2))$, i.e., gauge potentials which induce the same chiral index but differ in their C_3-flat directions. In the 4-fold geometry $\widehat{Y}_4$, these C_3-flat directions are described by the intermediate Jacobian $J^2(\widehat{Y}_4)$. Since $h^{3,0}(\widehat{Y}_4) = 0$, we have (see [45] and references therein) $J^2(\widehat{Y}_4) = H^{2,1}(\widehat{Y}_4)/H^3(\widehat{Y}_4, \mathbb{Z})$ and $\dim_{\mathbb{C}}(J^2(\widehat{Y}_4)) = h^{2,1}(\widehat{Y}_4)$. In particular, if a gauge potential in $H^4_D(\widehat{Y}_4, \mathbb{Z}(2))$ admits $(2\overline{K}^3_{X_{\Sigma(T)}})$-th roots, then it admits $(2\overline{K}^3_{X_{\Sigma(T)}})^{2h^{2,1}(\widehat{Y}_4)}$ roots. On the genus g curve $C_{(\mathbf{3},\mathbf{2})_{1/6}}$, we find $(2\overline{K}^3_{X_{\Sigma(T)}})^{2g}$ roots. Therefore, a necessary condition for many roots on $C_{(\mathbf{3},\mathbf{2})_{1/6}}$ to stem from F-theory gauge potentials is $h^{2,1}(\widehat{Y}_4) \geq g$:

$\overline{K}^3_B$	# Polytopes	$h^{21}(\widehat{Y}_4)$	g
6	7	$\{8, 9, 10, 12, 16\}$	4
10	54	$\{2, 3, \ldots, 11\} \cup \{13\}$	6
18	373	$\{0, 1, \ldots, 12\}$	10
30	274	$\{0, 1, \ldots, 9\}$	16

All 7 polytopes with $\overline{K}^3_B = 6$ satisfy this necessary condition. Their triangulations give at least 50% of the QSM 3-fold base spaces [30]. In addition, 27 polytopes with $\overline{K}^3_B = 10$ and three with $\overline{K}^3_B = 18$ have this property. For the $\overline{K}^3_B = 10$ polytope Δ°_{14} and the three $\overline{K}^3_B = 18$ polytopes Δ°_{72}, Δ°_{229} and Δ°_{527}, the quark-doublet curve has a component with genus larger than one. Hence, for these space the counting procedure introduced in [196] does not apply. However, for the remaining 33 polytopes, our computer implementation finds $\check{N}^{(3)}_P(C_{(\mathbf{3},\mathbf{2})_{1/6}})$ within a few minutes. These results are listed in 11.

Among these 33 polytopes, the ratio $\check{N}^{(3)}_P/N_P$ is largest for Δ°_8. In addition, within the QSMs, base spaces obtained from FRSTs of Δ°_8 have the maximal $16 = h^{21}(\widehat{Y}_4)$ and the

minimal $g = 4$. In this sense, they most positively satisfy the necessary condition for a top-down origin of at least some of the root bundles. In this sense, these $\mathcal{O}(10^{15})$ toric base 3-folds [30] are currently the most promising candidates to establish an F-theory Standard Model with exactly three quark-doublets and no vector-like exotics in this representation.

7.4 Discussion and Outlook

A construction of one Quadrillion globally consistent F-theory Standard Models (QSMs) with gauge coupling unification and no chiral exotics was presented in [32]. In this work, we apply the techniques introduced in [196] systematically to the toric QSM base 3-folds. Our goal is to identify toric base spaces, which are promising candidates to establish F-theory Standard Models with exactly three quark-doublets and no vector-like exotics in this representation.

We recall that vector-like spectra are counted by cohomologies of line bundles $L_{\mathbf{R}}$ on the matter curves $C_{\mathbf{R}}$. In [196], it was argued that these bundles must necessarily be root bundles. For instance, on the quark-doublet curve $C_{(\mathbf{3},\mathbf{2})_{1/6}}$ we consider line bundles $P_{(\mathbf{3},\mathbf{2})_{1/6}}$ which solve 7.3.4, where $\overline{K}_B^3$ is the triple intersection number of the anticanonical class of the 3-fold B_3. This constraint has $N_P(C_{(\mathbf{3},\mathbf{2})_{1/6}}) = (2\overline{K}_B^3)^{2g}$ solutions, where g is the genus of $C_{(\mathbf{3},\mathbf{2})_{1/6}}$. In every QSM vacuum, the zero mode spectrum is counted by the cohomologies of one of these solutions. It is currently not known exactly which roots stem from F-theory gauge potentials in the Deligne cohomology $H_D^4(\widehat{Y}_4, \mathbb{Z}(2))$ of the elliptic 4-fold $\widehat{Y}_4$.

In this work, we did not attempt to give a detailed answer to this question. Rather, we focused on base spaces for which it can be expected that many roots are induced from inequivalent F-theory gauge potentials, i.e., gauge potentials which induce the same chiral index but differ in their C_3-flat directions. In the 4-fold geometry $\widehat{Y}_4$, these C_3-flat directions are described by the intermediate Jacobian $J^2(\widehat{Y}_4)$. Since $h^{3,0}(\widehat{Y}_4) = 0$, it holds $J^2(\widehat{Y}_4) = H^{2,1}(\widehat{Y}_4)/H^3(\widehat{Y}_4, \mathbb{Z})$ (see [45] for details) and $\dim_{\mathbb{C}}(J^2(\widehat{Y}_4)) = h^{2,1}(\widehat{Y}_4)$. If

a gauge potential in $H^4_D(\widehat{Y}_4, \mathbb{Z}(2))$ admits $(2\overline{K}^3_B)$-th roots, then it admits $(2\overline{K}^3_B)^{2h^{2,1}(\widehat{Y}_4)}$ roots. On $C_{(\mathbf{3},\mathbf{2})_{1/6}}$, we find $(2\overline{K}_B)^{2g}$ roots. Therefore, a necessary condition for many roots on $C_{(\mathbf{3},\mathbf{2})_{1/6}}$ to stem from F-theory gauge potentials is $h^{2,1}(\widehat{Y}_4) \geq g$.

The QSM toric base 3-folds are obtained from fine, regular, star triangulations (FRSTs) of 708 3-dimensional, reflexive, lattice polytopes [32]. In these spaces, the gauge divisors are K3-surfaces. This leads to gauge coupling unification and emphasizes the physical significance of $\overline{K}_B$. Only 37 of the QSM polytopes lead to spaces with $h^{2,1}(\widehat{Y}_4) \geq g$. Still, the triangulations of these 37 polytopes provide the majority of the $\mathcal{O}(10^{15})$ toric QSM base 3-folds [30, 32].

The natural next step is to count the number $N_P^{(3)}$ of roots which solve 7.3.4 and admit exactly three global sections, thus ensuring no vector-like exotics on the quark-doublet curve. In following [196], we achieve this by studying limit roots on a nodal curve $C^{\bullet}_{(\mathbf{3},\mathbf{2})_{1/6}}$ introduced in [196], which establishes a lower bound $\check{N}_P^{(3)} \leq N_P^{(3)}$. Crucially, we argue that $\check{N}_P^{(3)}$ *is identical for all spaces* $B_3(\Delta^\circ)$ *obtained from FRSTs of* Δ°*, that is* $\check{N}_P^{(3)}$ *depends only on* Δ° *and not the FRSTs.*

We establish this result by arguing that the data, which specifies the limit roots, is identical for all spaces in $B_3(\Delta^\circ)$. This in turn follows by noting that the QSM base spaces are obtained from desingularizations of toric K3-hypersurfaces. Since the nodal curve $C^{\bullet}_{(\mathbf{3},\mathbf{2})_{1/6}}$ is closely related to the Picard lattice of the resulting smooth, toric K3-surface, we could employ powerful and well-known results about such desingularizations [198, 199, 200, 201] (see also [202] for recent work on related topics), and thereby establish the claim. Explicitly, this reduces to the FRST-invariance of topological triple-intersection numbers, which are related to FRST-independent counts of lattice points in the polytope Δ [199].

Among the 37 polytopes with $h^{21}(\widehat{Y}_4) \geq g$, there are four polytopes for which $C_{(\mathbf{3},\mathbf{2})_{1/6}}$ has components with genus larger than one, so that the techniques introduced in [196]

cannot be applied. For the remaining 33 polytopes, we list the lower bounds in 11. These counts were determined with the `Gap4` package *QSMExplorer*, which is part of the *ToricVarieties_project* [168]. We have optimized the input for this algorithm by simplifying the dual graph of $C^{\bullet}_{(\mathbf{3},\mathbf{2})_{1/6}}$. For one polytope and a personal computer, we expect runtimes from a few seconds to around 10 minutes for the lower bounds in 11.

Surprisingly, the simplifications of the dual graph of $C^{\bullet}_{(\mathbf{3},\mathbf{2})_{1/6}}$ lead to very similar graphs for distinct polytopes, and at times even identical lower bounds. For example, this applies to Δ°_{128}, Δ°_{130}, Δ°_{136} and Δ°_{236}. We reserve a detailed study of this phenomenon for future work.

We read-off from 11 that $\check{N}^{(3)}_P/N_P$ and $h^{21}(\widehat{Y}_4)/g(C_{(\mathbf{3},\mathbf{2})_{1/6}})$ are largest for $B_3(\Delta^{\circ}_8)$. At least every 3000-th root on $C_{(\mathbf{3},\mathbf{2})_{1/6}}$ has exactly three global sections. Furthermore, $16 = h^{21}(\widehat{Y}_4) \geq g \equiv g(C_{(\mathbf{3},\mathbf{2})_{1/6}}) = 4$, for these spaces, which is the largest, respectively smallest possible value among all QSMs. Therefore, the triangulations of Δ°_8 lead to $\mathcal{O}(10^{15})$ [30] promising toric base 3-folds for F-theory Standard Models with exactly three quark-doublets and no vector-like exotics in this representation.

The study of root bundles on the matter curves $C_{(\mathbf{1},\mathbf{1})_1}$ and $C_{(\mathbf{3},\mathbf{1})_{-2/3}}$ is identical to the presented study of roots on $C_{(\mathbf{3},\mathbf{2})_{1/6}}$. The matter curve $C_{(\mathbf{3},\mathbf{1})_{1/3}}$ is more complicated due to its higher genus, but can at least in principle be treated analogously. The real challenge however, is to establish one vector-like pair on the Higgs curve $C_{(\mathbf{1},\mathbf{2})_{-1/2}}$ and to investigate the "top-down" origin of the root bundles from F-theory gauge potentials. It can be anticipated that a detailed study of these questions will shed more light on the structure and construction of F-theory MSSMs. We hope to return to this thrilling and challenging task in the near future.

$\overline{K}_B^3 = 6$: $N_P(C_{(\mathbf{3},\mathbf{2})_{1/6}}) = 12^8$					
	$\check{N}_P^{(3)}$	$N_P/\check{N}_P^{(3)}$		$\check{N}_P^{(3)}$	$N_P/\check{N}_P^{(3)}$
Δ_8°	142560	$3.0 \cdot 10^3$	Δ_{130}°	8910	$4.8 \cdot 10^4$
Δ_4°	11110	$3.8 \cdot 10^4$	Δ_{136}°	8910	$4.8 \cdot 10^4$
Δ_{134}°	10100	$4.3 \cdot 10^4$	Δ_{236}°	8910	$4.8 \cdot 10^4$
Δ_{128}°	8910	$4.8 \cdot 10^4$			
$\overline{K}_B^3 = 10$: $N_P(C_{(\mathbf{3},\mathbf{2})_{1/6}}) = 20^{12}$					
	$\check{N}_P^{(3)}$	$N_P/\check{N}_P^{(3)}$		$\check{N}_P^{(3)}$	$N_P/\check{N}_P^{(3)}$
Δ_{88}°	781.680.888	$5.2 \cdot 10^6$	Δ_{762}°	32.858.151	$1.2 \cdot 10^8$
Δ_{110}°	738.662.983	$5.5 \cdot 10^6$	Δ_{417}°	32.857.596	$1.2 \cdot 10^8$
Δ_{272}°	736.011.640	$5.6 \cdot 10^6$	Δ_{838}°	32.845.047	$1.2 \cdot 10^8$
Δ_{274}°	736.011.640	$5.6 \cdot 10^6$	Δ_{782}°	32.844.379	$1.2 \cdot 10^8$
Δ_{387}°	733.798.30	$5.6 \cdot 10^6$	Δ_{377}°	30.846.440	$1.3 \cdot 10^8$
Δ_{798}°	690.950.608	$5.9 \cdot 10^6$	Δ_{499}°	30.846.440	$1.3 \cdot 10^8$
Δ_{808}°	690.950.608	$5.9 \cdot 10^6$	Δ_{503}°	30.846.440	$1.3 \cdot 10^8$
Δ_{810}°	690.950.608	$5.9 \cdot 10^6$	Δ_{1348}°	30.845.702	$1.3 \cdot 10^8$
Δ_{812}°	690.950.608	$5.9 \cdot 10^6$	Δ_{882}°	30.840.098	$1.3 \cdot 10^8$
Δ_{254}°	35.004.914	$1.2 \cdot 10^8$	Δ_{1340}°	28.954.543	$1.4 \cdot 10^8$
Δ_{52}°	34.980.351	$1.2 \cdot 10^8$	Δ_{1879}°	28.950.852	$1.4 \cdot 10^8$
Δ_{302}°	34.908.682	$1.2 \cdot 10^8$	Δ_{1384}°	27.178.020	$1.5 \cdot 10^8$
Δ_{786}°	32.860.461	$1.2 \cdot 10^8$	Δ_{856}°	22.807.749	$1.8 \cdot 10^8$

Table 11: $\check{N}_P^{(3)}$ for 33 QSM polytopes with $h^{21}(\widehat{Y}_4) \geq g$.

CHAPTER 8: Conclusions

In summary, F-theory is remarked by its powerful phenomenological model building potential due to its geometric description of compactification. It translates physics quantities in the effective low energy theory to the mathematical objects in en elliptic fibration $Y_{n+1} \to B_n$. This connection is built upon identifying the varying axio-dilaton field in type IIB supergravity theory with the complex structure modulus of an elliptic curve, which serves as the fiber of the elliptic fibration. In 4d compactifiation, this allows us to capture the non-perturbative back-reactions of seven branes onto the compactification space B_3 in elliptically fibered Calabi–Yau fourfold Y_4. The ingredients of SM physics, including gauge symmetries, charged matter, and Yukawa couplings, are then encoded beautifully in Y_4's singularities in codimensions one, two, and three, respectively. Moreover, many global consistency conditions, including the D3-tadpole cancellation, can be reduced to simple criteria on intersection numbers of base divisors.

In this thesis, we focus on searching for F-theory SM geometries that admit exact MSSM matter spectra. Our goal is to realize the gauge group, chiral and vector-like spectra of MSSM in F-theory. To begin with, Part I of the thesis constructs torus fibered Calabi–Yau fourfolds which realize a SM with exactly three chiral families in the presence of a G_4-flux. In chapter 3, we present a compactification which realize the SM gauge group with an additional $\mathbb{Z}_2$ matter parity. This additional discrete symmetry beyond the SM gauge group forbids proton decay. In chapter 4, we explicitly construct $\mathcal{O}(10^{15})$ globally consistent F-theory SMs without chiral exotics and support the gauge unificston. To our knowledge, this is the largest such ensemble in the literature, outnumbering existing results by about 5 orders of magnitude.

We advance to seek approaches towards exact matter spectra in 4d F-theory, i,e. the full determination of the vector-ike spectra. This is important to identify the number of Higgs pairs in this compactification. It is well known that certain line bundle cohomologies count

the massless zero modes localized on matter curves in the presenece of a gauge background. The 3-form potential C_3 in the dual M-theory encodes the full gauge data, whose field strength G_4-flux only controls the chiral spectra. In order to understand the line bundle cohomology's dependence on the moduli of the compactification geometry, we investigate this dependence of vector-like spectra in computationally simple geometry in chapter 5. We approach it by collecting the topological data extracted from various curve and line bundle setups on this surface for which we compute the vector-like spectra by brutal force. Utilizing machine learning techniques, we eventually achieve a comprehensive analysis of the input data by decision tree and successfully predict the appearance of vector-like jumps with accuracy of 95% accuracy. The pure topological data here surprisingly predict vector-like jumps, which is very unexpected since the vector-like spectra depend heavily on the complex structure moduli. We employ additional tools, particularly Brill–Noether theory. To explain cohomology jumps occurrence in the rest corner.

Moving to the realistic F-theory geometry, the appearance of fractional powers of line bundles in studies of vector-like spectra in 4d F-theory compactifications is presented in chapter 6. They are also known as root bundles and can be thought of as generalizations of spin bundles. We explain how these root bundles are linked to inequivalent F-theory gauge potentials of a G_4-flux. In aiming for MSSMs, it is desired to argue for the absence of vector-like exotics. We work out the root bundle constraints on all matter curves in the largest class of currently-known, globally consistent F-theory Standard Model constructions without chiral exotics and gauge coupling unification [32]. On a technical level, this systematic study is achieved by a well-known diagrammatic description of root bundles on nodal curves. We extend this description by a counting procedure, which determines the cohomologies of so-called limit root bundles on full blow-ups of nodal curves. Consequently, We identify roots on all matter curves except the Higgs curve in SM that admit exactly three sections.

In generalizing this and perform even further, we anticipate a scan over many of the F-

theory Standard model geometries in [32]. By studying root bundles on the quark doublet curve $C_{(\mathbf{3},\mathbf{2})_{1/6}}$ and employing well-known results about desingularizations of toric K3-surfaces, we derive a *triangulation independent lower bound* $\check{N}_P^{(3)}$ for the number $N_P^{(3)}$ of root bundles on $C_{(\mathbf{3},\mathbf{2})_{1/6}}$ with exactly three sections. The ratio $\check{N}_P^{(3)}/N_P$, where N_P is the total number of roots on $C_{(\mathbf{3},\mathbf{2})_{1/6}}$, provides a numerical discrimination. The larger the ratio computed on a specific base the higher chance that we catch a meaningful physics root on $C_{(\mathbf{3},\mathbf{2})_{1/6}}$ with exactly three global sections and thus no exotic vector-like quark-doublet modes. This discrimination indicates that the most promising base are associated with triangulations of the 8-th 3-dimensional polytope Δ_8° in the Kreuzer-Skarke list. For each of these $\mathcal{O}(10^{15})$ 3-folds, we expect that many root bundles on $C_{(\mathbf{3},\mathbf{2})_{1/6}}$ are induced from F-theory gauge potentials and that at least every 3000th root on $C_{(\mathbf{3},\mathbf{2})_{1/6}}$ has exactly three global sections and thus no exotic vector-like quark-doublet modes.

It remains to establish one vector-like pair on the Higgs curve $C_{(\mathbf{1},\mathbf{2})_{-1/2}}$ and to investigate the "top-down" origin of the root bundles from F-theory gauge potentials. It can be anticipated that a detailed study of these questions will shed more light on the structure and construction of F-theory MSSMs. We hope to return to this thrilling and challenging task in the near future. As a long-term goal, by a continued study of F-theory compactifications, we may hope to reproduce the whole picture of physics in the 4d effective low energy theory and thereby reveal new insights on the inner workings of our universe.

A.1 Homology classes of matter surfaces

In this appendix, we collect the matter surface homology classes of the two top combinations considered in Sections 3.3 and 3.4, in Table 12 and 13, respectively.

R	Matter surface homology classes
$\mathbf{2}_1$	$-(E_1F_1) - E_1\overline{K}_B + E_1S_7 - E_1S_9 + F_1W_2 + \overline{K}_BW_2 - S_7W_2 + S_9W_2 - W_2[x]$ $-W_2[x] - 2E_1[y] + 2W_2[y]$
$\mathbf{2}_2$	$3E_1\overline{K}_B - E_1S_7 - E_1S_9 + F_2W_2 - \overline{K}_BW_2 + S_9W_2 - W_2[x] + 2E_1[y]$
$\overline{\mathbf{3}}_1$	$F_2^2 - F_2\overline{K}_B + F_2S_9 + F_2W_2 - E_1W_3 - F_2W_3 + \overline{K}_BW_3 - S_9W_3 + W_3[x]$
$\mathbf{3}_2$	$-(E_1F_1) + F_2^2 + F_1\overline{K}_B + F_2\overline{K}_B - F_2S_7 + W_3[y]$
$\overline{\mathbf{3}}_3$	$-2F_1F_2 - F_2^2 + F_2S_7$
$\overline{\mathbf{3}}_4$	$E_1F_1 + 2F_1F_2 + F_2^2 - 2F_1\overline{K}_B - F_2\overline{K}_B - F_2S_9 + F_1W_3 + 2\overline{K}_BW_3$ $-S_7W_3 + S_9W_3 - W_3[x] + W_3[y]$
$(\overline{\mathbf{3}}, \mathbf{2})$	E_1F_0
$\mathbf{1}_1$	$-2F_1F_2 - F_2^2 + E_1\overline{K}_B + 3F_1\overline{K}_B + F_2\overline{K}_B + 2\overline{K}_B^2 - E_1S_7 - F_1S_7 - 3\overline{K}_BS_7 + S_7^2$ $+E_1S_9 - F_1S_9 + F_2S_9 + 2\overline{K}_BS_9 - S_7S_9 - F_1W_2 - \overline{K}_BW_2 + S_7W_2 - S_9W_2$ $-4\overline{K}_B[x] + 2S_7[x] + W_2[x] + 2E_1[y] + 2\overline{K}_B[y] + 2S_9[y] - 2W_2[y] - 2W_3[y] - 4[x][y]$
$\overline{\mathbf{1}}_2$	$-(E_1F_1) - 2F_1F_2 - F_2^2 - 2E_1\overline{K}_B + F_1\overline{K}_B - 3F_2\overline{K}_B + 2\overline{K}_B^2 - E_1S_7 - F_1S_7$ $+2\overline{K}_BS_7 + E_1S_9 - F_1S_9 + F_2S_9 - 3\overline{K}_BS_9 - S_7S_9 + S_9^2 + E_1W_2 + F_2W_2$ $-\overline{K}_BW_2 + 2E_1W_3 + F_1W_3 + 2F_2W_3 - 3\overline{K}_BW_3 + 2S_9W_3 + 2\overline{K}_B[x] + 2S_7[x]$ $-W_2[x] - 3W_3[x] + 2E_1[y] - 4\overline{K}_B[y] + 2S_9[y] + W_3[y] - 4[x][y]$

Table 12: Summary of matter homology classes restricted to CY of first top combination.

R	Matter surface homology classes
$\mathbf{2}_1$	$-(E_1\overline{K}_B) - E_1S_7 - E_1S_9 + \overline{K}_BW_2 + S_7W_2 + S_9W_2$ $+2E_1W_3 - 2W_2W_3 + W_2[x] + 2E_1[y] - 2W_2[y]$
$\mathbf{2}_2$	$-(E_1F_1) + 3E_1\overline{K}_B + E_1S_7 - E_1S_9 - 2E_1W_2 + F_2W_2$ $+\overline{K}_BW_2 - S_9W_2 - E_1W_3 + W_2[x] - 2E_1[y]$
$\overline{\mathbf{3}}_1$	$F_2^2 + F_2\overline{K}_B - F_2S_9 + W_3[x]$
$\overline{\mathbf{3}}_2$	$-(E_1F_1) - F_2^2 + F_1\overline{K}_B - F_2\overline{K}_B + F_1S_7 + F_2S_7 - F_1S_9 - F_1W_3 - W_3[y]$
$\mathbf{3}_3$	$2F_1F_2 + F_2^2 + F_2\overline{K}_B + F_2S_9 - 2F_2W_3$
$\mathbf{3}_4$	$E_1F_1 - 2F_1F_2 - F_2^2 - 3F_1\overline{K}_B - 2F_2\overline{K}_B + F_1S_7 + F_2S_7 + F_1S_9$ $-E_1W_3 - F_1W_3 + F_2W_3 + 2\overline{K}_BW_3 - S_9W_3 + W_3[x] - W_3[y]$
$(\overline{\mathbf{3}}, \mathbf{2})$	$-(E_1F_1) + F_1W_2$
$\mathbf{1}_1$	$2F_1F_2 + 3F_2^2 + E_1\overline{K}_B + F_1\overline{K}_B + 3F_2\overline{K}_B + 2\overline{K}_B^2 - E_1S_7 - F_1S_7 - 2F_2S_7 - 3\overline{K}_BS_7$ $+S_7^2 + E_1S_9 + F_1S_9 - F_2S_9 + 2\overline{K}_BS_9 - S_7S_9 - \overline{K}_BW_2 + S_7W_2 - S_9W_2 - 4\overline{K}_B[x]$ $+2S_7[x] + W_2[x] + 2E_1[y] + 2\overline{K}_B[y] + 2S_9[y] - 2W_2[y] - 2W_3[y] - 4[x][y]$
$\overline{\mathbf{1}}_2$	$E_1F_1 + 2F_1F_2 + 3F_2^2 - 2E_1\overline{K}_B - F_1\overline{K}_B + 5F_2\overline{K}_B + 2\overline{K}_B^2 - E_1S_7 - F_1S_7 - 2F_2S_7$ $+2\overline{K}_BS_7 + E_1S_9 + F_1S_9 - F_2S_9 - 3\overline{K}_BS_9 - S_7S_9 + S_9^2 + E_1W_2 - F_2W_2 - \overline{K}_BW_2$ $+S_9W_2 + E_1W_3 + F_1W_3 - F_2W_3 - 2\overline{K}_BW_3 + S_9W_3 + 2\overline{K}_B[x] + 2S_7[x] - W_2[x]$ $-3W_3[x] + 2E_1[y] - 4\overline{K}_B[y] + 2S_9[y] + W_3[y] - 4[x][y]$

Table 13: Matter surface homology classes of the second top restricted on the fourfold.

A.2 Towards the vector-like spectrum of the first top

In this section we want to give all information that is needed to compute the vector-like spectrum of our first model realizing $\mathbb{Z}_2^{M_2}$ using the methods of [46]. The key point is to assign to each matter curve $C_{\mathbf{R}} \subset B$ a divisor D, i.e., a collection of points on $C_{\mathbf{R}}$, based on the intersection properties between the G_4-flux and the matter surface $S_{\mathbf{R}}$. By expression the flux in terms of matter surfaces, evaluating this intersection product reduce to properly counting the points, in which various matter surfaces meet. In F-theory geometries, these points are in the fibers over codimension three enhancement loci, i.e., Yukawa points Y_i. Thus, the resulting divisor D is a linear combination $\sum_i \mu_i Y_i$ of these points. From this divisor, one can then extract the left- and right-handed fermions as the sheaf cohomologies

$$h^i(C_{\mathbf{R}}\,,\, \mathcal{O}_{C_{\mathbf{R}}}(D) \otimes \sqrt{K_{C_{\mathbf{R}}}})\,, \quad i = 0, 1\,, \tag{A.2.1}$$

where $\sqrt{K_{C_{\mathbf{R}}}}$ is the spin bundle on $C_{\mathbf{R}}$. These cohomologies depend on the complex structure parameters of the fourfold. However, the chiral index $\chi = h^0 - h^1$ is a topological invariant, which is simply the number of points (including signs) that constitutes $D \subset B$. More details and examples can be found in [46].

For the first top realizing the MSSM with matter parity $\mathbb{Z}_2^{M_2}$, we need, in addition to the particular flux basis (3.3.19) that we have picked, also algebraic equivalence relations between fluxes and other vertical 4-cycles. Explicitly, these are

$$\begin{aligned}
A(\mathbf{2}_2) - A((\mathbf{3},\mathbf{2})) + 2\, D_{U(1)} \cdot W_2 + [S_{\mathbf{2}_1}] + \frac{1}{2}\, E_1 \cdot [\{f_{\mathbf{2}_1}\}] - \frac{1}{2}\, C_{\mathbf{2}_1} = 0\,, \\
A((\mathbf{3},\mathbf{2})) - A(\mathbf{3}_2) - D_{U(1)} \cdot W_3 + [S_{\mathbf{3}_1}] + \frac{1}{3}\, (F_1 + 2\, F_2) \cdot [\{f_{\mathbf{3}_1}\}] - \frac{1}{6}\, C_{\mathbf{3}_1} = 0\,, \\
A(\mathbf{3}_4) + A((\mathbf{3},\mathbf{2})) + D_{U(1)} \cdot W_3 + [S_{\mathbf{3}_3}] + \frac{1}{3}\, (F_1 - F_2) \cdot [\{f_{\mathbf{3}_3}\}] - \frac{1}{6}\, C_{\mathbf{3}_3} = 0\,, \\
A((\mathbf{3},\mathbf{2})) - A(\mathbf{1}_{(1,+)}) + D_{U(1)} \cdot (6\, \overline{K}_B - 2\, W_2 - 3\, W_3) + [S_{\mathbf{1}_{(1,-)}}] - \frac{1}{2}\, C_{\mathbf{1}_{(1,-)}} = 0\,.
\end{aligned} \tag{A.2.2}$$

The Yukawa points and their homology classes are listed in Table 14. In terms of the homology classes, we can write the chiral indices of the matter states induced by the flux (3.3.19) as

$$\begin{aligned}
\chi(\overline{\mathbf{3}}_1) =& -\frac{2}{3} C_{\overline{\mathbf{3}}_1}\, F + a_1[Y_8] + \frac{1}{3} a_2[Y_{16}] + a_3\,(\frac{2}{3}\,[Y_9] - \frac{1}{3}\,[Y_{13}]) - \frac{1}{3} a_4[Y_8] - a_5[Y_{12}]\,, \\
\chi(\mathbf{3}_2) =& \frac{2}{3} C_{\mathbf{3}_2}\, F + a_2\,(\frac{1}{3}\,[Y_{16}] + \frac{1}{3}\,[Y_6] - \frac{2}{3}\, C_{\mathbf{3}_2}\, W_3) - a_3(\frac{4}{3}[Y_{11}] - \frac{1}{3}[Y_{15}]) \\
& + \frac{1}{3} a_4[Y_6] + a_5[Y_{15}]\,, \\
\chi(\overline{\mathbf{3}}_3) =& \frac{1}{3} C_{\overline{\mathbf{3}}_3}\, F - a_1[Y_7] + a_2(\frac{1}{3}[Y_{14}] - \frac{4}{3}[Y_{10}]) + a_3(\frac{2}{3}[Y_9] - \frac{1}{3}[Y_{17}]) - \frac{1}{3} a_4[Y_7] + a_5[Y_{12}]\,, \\
\chi(\overline{\mathbf{3}}_4) =& \frac{1}{3} C_{\overline{\mathbf{3}}_4}\, F + a_2(-\frac{4}{3}[Y_{11}] + \frac{1}{3}[Y_{15}]) + a_3(\frac{1}{3}[Y_5] - \frac{2}{3}[Y_{18}] - \frac{2}{3}[Y_9] + \frac{1}{3}[Y_{17}] - \frac{1}{3} C_{\overline{\mathbf{3}}_4} W_3) \\
& + a_4(-\frac{1}{3}[Y_5] + \frac{2}{3}[Y_{18}]) + a_5[Y_{15}]\,,
\end{aligned} \tag{A.2.3}$$

Coupling	Homology classes
$\mathbf{2}_1 \cdot \mathbf{2}_2 \cdot \overline{\mathbf{1}_{(1,-)}}$	$[Y_1] = W_2 \cdot (6\overline{K}_B^2 - 4\overline{K}_B S_7 + 2S_7^2 + 4\overline{K}_B S_9 - 2S_9^2 - 2\overline{K}_B W_2$ $-2S_9 W_2 - \overline{K}_B W_3 - 3S_7 W_3 - S_9 W_3 + W_2 W_3 + 2W_3^2)$
$\mathbf{2}_1 \cdot \mathbf{2}_1 \cdot \overline{\mathbf{1}_{(1,+)}}$	$[Y_2] = W_2 \cdot (2\overline{K}_B S_7 - S_7^2 + \overline{K}_B S_9 + S_9^2 - 2\overline{K}_B W_3 + S_7 W_3 - S_9 W_3)$
$\mathbf{2}_1 \cdot \overline{\mathbf{2}_2} \cdot \mathbf{1}_{(0,-)}$	$[Y_3] = W_2 \cdot (6\overline{K}_B^2 + 4\overline{K}_B S_7 - 2S_7^2 + 4\overline{K}_B S_9 - 2S_9^2 - 2\overline{K}_B W_2$ $-2S_9 W_2 - 9\overline{K}_B W_3 + 3S_7 W_3 - S_9 W_3 + W_2 W_3)$
$\mathbf{2}_2 \cdot \mathbf{2}_2 \cdot \overline{\mathbf{1}_{(1,+)}}$	$[Y_4] = W_2 \cdot (6\overline{K}_B^2 + 2\overline{K}_B S_7 - S_7^2 - 5\overline{K}_B S_9 + S_9^2 - 5\overline{K}_B W_2 + 2S_9 W_2$ $+W_2^2 - 7\overline{K}_B W_3 + 2S_7 W_3 + 2S_9 W_3 + 2W_2 W_3)$
$\mathbf{2}_1 \cdot \mathbf{3}_4 \cdot (\overline{\mathbf{3}}, \mathbf{2})$	$[Y_5] = W_2 \cdot W_3 \cdot (2\overline{K}_B - S_7 + S_9)$
$\mathbf{2}_1 \cdot \overline{\mathbf{3}_2} \cdot (\mathbf{3}, \mathbf{2})$	$[Y_6] = W_2 \cdot W_3 \cdot (S_7 + S_9 - W_3)$
$\mathbf{2}_2 \cdot \mathbf{3}_3 \cdot (\overline{\mathbf{3}}, \mathbf{2})$	$[Y_7] = W_2 \cdot W_3 \cdot (3\overline{K}_B + S_7 - S_9 - W_2 - 2W_3)$
$\mathbf{2}_2 \cdot \overline{\mathbf{3}}_1 \cdot (\mathbf{3}, \mathbf{2})$	$[Y_8] = W_2 \cdot W_3 \cdot (3\overline{K}_B - S_7 - S_9 - W_2)$
$\overline{\mathbf{3}}_1 \cdot \overline{\mathbf{3}}_3 \cdot \overline{\mathbf{3}}_4$	$[Y_9] = W_3 \cdot \overline{K}_B (3\overline{K}_B - S_7 - S_9 - W_2)$
$\mathbf{3}_2 \cdot \mathbf{3}_3 \cdot \mathbf{3}_3$	$[Y_{10}] = W_3 \cdot \overline{K}_B (S_7 - W_3)$
$\mathbf{3}_2 \cdot \mathbf{3}_4 \cdot \mathbf{3}_4$	$[Y_{11}] = W_3 \cdot \overline{K}_B S_9$
$\overline{\mathbf{3}}_1 \cdot \mathbf{3}_3 \cdot \mathbf{1}_{(1,+)}$	$[Y_{12}] = W_3 \cdot (3\overline{K}_B - S_7 - S_9 - W_2)(2\overline{K}_B + S_7 - S_9 - W_2 - 2W_3)$
$\overline{\mathbf{3}}_1 \cdot \mathbf{3}_4 \cdot \mathbf{1}_{(1,-)}$	$[Y_{13}] = W_3 \cdot (2\overline{K}_B - S_7 + S_9)(3\overline{K}_B - S_7 - S_9 - W_2)$
$\mathbf{3}_2 \cdot \overline{\mathbf{3}}_3 \cdot \overline{\mathbf{1}_{(1,-)}}$	$[Y_{14}] = W_3 \cdot (\overline{K}_B S_7 + S_7^2 + 3\overline{K}_B S_9 - S_9^2 - S_7 W_2 - S_9 W_2 - \overline{K}_B W_3$ $-3S_7 W_3 - S_9 W_3 + W_2 W_3 + 2W_3^2)$
$\mathbf{3}_2 \cdot \overline{\mathbf{3}}_4 \cdot \overline{\mathbf{1}_{(1,+)}}$	$[Y_{15}] = W_3 \cdot (3\overline{K}_B S_7 - S_7^2 + \overline{K}_B S_9 + S_9^2 - 3\overline{K}_B W_3 + S_7 W_3 - S_9 W_3)$
$\overline{\mathbf{3}}_1 \cdot \mathbf{3}_2 \cdot \mathbf{1}_{(0,-)}$	$[Y_{16}] = W_3 \cdot (3\overline{K}_B - S_7 - S_9 - W_2)(S_7 + S_9 - W_3)$
$\overline{\mathbf{3}}_3 \cdot \mathbf{3}_4 \cdot \mathbf{1}_{(0,-)}$	$[Y_{17}] = W_3 \cdot (6\overline{K}_B^2 + \overline{K}_B S_7 - S_7^2 + \overline{K}_B S_9 + 2S_7 S_9 - S_9^2 - 2\overline{K}_B W_2$ $+S_7 W_2 - S_9 W_2 - 6\overline{K}_B W_3 + 2S_7 W_3 - 2S_9 W_3)$
$(\overline{\mathbf{3}}, \mathbf{2}) \cdot (\overline{\mathbf{3}}, \mathbf{2}) \cdot \overline{\mathbf{3}}_4$	$[Y_{18}] = W_2 \cdot W_3 \cdot \overline{K}_B$

Table 14: Yukawa points of the first top.

$$
\begin{aligned}
\chi(\overline{\mathbf{3}}, \mathbf{2}) =& -\frac{1}{6} C_{(\overline{\mathbf{3}},\mathbf{2})}\, F + \frac{1}{2} a_1([Y_7] - [Y_8]) + \frac{1}{3} a_2 [Y_6] + \frac{1}{6} a_4 C_{(\overline{\mathbf{3}},\mathbf{2})}\, (6\overline{K}_B - 2W_2 - 3W_3) \\
& + a_3 (\frac{2}{3}[Y_{18}] - \frac{1}{3}[Y_5])\,, \\
\chi(\mathbf{2}_2) =& \frac{1}{2} C_{\mathbf{2}_2}\, F + a_1(-\frac{1}{2}[Y_8] + \frac{1}{2}[Y_7] - C_{\mathbf{2}_2}\, W_2 + \frac{1}{2}[Y_1] - \frac{1}{2}[Y_3]) \\
& + a_4(-\frac{1}{2}[Y_8] + \frac{1}{2}[Y_7]) + 2a_5 [Y_4]\,, \\
\chi(\mathbf{2}_1) =& \frac{1}{2} C_{\mathbf{2}_1}\, F + a_1(\frac{1}{2}[Y_1] - \frac{1}{2}[Y_3]) - a_2 [Y_6] - a_3 [Y_5] + a_4(\frac{1}{2}[Y_5] - \frac{1}{2}[Y_6]) + 2a_5 [Y_2]\,, \\
\chi(\mathbf{1}_{(1,-)}) =& -C_{\mathbf{1}_{(1,+)}}\, F + 2a_1 [Y_4] + a_2 [Y_{15}] + a_3 [Y_{15}] + a_5\, V\,, \\
\chi(\mathbf{1}_{(1,+)}) =& C_{\mathbf{1}_{(1,-)}}\, F - a_1 [Y_1] - a_2 [Y_{14}] - a_3 [Y_{13}] + a_5\, V\,,
\end{aligned}
\tag{A.2.4}
$$

where

$$
\begin{aligned}
V = &- C_{\mathbf{1}_{(1,+)}}\left(6\overline{K}_B - 2W_2 - 3W_3\right) - W_2^2 W_3 - 2W_2 W_3^2 + 2W_2^2\overline{K}_B \\
&+ 13W_2W_3\overline{K}_B + 12W_3^2\overline{K}_B - 10W_2\overline{K}_B^2 - 24W_3\overline{K}_B^2 + 12\overline{K}_B^3 - 2W_2W_3S_7 \\
&- 4W_3^2S_7 - 4W_2\overline{K}_BS_7 - W_3\overline{K}_BS_7 + 8\overline{K}_B^2S_7 + 2W_2S_7^2 + 3W_3S_7^2 - 4\overline{K}_BS_7^2 \\
&+ 2W_2^2S_9 + 4W_2W_3S_9 - 8W_2\overline{K}_BS_9 - 9W_3\overline{K}_BS_9 + 8\overline{K}_B^2S_9 + 2W_3S_7S_9 \\
&+ 2W_2S_9^2 + 3W_3S_9^2 - 4\overline{K}_BS_9^2\,.
\end{aligned}
\tag{A.2.5}
$$

A.3 Summary of toric tops

In this section we summarize the toric data of all four $SU(2)$ and $SU(3)$ tops over polygon F_2, following the prescription of [91]. The factorization of the generic hypersurface is given together with the SR-ideal and the abelian generators. Furthermore we present the matter loci, the class of fiber component we use for the matter surfaces, and the associated representations.

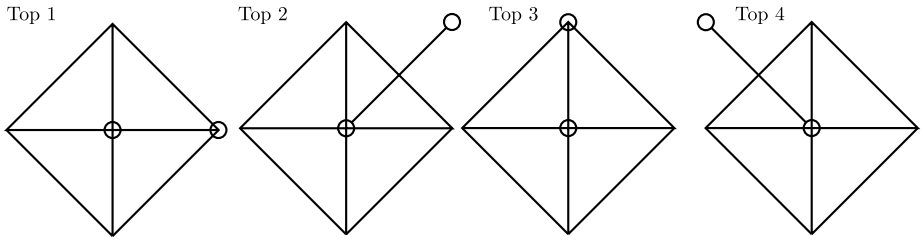

Figure 16: The toric diagram of the four inequivalent SU(2) tops over F_2.

Factorization:	$b_1 \to e_0 d_1 \quad b_2 \to e_0 d_2 \quad b_3 \to e_0 d_3$ $b_5 \to d_5 \quad b_6 \to d_6 \quad b_7 \to d_7$ $b_8 \to e_1 d_8 \quad b_9 \to e_1 d_9 \quad b_{10} \to e_1 d_{10}$
SRI:	$\{xt, xe_1, ys, te_0\}$
Charge Generators	$D_{U(1)} = [y] - [x] + 1/2[e_1]$ $D_{\mathbb{Z}_2} = [x]$

Locus	V(f, g, Δ)	matter $\mathbb{P}^1$	weight	Rep
$d_{10}^2 d_5^2 + d_{10} d_6^2 d_8 - 2 d_{10} d_5 d_7 d_8 + d_7^2 d_8^2$ $-d_6(d_{10} d_5 + d_7 d_8) d_9 + d_5 d_7 d_9^2 = 0$	$(0, 0, 3)$	$[e_0][s]$	$(-1, 1)_{(-\frac{1}{2}, 1)}$	$\mathbf{2}_{(-\frac{1}{2}, -)}$
$d_3^2 d_5^2 - d_2 d_3 d_5 d_6 + d_1 d_3 d_6^2 + d_2^2 d_5 d_7$ $-2 d_1 d_3 d_5 d_7 - d_1 d_2 d_6 d_7 + d_1^2 d_7^2 = 0$	$(0, 0, 3)$	$[e_1][s]$	$(1, -1)_{(-\frac{1}{2}, 0)}$	$\mathbf{2}_{(\frac{1}{2}, +)}$
$4 d_1 d_{10} - d_6^2 = 0$	$(1, 2, 3)$	-	-	-

Table 15: Summary of $SU(2)$ top 1.

Factorization:	$b_1 \to d_1 \quad b_2 \to e_0 d_2 \quad b_3 \to e_0^2 d_3$ $b_5 \to e_1 d_5 \quad b_6 \to d_6 \quad b_7 \to e_0 d_7$ $b_8 \to e_1^2 d_8 \quad b_9 \to e_1 d_9 \quad b_{10} \to d_{10}$
SRI:	$\{xt, ys, xe_0, se_1\}$
Charge Generators	$D_{U(1)} = [y] - [x] - [e_0]$ $D_{\mathbb{Z}_2} = [x]$

Locus	V(f, g, Δ)	matter $\mathbb{P}^1$	Weight	Rep
$d_1 = 0$	$(0, 0, 3)$	$[e_0][t]$	$(-1, 1)_{(1,0)}$	$\mathbf{2}_{(1,+)}$
$d_{10} = 0$	$(0, 0, 3)$	$[e_0][y]$	$(-1, 1)_{(-1,1)}$	$\mathbf{2}(-1, -)$
$-d_{10} d_2^2 + 4 d_1 d_{10} d_3$ $-d_3 d_6^2 + d_2 d_6 d_7 - d_1 d_7^2 = 0$	$(0, 0, 3)$	$[e_1][y]$	$(1, -1)_{(0,0)}$	$\mathbf{2}_{(0,+)}$
$-d_{10} d_5^2 + 4 d_1 d_{10} d_8 - d_6^2 d_8$ $+d_5 d_6 d_9 - d_1 d_9^2 = 0$	$(0, 0, 3)$	$[e_0][e_1 + t + y]$	$(1, -1)_{(0,1)}$	$\mathbf{2}_{(0,-)}$
$4 d_1 d_{10} - d_6^2 = 0$	$(1, 2, 3)$	-	-	-

Table 16: Summary of $SU(2)$ top 2.

Factorization:	$b_1 \to e_1 d_1 \quad b_2 \to d_2 \quad b_3 \to e_0 d_3$ $b_5 \to e_1 d_5 \quad b_6 \to d_6 \quad b_7 \to e_0 d_7$ $b_8 \to e_1 d_8 \quad b_9 \to d_9 \quad b_{10} \to e_0 d_{10}$			
SRI:	$\{xt, ys, ye_0, se_1\}$			
Charge Generators	$D_{U(1)} = [y] - [x] + 1/2[e_1]$ $D_{\mathbb{Z}_2} = [x] + 1/2[e_1]$			
Locus	V(f, g, Δ)	matter $\mathbb{P}^1$	Weight	Rep
$-d_2 d_5 d_6 d_8 + d_1 d_6^2 d_8 + d_2^2 d_8^2 + d_2 d_5^2 d_9$ $-d_1 d_5 d_6 d_9 - 2 d_1 d_2 d_8 d_9 + d_1^2 d_9^2 = 0$	$(0, 0, 3)$	$[e_1][x + t]$	$(1, -1)_{(\frac{1}{2}, -\frac{1}{2})}$	$\mathbf{2}_{(-\frac{1}{2}, \frac{1}{2})}$
$d_{10} d_3 d_6^2 - d_{10} d_2 d_6 d_7 - 2 d_{10} d_2 d_3 d_9$ $+ d_{10}^2 d_2^2 - d_3 d_6 d_7 d_9 + d_2 d_7^2 d_9 + d_3^2 d_9^2 = 0$	$(0, 0, 3)$	$[e_0][x + t]$	$(-1, 1)_{(\frac{1}{2}, \frac{1}{2})}$	$\mathbf{2}_{(\frac{1}{2}, \frac{1}{2})}$
$4 d_2 d_9 - d_6^2 = 0$	$(1, 2, 3)$	-	-	-

Table 17: Summary of $SU(2)$ top 3. In this model the discrete symmetry is enhanced to $\mathbb{Z}_2$ due to the form of $D_{\mathbb{Z}_2}$. Hence, the representations are labeled by $\mathbb{Z}_4$ charges, which here are multiples of $\frac{1}{2}$ modulo $2\mathbb{Z}$. Note that the charge assignments exhibit the global gauge group structure $[SU(2) \times U(1) \times \mathbb{Z}_4]/(\mathbb{Z}_2^{U(1)} \times \mathbb{Z}_2^{\text{bisec}})$. Both quotient factors are embedded in the center of $SU(2)$, however, the first one only affects the $U(1)$ charges while the second one restricts the $\mathbb{Z}_4$ charges.

Factorization:	$b_1 \to e_1^2 d_1 \quad b_2 \to e_1 d_2 \quad b_3 \to d_3$ $b_5 \to e_1 d_5 \quad b_6 \to d_6 \quad b_7 \to e_0 d_7$ $b_8 \to d_8 \quad b_9 \to e_0 d_9 \quad b_{10} \to e_0^2 d_{10}$			
SRI:	$\{xt, ys, xe_1, se_1\}$			
Charge Generators	$\sigma(s_1) = [y] - [x]$ $\sigma(s^{(2)}) = [x] + [e_1]$			
Locus	V(f, g, Δ)	matter $\mathbb{P}^1$	Weight	Rep
$d_3 = 0$	$(0, 0, 3)$	$[e_0][y]$	$(-1, 1)_{(-1,1)}$	$\mathbf{2}_{(-1,-)}$
$d_8 = 0$	$(0, 0, 3)$	$[e_0][x]$	$(-1, 1)_{(1,0)}$	$\mathbf{2}_{(1,+)}$
$d_3 d_5^2 - d_2 d_5 d_6 + d_1 d_6^2$ $+ d_2^2 d_8 - 4 d_1 d_3 d_8 = 0$	$(0, 0, 3)$	$[e_0][x + s]$	$(-1, 1)_{(0,1)}$	$\mathbf{2}_{(0,-)}$
$-d_{10} d_6^2 + 4 d_{10} d_3 d_8 - d_7^2 d_8$ $+ d_6 d_7 d_9 - d_3 d_9^2 = 0$	$(0, 0, 3)$	$[e_1][x + s]$	$(1, -1)_{(0,0)}$	$\mathbf{2}_{(0,+)}$
$4 d_3 d_8 - d_6^2 = 0$	$(1, 2, 3)$	-	-	-

Table 18: Summary of $SU(2)$ top 4.

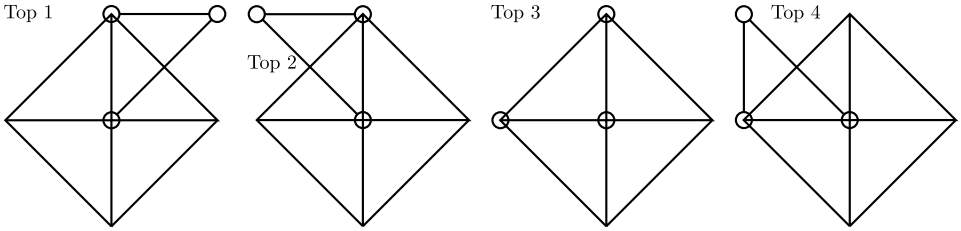

Figure 17: The toric diagram of the four inequivalent $SU(3)$ tops over F_2.

Factorization:	$b_1 \to f_2 d_1 \quad b_2 \to f_0 f_2 d_2 \quad b_3 \to f_0^2 d_3$ $b_5 \to f_1 f_2 d_5 \quad b_6 \to d_6 \quad b_7 \to f_0 d_7$ $b_8 \to f_1^2 f_2 d_8 \quad b_9 \to f_1 d_9 \quad b_{10} \to f_0 f_1 d_{10}$
vertices:	$f_0:(0,0,1), f_1:(1,1,1), f_2:(0,1,1)$
SRI:	$\{xt, xf_1, ys, yf_0, tf_2, sf_2, sf_1\}$
Charge Generators	$\sigma(s_1) = [y] - [x] + \frac{1}{3}(2[f_1] + [f_2])$ $\sigma(s^{(2)}) = [x] + + \frac{1}{3}(2[f_1] + [f_2])$

Locus	V(f,g,Δ)	matter $\mathbb{P}^1$	Weight	Rep
$d_1 = 0$	$(0,0,4)$	$[f_0][t]$	$(1,0)_{(\frac{2}{3},\frac{1}{3})}$	$\mathbf{3}_{(\frac{2}{3},-)}$
$d_{10}d_6 - d_7 d_9 = 0$	$(0,0,4)$	$[f_2][x]$	$(0,-1)_{(\frac{2}{3},-\frac{2}{3})}$	$\mathbf{3}_{(\frac{2}{3},+)}$
$d_3 d_6^2 - d_2 d_6 d_7$ $+ d_1 d_7^2 = 0$	$(0,0,4)$	$[f_1][y]$	$(-1,1)_{(-\frac{1}{3},\frac{1}{3})}$	$\mathbf{3}_{(-\frac{1}{3},-)}$
$d_6^2 d_8 - d_5 d_6 d_9$ $+ d_1 d_9^2 = 0$	$(0,0,4)$	$[f_0][x]$	$(0,1)_{(\frac{1}{3},-\frac{2}{3})}$	$\mathbf{3}_{(-\frac{1}{3},+)}$
$d_6 = 0$	$(2,2,4)$	-	-	-

Table 19: Summary of $SU(3)$ top 1.

Factorization:	$b_1 \to f_2 d_1 \quad b_2 \to f_1 d_2 \quad b_3 \to f_0 f_1 d_3$ $b_5 \to f_1 f_2 d_5 \quad b_6 \to d_6 \quad b_7 \to f_0 d_7$ $b_8 \to f_2 d_8 \quad b_9 \to f_0 f_2 d_9 \quad b_{10} \to f_0^2 f_2 d_{10}$
vertices:	$f_0:(0,0,1), f_1:(-1,1,1), f_2:(0,1,1)$
SRI:	$\{xt, xf_2, ys, yf_0, tf_1, sf_1, sf_2\}$
Charge Generators	$\sigma(s_1) = [y] - [x] - \frac{1}{3}([f_1] - [f_2])$ $\sigma(s^{(2)}) = [x] + \frac{2}{3}(2[f_1] + [f_2])$

Locus	V(f,g,Δ)	matter $\mathbb{P}^1$	Weight	Rep
$d_8 = 0$	$(0,0,4)$	$[f_0][x]$	$(1,0)_{(\frac{2}{3},\frac{1}{3})}$	$\mathbf{3}_{(\frac{2}{3},-)}$
$-d_3 d_6 + d_2 d_7 = 0$	$(0,0,4)$	$[f_2][t]$	$(0,-1)_{(\frac{2}{3},-\frac{2}{3})}$	$\mathbf{3}_{(\frac{2}{3},+)}$
$-d_2 d_5 d_6 + d_1 d_6^2$ $+ d_2^2 d_8 = 0$	$(0,0,4)$	$[f_0][t]$	$(0,1)_{(\frac{1}{3},\frac{2}{3})}$	$\mathbf{3}_{(-\frac{1}{3},+)}$
$d_1 0 d_6^2 + d_7^2 d_8$ $- d_6 d_7 d_9 = 0$	$(0,0,4)$	$[f_1][y]$	$(-1,1)_{(-\frac{1}{3},\frac{1}{3})}$	$\mathbf{3}_{(-\frac{1}{3},-)}$
$d_6 = 0$	$(2,2,4)$	-	-	-

Table 20: Summary of $SU(3)$ top 2.

Factorization:	$b_1 \to f_0 f_2 d_1$ $b_2 \to f_0 d_2$ $b_3 \to f_0^2 f_1 d_3$ $b_5 \to f_2 d_5$ $b_6 \to d_6$ $b_7 \to f_0 f_1 d_7$ $b_8 \to f_1 f_2^2 d_8$ $b_9 \to f_1 f_2 d_9$ $b_{10} \to f_1 d_{10}$
vertices:	$f_0 : (0,0,1), f_1 : (0,1,1), f_2 : (1,1,1)$
SRI:	$\{xt, xf_1, xf_2, ys, yf_1, tf_0, sf_2\}$
Charge Generators	$\sigma(s_1) = [y] - [x] + \frac{2}{3}([f_1] + 2[f_2])$ $\sigma(s^{(2)}) = [x]$

Locus	V(f, g, Δ)	matter $\mathbb{P}^1$	Weight	Rep
$d_{10} = 0$	$(0,0,4)$	$[f_0][y]$	$(0,1)_{(-\frac{2}{3},1)}$	$\mathbf{3}_{(\frac{2}{3},-)}$
$d_2 d_5 - d_1 d_6 = 0$	$(0,0,4)$	$[f_1][t]$	$(-1,1)_{(\frac{2}{3},0)}$	$\mathbf{3}_{(\frac{2}{3},+)}$
$d_1 0 d_2^2 + d_3 d_6^2$ $-d_2 d_6 d_7 = 0$	$(0,0,4)$	$[f_2][t]$	$(1,-1)_{(\frac{1}{3},0)}$	$\mathbf{3}_{(\frac{1}{3},+)}$
$d_1 0 d_5^2 + d_6^2 d_8$ $-d_5 d_6 d_9 = 0$	$(0,0,4)$	$[f_0][s]$	$(1,0)_{(-\frac{1}{3},1)}$	$\mathbf{3}_{(-\frac{1}{3},-)}$
$d_6 = 0$	$(2,2,4)$	-	-	-

Table 21: Summary of $SU(3)$ top 3.

Factorization:	$b_1 \to f_0 f_1^2 d_1$ $b_2 \to f_0 f_1 d_2$ $b_3 \to f_0 d_3$ $b_5 \to f_1 d_5$ $b_6 \to d_6$ $b_7 \to f_0 f_2 d_7$ $b_8 \to f_1 f_2 d_8$ $b_9 \to f_2 d_9$ $b_{10} \to f_0 f_2^2 d_{10}$
vertices:	$f_0 : (0,0,1), f_1 : (0,1,1), f_2 : (1,0,1)$
SRI:	$\{xt, xf_2, ys, yf_0, yf_2, sf_1, tf_0\}$
Charge Generators	$\sigma(s_1) = [y] - [x] + \frac{1}{3}(2[f_1] + [f_2])$ $\sigma(s^{(2)}) = [x] + \frac{1}{3}(2[f_1] + [f_2])$

Locus	V(f, g, Δ)	matter $\mathbb{P}^1$	Weight	Rep
$d_3 = 0$	(0,0,4)	$[f_1][t]$	$(-1,1)_{(\frac{2}{3},-\frac{1}{3})}$	$\mathbf{3}_{(\frac{2}{3},-)}$
$-d_6 d_8 + d_5 d_9 = 0$	(0,0,4)	$[f_0][x]$	$(1,0)_{(\frac{2}{3},\frac{2}{3})}$	$\mathbf{3}_{(\frac{2}{3},+)}$
$d_3 d_5^2 - d_2 d_5 d_6$ $+d_1 d_6^2 = 0$	$(0,0,4)$	$[f_2][s]$	$(0,-1)_{(-\frac{1}{3},-\frac{1}{3})}$	$\mathbf{3}_{(-\frac{1}{3},-)}$
$d_{10} d_6^2 - d_6 d_7 d_9$ $+d_3 d_9 = 0$	$(0,0,4)$	$[f_1][x]$	$(-1,0)_{(\frac{1}{3},-\frac{2}{3})}$	$\mathbf{3}_{(-\frac{1}{3},+)}$
$d_6 = 0$	$(2,2,4)$	-	-	-

Table 22: Summary of $SU(3)$ top 4.

B.1 Tools: Koszul resolution, Brill–Noether theory and fat points

The purpose of this appendix is to cover some of the necessary mathematical backgrounds, and also provide more details of computations carried out throughout the paper.

B.1.1 Brill–Noether theory

Our exposition of Brill–Noether theory is based on [151, 152]. We refer the interested reader to these references for more details.

The Jacobian of Riemann surfaces

To each smooth Riemann surface C_g one can associate a Jacobian variety $\mathrm{Jac}(C_g)$. This variety is of dimension g and classifies equivalence classes of line bundle divisors of degree 0:

$$\mathrm{Jac}(C_g) = \mathrm{Div}_0(C_g)/\mathrm{Prin}(C_g)\,. \tag{B.1.1}$$

In this expression $\mathrm{Div}^0(C_g)$ is the group of all divisors of degree 0 and $\mathrm{Prin}(C_g)$ the group of all principal divisors on C_g. Line bundles on C_g are isomorphic iff their divisors differ by a divisor in $\mathrm{Prin}(C_g)$. Hence, sheaf cohomologies of line bundles can only differ if the line bundles are not isomorphic, or equivalently if their divisors differ by more than elements of $\mathrm{Prin}(C_g)$. Consequently, the Jacobian of C_g plays an important role for our analysis and in Brill–Noether theory. Let us therefore introduce the Jacobian in more detail.

Historically, the Jacobian of a curve C_g of genus g was discovered by investigating integrals $\int_{\mathcal{P}} \omega$ where $\mathcal{P} \subset C_g$ is a (not necessarily closed) path and ω a holomorphic differential. More generally, mark a point $p_0 \in C_g$, let $(\omega_1, \ldots, \omega_g)$ be a basis of the holomorphic

differentials on C_g and consider the map

$$\phi\colon C_g \to \mathbb{C}^g\,,\; p \mapsto \left(\int_{p_0}^{p} \omega_1\,,\;\ldots\,,\;\int_{p_0}^{p} \omega_g\right)\,. \tag{B.1.2}$$

The value of this map strongly depends on the path $\mathcal{P} \subset C_g$ which we choose to connect p_0 and p. This redundancy can be removed by taking the period lattice of C_g into account. To this end, recall that there are $2g$ homologically distinct closed 1-cycles in C_g, i.e., $H_1(C_g, \mathbb{Z})$ is a $2g$-dimensional vector space over $\mathbb{Z}$.[1] We now consider the map

$$\phi\colon H_1(C_g, \mathbb{Z}) \to \mathbb{C}^g\,,\; \alpha \mapsto \left(\int_{\alpha} \omega_1\,,\;\ldots\,,\;\int_{\alpha} \omega_g\right)\,, \tag{B.1.3}$$

where ω_i denote the above basis of holomorphic differentials on C_g. Hence, for every of the $2g$-basis elements of $H_1(C_g, \mathbb{Z})$, we obtain an element $\phi(\alpha) \in \mathbb{C}^g$. It turns out that these $2g$ elements span a full-dimensional lattice Λ in $\mathbb{C}^g$ — the period lattice of C_g. By virtue of this lattice, we obtain a well-defined map

$$\phi\colon C_g \to \mathbb{C}^g/\Lambda\,,\; p \mapsto \left(\int_{p_0}^{p} \omega_1\,,\;\ldots\,,\;\int_{p_0}^{p} \omega_g\right)\,. \tag{B.1.4}$$

This map is known as the *Abel–Jacobi map*. It can easily be extended to divisors in C_g. Namely, for a divisor

$$D = \sum_{i=1}^{N} \lambda_i \cdot p_i\,,\; \lambda_i \in \mathbb{Z}, \qquad p_i \in C_g\,, \tag{B.1.5}$$

we define

$$\phi\colon \mathrm{Div}(C_g) \to \mathbb{C}^g/\Lambda\,,\; D \mapsto \sum_{i=1}^{N} \lambda_i \cdot \phi\,(p_i)\,. \tag{B.1.6}$$

The theorem of Abel (see [183] and references therein) states that two effective divisors D and E satisfy $\phi(D) = \phi(E)$ iff D and E are linearly equivalent. Consequently, we obtain

[1] See e.g. [151] for an explicit construction of the $2g$-generators A_i, B_i of $H_1(C_g, \mathbb{Z})$.

an injective group homomorphism

$$\Phi\colon \mathrm{Div}_0(C_g)/\mathrm{Prin}(C_g) \to \mathbb{C}^g/\Lambda\,,\ [D] \mapsto \sum_{i=1}^{N} \lambda_i \cdot \phi\,(p_i)\,, \tag{B.1.7}$$

of divisor classes of degree 0. It turns out that this map is also surjective (see [183] for a proof). Hence, there is a natural isomorphism

$$\mathrm{Jac}(C_g) = \mathrm{Div}_0(C_g)/\mathrm{Prin}(C_g) \cong \mathbb{C}^g/\Lambda\,. \tag{B.1.8}$$

Central results

For ease of notation let $\mathrm{Div}(C_g)_d$ denote all divisors of degree d. Then, let us consider the restriction of B.1.6 to $\mathrm{Div}(C_g)_d$, i.e.

$$\Phi_d\colon \mathrm{Div}(C_g)_d/\mathrm{Prim}(C_g) \to \mathbb{C}^g/\Lambda\,,\ D \mapsto \sum_{i=1}^{N} \lambda_i \cdot \phi\,(p_i)\,. \tag{B.1.9}$$

Let us pick an integer $r \geq -1$ and study the subvariety of $\mathrm{Jac}(C_g)$

$$G_d^r = \left\{ p \in \mathrm{im}\,(\Phi_d)\ ,\ h^0\left(C_g, \mathcal{O}_{C_g}(\Phi_d^{-1}(p))\right) = r+1 \right\}\,. \tag{B.1.10}$$

Then, the central result of Brill–Noether theory states [150]

$$\dim(G_d^r) \geq \rho\,(r,d,g) \equiv g - (r+1)\cdot((r+1) - (d-g+1))\,. \tag{B.1.11}$$

By use of the Riemann–Roch theorem

$$h^0\left(C_g, \mathcal{O}_{C_g}(D)\right) - h^1\left(C_g, \mathcal{O}_{C_g}(D)\right) = \deg\left(\mathcal{O}_{C_g}(D)\right) - g + 1 = d - g + 1\,, \tag{B.1.12}$$

we can rewrite this results in the suggestive form

$$\dim(G_d^r) \geq \rho\,(r,d,g) \equiv g - n^0 \cdot n^1\,, \tag{B.1.13}$$

with $n^0 \equiv r+1$ and $n^1 = r+1-(d-g+1)$. We may thus use $\rho\,(r,d,g)$ as a measure for how likely it is that a line bundle of degree d on a genus g curve C_g has $n^0 = r+1$ global sections.

Let us demonstrate this for degree $d=2$ bundles on a genus-3 curve. By general theory, the number of section of a line bundle on a curve C_g with $g \geq 1$ can never exceed its degree. Hence $n^0 \in \{0,1,2\}$. With this information, let us compute $\rho(r,d,g)$ for the admissible values of r:

r	(n^0, n^1)	$\rho(r,d,g)$
-1	$(0,0)$	3
0	$(1,1)$	2
1	$(2,2)$	-1

(B.1.14)

From this we learn, that most line bundles $\mathcal{L}$ of degree 2 on a genus-3 curve C_3 satisfy $h^0\,(C_3,\mathcal{L}) = 0$. Since for these bundles ρ matches the dimension of the Jacobian of C_3, we can say that these line bundles are associated to generic points of the Jacobian. Furthermore, we learn that there are such line bundles with $h^0\,(C_3,\mathcal{L}) = 1$. However, these are special in the sense that they are associated to a codimension-1 locus in the Jacobian $\mathrm{Jac}(C_3)$.

Finally, $\rho = -1$ for $r=1$ begs for an explanation. This explanation follows from work of Griffiths and Harris [153]:

$$\text{On } \textbf{generic} \text{ curves, } \dim(G^r_d) = \rho\,(r,d,g).$$

So in particular, on generic curves it holds $G^r_d = \emptyset$ if and only if $\rho\,(r,d,g) < 0$. Consequently, we conclude from B.1.14, that on generic genus $g=3$ curve, there is no line bundle $\mathcal{L}$ of degree 2 such that $h^0(C_3,\mathcal{L}) = 2$.

Note however, that this does not rule out the possibility that non-generic curves may host such line bundles. In the case at hand, it follows from the theorem of Cliffford [153] that

hyperelliptic curves H_3 of genus $g = 3$ admit line bundles $\mathcal{L}$ of degree 2 and $h^0(H_3, \mathcal{L}) = 2$.

Brill–Noether jump

As we see from B.1.14, we can in general modify a line bundle on a generic curve such that it admits additional sections. A jump from $r = r_{\text{generic}}$ to $r_{\text{generic}} + 1$ is equivalent to saying that the Serre-dual bundle admits a section, i.e., becomes effective:

$$K_C - D > 0 \quad \Leftrightarrow \quad \exists p_i \colon K_C - D \sim \sum_i p_i \,. \tag{B.1.15}$$

where $\sim$ represents linear equivalence of divisors. Obviously, this requires the line bundle divisor D to move into special alignment relative to K_C. Such a divisor is termed a *special* divisor. We term a change in h^0, which is solely attributed to a special alignment of the line bundle divisor, a *Brill–Noether jump*.

B.1.2 Koszul resolution

Generalities

Given a curve C and a line bundle $\mathcal{L}$ on C, we wish to identify which deformations of the curve lead to an increased number of global sections for $\mathcal{L}$. For hypersurface curves in dP_3, the answer follows from a study of the Koszul resolution. In this case $C(\mathbf{c}) = V(P(\mathbf{c}))$ for a polynomial $P(\mathbf{c})$. The coefficients $\mathbf{c}$ model the complex structure moduli of a global F-theory setting.

For such a setup, the Koszul resolution is given by the short-exact sequence

$$0 \to \mathcal{O}_{dP_3}\left(D_L - D_C\right) \xrightarrow{\alpha} \mathcal{O}_{dP_3}\left(D_L\right) \to \mathcal{L}(\mathbf{c}) \to 0 \,. \tag{B.1.16}$$

The map α is induced by the polynomial $P(\mathbf{c})$. Namely, for $U \subseteq dP_3$ open, α is given by

$$s \in \mathcal{O}_{dP_3}\left(D_L - D_C\right)(U) \mapsto s \cdot P(\mathbf{c}) \in \mathcal{O}_{dP_3}\left(D_L\right)(U) \,. \tag{B.1.17}$$

The Koszul resolution then induces the following long exact sequence in sheaf cohomology:

$$\begin{aligned} 0 \longrightarrow & H^0\left(dP_3, D_L - D_C\right) \xrightarrow{\varphi_0} H^0\left(dP_3, D_L\right) \longrightarrow H^0\left(C(\mathbf{c}), \mathcal{L}(\mathbf{c})\right) \\ \hookrightarrow & H^1\left(dP_3, D_L - D_C\right) \xrightarrow{\varphi_1} H^1\left(dP_3, D_L\right) \longrightarrow H^1\left(C(\mathbf{c}), \mathcal{L}(\mathbf{c})\right) \\ \hookrightarrow & H^2\left(dP_3, D_L - D_C\right) \xrightarrow{\varphi_2} H^2\left(dP_3, D_L\right) \longrightarrow 0 \longrightarrow 0\,. \end{aligned} \tag{B.1.18}$$

The maps $\varphi_i = \varphi_i(\mathbf{c})$ are induced from multiplication with $P(\mathbf{c})$. Therefore, these maps are sensitive to the choice of parameters $\mathbf{c}$ for the curve $C(\mathbf{c})$. Explicitly, the maps φ_i are vector-space morphisms and the entries of their defining matrices are functions of the parameters c_i. Provided that we know these mapping matrices, we may thus use the exactness of the Koszul resolution of infer $h^i\left(C(\mathbf{c}), \mathcal{L}(\mathbf{c})\right)$ as a function of the coefficients c_i in $P(\mathbf{c})$.

For example, in 5.4.1, we consider $D_C = (4; -1, -2, -1)$ and $D_L = (3; -3, -1, -2)$. In this case, the Koszul resolution simplifies and takes the form

$$\begin{aligned} 0 \longrightarrow & 0 \longrightarrow 0 \longrightarrow H^0\left(C(\mathbf{c}), \mathcal{L}(\mathbf{c})\right) \\ \hookrightarrow & H^1\left(dP_3, D_L - D_C\right) \cong \mathbb{C}^4 \xrightarrow{\varphi} H^1\left(dP_3, D_L\right) \cong \mathbb{C}^1 \longrightarrow H^1\left(C(\mathbf{c}), \mathcal{L}(\mathbf{c})\right) \\ \hookrightarrow & 0 \longrightarrow 0 \longrightarrow 0 \longrightarrow 0\,. \end{aligned} \tag{B.1.19}$$

Then it follows

$$\begin{aligned} H^1\left(C(\mathbf{c}), \mathcal{L}(\mathbf{c})\right) &\cong \mathrm{coker}\varphi\,, \\ h^1(C(\mathbf{c}), \mathcal{L}(\mathbf{c})) &= 1 - \dim\left(\mathrm{im}\varphi\right)\,. \end{aligned} \tag{B.1.20}$$

A detailed study of Čech cohomology [203] shows that in this geometry we have $M_\varphi = (c_3, c_6, c_9, 0)$. Hence, $h^1(C(\mathbf{c}), \mathcal{L}(\mathbf{c})) = 1$ on curves with $c_3 = c_6 = c_9 = 0$ and otherwise $h^1(C(\mathbf{c}), \mathcal{L}(\mathbf{c})) = 0$. Along these lines, we classify the curve geometries according to their

admitted number of global sections.

Recall that Čech cohomology expresses $H^i(dP_3, \mathcal{O}_{dP_3}(D_L - D_C))$ and $H^i(dP_3, \mathcal{O}_{dP_3}(D_L))$ as collections of local sections. The mappings of these local sections follow from B.1.17, i.e., are given by multiplication with the polynomial $P(\mathbf{c})$ which defines the curve $C(\mathbf{c})$. Importantly, these bases are expressed modulo equivalence relations induced from Čech coboundaries. Therefore, these computations are typically fairly tedious.

Oftentimes, *cohomCalg* [205, 206, 207, 208, 209, 210, 211] can help to simplify this task. Namely, it identifies bases of $H^i(dP_3, \mathcal{O}_{dP_3}(D_L - D_C))$ and $H^i(dP_3, \mathcal{O}_{dP_3}(D_L))$ in terms of rationoms — quotients of monomials in the homogeneous coordinates — and therefore simplifies the task to find the bases in Čech cohomology. Even more, we may be tempted to simply multiply the basis elements identifed by *cohomCalg* [205, 206, 207, 208, 209, 210, 211] with the polynomial $P(\mathbf{c})$ and ignore all image rationoms that have not been identified as bases for $H^i(dP_3, \mathcal{O}_{dP_3}(D_L))$ by *cohomCalg* under the assumption that they correspond to Čech coboundaries.

This procedure fails whenever *Čech cohomology chamber factors* greater than 1 appear. In this case, *cohomCalg* finds that one rationom R spans a vector space of dimension greater than 1 in sheaf cohomology. The interpretation of this is, that there are at least two distinct Čech cochains, i.e., collections of local sections, in which the rationom R is the only non-trivial entry. Hence, these distinct Čech cochains are both canonically isomorphic to R. However, to identify the mapping matrices of the line bundle cohomologies correctly, the information about R is insufficient. Rather, the corresponding Čech cochains need to be identified explicitly.

Given these insights, we have taken extra care, to work out the mappings presented in this work carefully with Čech cohomology. We present such a computation in large detail in the following section.

Before we come to this, let us mentioned that a detailed study of the Koszul resolution is not original to this work. For example, in the context of heterotic compactifications, these resolutions — including the mappings in the induced long exact sequence — have been studied extensively [212, 213, 162, 163, 108]. However, to the best of our knowledge, chamber factor greater than 1 do not show in products of projective spaces. Hence, this complication does not arise in heterotic compactifications with CICYs.

Čech cohomologies for 5.4.2

Here, we present a more detailed computation of the example discussed in 5.4.2. Recall that the curve and line bundle in question are given by

$$D_C = (4; -1, -1, -1)\,, \qquad D_L = (1; 2, -2, -1)\,. \tag{B.1.21}$$

Moreover, recall that in this case $h^0\left(C(\mathbf{c}), \mathcal{L}(\mathbf{c})\right)$ is uniquely determined by the mapping

$$\varphi\colon H^1\left(dP_3, \mathcal{O}_{dP_3}\left(D_L - D_C\right)\right) \xrightarrow{\cdot P(\mathbf{c})} H^1\left(dP_3, \mathcal{O}_{dP_3}\left(D_L\right)\right)\,, \tag{B.1.22}$$

where

$$\begin{aligned} P(\mathbf{c}) = {} & c_1 x_1^3 x_2^3 x_3^2 x_4 + c_2 x_1^2 x_2^3 x_3 x_4^2 x_6 + c_3 x_1 x_2^3 x_4^3 x_6^2 + c_4 x_1^3 x_2^2 x_3^3 x_5 + c_5 x_1^2 x_2^2 x_3^2 x_4 x_5 x_6 \\ & + c_6 x_1 x_2^2 x_3 x_4^2 x_5 x_6^2 + c_7 x_2^2 x_4^3 x_5 x_6^3 + c_8 x_1^2 x_2 x_3^3 x_5^2 x_6 + c_9 x_1 x_2 x_3^2 x_4 x_5^2 x_6^2 \\ & + c_{10} x_2 x_3 x_4^2 x_5^2 x_6^3 + c_{11} x_1 x_3^3 x_5^3 x_6^2 + c_{12} x_3^2 x_4 x_5^3 x_6^3\,. \end{aligned} \tag{B.1.23}$$

Namely, $h^0(C(\mathbf{c}), \mathcal{L}(\mathbf{c})) = 3 - \mathrm{rk}\left(M_\varphi\right)$. With *cohomCalg* [205, 207, 208, 209, 210, 206, 211], we obtain a basis of the line bundle cohomologies:

$$H^1(D_L - D_C) \cong \mathrm{Span}_{\mathbb{C}}\left\{\frac{1}{x_3 x_4^3 x_6^3}, \frac{1}{x_1 x_3^2 x_4^2 x_6^2}, \frac{1}{x_1^2 x_3^3 x_4 x_6}\right\} \cong \mathbb{C}^3\,, \tag{B.1.24}$$

$$H^1(D_L) \cong \mathrm{Span}_{\mathbb{C}}\left\{\frac{x_5^3 x_6}{x_1 x_4}, \frac{x_1 x_2^3}{x_3 x_6}\right\} \cong \mathbb{C}^2\,. \tag{B.1.25}$$

By polynomial multiplication we then have

$$\frac{1}{x_3x_4^3x_6^3}\cdot P(\mathbf{c}) = c_3\frac{x_1x_2^3}{x_3x_6} + \dots\,, \tag{B.1.26}$$

$$\frac{1}{x_1x_3^2x_4^2x_6^2}\cdot P(\mathbf{c}) = c_2\frac{x_1x_2^3}{x_3x_6} + c_{12}\frac{x_5^3x_6}{x_1x_4} + \dots\,, \tag{B.1.27}$$

$$\frac{1}{x_1^2x_3^3x_4x_6}\cdot P(\mathbf{c}) = c_1\frac{x_1x_2^3}{x_3x_6} + c_{11}\frac{x_5^3x_6}{x_1x_4} + \dots\,. \tag{B.1.28}$$

On the RHS of these equations, we have omitted all rationoms which cannot be expressed as $\mathbb{Z}$-linear combinations of those listed in B.1.25. The remainder of this section will justify that we can indeed omit these terms. For the time being, note that this leads to

$$M_\varphi = \left(\begin{smallmatrix} c_3 & c_2 & c_1 \\ 0 & c_{12} & c_{11}\end{smallmatrix}\right), \tag{B.1.29}$$

which is the matrix analyzed in 5.4.2.

Strategy In order to justify that all omitted terms in B.1.28 can be ignored, we will now analyse $H^1(dP_3, \mathcal{O}_{dP_3}(D_L))$ and $H^1(dP_3, \mathcal{O}_{dP_3}(D_L - D_C))$ from the perspective of Čech cohomology. For additional background we refer the interested reader to [203]. Recall that for $H^1(dP_3, \mathcal{O}_{dP_3}(D_L))$ it holds

$$H^1(dP_3, \mathcal{O}_{dP_3}(D_L)) \cong \check{H}^1(\mathcal{U}, \mathcal{O}_{dP_3}(D_L)) = \ker(\delta_1)/\mathrm{im}(\delta_0)\,. \tag{B.1.30}$$

In this expression, $\mathcal{U}$ is the affine open cover of the dP_3 surface — we will discuss this momentarily — and the maps δ_i are the boundary morphisms in the Čech complex

$$0 \to \check{C}^0(\mathcal{U}, \mathcal{O}_{dP_3}(D_L)) \xrightarrow{\delta_0} \check{C}^1(\mathcal{U}, \mathcal{O}_{dP_3}(D_L)) \xrightarrow{\delta_1} \dots\,. \tag{B.1.31}$$

Thereby, let us specify our statement regarding the RHS of B.1.28. We claim that all omitted terms are in $\mathrm{im}(\delta_0)$, i.e., are Čech coboundaries. To justify this statement, we proceed by investigating the following objects:

1. $\mathrm{im}\,(\delta_0(D_L))$.

2. $\ker\,(\delta_1(D_L))$,

3. $\ker\,(\delta_1(D_L - D_C))$,

4. the map $\ker\,(\delta_1(D_L - D_C)) \to \ker\,(\delta_1(D_L))$.

Čech 0-cocycles of D_L To understand $\check{C}^0(\mathcal{U}, \mathcal{O}_{dP_3}(D_L))$, recall that dP_3 has 6 homogeneous variables x_i. These correspond to the ray generators

$$u_1 = (0,-1)\,, \qquad u_2 = (-1,0)\,, \qquad u_3 = (1,-1)\,, \tag{B.1.32}$$

$$u_4 = (-1,1)\,, \qquad u_5 = (1,0)\,, \qquad u_6 = (0,1)\,. \tag{B.1.33}$$

In terms of these, the maximal cones in the fan of dP_3 are given by

$$\begin{aligned} &U_1 = \mathrm{Span}_{\geq 0}\,\{u_1, u_3\}\,, \qquad U_2 = \mathrm{Span}_{\geq 0}\,\{u_3, u_5\}\,, \qquad U_3 = \mathrm{Span}_{\geq 0}\,\{u_5, u_6\}\,, \\ &U_4 = \mathrm{Span}_{\geq 0}\,\{u_6, u_4\}\,, \qquad U_5 = \mathrm{Span}_{\geq 0}\,\{u_4, u_2\}\,, \qquad U_6 = \mathrm{Span}_{\geq 0}\,\{u_2, u_1\}\,. \end{aligned} \tag{B.1.34}$$

These cones correspond to open affine subsets of the dP_3, namely the subsets of the form $\{x_i \neq 0\}$. Collectively, $\mathcal{U} = \{U_i\}_{1\leq i\leq 6}$ is the open affine cover of dP_3. To compute $\check{C}^0(\mathcal{U}, \mathcal{O}_{X_\Sigma}(D_L))$ with respect to this open affine cover $\mathcal{U}$, we note

$$D_L = (1;2,-2,-1) = H + 2E_1 - 2E_2 - E_3 = \sum_{i=1}^{6} a_i V(x_i)\,, \tag{B.1.35}$$

with $a_1 = a_4 = a_6 = 0$ and $a_2 = 2$, $a_3 = -1$, $a_5 = 1$. Now, we can quote from [203] that

$$\check{C}^0(\mathcal{U}, \mathcal{O}_{X_\Sigma}(D_L)) = \bigoplus_{1\leq i\leq 6} H^0(U_i, \mathcal{O}_{X_\Sigma}(D_L)|_{U_i}\,, \tag{B.1.36}$$

$$H^0(U_i, \mathcal{O}_{X_\Sigma}(D_L)|_{U_i}) \cong \left(\prod_{j=1}^{6} x_j^{a_j}\right) \cdot \bigoplus_{m\in P_D(U_i)} \mathbb{C} \cdot \left(\prod_{j=1}^{6} x_j^{\langle m, u_j\rangle}\right), \tag{B.1.37}$$

$$P_D(U_i) = \{m \in \mathbb{Z}^2\,,\, \langle m, u_\rho\rangle \geq -a_\rho\ \forall \rho \in \sigma(1)\}\,. \tag{B.1.38}$$

The normalization in B.1.37 ensures that we are looking at rationoms of degree D_L, as analysed by *cohomCalg*. Explicitly, it holds

$$P_D(U_1) = \{m \in \mathbb{Z}^2\,, -m_2 \geq 0 \text{ and } m_1 - m_2 \geq 1\}\,, \tag{B.1.39}$$

$$P_D(U_2) = \{m \in \mathbb{Z}^2\,, m_1 - m_2 \geq 1 \text{ and } m_1 \geq -1\}\,, \tag{B.1.40}$$

$$P_D(U_3) = \{m \in \mathbb{Z}^2\,, m_1 \geq -1 \text{ and } m_2 \geq 0\}\,, \tag{B.1.41}$$

$$P_D(U_4) = \{m \in \mathbb{Z}^2\,, m_2 \geq 0 \text{ and } -m_1 + m_2 \geq 0\}\,, \tag{B.1.42}$$

$$P_D(U_5) = \{m \in \mathbb{Z}^2\,, -m_1 + m_2 \geq 0 \text{ and } -m_1 \geq -2\}\,, \tag{B.1.43}$$

$$P_D(U_6) = \{m \in \mathbb{Z}^2\,, -m_1 \geq -2 \text{ and } -m_2 \geq 0\}\,. \tag{B.1.44}$$

To express these polytopes in simpler terms, we define the regions A, B, C, D, E, F, G, H:

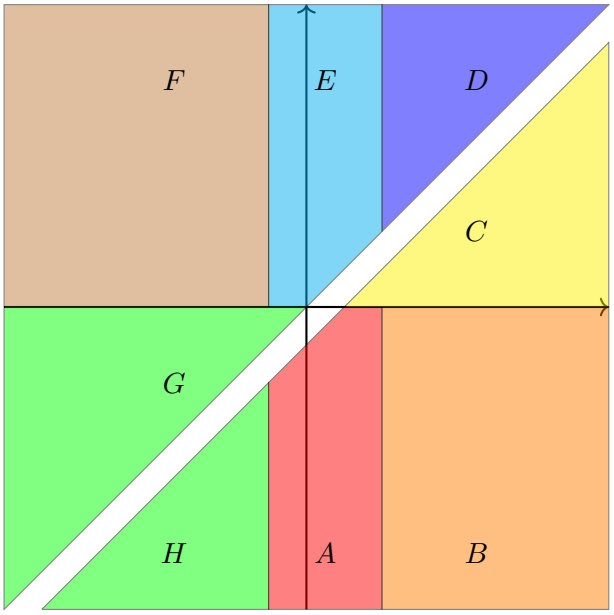

In an abuse of terminology, we use A to denote all polynomials formed from linear combination of the Laurent monomials associated to the lattice points of the region A. Similarly,

we use the names for the other regions. Thereby, we can write

$$\check{C}^0(\mathcal{U}, \mathcal{O}_{X_\Sigma}(D_L)) = \frac{x_2^2 x_5}{x_3} \cdot (H + A + B, A + B + C, C + D + E, \tag{B.1.45}$$

$$D + E + F, E + F + G, G + H + A) \; . \tag{B.1.46}$$

Finally note that the map $\delta_0 \colon \check{C}^0(\mathcal{U}, \mathcal{O}_{X_\Sigma}(D_L)) \to \check{C}^1(\mathcal{U}, \mathcal{O}_{X_\Sigma}(D_L))$ is given by multiplication with the following matrix:

$$M_{\delta_0} = \begin{pmatrix} -1 & 1 & 0 & 0 & 0 & 0 \\ -1 & 0 & 1 & 0 & 0 & 0 \\ -1 & 0 & 0 & 1 & 0 & 0 \\ -1 & 0 & 0 & 0 & 1 & 0 \\ -1 & 0 & 0 & 0 & 0 & 1 \\ 0 & -1 & 1 & 0 & 0 & 0 \\ 0 & -1 & 0 & 1 & 0 & 0 \\ 0 & -1 & 0 & 0 & 1 & 0 \\ 0 & -1 & 0 & 0 & 0 & 1 \\ 0 & 0 & -1 & 1 & 0 & 0 \\ 0 & 0 & -1 & 0 & 1 & 0 \\ 0 & 0 & -1 & 0 & 0 & 1 \\ 0 & 0 & 0 & -1 & 1 & 0 \\ 0 & 0 & 0 & -1 & 0 & 1 \\ 0 & 0 & 0 & 0 & -1 & 1 \end{pmatrix} . \tag{B.1.47}$$

Čech 1-cocycles of D_L We repeat this analysis for $\check{C}^1(\mathcal{U}, \mathcal{O}_{dP_3}(D_L))$. The elements in this Čech cohomology are given by local sections on pairwise intersections of the U_i which form the affine open cover of dP_3. These pairwise intersections and the corresponding polytopes are as follows:

Intersection	Cone	$P_D(U_{ij})$	Presentation
$U_1 \cap U_2$	$\mathrm{Span}_{\geq 0}(u_3)$	$\{m \in \mathbb{Z}^2\,,\, m_1 \geq 1 + m_2\}$	B, C, D, E, F, N
$U_1 \cap U_3$	$\mathrm{Span}_{\geq 0}(0)$	$\mathbb{Z}^2$	
$U_1 \cap U_4$	$\mathrm{Span}_{\geq 0}(0)$	$\mathbb{Z}^2$	
$U_1 \cap U_5$	$\mathrm{Span}_{\geq 0}(0)$	$\mathbb{Z}^2$	
$U_1 \cap U_6$	$\mathrm{Span}_{\geq 0}(u_1)$	$\{m \in \mathbb{Z}^2\,,\, m_1 \leq 0\}$	A, B, C, I, K, L
$U_2 \cap U_3$	$\mathrm{Span}_{\geq 0}(u_5)$	$\{m \in \mathbb{Z}^2\,,\, m_1 \geq -1\}$	$C, D, E, F, G, H, I, L, M, N$
$U_2 \cap U_4$	$\mathrm{Span}_{\geq 0}(0)$	$\mathbb{Z}^2$	
$U_2 \cap U_5$	$\mathrm{Span}_{\geq 0}(0)$	$\mathbb{Z}^2$	
$U_2 \cap U_6$	$\mathrm{Span}_{\geq 0}(0)$	$\mathbb{Z}^2$	
$U_3 \cap U_4$	$\mathrm{Span}_{\geq 0}(u_6)$	$\{m \in \mathbb{Z}^2\,,\, m_2 \geq 0\}$	A, B, C, D, E, L,M
$U_3 \cap U_5$	$\mathrm{Span}_{\geq 0}(0)$	$\mathbb{Z}^2$	
$U_3 \cap U_6$	$\mathrm{Span}_{\geq 0}(0)$	$\mathbb{Z}^2$	
$U_4 \cap U_5$	$\mathrm{Span}_{\geq 0}(u_4)$	$\{m \in \mathbb{Z}^2\,,\, m_2 \geq m_1\}$	A, G, H, I, K, L
$U_4 \cap U_6$	$\mathrm{Span}_{\geq 0}(0)$	$\mathbb{Z}^2$	
$U_5 \cap U_6$	$\mathrm{Span}_{\geq 0}(u_2)$	$\{m \in \mathbb{Z}^2\,,\, m_1 \leq 2\}$	$A, B, C, D, H, I, K, L, M, N$

In this table, we have use the following geometric loci to express the polytopes in question:

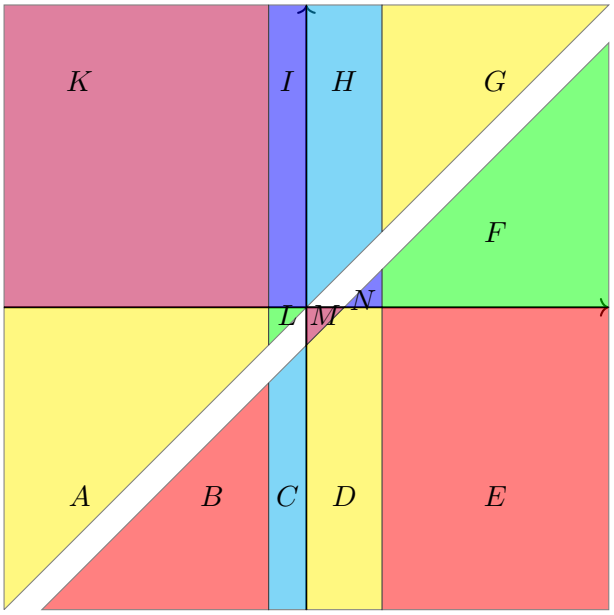

To identify a basis of $\ker(\delta_1)$, we look at the corresponding mapping matrix

$$M_{\delta_1} = \begin{pmatrix}
-1 & 1 & 0 & 0 & 0 & -1 & 0 & 0 & 0 & 0 & 0 & 0 & 0 & 0 & 0 \\
-1 & 0 & 1 & 0 & 0 & 0 & -1 & 0 & 0 & 0 & 0 & 0 & 0 & 0 & 0 \\
-1 & 0 & 0 & 1 & 0 & 0 & 0 & -1 & 0 & 0 & 0 & 0 & 0 & 0 & 0 \\
-1 & 0 & 0 & 0 & 1 & 0 & 0 & 0 & -1 & 0 & 0 & 0 & 0 & 0 & 0 \\
0 & -1 & 1 & 0 & 0 & 0 & 0 & 0 & 0 & -1 & 0 & 0 & 0 & 0 & 0 \\
0 & -1 & 0 & 1 & 0 & 0 & 0 & 0 & 0 & 0 & -1 & 0 & 0 & 0 & 0 \\
0 & -1 & 0 & 0 & 1 & 0 & 0 & 0 & 0 & 0 & 0 & -1 & 0 & 0 & 0 \\
0 & 0 & -1 & 1 & 0 & 0 & 0 & 0 & 0 & 0 & 0 & 0 & -1 & 0 & 0 \\
0 & 0 & -1 & 0 & 1 & 0 & 0 & 0 & 0 & 0 & 0 & 0 & 0 & -1 & 0 \\
0 & 0 & 0 & -1 & 1 & 0 & 0 & 0 & 0 & 0 & 0 & 0 & 0 & 0 & -1 \\
0 & 0 & 0 & 0 & 0 & -1 & 1 & 0 & 0 & -1 & 0 & 0 & 0 & 0 & 0 \\
0 & 0 & 0 & 0 & 0 & -1 & 0 & 1 & 0 & 0 & -1 & 0 & 0 & 0 & 0 \\
0 & 0 & 0 & 0 & 0 & -1 & 0 & 0 & 1 & 0 & 0 & -1 & 0 & 0 & 0 \\
0 & 0 & 0 & 0 & 0 & 0 & -1 & 1 & 0 & 0 & 0 & 0 & -1 & 0 & 0 \\
0 & 0 & 0 & 0 & 0 & 0 & -1 & 0 & 1 & 0 & 0 & 0 & 0 & -1 & 0 \\
0 & 0 & 0 & 0 & 0 & 0 & 0 & -1 & 1 & 0 & 0 & 0 & 0 & 0 & -1 \\
0 & 0 & 0 & 0 & 0 & 0 & 0 & 0 & 0 & -1 & 1 & 0 & -1 & 0 & 0 \\
0 & 0 & 0 & 0 & 0 & 0 & 0 & 0 & 0 & -1 & 0 & 1 & 0 & -1 & 0 \\
0 & 0 & 0 & 0 & 0 & 0 & 0 & 0 & 0 & 0 & -1 & 1 & 0 & 0 & -1 \\
0 & 0 & 0 & 0 & 0 & 0 & 0 & 0 & 0 & 0 & 0 & 0 & -1 & 1 & -1
\end{pmatrix}. \tag{B.1.48}$$

Let us introduce the points

$$p_2 = (2, 1)\,, \qquad p_9 = (-1, -1)\,. \tag{B.1.49}$$

The corresponding Laurent monomials, once multiplied by $x^a \equiv \prod_{j=1}^{6} x_j^{a_j}$, are $\frac{x_5^3 x_6}{x_1 x_4}$, $\frac{x_1 x_2^3}{x_3 x_6}$, i.e., exactly those rationoms which *cohomCalg* identified in B.1.25 as basis of the coho-

mology:

$$H^1(D_L) \cong \mathrm{Span}_{\mathbb{C}} \left\{ \frac{x_5^3 x_6}{x_1 x_4}, \frac{x_1 x_2^3}{x_3 x_6} \right\} . \tag{B.1.50}$$

However, here we can make this isomorphism explicit. In an abuse of terminology let p_2, p_9 denote their Laurent monomials. Then it is readily verified that the following Čech 1-cocycles furnish a basis of $\ker(\delta_1)$:

$$(0, -p_2, -p_2, -p_2, 0, -p_2, -p_2, -p_2, 0, 0, 0, p_2, 0, p_2, p_2) \cong \frac{x_5^3 x_6}{x_1 x_4} , \tag{B.1.51}$$

$$(0, -p_9, -p_9, -p_9, 0, -p_9, -p_9, -p_9, 0, 0, 0, p_9, 0, p_9, p_9) \cong \frac{x_1 x_2^3}{x_3 x_6} . \tag{B.1.52}$$

Čech 1-cocycles of $D_L - D_C$ Finally, let us identify $\check{C}^1(\mathcal{U}, \mathcal{O}_{dP_3}(D_L - D_C))$. We have

$$D_L - D_C = (-3; 3, -1, 0) = 3V(x_2) - 4V(x_3) - 3V(x_5) - 3V(x_6) . \tag{B.1.53}$$

Thus $a_1 = a_4 = 0$, $a_2 = 3$, $a_3 = -4$ and $a_5 = a_6 = -3$. The points associated to the Laurent monomials identified by *cohomCalg* in B.1.24 are:

$$\begin{aligned}
\frac{1}{x_3 x_4^3 x_6^3} &= \frac{x_2^3}{x_3^4 x_5^3 x_6^3} \cdot \frac{x_3^3 x_5^3}{x_2^3 x_4^3} && \leftrightarrow && q_1 = (3, 0) , \\
\frac{1}{x_1 x_3^2 x_4^2 x_6^2} &= \frac{x_2^3}{x_3^4 x_5^3 x_6^3} \cdot \frac{x_3^2 x_5^3 x_6}{x_2^3 x_4^2 x_1} && \leftrightarrow && q_2 = (3, 1) , \\
\frac{1}{x_1^2 x_3^3 x_4 x_6} &= \frac{x_2^3}{x_3^4 x_5^3 x_6^3} \cdot \frac{x_3 x_5^3 x_6^2}{x_4 x_2^3 x_1^2} && \leftrightarrow && q_3 = (3, 2) .
\end{aligned} \tag{B.1.54}$$

The relevant pairwise intersection and polytopes are as follows:

Intersection	Cone	$P_D(U_{ij})$	Points contained
$U_1 \cap U_2$	$\mathrm{Span}_{\geq 0}(u_3)$	$\{m \in \mathbb{Z}^2\,,\, m_1 - m_2 \geq 4\}$	$\emptyset$
$U_1 \cap U_3$	$\mathrm{Span}_{\geq 0}(0)$	$\mathbb{Z}^2$	q_1, q_2, q_3
$U_1 \cap U_4$	$\mathrm{Span}_{\geq 0}(0)$	$\mathbb{Z}^2$	q_1, q_2, q_3
$U_1 \cap U_5$	$\mathrm{Span}_{\geq 0}(0)$	$\mathbb{Z}^2$	q_1, q_2, q_3
$U_1 \cap U_6$	$\mathrm{Span}_{\geq 0}(u_1)$	$\{m \in \mathbb{Z}^2\,,\, -m_2 \geq 0\}$	q_1
$U_2 \cap U_3$	$\mathrm{Span}_{\geq 0}(u_5)$	$\{m \in \mathbb{Z}^2\,,\, m_1 \geq 3\}$	q_1, q_2, q_3
$U_2 \cap U_4$	$\mathrm{Span}_{\geq 0}(0)$	$\mathbb{Z}^2$	q_1, q_2, q_3
$U_2 \cap U_5$	$\mathrm{Span}_{\geq 0}(0)$	$\mathbb{Z}^2$	q_1, q_2, q_3
$U_2 \cap U_6$	$\mathrm{Span}_{\geq 0}(0)$	$\mathbb{Z}^2$	q_1, q_2, q_3
$U_3 \cap U_4$	$\mathrm{Span}_{\geq 0}(u_6)$	$\{m \in \mathbb{Z}^2\,,\, m_2 \geq 3\}$	$\emptyset$
$U_3 \cap U_5$	$\mathrm{Span}_{\geq 0}(0)$	$\mathbb{Z}^2$	q_1, q_2, q_3
$U_3 \cap U_6$	$\mathrm{Span}_{\geq 0}(0)$	$\mathbb{Z}^2$	q_1, q_2, q_3
$U_4 \cap U_5$	$\mathrm{Span}_{\geq 0}(u_4)$	$\{m \in \mathbb{Z}^2\,,\, -m_1 + m_2 \geq 0\}$	$\emptyset$
$U_4 \cap U_6$	$\mathrm{Span}_{\geq 0}(0)$	$\mathbb{Z}^2$	q_1, q_2, q_3
$U_5 \cap U_6$	$\mathrm{Span}_{\geq 0}(u_2)$	$\{m \in \mathbb{Z}^2\,,\, -m_1 \leq -3\}$	q_1, q_2, q_3

It is not hard to verify that $\ker(\delta_1) = \mathrm{Span}_{\mathbb{Z}}\{b_1, b_2, b_3\}$ where

$$\begin{aligned} b_1 &= (0, q_1, q_1, q_1, 0, q_1, q_1, q_1, 0, 0, 0, -q_1, 0, -q_1, -q_1)\ , \\ b_2 &= (0, q_2, q_2, q_2, 0, q_2, q_2, q_2, 0, 0, 0, -q_2, 0, -q_2, -q_2)\ , \\ b_3 &= (0, q_3, q_3, q_3, 0, q_3, q_3, q_3, 0, 0, 0, -q_3, 0, -q_3, -q_3)\ . \end{aligned} \tag{B.1.55}$$

Images of b_1, b_2, b_3 in $\check{C}^1(\mathcal{U}, D_L)$ The mapping between the Čech cocycles happens through the following mapping of complexes

$$\begin{array}{ccccccccc} 0 & \longrightarrow & \check{C}^0(\mathcal{U}, D_L - D_C) & \xrightarrow{\delta_0} & \check{C}^1(\mathcal{U}, D_L - D_C) & \xrightarrow{\delta_1} & \check{C}^2(\mathcal{U}, D_L - D_C) & \to & \cdots \\ & & \cdot P(\mathbf{c}) \downarrow & & \cdot P(\mathbf{c}) \downarrow & & \cdot P(\mathbf{c}) \downarrow & & \\ 0 & \longrightarrow & \check{C}^0(\mathcal{U}, D_L) & \xrightarrow{\delta_0} & \check{C}^1(\mathcal{U}, D_L) & \xrightarrow{\delta_1} & \check{C}^2(\mathcal{U}, D_L) & \longrightarrow & \cdots \end{array} \tag{B.1.56}$$

where $P(\mathbf{c})$ is the global section of D_C in B.1.23. From this it is now readily verified, that the terms omitted on the RHS of B.1.28 correspond to elements of $\check{C}^1(\mathcal{U}, D_L)$ of the form

$$\varphi_i = (0, r_i, r_i, r_i, 0, r_i, r_i, r_i, 0, 0, 0, -r_i, 0, -r_i, -r_i) \ , \tag{B.1.57}$$

where r_i is the Laurent monomial associated — upon multiplication by $x^a = \frac{x_2^2 x_5}{x_3}$ — to

$$\begin{array}{llll} r_1 = (-1, -3), & r_2 = (-1, -2), & r_3 = (2, -1), & r_4 = (-1, 0), \\ r_5 = (2, 0), & r_6 = (-1, 1), & r_7 = (1, 1). & \end{array} \tag{B.1.58}$$

From this we can verify that $\varphi_i = \delta_0(\mu_i)$ for $\mu_i \in \check{C}^0(\mathcal{U}, D_L)$ as follows:

φ_i	μ_i
φ_1	$(r_1, r_1, 0, 0, 0, r_1)$
φ_2	$(r_2, r_2, 0, 0, 0, r_2)$
φ_3	$(-r_3, -r_3, 0, 0, 0, -r_3)$
φ_4	$(0, 0, r_4, r_4, r_4, 0)$
φ_5	$(-r_5, -r_5, 0, 0, 0, -r_5)$
φ_6	$(0, 0, r_6, r_6, r_6, 0)$
φ_7	$(0, 0, r_7, r_7, r_7, 0)$

Hence, we conclude

$$\varphi\left(b_1\right) \cong c_3 \frac{x_1 x_2^3}{x_3 x_6}\,, \quad \varphi\left(b_2\right) \cong c_2 \frac{x_1 x_2^3}{x_3 x_6} + c_{12} \frac{x_5^3 x_6}{x_1 x_4}\,, \quad \varphi\left(b_3\right) \cong c_1 \frac{x_1 x_2^3}{x_3 x_6} + c_{11} \frac{x_5^3 x_6}{x_1 x_4}\,. \tag{B.1.59}$$

Application to GUT-example

For the example in 5.3 we consider $D_C = (10; -3, -3, -4)$ and $D_L = (5; -4, -4, 3)$. This curve $C_{\mathbf{5}_3}$ is cut-out by the following polynomial $a_{3,2}$:

$$\begin{aligned}
a_{3,2} = {} & c_{44} x_1^6 x_2^7 x_3^3 x_4^4 + c_{43} x_1^6 x_2^6 x_3^4 x_4^3 x_5 + c_{42} x_1^6 x_2^5 x_3^5 x_4^2 x_5^2 + c_{41} x_1^6 x_2^4 x_3^6 x_4 x_5^3 + c_{40} x_1^6 x_2^3 x_3^7 x_5^4 \\
& + c_{39} x_1^5 x_2^7 x_3^2 x_4^5 x_6 + c_{38} x_1^5 x_2^6 x_3^3 x_4^4 x_5 x_6 + c_{37} x_1^5 x_2^5 x_3^4 x_4^3 x_5^2 x_6 + c_{36} x_1^5 x_2^4 x_3^5 x_4^2 x_5^3 x_6 \\
& + c_{35} x_1^5 x_2^3 x_3^6 x_4 x_5^4 x_6 + c_{34} x_1^5 x_2^2 x_3^7 x_5^5 x_6 + c_{33} x_1^4 x_2^7 x_3 x_4^6 x_6^2 + c_{32} x_1^4 x_2^6 x_3^2 x_4^5 x_5 x_6^2 \\
& + c_{31} x_1^4 x_2^5 x_3^3 x_4^4 x_5^2 x_6^2 + c_{30} x_1^4 x_2^4 x_3^4 x_4^3 x_5^3 x_6^2 + c_{29} x_1^4 x_2^3 x_3^5 x_4^2 x_5^4 x_6^2 + c_{28} x_1^4 x_2^2 x_3^6 x_4 x_5^5 x_6^2 \\
& + c_{27} x_1^4 x_2 x_3^7 x_5^6 x_6^2 + c_{26} x_1^3 x_2^7 x_4^7 x_6^3 + c_{25} x_1^3 x_2^6 x_3 x_4^6 x_5 x_6^3 + c_{24} x_1^3 x_2^5 x_3^2 x_4^5 x_5^2 x_6^3 \\
& + c_{23} x_1^3 x_2^4 x_3^3 x_4^4 x_5^3 x_6^3 + c_{22} x_1^3 x_2^3 x_3^4 x_4^3 x_5^4 x_6^3 + c_{21} x_1^3 x_2^2 x_3^5 x_4^2 x_5^5 x_6^3 + c_{20} x_1^3 x_2 x_3^6 x_4 x_5^6 x_6^3 \\
& + c_{19} x_1^3 x_3^7 x_5^7 x_6^3 + c_{18} x_1^2 x_2^6 x_4^7 x_5 x_6^4 + c_{17} x_1^2 x_2^5 x_3 x_4^6 x_5^2 x_6^4 + c_{16} x_1^2 x_2^4 x_3^2 x_4^5 x_5^3 x_6^4 \\
& + c_{15} x_1^2 x_2^3 x_3^3 x_4^4 x_5^4 x_6^4 + c_{14} x_1^2 x_2^2 x_3^4 x_4^3 x_5^5 x_6^4 + c_{13} x_1^2 x_2 x_3^5 x_4^2 x_5^6 x_6^4 + c_{12} x_1^2 x_3^6 x_4 x_5^7 x_6^4 \\
& + c_{11} x_1 x_2^5 x_4^7 x_5^2 x_6^5 + c_{10} x_1 x_2^4 x_3 x_4^6 x_5^3 x_6^5 + c_9 x_1 x_2^3 x_3^2 x_4^5 x_5^4 x_6^5 + c_8 x_1 x_2^2 x_3^3 x_4^4 x_5^5 x_6^5 \\
& + c_7 x_1 x_2 x_3^4 x_4^3 x_5^6 x_6^5 + c_6 x_1 x_3^5 x_4^2 x_5^7 x_6^5 + c_5 x_2^4 x_4^7 x_5^3 x_6^6 + c_4 x_2^3 x_3 x_4^6 x_5^4 x_6^6 \\
& + c_3 x_2^2 x_3^2 x_4^5 x_5^5 x_6^6 + c_2 x_2 x_3^3 x_4^4 x_5^6 x_6^6 + c_1 x_3^4 x_4^3 x_5^7 x_6^6
\end{aligned} \tag{B.1.60}$$

Hence, the Koszul resolution of the line bundle $\mathcal{L} = \mathcal{O}_{dP_3}\left(D_L\right)|_{C_{\mathbf{5}_3}}$ is given by

$$0 \to \mathcal{O}_{dP_3}\left(D_L - D_C\right) \xrightarrow{\phi} \mathcal{O}_{dP_3}\left(D_L\right) \to \mathcal{L} \to 0\,, \tag{B.1.61}$$

and the map ϕ is induced from multiplication with $a_{3,2}$. The associated long exact sequence in sheaf cohomology is then:

$$\begin{aligned} 0 \longrightarrow 0 \longrightarrow H^0\left(dP_3, D_L\right) \cong \mathbb{C}^4 \longrightarrow H^0\left(D_C, \mathcal{L}\right) \\ \hookrightarrow H^1\left(dP_3, D_L - D_C\right) \cong \mathbb{C}^4 \xrightarrow{\varphi} H^1\left(dP_3, D_L\right) \cong \mathbb{C}^6 \longrightarrow H^1\left(C_{\mathbf{5}_3}, \mathcal{L}\right) \\ \hookrightarrow 0 \longrightarrow 0 \longrightarrow 0 \longrightarrow 0\,. \end{aligned} \tag{B.1.62}$$

By exactness of this sequence, we have $h^1(C_{\mathbf{5}_3}, \mathcal{L}) = 6 - \mathrm{rk}(M_\varphi)$, where the mapping matrix M_φ is determined by the coefficients of $a_{3,2}$:

$$M_\varphi = \begin{pmatrix} 0 & c_1 & 0 & 0 & c_2 & c_3 & c_4 & c_5 & 0 & 0 & 0 & 0 & 0 & 0 & 0 & 0 & 0 \\ c_5 & 0 & 0 & 0 & c_1 & c_2 & c_3 & c_4 & 0 & 0 & 0 & 0 & 0 & 0 & 0 & 0 & 0 \\ c_{11} & c_6 & 0 & 0 & c_7 & c_8 & c_9 & c_{10} & c_1 & c_2 & c_3 & c_4 & c_5 & 0 & 0 & 0 & 0 \\ 0 & 0 & c_{39} & c_{34} & 0 & 0 & 0 & 0 & c_{40} & c_{41} & c_{42} & c_{43} & c_{44} & c_{35} & c_{36} & c_{37} & c_{38} \\ 0 & 0 & c_{44} & 0 & 0 & 0 & 0 & 0 & 0 & 0 & 0 & 0 & 0 & c_{40} & c_{41} & c_{42} & c_{43} \\ 0 & 0 & 0 & c_{40} & 0 & 0 & 0 & 0 & 0 & 0 & 0 & 0 & 0 & c_{41} & c_{42} & c_{43} & c_{44} \end{pmatrix}. \tag{B.1.63}$$

Some linear algebra yields that the rank of this map drops by one, if

$$\begin{aligned} &c_1 = c_2 = c_3 = c_4 = c_5 = c_7 = c_8 = c_9 = c_{10} = c_{35} = c_{36} = c_{37} = c_{38} = 1 \\ &c_{40} = c_{41} = c_{42} = c_{43} = c_{44} = 1, \quad c_{11} = c_{34} = -1, \quad c_6 = c_{39} = 2\,. \end{aligned} \tag{B.1.64}$$

One can easily verify that the polynomial B.1.60 does not factorize for generic other coefficients not tuned above. Hence the curve $C_{\mathbf{5}_3}$ remains irreducible. By applying *sagemath* [169], one can further justify the smoothness of $C_{\mathbf{5}_3}$. Therefore, this tuning condition leads to one additional section without topology change for $C_{\mathbf{5}_3}$. This is an example of jump from Brill–Noether theory.

B.1.3 The fat point

Finally, in our analysis, non-reduced curves feature prominently. Consequently, a basic understanding of such curves is required. Let us therefore briefly discuss the mother of all non-reduced varieties, the *fat point*. This is an example in non-compact affine space $\mathbb{C}^2$ with coordinates x, y. Most of this intuition carries over to compact curves. More details can for example be found in [152, 214].

Let us consider $V(x) \subseteq \mathbb{C}^2$. This is the complex (non-compact) curve with coordinate y. The difference between $V(x)$ and $V(x^2)$ is not the collection of points, which these vanishing sets contain, but rather the allowed functions on these spaces. Namely, recall that in the modern language of algebraic geometry, a scheme (or equivalently in the analytic regime — a *geometric space*) is a pair of a topological space and a structure sheaf. The difference between $V(x)$ and $V(x^2)$ is this very structure sheaf.

In staying within the regime of algebraic geometry, the structure sheaf of $\mathbb{C}^2$ is given by (the sheafification of) the total coordinate ring $\mathbb{C}[x, y]$ — the ring of all polynomials in the variables x and y. Likewise, we can understand the structure sheaf on $V(x)$ from its coordinate ring:

$$R_{V(x)} = \mathbb{C}[x, y]/\langle x \rangle = \mathbb{C}[y]\,. \tag{B.1.65}$$

Hence, functions on the variety $V(x)$ correspond to polynomials in y. How about $V(x^2)$? On this space it holds

$$R_{V(x^2)} = \mathbb{C}[x, y]/\left\langle x^2 \right\rangle = \mathbb{C}[y] \oplus \langle x \rangle\ . \tag{B.1.66}$$

Consequently, on $V(x^2)$, the polynomial x provides a *non-trivial* function! This is the difference between $V(x)$ and $V(x^2)$.

We can extend this example slightly by looking at $V(y, x^2)$. For this space we find

$$R_{V(y,x^2)} = \mathbb{C}[x, y]/\left\langle y, x^2 \right\rangle = \langle x \rangle \ . \tag{B.1.67}$$

Hence, on this point in the affine plane $\mathbb{C}$, the set of non-trivial functions is 1-dimensional and is generated by the polynomial x. This lends $V(y, x^2)$ its name — as point set it is just a single point, yet this point is large enough to admit non-trivial functions — it is a *fat point*.

B.2 Collection of data

B.2.1 Curve splittings and jumps

Recall that the six toric $\mathbb{P}^1$s of dP_3 correspond to the exceptional divisors E_1, E_2, E_3 and the following three divisors:

$$E_4 = H - E_1 - E_2 \,, \qquad E_5 = H - E_1 - E_3 \,, \qquad E_6 = H - E_2 - E_3 \,. \tag{B.2.1}$$

$\mathbf{D_C} = (\mathbf{3}; \mathbf{-1}, \mathbf{-1}, \mathbf{-1})$

For this genus-1 curve we find:

bundle	h^0-values	E_1-splits	E_2-splits	E_3-splits	E_4-splits	E_5-splits	E_6-splits
(2, 1, -4, 1)	(4, 5, 6)	(4, 5, 6)	(4, 5, 6)	(4, 5, 6)	(4, 5, 6)	(4, 5, 6)	(4, 5, 6)
(1, -3, -3, -2)	(0, 1, 2, 3, 4, 5)	(2, 3, 4, 5)	(2, 3, 4, 5)	(1, 3, 4, 5)	(0, 1, 2, 3, 4, 5)	(0, 1, 2, 3, 4, 5)	(0, 1, 2, 3, 4, 5)
(1, -1, -3, 0)	(0, 1, 2, 3)	(0, 1, 2, 3)	(2)	(0, 1, 2, 3)	(1, 2, 3)	(0, 1, 2)	(0, 2, 3)
(1, -2, -3, -2)	(0, 1, 2, 3, 4)	(1, 2, 3, 4)	(2, 3, 4)	(1, 2, 3, 4)	(0, 1, 2, 3, 4)	(0, 1, 2, 3, 4)	(0, 1, 2, 3, 4)
(1, -1, -3, -1)	(0, 2, 3)	(0, 2, 3)	(2)	(0, 2, 3)	(0, 2, 3)	(0, 2)	(0, 2, 3)
(1, -3, -4, -2)	(0, 1, 2, 3, 4) (5, 6, 7)	(2, 3, 5, 6, 7)	(3, 4, 5, 6)	(1, 3, 4, 6)	(0, 1, 2, 3, 4) (5, 6)	(0, 1, 2, 3, 4) (5, 6)	(0, 1, 2, 3, 4) (5, 6, 7)
(2, 1, -4, 2)	(5, 6, 7)	(5, 6, 7)	(5, 6, 7)	(6, 7)	(5, 6, 7)	(5, 6, 7)	(5, 6, 7)
(2, 2, -4, 2)	(6, 7, 8, 9)	(7, 8, 9)	(6, 7, 8)	(7, 8, 9)	(6, 7, 8, 9)	(6, 7, 8)	(6, 7, 8, 9)
(1, -1, -4, -1)	(0, 3, 5)	(0, 3, 5)	(3)	(0, 3, 5)	(0, 3, 5)	(0, 3)	(0, 3, 5)
(1, 1, -3, 1)	(2, 3, 4)	(2, 3, 4)	(2, 3, 4)	(2, 3, 4)	(2, 3, 4)	(2, 3, 4)	(2, 3, 4)
(1, 1, -3, 0)	(1, 2, 3)	(1, 2, 3)	(2, 3)	(1, 2, 3)	(1, 2, 3)	(1, 2, 3)	(2, 3)
(1, -1, -2, 0)	(0, 1)	(0, 1)	(1)	(0, 1)	(1)	(0, 1)	(0, 1)
(1, 1, -3, 2)	(3, 4, 5)	(3, 4, 5)	(3, 4, 5)	(4, 5)	(3, 4, 5)	(3, 4, 5)	(3, 4, 5)

$\mathbf{D_C = (4; -1, -2, 1)}$

For this (generically disjoint) union of a genus-0 and a genus-2 curve, we find:

bundle	h^0-values	E_1-splits	E_2-splits	E_3-splits	E_4-splits	E_5-splits	E_6-splits
(2, -1, -2, 5)	(2, 5, 7, 8)	(2, 5, 7, 8)	(2, 5, 7, 8)	(2)	(2, 5, 7, 8)	(5, 7, 8)	(5, 7, 8)
(1, -1, -2, -1)	(2, 3)	(2, 3)	(2, 3)	(2)	(2, 3)	(3)	(3)
(1, -2, -2, -2)	(3, 4, 5, 6, 7)	(4, 6, 7)	(3, 4, 5, 6, 7)	(3, 4)	(3, 4, 5, 6, 7)	(5, 6, 7)	(5, 6, 7)
(2, -3, -2, -1)	(2, 3, 4, 5, 6)	(4, 5)	(2, 3, 4, 5, 6)	(2, 3, 4, 5)	(4, 5, 6)	(3, 5, 6)	(3, 4, 5, 6)
(1, -2, -1, 4)	(0, 1, 2, 3)	(1, 2, 3)	(0, 1, 2, 3)	(0, 1)	(1, 2, 3)	(1, 2, 3)	(1, 2, 3)
(1, -2, -2, -3)	(4, 5, 7, 8, 9) (10, 11)	(5, 8, 10, 11)	(4, 5, 7, 8, 9) (10, 11)	(4,5)	(4, 5, 7, 8, 9) (10, 11)	(7, 8, 9, 10, 11)	(7, 8, 9, 10, 11)
(2, -3, -2, -2)	(3, 4, 5, 6, 7) (8, 9)	(5, 6, 7, 8)	(3, 5, 6, 7, 8, 9)	(3, 4, 5, 6)	(5, 6, 7, 8, 9)	(5, 6, 7, 8, 9)	(5, 6, 7, 8, 9)
(1, -2, 1, -1)	(5, 6)	(5, 6)	(5, 6)	(5)	(5, 6)	(6)	(5, 6)
(2, -2, -1, -2)	(6, 7)	(6, 7)	(6, 7)	(6)	(6, 7)	(7)	(6, 7)
(2, -2, -2, 7)	(1, 2, 6, 7, 10) (11, 13, 14, 15)	(2, 6, 7, 10, 11) (11, 13, 14, 15)	(1, 2, 6, 7, 10) (13, 14, 15)	(1, 2)	(2, 7, 11, 14)	(6, 7, 10, 11, 13) (13, 14, 15)	(6, 7, 10, 11, 13) (14)
(3, -1, -2, 10)	(6, 14, 21, 27, 32)	(6, 14, 21, 27, 32)	(6, 14, 21, 27, 32)	(6)	(6, 14, 21, 27)	(14, 21, 27, 32)	(14, 21, 27)
(1, -3, 1, -1)	(4, 5, 6, 7)	(4, 5, 6, 7)	(4, 5, 6, 7)	(4, 5, 6)	(4, 5, 6, 7)	(6, 7)	(4, 5, 6, 7)

$\mathbf{D_C = (4; -1, -2, -1)}$

For this genus-2 curve we find:

bundle	h^0-values	E_1-splits	E_2-splits	E_3-splits	E_4-splits	E_5-splits	E_6-splits
(2, 3, -3, 1)	(5, 7, 8)	(7)	(5, 7, 8)	(5, 7, 8)	(5, 7, 8)	(5, 7, 8)	(5, 7, 8)
(3, 1, -4, -1)	(3, 4)	(3, 4)	(3, 4)	(3, 4)	(3, 4)	(3, 4)	(4)
(2, 2, -4, 0)	(1, 2, 3, 4)	(2, 3, 4)	(2, 3, 4)	(1, 2, 3, 4)	(1, 2, 3, 4)	(2, 3, 4)	(2, 3, 4)
(2, 1, -4, -3)	(0, 1, 2, 3, 4) (5, 6)	(0, 1, 2, 3, 4) (5)	(2, 3, 4, 5, 6)	(2, 3, 4, 5)	(0, 1, 2, 3, 4) (5, 6)	(0, 1, 2, 3, 4) (5, 6)	(1, 2, 3, 4)
(1, -1, -3, -2)	(0, 1, 2)	(0, 1, 2)	(1, 2)	(1, 2)	(0, 1, 2)	(0, 1, 2)	(0, 1, 2)
(1, -2, -4, 2)	(0, 1, 2, 3, 4)	(1, 2, 3, 4)	(2, 3, 4)	(0, 1, 2, 3, 4)	(0, 1, 2, 3)	(0, 1, 2, 3, 4)	(0, 1, 2, 3, 4)
(4, 3, -3, -8)	(4, 5, 6, 7, 8) (10, 12, 13, 15) (16, 17, 18, 19)	(6, 7, 8, 9, 10) (12, 13, 15, 16) (17, 18)	(4, 5, 6, 7, 8) (9, 10, 12, 13) (15, 17, 18, 19)	(7, 10, 12, 13, 15) (17)	(4, 5, 6, 7, 8) (9, 10, 12, 13, 15) (16, 17, 18, 19)	(4, 7, 9, 10, 12) (13, 15, 16, 18, 19)	(10, 12, 13, 15, 16)
(1, 3, -4, -5)	(0, 1, 2, 4, 6) (7, 8, 9, 11)	(0, 2, 4, 6, 7) (8, 9)	(2, 4, 6, 8, 9) (11)	(4, 6, 8)	(0, 1, 2, 4, 6) (7, 8, 9, 11)	(0, 2, 4, 6, 7) (9,11)	(0, 1, 2, 4, 6) (7)
(3, 1, -4, -5)	(0, 1, 2, 4, 5) (6, 7, 8, 9, 11)	(0, 1, 2, 4, 5) (6, 7, 8, 9)	(2, 4, 6, 8, 9) (11)	(4, 5, 6, 8)	(0, 1, 2, 4, 5) (6, 7, 8, 9, 11)	(0, 1, 2, 4, 5) (6, 7, 8, 9, 11)	(4, 5, 6, 7)
(3, 2, -3, -7)	(0, 1, 2, 3, 4) (6, 7, 9, 10, 11) (12, 14, 15, 16)	(1, 2, 3, 4, 6) (7, 9, 10, 11) (12, 14, 15)	(1, 3, 4, 6, 7) (7, 9, 10, 11) (12, 14, 15, 16)	(6, 7, 9, 10, 11) (12)	(1, 2, 3, 4, 6) (7, 9, 10, 11) (12, 14, 15)	(1, 3, 4, 6, 7) (9, 10, 11, 12) (14, 15, 16)	(6, 7, 9, 10, 11) (12)
(3, 2, -3, -5)	(2, 3, 4, 5, 6) (7, 8, 9, 10, 11)	(3, 4, 5, 7, 8) (10)	(2, 3, 4, 6, 7) (8, 9, 10, 11)	(4, 5, 6, 7, 8) (9,10)	(2, 3, 4, 5, 6) (7, 8, 9, 10, 11)	(2, 3, 4, 5, 6) (7, 8, 9, 10, 11)	(6, 7, 8)
(1, 1, -4, 2)	(0, 1, 2, 3, 4)	(0, 1, 2, 3, 4)	(2, 3, 4)	(0, 1, 2, 3, 4)	(0, 1, 2, 3, 4)	(2, 3, 4)	(0, 1, 2, 3, 4)
(1, 0, -4, -1)	(0, 2, 3)	(0, 2, 3)	(2)	(0, 2, 3)	(0, 2, 3)	(0, 2)	(0, 2, 3)
(3, -3, -1, -2)	(4, 5)	(4, 5)	(4, 5)	(4, 5)	(4, 5)	(4, 5)	(4, 5)
(4, -7, -1, -3)	(3, 4, 5, 6, 7) (8, 10, 11, 12) (13, 15, 17)	(3, 4, 5, 6, 7) (8, 10, 11, 12)	(3, 4, 5, 6, 7) (8, 10, 11, 13, 15)	(3, 4, 5, 6, 8) (10, 11, 12, 13) (15, 17)	(3, 4, 5, 6, 7) (8, 11, 13, 15)	(3, 4, 5, 6, 8) (10, 11, 13, 15)	(3, 4, 5, 6, 7) (10, 11, 12, 13, 15)

$\mathbf{D_C = (4; -1, -2, 0)}$

For this genus-2 curve we find:

bundle	h^0-values	E_1-splits	E_2-splits	E_3-splits	E_4-splits	E_5-splits	E_6-splits
(1, -2, -1, 4)	(0, 1, 2, 3, 4, 5, 6)	(1, 2, 3, 4, 5, 6)	(0, 1, 2, 3, 4, 5, 6)	(2, 3)	(1, 3, 5, 6)	(2, 3, 4, 5, 6)	(2, 3, 4, 5, 6)

$\mathbf{D_C = (4; -1, -1, -1)}$

On this genus-3 curve we find:

bundle	h^0-values	E_1-splits	E_2-splits	E_3-splits	E_4-splits	E_5-splits	E_6-splits
(1, -2, -3, -1)	(0, 1, 2, 3, 4)	(1, 3, 4)	(2, 3)	(0, 1, 2, 3, 4)	(0, 1, 2, 3, 4)	(0, 1, 2, 3, 4)	(0, 1, 2, 3, 4)
(1, -3, -4, -3)	(0, 2, 3, 4, 5) (6, 7, 8, 9, 10)	(2, 4, 5, 7, 8) (9, 10)	(3, 5, 6, 7, 8) (9)	(2, 4, 5, 7, 8) (9, 10)	(0, 2, 3, 4, 5) (6, 7, 8, 9, 10)	(0, 2, 3, 4, 5) (6, 7, 8, 9, 10)	(0, 2, 3, 4, 5) (6, 7, 8, 9, 10)
(1, 1, -3, 0)	(0, 1, 2, 3)	(0, 1, 2, 3)	(2)	(0, 1, 2, 3)	(1, 2, 3)	(0, 1, 2, 3)	(1, 2, 3)
(1, -3, -3, -3)	(0, 2, 3, 4, 5) (6, 7, 8)	(2, 4, 5, 6, 7) (8)	(2, 4, 5, 6, 7) (8)	(2, 4, 5, 6, 7) (8)	(0, 2, 3, 4, 5) (6, 7, 8)	(0, 2, 3, 4, 5) (6, 7, 8)	(0, 2, 3, 4, 5) (6, 7, 8)
(1, -3, -2, -3)	(0, 1, 2, 3, 4) (5, 6, 7)	(2, 3, 4, 5, 6)	(1, 3, 4, 5, 6) (7)	(2, 3, 4, 5, 6)	(0, 1, 2, 3, 4) (5, 6, 7)	(0, 1, 2, 3, 4) (5, 6)	(0, 1, 2, 3, 4) (5, 6, 7)
(1, 2, -2, -1)	(1, 2, 3)	(2, 3)	(1, 2, 3)	(1, 2, 3)	(1, 2, 3)	(1, 2, 3)	(2, 3)
(1, 1, -3, -3)	(0, 1, 2, 3, 4) (5, 6)	(0, 1, 2, 3, 4) (5, 6)	(2, 4, 5)	(2, 4, 5)	(0, 2, 3, 4, 5) (6)	(0, 2, 3, 4, 5) (6)	(1, 2, 3, 4, 5)
(2, 3, -4, -1)	(4, 5, 6, 7, 8, 9)	(6, 7, 8, 9)	(4, 5, 6, 7, 8, 9)	(4, 5, 6, 7, 8, 9)	(4, 5, 6, 7, 8, 9)	(4, 5, 6, 7, 8, 9)	(6, 7, 8, 9)
(1, 2, -4, 2)	(2, 3, 4, 5, 6) (7, 8)	(3, 4, 5, 6, 7) (8)	(3, 4, 5, 6, 7) (8)	(3, 4, 5, 6, 7) (8)	(2, 3, 4, 5, 6) (7, 8)	(3, 4, 5, 6, 7) (8)	(2, 3, 4, 5, 6) (7, 8)
(1, -2, -3, -2)	(0, 1, 2, 3, 4, 5)	(1, 2, 3, 4, 5)	(2, 3, 4)	(1, 2, 3, 4, 5)	(0, 1, 2, 3, 4, 5)	(0, 1, 2, 3, 4, 5)	(0, 1, 2, 3, 4, 5)
(1, 3, -3, 1)	(3, 4, 5, 6, 7)	(5, 6, 7)	(3, 4, 5, 6, 7)	(3, 4, 5, 6, 7)	(3, 4, 5, 6, 7)	(3, 4, 5, 6, 7)	(3, 4, 5, 6, 7)
(1, -1, -3, 0)	(0, 1, 2, 3)	(0, 1, 2, 3)	(2)	(0, 1, 2, 3)	(1, 2, 3)	(0, 1, 2, 3)	(0, 2, 3)

$$\mathbf{D_C} = (\mathbf{5}; -\mathbf{2}, -\mathbf{2}, -\mathbf{1})$$

On this genus-4 curve we find:

bundle	h^0-values	E_1-splits	E_2-splits	E_3-splits	E_4-splits	E_5-splits	E_6-splits
(2, -2, -4, -2)	(0, 1, 2, 3, 4)	(0, 1, 2, 3, 4)	(2, 3)	(1, 3, 4)	(0, 1, 2, 3, 4)	(0, 1, 2, 3, 4)	(0, 1, 2, 3, 4)
(1, -1, -3, 0)	(0, 1)	(0, 1)	(1)	(0, 1)	(0, 1)	(0, 1)	(0, 1)
(1, 2, -2, 0)	(2, 3)	(3)	(2, 3)	(2, 3)	(2, 3)	(2, 3)	(2, 3)
(1, 2, -2, 1)	(3, 4)	(4)	(3, 4)	(3, 4)	(3, 4)	(3, 4)	(3, 4)
(1, 1, -4, -1)	(0, 2, 3)	(0, 2, 3)	(2)	(0, 2, 3)	(0, 2, 3)	(0, 2, 3)	(0, 2, 3)
(1, -1, -4, -1)	(0, 2, 3)	(0, 2, 3)	(2)	(0, 2, 3)	(0, 2, 3)	(0, 2, 3)	(0, 2, 3)
(1, -2, -4, 2)	(0, 2, 3)	(0, 2, 3)	(2)	(0, 2, 3)	(0, 2, 3)	(0, 2, 3)	(0, 2, 3)
(1, 1, -4, 1)	(0, 1, 2, 3, 4)	(0, 1, 2, 3, 4)	(2, 3)	(0, 1, 2, 3, 4)	(0, 1, 2, 3, 4)	(1, 3, 4)	(0, 1, 2, 3, 4)
(1, -1, -2, 3)	(0, 1, 2, 3)	(0, 1, 2, 3)	(0, 1, 2, 3)	(1, 2)	(0, 1, 2, 3)	(1, 2, 3)	(0, 1, 2, 3)
(2, -1, -4, 1)	(0, 1, 2, 3)	(0, 1, 2, 3)	(2)	(0, 1, 2, 3)	(0, 1, 2, 3)	(0, 1, 2, 3)	(0, 1, 2, 3)
(1, 2, -3, 1)	(1, 2, 3, 4)	(2, 3, 4)	(1, 2, 3, 4)	(1, 2, 3, 4)	(1, 2, 3, 4)	(2, 3, 4)	(1, 2, 3, 4)
(1, 1, -4, 0)	(0, 2, 3)	(0, 2, 3)	(2)	(0, 2, 3)	(0, 2, 3)	(0, 2, 3)	(0, 2, 3)
(1, 2, -2, -2)	(0, 1, 2, 3, 4)	(1, 2, 3, 4)	(0, 1, 2, 3, 4)	(1, 2, 3, 4)	(0, 1, 2, 3, 4)	(0, 1, 2, 3, 4)	(2, 3)

$\mathbf{D_C} = (\mathbf{5}; -\mathbf{1}, -\mathbf{1}, -\mathbf{2})$

On this genus-5 curve we find:

bundle	h^0-values	E_1-splits	E_2-splits	E_3-splits	E_4-splits	E_5-splits	E_6-splits
(1, -2, -2, -3)	(0, 1, 2, 3)	(1, 2, 3)	(1, 2, 3)	(1, 2, 3)	(0, 1, 2, 3)	(0, 1, 2, 3)	(0, 1, 2, 3)
(1, 1, -4, 2)	(2, 3, 4, 5, 6) (7, 8)	(2, 3, 4, 5, 6) (7, 8)	(3, 4, 5, 6, 7)	(3, 4, 5, 6, 7) (8)	(3, 4, 5, 6, 7) (8)	(2, 3, 4, 5, 6) (7, 8)	(2, 3, 4, 5, 6) (7, 8)
(1, 1, -4, 1)	(0, 1, 2, 3, 4) (5, 6, 7)	(0, 1, 2, 3, 4) (5, 6, 7)	(3, 4)	(0, 1, 2, 3, 4) (5, 6, 7)	(1, 2, 3, 4, 5) (5, 6, 7)	(1, 2, 4, 6, 7)	(1, 2, 3, 4, 5) (6, 7)
(1, -1, -3, -2)	(0, 2, 3)	(0, 2, 3)	(2)	(0, 2, 3)	(0, 2, 3)	(0, 2, 3)	(0, 2, 3)
(1, 1, -3, -1)	(0, 1, 2, 3)	(0, 1, 2, 3)	(2)	(0, 1, 2, 3)	(0, 2, 3)	(0, 1, 2, 3)	(1, 2, 3)
(1, 1, -3, -2)	(0, 2, 3)	(0, 2, 3)	(2)	(0, 2, 3)	(0, 2, 3)	(0, 2, 3)	(0, 2, 3)
(1, 2, -2, -1)	(0, 1)	(0, 1)	(1)	(0, 1)	(0, 1)	(0, 1)	(1)
(1, 1, -4, 0)	(0, 1, 3, 5, 6)	(0, 1, 3, 5, 6)	(3)	(0, 1, 3, 5, 6)	(1, 3, 5, 6)	(0, 1, 3, 5, 6)	(1, 3, 5, 6)
(1, -2, -1, -3)	(0, 1, 2)	(1, 2)	(0, 1, 2)	(1, 2)	(0, 1, 2)	(0, 1, 2)	(0, 1, 2)
(1, 1, -3, 1)	(1, 2, 3, 4)	(1, 2, 3, 4)	(2, 3)	(1, 2, 3, 4)	(1, 2, 3, 4)	(1, 2, 3, 4)	(1, 2, 3, 4)
(1, -1, -2, -2)	(0, 1)	(0, 1)	(1)	(0, 1)	(0, 1)	(0, 1)	(0, 1)
(1, -2, -3, -3)	(0, 1, 2, 3, 4, 5)	(1, 2, 3, 4, 5)	(2, 3, 4)	(1, 2, 3, 4, 5)	(0, 1, 2, 3, 4, 5)	(0, 1, 2, 3, 4, 5)	(0, 1, 2, 3, 4, 5)
(1, 1, -4, -1)	(0, 1, 3, 5, 6)	(0, 1, 3, 5, 6)	(3)	(0, 1, 3, 5, 6)	(0, 3, 5, 6)	(0, 1, 3, 5, 6)	(1, 3, 5, 6)

$\mathbf{D_C} = (\mathbf{6}; -\mathbf{3}, -\mathbf{2}, -\mathbf{1})$

On this genus-6 curve we find:

bundle	h^0-values	E_1-splits	E_2-splits	E_3-splits	E_4-splits	E_5-splits	E_6-splits
(1, 1, -4, 1)	(0, 1, 2, 3, 4)	(0, 1, 2, 3, 4)	(2, 3)	(0, 1, 2, 3, 4)	(0, 1, 2, 3, 4)	(1, 3, 4)	(0, 1, 2, 3, 4)
(1, 0, -3, 1)	(0, 1)	(0, 1)	(1)	(0, 1)	(0, 1)	(0, 1)	(0, 1)

B.2.2 Local to global section counting applied to our database

In this section, we list results which quantify how good the counting procedure proposed in 5.5.2 works, when applied to our database. We have preformed two tests:

1. We consider those curves in our data, for which we can quickly identify the exact number of sections on all curve components. This can be done quickly for non-split curves and for curves with only smooth components. For the latter curves, we have

read-off the genus g and the line bundle degree d from our database. If $d < 0$, we know that there are no non-trivial sections on this curve component. However, if $d > 2g - 2$, then $h^0(C, \mathcal{L}) = d - g + 1$. Based on these exact local section counts, we have then tried to predict the number of global sections. The accuracy for this is listed in B.2.2.

2. Our second test is based on our *H0Approximator*-program [148], which is part of [168]. This program considers curve degeneration, which split-off combinations of the 6 toric $\mathbb{P}^1$s in dP_3. For each such curve splitting, the program assumes that the number of local sections on each curve component is generic. Since this generic value is a lower bound to the actual number of local sections, we can use these estimates to derive a lower bound on the number of global sections. By repeating this strategy for many curve splittings, we obtain an estimate for the allowed h^0-values over the parameter space of the curve in question. We list the so-obtained results for all pairs (D_C, D_L) in our database [147] in B.2.2.

Accuracy

Table 23: Accuracy of counting procedure for exact numbers of local sections

$\mathbf{D_C}$	$\mathbf{D_L}$	**Applicable data sets** [%]	**Accuracy** [%]
(3, -1, -1, -1)	(1, 1, -3, 0)	62.2	100
(3, -1, -1, -1)	(1, 1, -3, 1)	71.6	100
(3, -1, -1, -1)	(1, 1, -3, 2)	52.7	100
(3, -1, -1, -1)	(1, -1, -2, 0)	52.7	100
(3, -1, -1, -1)	(1, -1, -3, 0)	66.9	100
(3, -1, -1, -1)	(1, -1, -3, -1)	76.4	100
(3, -1, -1, -1)	(1, -1, -4, -1)	76.4	100
(3, -1, -1, -1)	(1, -2, -3, -2)	90.5	100
(3, -1, -1, -1)	(1, -3, -3, -2)	90.5	100
(3, -1, -1, -1)	(1, -3, -4, -2)	90.5	100
(3, -1, -1, -1)	(2, 1, -4, 1)	62.2	100
(3, -1, -1, -1)	(2, 1, -4, 2)	48.0	100

Continued on next page

Table 23 – *Continued from previous page*

$\mathbf{D_C}$	$\mathbf{D_L}$	**Applicable data sets [%]**	**Accuracy [%]**
(3, -1, -1, -1)	(2, 2, -4, 2)	37.0	100
(4, -1, -2, 1)	(1, -1, -2, 0)	38.7	100
(4, -1, -2, 1)	(1, -1, -2, -1)	38.7	100
(4, -1, -2, 1)	(1, -2, 1, -1)	26.9	100
(4, -1, -2, 1)	(1, -2, -1, 4)	12.6	65.1
(4, -1, -2, 1)	(1, -2, -2, -2)	43.4	100
(4, -1, -2, 1)	(1, -2, -2, -3)	43.4	100
(4, -1, -2, 1)	(1, -3, 1, -1)	9.2	100
(4, -1, -2, 1)	(2, -1, -2, 5)	4.3	100
(4, -1, -2, 1)	(2, -2, -1, -2)	28.3	100
(4, -1, -2, 1)	(2, -2, -2, 7)	4.4	100
(4, -1, -2, 1)	(2, -3, -2, -1)	12.6	100
(4, -1, -2, 1)	(2, -3, -2, -2)	12.6	100
(4, -1, -2, 1)	(3, -1, -2, 10)	23.9	100
(4, -1, -2, -1)	(1, 0, -4, -1)	80.4	100
(4, -1, -2, -1)	(1, 3, -4, -5)	83.4	99
(4, -1, -2, -1)	(1, -1, -3, -2)	88.3	100
(4, -1, -2, -1)	(1, -2, -4, 2)	84.2	100
(4, -1, -2, -1)	(3, 2, -3, -7)	71.8	100
(4, -1, -2, -1)	(2, 1, -4, -3)	76.4	100
(4, -1, -2, -1)	(2, 2, -4, 0)	50.6	100
(4, -1, -2, -1)	(2, 3, -3, 1)	44.8	100
(4, -1, -2, -1)	(3, 1, -4, -1)	45.4	100
(4, -1, -2, -1)	(3, 1, -4, -5)	69.4	100
(4, -1, -2, -1)	(3, 2, -3, -5)	54.3	100
(4, -1, -2, -1)	(1, 1, -4, 2)	76.3	98.6
(4, -1, -2, -1)	(4, 3, -3, -8)	60.6	100
(4, -1, -2, -1)	(3, -3, -1, -2)	66.5	98.7
(4, -1, -2, -1)	(4, -7, -1, -3)	74.1	92.6
(4, -1, -2, 0)	(1, -2, -1, 4)	58.7	92.5
(4, -1, -1, -1)	(1, 1, -3, 0)	52.2	95.8

Continued on next page

Table 23 – *Continued from previous page*

$\mathbf{D_C}$	$\mathbf{D_L}$	**Applicable data sets [%]**	**Accuracy [%]**
(4, -1, -1, -1)	(1, 1, -3, -1)	56.5	100
(4, -1, -1, -1)	(1, 1, -3, -3)	73.8	100
(4, -1, -1, -1)	(1, 2, -2, -1)	45.6	100
(4, -1, -1, -1)	(1, 2, -4, 2)	65.3	100
(4, -1, -1, -1)	(1, 3, -3, 1)	56.9	100
(4, -1, -1, -1)	(1, -1, -3, 0)	64.3	96.6
(4, -1, -1, -1)	(1, -2, -3, -1)	82.4	100
(4, -1, -1, -1)	(1, -2, -3, -2)	87.5	100
(4, -1, -1, -1)	(1, -3, -2, -3)	85.8	100
(4, -1, -1, -1)	(1, -3, -3, -3)	84.0	100
(4, -1, -1, -1)	(1, -3, -4, -3)	86.2	100
(4, -1, -1, -1)	(2, 3, -4, -1)	45.5	100
(5, -2, -2, -1)	(1, 1, -4, 0)	62.0	100
(5, -2, -2, -1)	(1, 1, -4, 1)	58.4	99.7
(5, -2, -2, -1)	(1, 1, -4, -1)	67.9	100
(5, -2, -2, -1)	(1, 2, -2, 0)	45.2	100
(5, -2, -2, -1)	(1, 2, -2, 1)	50.8	100
(5, -2, -2, -1)	(1, 2, -2, -2)	46.7	98.9
(5, -2, -2, -1)	(1, 2, -3, 1)	48.9	99.0
(5, -2, -2, -1)	(1, -1, -2, 3)	45.1	99.9
(5, -2, -2, -1)	(1, -1, -3, 0)	72.7	100
(5, -2, -2, -1)	(1, -1, -4, -1)	88.6	100
(5, -2, -2, -1)	(1, -2, -4, 2)	77.3	100
(5, -2, -2, -1)	(2, -1, -4, 1)	51.4	97.9
(5, -2, -2, -1)	(2, -2, -4, -2)	75.2	100
(5, -1, -1, -2)	(1, -2, -2, -3)	88.1	100
(5, -1, -1, -2)	(1, -2, -1, -3)	84.4	100
(5, -1, -1, -2)	(1, -1, -3, -2)	82.7	100
(5, -1, -1, -2)	(1, -1, -2, -2)	79.3	100
(5, -1, -1, -2)	(1, 2, -2, -1)	42.1	100
(5, -1, -1, -2)	(1, 1, -4, 2)	54.3	99.2
(5, -1, -1, -2)	(1, 1, -4, 1)	47.5	99.2

Continued on next page

Table 23 – *Continued from previous page*

$\mathbf{D_C}$	$\mathbf{D_L}$	**Applicable data sets [%]**	**Accuracy [%]**
(5, -1, -1, -2)	(1, 1, -4, 0)	56.8	95.0
(5, -1, -1, -2)	(1, 1, -3, -2)	65.9	100
(5, -1, -1, -2)	(1, 1, -3, -1)	55.5	98.6
(5, -1, -1, -2)	(1, 1, -3, 1)	46.1	99.4
(5, -1, -1, -2)	(1, -2, -3, -3)	88.1	100
(5, -1, -1, -2)	(1, 1, -4, -1)	64.4	98.8
(6, -3, -2, -1)	(1, 0, -3, 1)	51.8	100
(6, -3, -2, -1)	(1, 1, -4, 1)	52.4	99.7

Spectrum estimate

Table 24: Spectrum estimates from the *H0Approximator*

$\mathbf{D_C}$	$\mathbf{D_L}$	**Predicted spectrum**	**Missing values**
(5, -2, -2, -1)	(2, -2, -4, -2)	(0, 1, 2, 3, 4)	–
(5, -2, -2, -1)	(1, -1, -3, 0)	(0, 1)	–
(5, -2, -2, -1)	(1, 2, -2, 0)	(2, 3)	–
(5, -2, -2, -1)	(1, 2, -2, 1)	(3, 4)	–
(5, -2, -2, -1)	(1, 1, -4, -1)	(0, 2, 3)	–
(5, -2, -2, -1)	(1, -1, -4, -1)	(0, 2, 3)	–
(5, -2, -2, -1)	(1, -2, -4, 2)	(0, 2, 3)	–
(5, -2, -2, -1)	(1, 1, -4, 1)	(0, 1, 2, 3, 4)	–
(5, -2, -2, -1)	(1, -1, -2, 3)	(0, 1, 2, 3)	–
(5, -2, -2, -1)	(2, -1, -4, 1)	(0, 1, 2, 3)	–
(5, -2, -2, -1)	(1, 2, -3, 1)	(1, 2, 3, 4)	–
(5, -2, -2, -1)	(1, 1, -4, 0)	(0, 2, 3)	–
(5, -2, -2, -1)	(1, 2, -2, -2)	(0, 1, 2, 3, 4)	–
(3, -1, -1, -1)	(2, 1, -4, 1)	(4, 5, 6)	–
(3, -1, -1, -1)	(1, -3, -3, -2)	(0, 1, 2, 3, 4)	(5)
(3, -1, -1, -1)	(1, -1, -3, 0)	(0, 1, 2, 3)	–
(3, -1, -1, -1)	(1, -2, -3, -2)	(0, 1, 2, 3)	(4)

Continued on next page

Table 24 – *Continued from previous page*

$\mathbf{D_C}$	$\mathbf{D_L}$	**Predicted spectrum**	**Missing values**
(3, -1, -1, -1)	(1, -1, -3, -1)	(0, 2, 3)	–
(3, -1, -1, -1)	(1, -3, -4, -2)	(0, 1, 2, 3, 4, 5)	(6, 7)
(3, -1, -1, -1)	(2, 1, -4, 2)	(5, 6, 7)	–
(3, -1, -1, -1)	(2, 2, -4, 2)	(6, 7, 8, 9)	–
(3, -1, -1, -1)	(1, -1, -4, -1)	(0, 3, 5)	–
(3, -1, -1, -1)	(1, 1, -3, 1)	(2, 3, 4)	–
(3, -1, -1, -1)	(1, 1, -3, 0)	(1, 2, 3)	–
(3, -1, -1, -1)	(1, -1, -2, 0)	(0, 1)	–
(3, -1, -1, -1)	(1, 1, -3, 2)	(3, 4, 5)	–
(5, -1, -1, -2)	(1, -2, -2, -3)	(0, 1, 2, 3)	–
(5, -1, -1, -2)	(1, 1, -4, 2)	(2, 3, 4, 5, 6, 7, 8)	–
(5, -1, -1, -2)	(1, 1, -4, 1)	(0, 1, 2, 3, 4, 5, 6, 7)	–
(5, -1, -1, -2)	(1, -1, -3, -2)	(0, 2, 3)	–
(5, -1, -1, -2)	(1, 1, -3, -1)	(0, 2, 3)	(1)
(5, -1, -1, -2)	(1, 1, -3, -2)	(0, 2, 3)	–
(5, -1, -1, -2)	(1, 2, -2, -1)	(0, 1)	–
(5, -1, -1, -2)	(1, 1, -4, 0)	(0, 3, 5, 6)	(1)
(5, -1, -1, -2)	(1, -2, -1, -3)	(0, 1, 2)	–
(5, -1, -1, -2)	(1, 1, -3, 1)	(1, 2, 3, 4)	–
(5, -1, -1, -2)	(1, -1, -2, -2)	(0, 1)	–
(5, -1, -1, -2)	(1, -2, -3, -3)	(0, 1, 2, 3, 4, 5)	–
(5, -1, -1, -2)	(1, 1, -4, -1)	(0, 3, 5, 6)	(1)
(4, -1, -1, -1)	(1, -2, -3, -1)	(0, 1, 2, 3, 4)	–
(4, -1, -1, -1)	(1, -3, -4, -3)	(0, 2, 3, 4, 5, 6, 7, 8, 9)	(10)
(4, -1, -1, -1)	(1, 1, -3, 0)	(0, 1, 2, 3)	–
(4, -1, -1, -1)	(1, -3, -3, -3)	(0, 2, 3, 4, 5, 6, 7)	(8)
(4, -1, -1, -1)	(1, -3, -2, -3)	(0, 1, 2, 3, 4, 5, 6)	(7)
(4, -1, -1, -1)	(1, 2, -2, -1)	(1, 2, 3)	–
(4, -1, -1, -1)	(1, 1, -3, -3)	(0, 1, 2, 3, 4, 5, 6)	–
(4, -1, -1, -1)	(1, 1, -3, -3)	(0, 1, 2, 3, 4, 5, 6)	–
(4, -1, -1, -1)	(2, 3, -4, -1)	(4, 5, 6, 7, 8, 9)	–
(4, -1, -1, -1)	(1, 2, -4, 2)	(2, 3, 4, 5, 6, 7, 8)	–

Continued on next page

Table 24 – *Continued from previous page*

$\mathbf{D_C}$	$\mathbf{D_L}$	Predicted spectrum	Missing values
(4, -1, -1, -1)	(1, -2, -3, -2)	(0, 1, 2, 3, 4, 5)	–
(4, -1, -1, -1)	(1, 3, -3, 1)	(3, 4, 5, 6, 7)	–
(4, -1, -1, -1)	(1, -1, -3, 0)	(0, 2, 3)	(1)
(4, -1, -2, 0)	(1, -2, -1, 4)	(0, 1, 2, 3, 4, 5, 6)	–
(4, -1, -2, 1)	(2, -1, -2, 5)	(2, 5, 7, 8)	–
(4, -1, -2, 1)	(1, -1, -2, -1)	(2, 3)	–
(4, -1, -2, 1)	(1, -2, -2, -2)	(3, 4, 5, 6, 7)	–
(4, -1, -2, 1)	(2, -3, -2, -1)	(2, 3, 4, 5, 6)	–
(4, -1, -2, 1)	(1, -2, -1, 4)	(0, 1, 2, 3)	–
(4, -1, -2, 1)	(1, -2, -2, -3)	(4, 5, 7, 8, 9, 10, 11)	–
(4, -1, -2, 1)	(2, -3, -2, -2)	(3, 5, 6, 7, 8, 9)	(4)
(4, -1, -2, 1)	(1, -2, 1, -1)	(5, 6)	–
(4, -1, -2, 1)	(2, -2, -1, -2)	(6, 7)	–
(4, -1, -2, 1)	(2, -2, -2, 7)	(1, 2, 6, 7, 10, 11, 13, 14, 15)	–
(4, -1, -2, 1)	(3, -1, -2, 10)	(6, 14, 21, 27, 32)	–
(4, -1, -2, 1)	(1, -3, 1, -1)	(4, 5, 6, 7)	–
(6, -3, -2, -1)	(1, 1, -4, 1)	(0, 1, 2, 3, 4)	–
(6, -3, -2, -1)	(1, 0, -3, 1)	(0, 1)	–
(4, -1, -2, -1)	(3, -3, -1, -2)	(4, 5)	–
(4, -1, -2, -1)	(4, -7, -1, -3)	(3, 6, 8, 11, 12, 13, 15)	(4, 5, 7, 10, 17)
(4, -1, -2, -1)	(2, 3, -3, 1)	(5, 7, 8)	–
(4, -1, -2, -1)	(3, 1, -4, -1)	(3, 4)	–
(4, -1, -2, -1)	(2, 2, -4, 0)	(1, 2, 3, 4)	–
(4, -1, -2, -1)	(2, 1, -4, -3)	(0, 1, 2, 3, 4, 5, 6)	–
(4, -1, -2, -1)	(1, -1, -3, -2)	(0, 1, 2)	–
(4, -1, -2, -1)	(1, -2, -4, 2)	(0, 1, 2, 3, 4)	–
(4, -1, -2, -1)	(4, 3, -3, -8)	(4, 6, 7, 9, 10, 12, 13, 15, 16, 17, 18, 19)	(5, 8)
(4, -1, -2, -1)	(1, 3, -4, -5)	(0, 2, 4, 6, 7, 8, 9, 11)	(1)
(4, -1, -2, -1)	(3, 1, -4, -5)	(0, 2, 4, 5, 6, 7, 8, 9, 11)	(1)
(4, -1, -2, -1)	(3, 2, -3, -7)	(0, 1, 3, 4, 6, 7, 9, 10, 11, 12, 14, 15)	(2, 16)

Continued on next page

Table 24 – *Continued from previous page*

$\mathbf{D_C}$	$\mathbf{D_L}$	**Predicted spectrum**	**Missing values**
(4, -1, -2, -1)	(3, 2, -3, -5)	(2, 3, 4, 5, 6, 7, 8, 9, 10, 11)	–
(4, -1, -2, -1)	(1, 1, -4, 2)	(0, 1, 2, 3, 4)	–
(4, -1, -2, -1)	(1, 0, -4, -1)	(0, 2, 3)	–

C.1 Fiber structure of F-theory Standard Models

In this section, we investigate the fiber structure of the resolved 4-fold with the SM gauge symmetry as employed in the largest currently-known class of globally consistent F-theory Standard Models without chiral exotics and gauge coupling unification [32]. We work out the intersection numbers in the fibers over generic points of the gauge divisors, matter curves and Yukawa loci. The knowledge of the fiber structure determines the vector-like spectrum in this F-theory vacuum.

C.1.1 Away from Matter Curves

$SU(2)$ Gauge Divisor

This gauge divisor is $V(s_3)$. Here, the defining equation of $P_{F_{11}}$ factors as

$$p_{F_{11}} = e_1\left(e_1e_2^2e_3e_4^4s_1u^3 + e_2^2e_3^2e_4^2s_2u^2v + e_1e_2e_4^3s_5u^2w + e_2e_3e_4s_6uvw + s_9vw^2\right) . \tag{C.1.1}$$

The Cartan divisors are therefore as follows

$$\begin{aligned} D_0^{SU(2)} &= V\left(e_1e_2^2e_3e_4^4s_1u^3 + e_2^2e_3^2e_4^2s_2u^2v + e_1e_2e_4^3s_5u^2w + e_2e_3e_4s_6uvw + s_9vw^2, s_3\right) , \\ D_1^{SU(2)} &= V\left(e_1, s_3\right) . \end{aligned} \tag{C.1.2}$$

The intersection numbers in the fiber over a generic base point $p \in V(s_3)$ are:

$D_i^{SU(2)} \cdot D_j^{SU(2)} \cdot \hat{\pi}^{-1}(p)$	$D_0^{SU(2)}$	$D_1^{SU(2)}$	$U(1)_Y$
$D_0^{SU(2)}$	-2	2	0
$D_1^{SU(2)}$	2	-2	0

(C.1.3)

$SU(3)$ Gauge Divisor

This $SU(3)$ gauge divisor $V(s_9)$ relates to the Cartan divisors as follows:

$$\begin{aligned} D_0^{SU(3)} &= V\left(e_1^2 e_2 e_3 e_4^4 s_1 u^2 + e_1 e_2 e_3^2 e_4^2 s_2 uv + e_2 e_3^3 s_3 v^2 + e_1^2 e_4^3 s_5 uw + e_1 e_3 e_4 s_6 vw, s_9\right), \\ D_1^{SU(3)} &= V\left(e_2, s_9\right), \qquad D_2^{SU(3)} = V\left(u, s_9\right). \end{aligned} \tag{C.1.4}$$

The intersection numbers in the fiber over a generic base point $p \in V(s_9)$ are:

$D_i^{SU(3)} \cdot D_j^{SU(3)} \cdot \hat{\pi}^{-1}(p)$	$D_0^{SU(3)}$	$D_1^{SU(3)}$	$D_3^{SU(3)}$	$U(1)_Y$
$D_0^{SU(3)}$	-2	1	1	0
$D_1^{SU(3)}$	1	-2	1	0
$D_2^{SU(3)}$	1	1	-2	0

(C.1.5)

C.1.2 Over Matter Curves

Intersection Structure over $\mathbf{C}_{(\mathbf{3},\mathbf{2})_{1/6}}$ away from Yukawa Loci

Over the matter curves, singularity enhancements occur. They are geometrically related to the presence of new $\mathbb{P}^1$-fibrations, of which linear combinations eventually serve as matter surfaces. Over $C_{(\mathbf{3},\mathbf{2})_{1/6}} = V(s_3, s_9)$ the following $\mathbb{P}^1$-fibrations are present:

$$\begin{aligned} \mathbb{P}_0^1\left((\mathbf{3},\mathbf{2})_{1/6}\right) &= V(s_3, s_9, e_1 e_2 e_3 e_4^3 s_1 u^2 + e_2 e_3^2 e_4 s_2 uv + e_1 e_4^2 s_5 uw + e_3 s_6 vw), \\ \mathbb{P}_1^1\left((\mathbf{3},\mathbf{2})_{1/6}\right) &= V(s_3, s_9, e_1), \qquad \mathbb{P}_2^1\left((\mathbf{3},\mathbf{2})_{1/6}\right) = V(s_3, s_9, e_4), \\ \mathbb{P}_3^1\left((\mathbf{3},\mathbf{2})_{1/6}\right) &= V(s_3, s_9, u), \qquad \mathbb{P}_4^1\left((\mathbf{3},\mathbf{2})_{1/6}\right) = V(s_3, s_9, e_2). \end{aligned} \tag{C.1.6}$$

These $\mathbb{P}^1$-fibrations relate to restrictions of the $SU(3)$ and $SU(2)$ Cartan divisors:

Original	Split components over $C_{\mathbf{R}}$
$D_0^{SU(2)}$	$\mathbb{P}^1_0\left((\mathbf{3},\mathbf{2})_{1/6}\right)+\mathbb{P}^1_2\left((\mathbf{3},\mathbf{2})_{1/6}\right)+\mathbb{P}^1_3\left((\mathbf{3},\mathbf{2})_{1/6}\right)+\mathbb{P}^1_4\left((\mathbf{3},\mathbf{2})_{1/6}\right)$
$D_1^{SU(2)}$	$\mathbb{P}^1_1\left((\mathbf{3},\mathbf{2})_{1/6}\right)$
$D_0^{SU(3)}$	$\mathbb{P}^1_0\left((\mathbf{3},\mathbf{2})_{1/6}\right)+\mathbb{P}^1_1\left((\mathbf{3},\mathbf{2})_{1/6}\right)+\mathbb{P}^1_2\left((\mathbf{3},\mathbf{2})_{1/6}\right)$
$D_1^{SU(3)}$	$\mathbb{P}^1_4\left((\mathbf{3},\mathbf{2})_{1/6}\right)$
$D_2^{SU(3)}$	$\mathbb{P}^1_3\left((\mathbf{3},\mathbf{2})_{1/6}\right)$

(C.1.7)

Over $p\in C_{(\mathbf{3},\mathbf{2})_{1/6}}$ which is not a Yukawa point, these $\mathbb{P}^1$-fibrations intersect as follows:

	$\mathbb{P}^1_0\left((\mathbf{3},\mathbf{2})_{1/6}\right)$	$\mathbb{P}^1_1\left((\mathbf{3},\mathbf{2})_{1/6}\right)$	$\mathbb{P}^1_2\left((\mathbf{3},\mathbf{2})_{1/6}\right)$	$\mathbb{P}^1_3\left((\mathbf{3},\mathbf{2})_{1/6}\right)$	$\mathbb{P}^1_4\left((\mathbf{3},\mathbf{2})_{1/6}\right)$
$\mathbb{P}^1_0\left((\mathbf{3},\mathbf{2})_{1/6}\right)$	-2	1	0	0	1
$\mathbb{P}^1_1\left((\mathbf{3},\mathbf{2})_{1/6}\right)$	1	-2	1	0	0
$\mathbb{P}^1_2\left((\mathbf{3},\mathbf{2})_{1/6}\right)$	0	1	-2	1	0
$\mathbb{P}^1_3\left((\mathbf{3},\mathbf{2})_{1/6}\right)$	0	0	1	-2	1
$\mathbb{P}^1_4\left((\mathbf{3},\mathbf{2})_{1/6}\right)$	1	0	0	1	-2

(C.1.8)

The intersection numbers between the pullbacks of the Cartan divisors and the $\mathbb{P}^1$-fibrations over $C_{(\mathbf{3},\mathbf{2})_{1/6}}$ and are readily computed as follows:

	$D_0^{SU(2)}$	$D_1^{SU(2)}$	$D_0^{SU(3)}$	$D_1^{SU(3)}$	$D_2^{SU(3)}$	$U(1)_Y$
$\mathbb{P}^1_0\left((\mathbf{3},\mathbf{2})_{1/6}\right)$	-1	1	-1	1	0	-1/6
$\mathbb{P}^1_1\left((\mathbf{3},\mathbf{2})_{1/6}\right)$	2	-2	0	0	0	0
$\mathbb{P}^1_2\left((\mathbf{3},\mathbf{2})_{1/6}\right)$	0	1	0	0	1	1/6
$\mathbb{P}^1_3\left((\mathbf{3},\mathbf{2})_{1/6}\right)$	0	0	1	1	-2	0
$\mathbb{P}^1_4\left((\mathbf{3},\mathbf{2})_{1/6}\right)$	0	0	1	-2	1	0

(C.1.9)

The matter surfaces $S^{(a)}_{(\mathbf{3},\mathbf{2})_{1/6}}$ over $C_{(\mathbf{3},\mathbf{2})_{1/6}}$ are linear combinations of the above $\mathbb{P}^1$-fibrations. We use $\mathbf{P}$ to denote such a linear combination compactly. Explicitly, $\mathbf{P}$ is a list of the

multiplicities with which these $\mathbb{P}^1$-fibrations appear in the above order:

$$\mathbf{P} = (0,1,0,4,0) \quad \leftrightarrow \quad 1 \cdot \mathbb{P}^1_1\left((\mathbf{3},\mathbf{2})_{1/6}\right) + 4 \cdot \mathbb{P}^1_3\left((\mathbf{3},\mathbf{2})_{1/6}\right) .$$

We apply β to indicate the Cartan charges of such a linear combination, these notations will also be adopted for the other matter curves. All that said, the matter surfaces over $C_{(\mathbf{3},\mathbf{2})_{1/6}}$ take the following form:

Label	$\vec{P}$	β	Label	$\vec{P}$	β
$S^{(1)}_{(\mathbf{3},\mathbf{2})_{1/6}}$	$(0,0,1,0,0)$	$(1)\otimes(0,1)$	$S^{(4)}_{(\mathbf{3},\mathbf{2})_{1/6}}$	$(0,1,1,1,0)$	$(-1)\otimes(1,-1)$
$S^{(2)}_{(\mathbf{3},\mathbf{2})_{1/6}}$	$(0,1,1,0,0)$	$(-1)\otimes(0,1)$	$S^{(5)}_{(\mathbf{3},\mathbf{2})_{1/6}}$	$(0,0,1,1,1)$	$(1)\otimes(-1,0)$
$S^{(3)}_{(\mathbf{3},\mathbf{2})_{1/6}}$	$(0,0,1,1,0)$	$(1)\otimes(1,-1)$	$S^{(6)}_{(\mathbf{3},\mathbf{2})_{1/6}}$	$(0,1,1,1,1)$	$(-1)\otimes(-1,0)$

(C.1.10)

Intersection Structure over $\mathbf{C}_{(\mathbf{1},\mathbf{2})_{-\mathbf{1/2}}}$ away from Yukawa Loci

For convenience, we employ p_i^H to denote the following polynomials:

$$\begin{aligned}
p_1^H &= s_1 e_2 e_3 e_4 u + s_5 w\,, \qquad p_2^H = s_1^2 e_1 e_2 e_4^3 u^2 + s_1 s_2 e_2 e_3 e_4 uv - s_2 s_5 vw + s_1 s_6 vw\,,\\
p_3^H &= s_2 e_2^2 e_3^2 e_4^2 u^2 + s_6 e_2 e_3 e_4 uw + s_9 w^2\,, \qquad p_4^H = s_2 s_5 e_2 e_3 e_4 u + s_5 s_6 w - s_1 s_9 w\,,\\
p_5^H &= s_2 s_5^2 + s_1^2 s_9 - s_1 s_5 s_6\,, \qquad p_6^H = s_1 s_5 e_1 e_2 e_4^3 u^2 + s_2 s_5 e_2 e_3 e_4 uv + s_1 s_9 vw\,,\\
p_7^H &= s_5^2 e_1 e_2 e_4^3 u^2 + s_5 s_6 e_2 e_3 e_4 uv - s_1 s_9 e_2 e_3 e_4 uv + s_5 s_9 vw\,.
\end{aligned}$$

(C.1.11)

Over $C_{(\mathbf{1},\mathbf{2})_{-1/2}}$ which is not a Yukawa point, the following $\mathbb{P}^1$-fibrations are present:

$$\begin{aligned}
&\mathbb{P}^1_0\left((\mathbf{1},\mathbf{2})_{-1/2}\right) = V(s_3, p_1^H, p_3^H, p_4^H, p_5^H)\,,\\
&\mathbb{P}^1_1\left((\mathbf{1},\mathbf{2})_{-1/2}\right) = V(s_3, p_2^H, p_5^H, p_6^H, p_7^H, p_1^H \cdot e_1 e_2 e_4^3 u^2 + p_3^H \cdot v)\,,\\
&\mathbb{P}^1_2\left((\mathbf{1},\mathbf{2})_{-1/2}\right) = V(s_3, p_5^H, e_1)\,.
\end{aligned}$$

(C.1.12)

Equivalently, $\mathbb{P}^1_0 = V(s_3, p_1^H, p_3^H)$ arises from the analysis of a primary decomposition. The above $\mathbb{P}^1$-fibrations relate to restrictions of the $SU(2)$ Cartan divisors as follows:

Original	Split components over $C_{\mathbf{R}}$	Original	Split components over $C_{\mathbf{R}}$
$D_0^{SU(2)}$	$\mathbb{P}^1_0\left((\mathbf{1},\mathbf{2})_{-1/2}\right) + \mathbb{P}^1_1\left((\mathbf{1},\mathbf{2})_{-1/2}\right)$	$D_1^{SU(2)}$	$\mathbb{P}^1_2\left((\mathbf{1},\mathbf{2})_{-1/2}\right)$

(C.1.13)

Over $p \in C_{(\mathbf{1},\mathbf{2})_{-1/2}}$ which is not a Yukawa point, these $\mathbb{P}^1$-fibrations correspond to the representation state at the right column and intersect each other as follows:

	$\mathbb{P}^1_0\left((\mathbf{1},\mathbf{2})_{-1/2}\right)$	$\mathbb{P}^1_1\left((\mathbf{1},\mathbf{2})_{-1/2}\right)$	$\mathbb{P}^1_2\left((\mathbf{1},\mathbf{2})_{-1/2}\right)$
$\mathbb{P}^1_0\left((\mathbf{1},\mathbf{2})_{-1/2}\right)$	-2	1	1
$\mathbb{P}^1_1\left((\mathbf{1},\mathbf{2})_{-1/2}\right)$	1	-2	1
$\mathbb{P}^1_2\left((\mathbf{1},\mathbf{2})_{-1/2}\right)$	1	1	-2

(C.1.14)

The matter surfaces are

Label	$\vec{P}$	β	Label	$\vec{P}$	β
$S^{(1)}_{(\mathbf{1},\mathbf{2})_{-1/2}}$	$(1,0,0)$	(1)	$S^{(2)}_{(\mathbf{1},\mathbf{2})_{-1/2}}$	$(1,0,1)$	(-1)

(C.1.15)

Intersection Structure over $\mathbf{C}_{(\overline{\mathbf{3}},\mathbf{1})_{-\mathbf{2/3}}}$ away from Yukawa Loci

Over $C_{(\overline{\mathbf{3}},\mathbf{1})_{-2/3}} = V(s_5, s_9)$ the following $\mathbb{P}^1$-fibrations are present:

$$\begin{aligned}
&\mathbb{P}^1_0\left((\overline{\mathbf{3}},\mathbf{1})_{-2/3}\right) = V(s_5, s_9, e_1^2 e_2 e_4^4 s_1 u^2 + e_1 e_2 e_3 e_4^2 s_2 uv + e_2 e_3^2 s_3 v^2 + e_1 e_4 s_6 vw)\,,\\
&\mathbb{P}^1_1\left((\overline{\mathbf{3}},\mathbf{1})_{-2/3}\right) = V(s_5, s_9, u)\,, \qquad \mathbb{P}^1_2\left((\overline{\mathbf{3}},\mathbf{1})_{-2/3}\right) = V(s_5, s_9, e_2)\,,\\
&\mathbb{P}^1_3\left((\overline{\mathbf{3}},\mathbf{1})_{-2/3}\right) = V(s_5, s_9, e_3)\,.
\end{aligned} \tag{C.1.16}$$

These $\mathbb{P}^1$-fibrations relate to restrictions of the $SU(3)$ Cartan divisors as follows:

Original	Split components over $C_{\mathbf{R}}$	Original	Split components over $C_{\mathbf{R}}$
$D_0^{SU(3)}$	$\mathbb{P}^1_0\left((\overline{\mathbf{3}},\mathbf{1})_{-2/3}\right)+\mathbb{P}^1_3\left((\overline{\mathbf{3}},\mathbf{1})_{-2/3}\right)$	$D_1^{SU(3)}$	$\mathbb{P}^1_2\left((\overline{\mathbf{3}},\mathbf{1})_{-2/3}\right)$
$D_2^{SU(3)}$	$\mathbb{P}^1_1\left((\overline{\mathbf{3}},\mathbf{1})_{-2/3}\right)$		

(C.1.17)

Over $p \in C_{(\overline{\mathbf{3}},\mathbf{1})_{-2/3}}$ which is not a Yukawa point, these $\mathbb{P}^1$-fibrations intersect as follows:

	$\mathbb{P}^1_0\left((\overline{\mathbf{3}},\mathbf{1})_{-2/3}\right)$	$\mathbb{P}^1_1\left((\overline{\mathbf{3}},\mathbf{1})_{-2/3}\right)$	$\mathbb{P}^1_2\left((\overline{\mathbf{3}},\mathbf{1})_{-2/3}\right)$	$\mathbb{P}^1_3\left((\overline{\mathbf{3}},\mathbf{1})_{-2/3}\right)$
$\mathbb{P}^1_0\left((\overline{\mathbf{3}},\mathbf{1})_{-2/3}\right)$	-2	1	0	1
$\mathbb{P}^1_1\left((\overline{\mathbf{3}},\mathbf{1})_{-2/3}\right)$	1	-2	1	0
$\mathbb{P}^1_2\left((\overline{\mathbf{3}},\mathbf{1})_{-2/3}\right)$	0	1	-2	1
$\mathbb{P}^1_3\left((\overline{\mathbf{3}},\mathbf{1})_{-2/3}\right)$	1	0	1	-2

(C.1.18)

The matter surfaces $S^{(a)}_{(\overline{\mathbf{3}},\mathbf{1})_{-2/3}}$ take the following form:

Label	$\vec{P}$	β	Label	$\vec{P}$	β	Label	$\vec{P}$	β
$S^{(1)}_{(\overline{\mathbf{3}},\mathbf{1})_{-2/3}}$	$(0,0,0,1)$	$(1,0)$	$S^{(2)}_{(\overline{\mathbf{3}},\mathbf{1})_{-2/3}}$	$(0,0,1,1)$	$(-1,1)$	$S^{(3)}_{(\overline{\mathbf{3}},\mathbf{1})_{-2/3}}$	$(0,1,1,1)$	$(0,-1)$

(C.1.19)

Intersection Structure over $\mathbf{C}_{(\overline{\mathbf{3}},\mathbf{1})_{1/3}}$ away from Yukawa Loci

Over $C_{(\overline{\mathbf{3}},\mathbf{1})_{1/3}}$ which is not a Yukawa point, the following $\mathbb{P}^1$-fibrations are present:

$$\begin{aligned}
\mathbb{P}^1_0\left((\overline{\mathbf{3}},\mathbf{1})_{1/3}\right) &= V(s_9, s_3s_5^2 - s_2s_5s_6 + s_1s_6^2, s_5e_1e_4^2u + s_6e_3v,\\
&\qquad s_1s_6e_1e_4^2u - s_3s_5e_3v + s_2s_6e_3v, s_1e_1^2e_4^4u^2 + s_2e_1e_3e_4^2uv + s_3e_3^2v^2)\,,\\
\mathbb{P}^1_1\left((\overline{\mathbf{3}},\mathbf{1})_{1/3}\right) &= V(s_9, s_3s_5^2 - s_2s_5s_6 + s_1s_6^2, s_1s_6e_1e_2e_3e_4^2u + s_3s_5e_2e_3^2v + s_5s_6e_1e_4w,\\
&\qquad s_1e_1^2e_2e_3e_4^4u^2 + s_2e_1e_2e_3^2e_4^2uv + s_5e_1^2e_4^3uw + s_3e_2e_3^3v^2 + s_6e_1e_3e_4vw,\\
&\qquad s_3s_5e_1e_2e_3e_4^2u - s_2s_6e_1e_2e_3e_4^2u - s_3s_6e_2e_3^2v - s_6^2e_1e_4w,\\
&\qquad s_1s_5e_1e_2e_3e_4^2u + s_2s_5e_2e_3^2v - s_1s_6e_2e_3^2v + s_5^2e_1e_4w)\,,\\
\mathbb{P}^1_2\left((\overline{\mathbf{3}},\mathbf{1})_{1/3}\right) &= V(s_9, s_3s_5^2 + s_1s_6^2 - s_2s_5s_6, u)\,,\\
\mathbb{P}^1_3\left((\overline{\mathbf{3}},\mathbf{1})_{1/3}\right) &= V(s_9, s_3s_5^2 + s_1s_6^2 - s_2s_5s_6, e_2)\,.
\end{aligned} \tag{C.1.20}$$

Due to primary decomposition analysis, $\mathbb{P}^1_0\left((\overline{\mathbf{3}},\mathbf{1})_{1/3}\right)$ can be rewritten as

$$\mathbb{P}^1_0\left((\overline{\mathbf{3}},\mathbf{1})_{1/3}\right) = V(s_9, us_5e_1e_4^2 + vs_6e_3, s_1s_6e_1e_4^2u - s_3s_5e_3v + s_2s_6e_3v) - V(s_9, s_5, s_6)\,. \tag{C.1.21}$$

The above $\mathbb{P}^1$-fibrations relate to restrictions of the $SU(3)$ Cartan divisors as follows:

Original	Split components over $C_{(\overline{\mathbf{3}},\mathbf{1})_{1/3}}$	Original	Split components over $C_{(\overline{\mathbf{3}},\mathbf{1})_{1/3}}$
$D_0^{SU(3)}$	$\mathbb{P}^1_0\left((\overline{\mathbf{3}},\mathbf{1})_{1/3}\right) + \mathbb{P}^1_1\left((\overline{\mathbf{3}},\mathbf{1})_{1/3}\right)$	$D_1^{SU(3)}$	$\mathbb{P}^1_3\left((\overline{\mathbf{3}},\mathbf{1})_{1/3}\right)$
$D_2^{SU(3)}$	$\mathbb{P}^1_2\left((\overline{\mathbf{3}},\mathbf{1})_{1/3}\right)$		

(C.1.22)

Over $p \in C_{(\overline{\mathbf{3}},\mathbf{1})_{1/3}}$ which is not a Yukawa point, these $\mathbb{P}^1$-fibrations intersect as follows:

	$\mathbb{P}^1_0\left((\overline{\mathbf{3}},\mathbf{1})_{1/3}\right)$	$\mathbb{P}^1_1\left((\overline{\mathbf{3}},\mathbf{1})_{1/3}\right)$	$\mathbb{P}^1_2\left((\overline{\mathbf{3}},\mathbf{1})_{1/3}\right)$	$\mathbb{P}^1_3\left((\overline{\mathbf{3}},\mathbf{1})_{1/3}\right)$
$\mathbb{P}^1_0\left((\overline{\mathbf{3}},\mathbf{1})_{1/3}\right)$	-2	1	0	1
$\mathbb{P}^1_1\left((\overline{\mathbf{3}},\mathbf{1})_{1/3}\right)$	1	-2	1	0
$\mathbb{P}^1_2\left((\overline{\mathbf{3}},\mathbf{1})_{1/3}\right)$	0	1	-2	1
$\mathbb{P}^1_3\left((\overline{\mathbf{3}},\mathbf{1})_{1/3}\right)$	1	0	1	-2

(C.1.23)

The matter surfaces $S^{(a)}_{(\overline{\mathbf{3}},\mathbf{1})_{1/3}}$ take the following form:

Label	$\vec{P}$	β	Label	$\vec{P}$	β	Label	$\vec{P}$	β
$S^{(1)}_{(\overline{\mathbf{3}},\mathbf{1})_{1/3}}$	$(1,0,0,0)$	$(1,0)$	$S^{(2)}_{(\overline{\mathbf{3}},\mathbf{1})_{1/3}}$	$(1,0,0,1)$	$(-1,1)$	$S^{(3)}_{(\overline{\mathbf{3}},\mathbf{1})_{1/3}}$	$(1,0,1,1)$	$(0,-1)$

(C.1.24)

Intersection Structure over $\mathbf{C}_{(\overline{\mathbf{1}},\mathbf{1})_\mathbf{1}}$ away from Yukawa Loci

Over the singlet curve $C_{(\mathbf{1},\mathbf{1})_1} = V(s_1, s_5)$ the following two $\mathbb{P}^1$-fibrations are present:

$$\begin{aligned}\mathbb{P}^1_0((\mathbf{1},\mathbf{1})_1) &= V\left(s_1, s_5, e_1e_2^2e_3^2e_4^2s_2u^2 + e_2^2e_3^3s_3uv + e_1e_2e_3e_4s_6uw + e_1s_9w^2\right), \\ \mathbb{P}^1_1((\mathbf{1},\mathbf{1})_1) &= V(s_1, s_5, v)\ .\end{aligned} \tag{C.1.25}$$

These fibrations intersect as follows:

	$\mathbb{P}^1_0((\mathbf{1},\mathbf{1})_1)$	$\mathbb{P}^1_1((\mathbf{1},\mathbf{1})_1)$	$U(1)_Y$
$\mathbb{P}^1_0((\mathbf{1},\mathbf{1})_1)$	-2	2	-1
$\mathbb{P}^1_1((\mathbf{1},\mathbf{1})_1)$	2	-2	1

(C.1.26)

We use $\mathbb{P}^1_1((\mathbf{1},\mathbf{1})_1)$ as matter surface for the singlet state with $q_{U(1)_Y} = 1$.

C.1.3 Over Yukawa Loci

Intersection Structure over Yukawa Locus $\mathbf{Y_1}$

Over the Yukawa point $Y_1 = V(s_3, s_5, s_9)$ the following $\mathbb{P}^1$-fibrations are present:

$$\begin{aligned}
&\mathbb{P}^1_0(Y_1) = V(s_3, s_5, s_9, e_1)\ , \quad \mathbb{P}^1_1(Y_1) = V(s_3, s_5, s_9, e_2)\ , \quad \mathbb{P}^1_2(Y_1) = V(s_3, s_5, s_9, e_3)\ , \\
&\mathbb{P}^1_3(Y_1) = V(s_3, s_5, s_9, e_4)\ , \quad \mathbb{P}^1_4(Y_1) = V(s_3, s_5, s_9, u)\ , \\
&\mathbb{P}^1_5(Y_1) = V\left(s_3, s_5, s_9, e_1e_2e_4^3s_1u^2 + e_2e_3e_4s_2uv + s_6vw\right)\ .
\end{aligned} \tag{C.1.27}$$

The intersection numbers in the fiber over Y_1 are as follows:

	$\mathbb{P}^1_0(Y_1)$	$\mathbb{P}^1_1(Y_1)$	$\mathbb{P}^1_2(Y_1)$	$\mathbb{P}^1_3(Y_1)$	$\mathbb{P}^1_4(Y_1)$	$\mathbb{P}^1_5(Y_1)$
$\mathbb{P}^1_0(Y_1)$	-2	0	0	1	0	1
$\mathbb{P}^1_1(Y_1)$	0	-2	1	0	1	0
$\mathbb{P}^1_2(Y_1)$	0	1	-2	0	0	1
$\mathbb{P}^1_3(Y_1)$	1	0	0	-2	1	0
$\mathbb{P}^1_4(Y_1)$	0	1	0	1	-2	0
$\mathbb{P}^1_5(Y_1)$	1	0	1	0	0	-2

(C.1.28)

Restrictions of the fibrations over the matter curves relate to the $\mathbb{P}^1_i(Y_1)$ as follows:

Split $\mathbb{P}^1$ over $C_{\mathbf{R}}$	Split $\mathbb{P}^1$ over Y_1	Split $\mathbb{P}^1$ over $C_{\mathbf{R}}$	Split $\mathbb{P}^1$ over Y_1
$\mathbb{P}^1_0\left((\mathbf{3},\mathbf{2})_{1/6}\right)$	$\mathbb{P}^1_2(Y_1) + \mathbb{P}^1_5(Y_1)$	$\mathbb{P}^1_1\left((\mathbf{1},\mathbf{2})_{-1/2}\right)$	$\mathbb{P}^1_5(Y_1)$
$\mathbb{P}^1_1\left((\mathbf{3},\mathbf{2})_{1/6}\right)$	$\mathbb{P}^1_0(Y_1)$	$\mathbb{P}^1_2\left((\mathbf{1},\mathbf{2})_{-1/2}\right)$	$\mathbb{P}^1_0(Y_1)$
$\mathbb{P}^1_2\left((\mathbf{3},\mathbf{2})_{1/6}\right)$	$\mathbb{P}^1_3(Y_1)$	$\mathbb{P}^1_0\left((\overline{\mathbf{3}},\mathbf{1})_{-2/3}\right)$	$\mathbb{P}^1_0(Y_1) + \mathbb{P}^1_3(Y_1) + \mathbb{P}^1_5(Y_1)$
$\mathbb{P}^1_3\left((\mathbf{3},\mathbf{2})_{1/6}\right)$	$\mathbb{P}^1_4(Y_1)$	$\mathbb{P}^1_1\left((\overline{\mathbf{3}},\mathbf{1})_{-2/3}\right)$	$\mathbb{P}^1_4(Y_1)$
$\mathbb{P}^1_4\left((\mathbf{3},\mathbf{2})_{1/6}\right)$	$\mathbb{P}^1_1(Y_1)$	$\mathbb{P}^1_2\left((\overline{\mathbf{3}},\mathbf{1})_{-2/3}\right)$	$\mathbb{P}^1_1(Y_1)$
$\mathbb{P}^1_0\left((\mathbf{1},\mathbf{2})_{-1/2}\right)$	$\sum_{i=1}^4 \mathbb{P}^1_i(Y_1)$	$\mathbb{P}^1_3\left((\overline{\mathbf{3}},\mathbf{1})_{-2/3}\right)$	$\mathbb{P}^1_2(Y_1)$

(C.1.29)

Intersection Structure over Yukawa Locus $\mathbf{Y_2}$

Over the Yukawa point $Y_2 = V(s_3, s_9, s_2s_5 - s_1s_6)$ the following $\mathbb{P}^1$-fibrations are present:

$$\begin{aligned}
&\mathbb{P}^1_0(Y_2) = V\left(s_9, s_3, s_2s_5 - s_1s_6, s_5e_1e_4^2u + s_6e_3v, s_1e_1e_4^2u + s_2e_3v\right),\\
&\mathbb{P}^1_1(Y_2) = V(s_9, s_3, s_2s_5 - s_1s_6, e_1), \qquad \mathbb{P}^1_2(Y_2) = V(s_9, s_3, s_2s_5 - s_1s_6, e_2),\\
&\mathbb{P}^1_3(Y_2) = V(s_9, s_3, s_2s_5 - s_1s_6, e_4), \qquad \mathbb{P}^1_4(Y_2) = V(s_9, s_3, s_2s_5 - s_1s_6, u),\\
&\mathbb{P}^1_5(Y_2) = V(s_9, s_3, s_2s_5 - s_1s_6, s_2e_2e_3e_4u + s_6w, s_1e_2e_3e_4u + s_5w).
\end{aligned} \tag{C.1.30}$$

The intersection numbers in the fiber over Y_2 are as follows:

	$\mathbb{P}^1_0(Y_2)$	$\mathbb{P}^1_1(Y_2)$	$\mathbb{P}^1_2(Y_2)$	$\mathbb{P}^1_3(Y_2)$	$\mathbb{P}^1_4(Y_2)$	$\mathbb{P}^1_5(Y_2)$
$\mathbb{P}^1_0(Y_2)$	-2	0	1	0	0	1
$\mathbb{P}^1_1(Y_2)$	0	-2	0	1	0	1
$\mathbb{P}^1_2(Y_2)$	1	0	-2	0	1	0
$\mathbb{P}^1_3(Y_2)$	0	1	0	-2	1	0
$\mathbb{P}^1_4(Y_2)$	0	0	1	1	-2	0
$\mathbb{P}^1_5(Y_2)$	1	1	0	0	0	-2

(C.1.31)

Restrictions of the fibrations over the matter curves relate to the $\mathbb{P}^1_i(Y_2)$ as follows:

Split $\mathbb{P}^1$ over $C_{\mathbf{R}}$	Split $\mathbb{P}^1$ over Y_2	Split $\mathbb{P}^1$ over $C_{\mathbf{R}}$	Split $\mathbb{P}^1$ over Y_2
$\mathbb{P}^1_0\left((\mathbf{3},\mathbf{2})_{1/6}\right)$	$\mathbb{P}^1_0(Y_2) + \mathbb{P}^1_5(Y_2)$	$\mathbb{P}^1_1\left((\mathbf{1},\mathbf{2})_{-1/2}\right)$	$\mathbb{P}^1_0(Y_2) + \sum_{i=2}^4 \mathbb{P}^1_i(Y_2)$
$\mathbb{P}^1_1\left((\mathbf{3},\mathbf{2})_{1/6}\right)$	$\mathbb{P}^1_1(Y_2)$	$\mathbb{P}^1_2\left((\mathbf{1},\mathbf{2})_{-1/2}\right)$	$\mathbb{P}^1_1(Y_2)$
$\mathbb{P}^1_2\left((\mathbf{3},\mathbf{2})_{1/6}\right)$	$\mathbb{P}^1_3(Y_2)$	$\mathbb{P}^1_0\left((\overline{\mathbf{3}},\mathbf{1})_{1/3}\right)$	$\mathbb{P}^1_0(Y_2)$
$\mathbb{P}^1_3\left((\mathbf{3},\mathbf{2})_{1/6}\right)$	$\mathbb{P}^1_4(Y_2)$	$\mathbb{P}^1_1\left((\overline{\mathbf{3}},\mathbf{1})_{1/3}\right)$	$\mathbb{P}^1_1(Y_2) + \mathbb{P}^1_3(Y_2) + \mathbb{P}^1_5(Y_2)$
$\mathbb{P}^1_4\left((\mathbf{3},\mathbf{2})_{1/6}\right)$	$\mathbb{P}^1_2(Y_2)$	$\mathbb{P}^1_2\left((\overline{\mathbf{3}},\mathbf{1})_{1/3}\right)$	$\mathbb{P}^1_4(Y_2)$
$\mathbb{P}^1_0\left((\mathbf{1},\mathbf{2})_{-1/2}\right)$	$\mathbb{P}^1_5(Y_2)$	$\mathbb{P}^1_3\left((\overline{\mathbf{3}},\mathbf{1})_{1/3}\right)$	$\mathbb{P}^1_2(Y_2)$

(C.1.32)

Intersection Structure over Yukawa Locus $\mathbf{Y_3}$

Over the Yukawa point $Y_3 = V(s_3, s_6, s_9)$, we use A_i^1 to denote the reduced $\mathbb{P}^1$-fibrations such that the following structure is presented:

$$\begin{aligned}
&\mathbb{P}_0^1(Y_3) = A_0^1(Y_3) = V(s_3, s_6, s_9, e_1)\ , \qquad \mathbb{P}_1^1(Y_3) = A_1^1(Y_3) = V(s_3, s_6, s_9, e_2)\ , \\
&\mathbb{P}_2^1(Y_3) = 2A_2^1(Y_3) = V\left(s_3, s_6, s_9, e_4^2\right)\ , \quad \mathbb{P}_3^1(Y_3) = 2A_3^1(Y_3) = V\left(s_3, s_6, s_9, u^2\right)\ , \\
&\mathbb{P}_4^1(Y_3) = A_4^1(Y_3) = V\left(s_3, s_6, s_9, us_1e_1e_2e_3e_4^2 + vs_2e_2e_3^2 + ws_5e_1e_4\right)\ .
\end{aligned} \tag{C.1.33}$$

Restrictions of the fibrations over the matter curves relate to the $\mathbb{P}_i^1(Y_3)$ as follows:

Split $\mathbb{P}^1$ over $C_{\mathbf{R}}$	Split $\mathbb{P}^1$ over Y_3	Split $\mathbb{P}^1$ over $C_{\mathbf{R}}$	Split $\mathbb{P}^1$ over Y_3
$\mathbb{P}_0^1\left((\mathbf{3},\mathbf{2})_{1/6}\right)$	$\sum_{i=2}^4 A_i^1(Y_3)$	$\mathbb{P}_0^1\left((\overline{\mathbf{3}},\mathbf{1})_{1/3}\right)$	$A_0^1(Y_3) + A_3^1(Y_3) + A_2^1(Y_3)$
$\mathbb{P}_1^1\left((\mathbf{3},\mathbf{2})_{1/6}\right)$	$A_0^1(Y_3)$	$\mathbb{P}_1^1\left((\overline{\mathbf{3}},\mathbf{1})_{1/3}\right)$	$A_4^1(Y_3)$
$\mathbb{P}_2^1\left((\mathbf{3},\mathbf{2})_{1/6}\right)$	$A_2^1(Y_3)$	$\mathbb{P}_2^1\left((\overline{\mathbf{3}},\mathbf{1})_{1/3}\right)$	$A_3^1(Y_3)$
$\mathbb{P}_3^1\left((\mathbf{3},\mathbf{2})_{1/6}\right)$	$A_3^1(Y_3)$	$\mathbb{P}_3^1\left((\overline{\mathbf{3}},\mathbf{1})_{1/3}\right)$	$A_1^1(Y_3)$
$\mathbb{P}_4^1\left((\mathbf{3},\mathbf{2})_{1/6}\right)$	$A_1^1(Y_3)$		

(C.1.34)

Their intersection numbers are slightly away from standard, namely

	$A_0^1(Y_3)$	$A_1^1(Y_3)$	$A_2^1(Y_3)$	$A_3^1(Y_3)$	$A_4^1(Y_3)$
$A_0^1(Y_3)$	-2	0	1	0	0
$A_1^1(Y_3)$	0	-2	0	1	0
$A_2^1(Y_3)$	1	0	$-\frac{3}{2}$	1	0
$A_3^1(Y_3)$	0	1	1	-2	1
$A_4^1(Y_3)$	0	0	0	1	-2

(C.1.35)

The meaning of $\left(A_2^1\left(Y_3\right)\right)^2 = -\frac{3}{2}$ becomes clear once we draw the associated diagram:

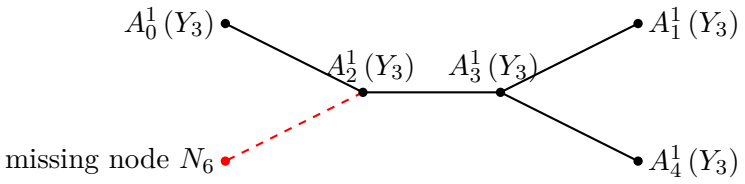

(C.1.36)

Consequently, we see that the node N_6 is missing and it holds $\mathbb{P}_2^1(Y_3) = 2 \cdot N_2 + N_6$, where N_2 is the standard node that ordinarily appear instead of $\mathbb{P}_2^1(Y_3)$. It follows

$$\left(\mathbb{P}_2^1(Y_3)\right)^2 = 4 \cdot N_2^2 + 4 N_2 N_6 + N_6^2 = 4 \cdot (-2) + 4 \cdot 1 + (-2) = -6\,. \tag{C.1.37}$$

Likewise, $A_2^1(Y_3) = N_2 + \frac{1}{2} \cdot N_6$ leads to the half-integer intersection in C.1.35.

Intersection Structure over Yukawa Locus $\mathbf{Y_4}$

Over the Yukawa point $Y_4 = V(s_1, s_3, s_5)$ the following $\mathbb{P}^1$-fibrations are present:

$$\begin{aligned} &\mathbb{P}_0^1\left(Y_4\right) = V\left(s_1, s_3, s_5, e_1\right)\,, \qquad \mathbb{P}_1^1\left(Y_4\right) = V\left(s_1, s_3, s_5, v\right)\,, \\ &\mathbb{P}_2^1\left(Y_4\right) = V\left(s_1, s_3, s_5, s_2 e_2^2 e_3^2 e_4^2 u^2 + s_6 e_2 e_3 e_4 u w + s_9 w^2\right)\,. \end{aligned} \tag{C.1.38}$$

Restrictions of the fibrations over the matter curves relate to the $\mathbb{P}_i^1\left(Y_4\right)$ as follows:

Split $\mathbb{P}^1$ over $C_{\mathbf{R}}$	Split $\mathbb{P}^1$ over Y_4	Split $\mathbb{P}^1$ over $C_{\mathbf{R}}$	Split $\mathbb{P}^1$ over Y_4
$\mathbb{P}_0^1\left((\mathbf{1},\mathbf{2})_{1/2}\right)$	$\mathbb{P}_2^1\left(Y_4\right)$	$\mathbb{P}_1^1\left((\mathbf{1},\mathbf{1})_0\right)$	$\mathbb{P}_1^1\left(Y_4\right) + \mathbb{P}_2^1\left(Y_4\right)$
$\mathbb{P}_1^1\left((\mathbf{1},\mathbf{2})_{1/2}\right)$	$\mathbb{P}_1^1\left(Y_4\right)$	$\mathbb{P}_2^1\left((\mathbf{1},\mathbf{1})_0\right)$	$\mathbb{P}_0^1\left(Y_4\right)$
$\mathbb{P}_2^1\left((\mathbf{1},\mathbf{2})_{1/2}\right)$	$\mathbb{P}_0^1\left(Y_4\right)$		

(C.1.39)

The intersection numbers in the fiber over Y_4 are as follows:

	$\mathbb{P}^1_0(Y_4)$	$\mathbb{P}^1_1(Y_4)$	$\mathbb{P}^1_2(Y_4)$
$\mathbb{P}^1_0(Y_4)$	-2	1	1
$\mathbb{P}^1_1(Y_4)$	1	-2	1
$\mathbb{P}^1_2(Y_4)$	1	1	-2

(C.1.40)

Intersection Structure over Yukawa Locus $\mathbf{Y_5}$

Over the Yukawa point $Y_5 = V(s_5, s_6^2, s_9)$ the following $\mathbb{P}^1$-fibrations are present:

$$\begin{aligned}
\mathbb{P}^1_0(Y_5) &= V\left(s_5, s_6^2, s_9, e_2^3, s_6e_2^2, u^2s_1e_1^2e_2^2e_4^4 + uvs_2e_1e_2^2e_3e_4^2 + v^2s_3e_2^2e_3^2 + vws_6e_1e_2e_4\right) \\
&= n_0 \cdot V(s_5, s_6, s_9, e_2) = n_0 \cdot A_0(Y_5)\,, \\
\mathbb{P}^1_1(Y_5) &= V\left(s_5, s_6^2, s_9, e_3\right) = n_1 \cdot V(s_5, s_6, s_9, e_3) = n_1 \cdot A_1(Y_5)\,, \\
\mathbb{P}^1_2(Y_5) &= V\left(s_5, s_6^2, s_9, u\right) = n_2 \cdot V(s_5, s_6, s_9, u) = n_2 \cdot A_2(Y_5)\,, \\
\mathbb{P}^1_3(Y_5) &= V(s_5, s_6^2, s_9, u^2s_1e_1^2e_2e_4^4 + uvs_2e_1e_2e_3e_4^2 + v^2s_3e_2e_3^2 + vws_6e_1e_4, \\
&\qquad u^4s_1^2e_1^4e_4^8 + 2u^3vs_1s_2e_1^3e_3e_4^6 + u^2v^2s_2^2e_1^2e_3^2e_4^4 + 2u^2v^2s_1s_3e_1^2e_3^2e_4^4 \\
&\qquad + 2uv^3s_2s_3e_1e_3^3e_4^2 + v^4s_3^2e_3^4, u^2s_1s_6e_1^2e_4^4 + uvs_2s_6e_1e_3e_4^2 + v^2s_3s_6e_3^2) \\
&= n_3 \cdot V\left(s_5, s_6, s_9, u^2s_1e_1^2e_4^4 + uvs_2e_1e_3e_4^2 + v^2s_3e_3^2\right) = n_3 \cdot A_3(Y_5)\,.
\end{aligned} \tag{C.1.41}$$

The total elliptic fiber over Y_5 is given

$$T^2(Y_5) = \sum_{i=0}^{3} \mathbb{P}^1_i(Y_5) = n_0 \cdot A_0(Y_5) + n_1 \cdot A_1(Y_5) + n_2 \cdot A_2(Y_5) + n_3 \cdot A_3(Y_5)\,. \tag{C.1.42}$$

Restrictions of the fibrations over the gauge divisor $D_i^{SU(3)}$ are:

$$\begin{aligned}
D_0^{SU(3)}|_{Y_5} &= n_3 \cdot A_3(Y_5) + n_1 \cdot A_1(Y_5) + n_4 \cdot A_0(Y_5)\,, \\
D_1^{SU(3)}|_{Y_5} &= n_5 \cdot A_0(Y_5)\,, \\
D_2^{SU(3)}|_{Y_5} &= n_2 \cdot A_2(Y_5)\,.
\end{aligned} \tag{C.1.43}$$

The total elliptic fiber can be obtained from the total torus over the gauge divisor $D_i^{SU(3)}$:

$$T^2\left(D_i^{SU(3)}|_{Y_5}\right) = (n_4+n_5)\cdot A_0(Y_5) + n_1\cdot A_1(Y_5) + n_2\cdot A_2(Y_5) + n_3\cdot A_3(Y_5)\,. \tag{C.1.44}$$

Since this must recover (C.1.42), we conclude that

$$n_0 = n_4 + n_5 \tag{C.1.45}$$

Restrictions of the fibrations over the matter curves $(\overline{\mathbf{3}},\mathbf{1})_{1/3}$) are as follows:

$$\begin{aligned}
&\mathbb{P}^1_0\left((\overline{\mathbf{3}},\mathbf{1})_{1/3}\right)|_{Y_5} = V\left(s_5, s_6, s_9, u^2 s_1 e_1^2 e_4^4 + uvs_2 e_1 e_3 e_4^2 + v^2 s_3 e_3^2\right) = A_3(Y_5)\,,\\
&\mathbb{P}^1_1\left((\overline{\mathbf{3}},\mathbf{1})_{1/3}\right)|_{Y_5} = V\left(s_5, s_6, s_9, u^2 s_1 e_1^2 e_4^4 + uvs_2 e_1 e_3 e_4^2 + v^2 s_3 e_3^2\right) + \mathbb{P}^1_1(Y_5) +\\
&\qquad\qquad V(s_5, s_6^2, s_9, e_2^2, s_6 e_2, u^2 s_1 e_1^2 e_2^2 e_4^4 + uvs_2 e_1 e_2^2 e_3 e_4^2 + v^2 s_3 e_2^2 e_3^2 + vws_6 e_1 e_2 e_4)\\
&\qquad\qquad = A_3(Y_5) + n_1\cdot A_1(Y_5) + n_4\cdot A_0(Y_5)\,,\\
&\mathbb{P}^1_2\left((\overline{\mathbf{3}},\mathbf{1})_{1/3}\right)|_{Y_5} = V\left(s_5, s_6^2, s_9, e_2\right) = n_5\cdot A_0(Y_5)\,,\\
&\mathbb{P}^1_3\left((\overline{\mathbf{3}},\mathbf{1})_{1/3}\right)|_{Y_5} = V\left(s_5, s_6^2, s_9, u\right) = n_2\cdot A_2(Y_5)\,.
\end{aligned} \tag{C.1.46}$$

The fibrations over the matter curves $(\overline{\mathbf{3}},\mathbf{1})_{1/3}$ give the total elliptic fiber over Y_5 as:

$$T^2\left((\overline{\mathbf{3}},\mathbf{1})_{1/3}|_{Y_5}\right) = (n_4+n_5)\cdot A_0(Y_5) + n_1\cdot A_1(Y_5) + n_2\cdot A_2(Y_5) + 2\cdot A_3(Y_5)\,. \tag{C.1.47}$$

Restrictions of the fibrations over the matter curves $(\overline{\mathbf{3}},\mathbf{1})_{-2/3}$ are:

$$\begin{aligned}
&\mathbb{P}^1_0\left((\overline{\mathbf{3}},\mathbf{1})_{-2/3}\right)|_{Y_5} = V(s_5, s_6^2, s_9, e_2^2, s_6 e_2, u^2 s_1 e_1^2 e_2^2 e_4^4 + uvs_2 e_1 e_2^2 e_3 e_4^2 + v^2 s_3 e_2^2 e_3^2 + vws_6 e_1 e_2 e_4)\\
&\qquad\qquad + \mathbb{P}^1_3(Y_5) = n_3\cdot A_3(Y_5) + n_4\cdot A_0(Y_5)\,,\\
&\mathbb{P}^1_1\left((\overline{\mathbf{3}},\mathbf{1})_{-2/3}\right)|_{Y_5} = V\left(s_5, s_6^2, s_9, u\right) = n_2\cdot A_2(Y_5)\,,\\
&\mathbb{P}^1_2\left((\overline{\mathbf{3}},\mathbf{1})_{-2/3}\right)|_{Y_5} = V\left(s_5, s_6^2, s_9, e_2\right) = n_5\cdot A_0(Y_5)\,,\\
&\mathbb{P}^1_3\left((\overline{\mathbf{3}},\mathbf{1})_{-2/3}\right)|_{Y_5} = V\left(s_5, s_6^2, s_9, e_3\right) = n_1\cdot A_1(Y_5)\,.
\end{aligned} \tag{C.1.48}$$

The fibrations over the matter curves $(\overline{\mathbf{3}},\mathbf{1})_{-2/3}$ give the total elliptic fiber over Y_5 as:

$$T^2\left((\overline{\mathbf{3}},\mathbf{1})_{-2/3}|_{Y_5}\right) = (n_4+n_5)\cdot A_0(Y_5) + n_1\cdot A_1(Y_5) + n_2\cdot A_2(Y_5) + n_3\cdot A_3(Y_5)\,. \tag{C.1.49}$$

We conclude that the restriction from the two triplet matter curves to the Yukawa point Y_5 preserve the elliptic fiber structure as presented in (C.1.42) iff $n_3 = 2$.

Before we continue our discussion of the factors n_i, let us look at the intersection numbers among the $A_i(Y_5)$ as follows:

	$A_0^1(Y_5)$	$A_1^1(Y_5)$	$A_2^1(Y_5)$	$A_3^1(Y_5)$
$A_0^1(Y_5)$	-2	1	1	2
$A_1^1(Y_5)$	1	-2	0	0
$A_2^1(Y_5)$	1	0	-2	0
$A_3^1(Y_5)$	2	0	0	-2

(C.1.50)

Let us return to the factors n_i we can fix $n_1 = n_2 = 2$ intuitively. Then, by infering that $-2 = \left(P_0((\overline{\mathbf{3}},\mathbf{1})_{-2/3})\Big|_{Y_5}\right)^2$, we find $n_4 \in \{1,3\}$. Intuitively, we discard $n_4 = 1$ and pick $n_4 = 3$ instead. By accepting all these steps above, we are then left to conclude

$$n_0 = 5, \qquad n_1 = n_2 = n_3 = 2\,, \qquad n_4 = 3\,, \qquad n_5 = 2\,. \tag{C.1.51}$$

This finally, completes our understanding of the fiber structure over Y_5.

Intersection Structure over Yukawa Locus $\mathbf{Y_6}$

Over the Yukawa point $Y_6 = V(s_1, s_5, s_9)$ the following $\mathbb{P}^1$-fibrations are present:

$$\begin{aligned}
&\mathbb{P}_0^1(Y_6) = V(s_1, s_5, s_9, e_2)\,, \quad \mathbb{P}_1^1(Y_6) = V(s_1, s_5, s_9, e_3)\,, \quad \mathbb{P}_2^1(Y_6) = V(s_1, s_5, s_9, u)\,,\\
&\mathbb{P}_3^1(Y_6) = V(s_1, s_5, s_9, v)\,, \quad \mathbb{P}_4^1(Y_6) = V\left(s_1, s_5, s_9, s_2e_1e_2e_3e_4^2u + s_3e_2e_3^2v + s_6e_1e_4w\right)\,.
\end{aligned} \tag{C.1.52}$$

Restrictions of the fibrations over the matter curves relate to the $\mathbb{P}^1_i(Y_6)$ as follows:

Split $\mathbb{P}^1$ over $C_{\mathbf{R}}$	Split $\mathbb{P}^1$ over Y_6	Split $\mathbb{P}^1$ over $C_{\mathbf{R}}$	Split $\mathbb{P}^1$ over Y_6
$\mathbb{P}^1_0\left((\overline{\mathbf{3}},\mathbf{1})_{1/3}\right)$	$\mathbb{P}^1_1(Y_6)+\mathbb{P}^1_3(Y_6)$	$\mathbb{P}^1_1\left((\overline{\mathbf{3}},\mathbf{1})_{-2/3}\right)$	$\mathbb{P}^1_2(Y_6)$
$\mathbb{P}^1_1\left((\overline{\mathbf{3}},\mathbf{1})_{1/3}\right)$	$\mathbb{P}^1_4(Y_6)$	$\mathbb{P}^1_2\left((\overline{\mathbf{3}},\mathbf{1})_{-2/3}\right)$	$\mathbb{P}^1_0(Y_6)$
$\mathbb{P}^1_2\left((\overline{\mathbf{3}},\mathbf{1})_{1/3}\right)$	$\mathbb{P}^1_2(Y_6)$	$\mathbb{P}^1_3\left((\overline{\mathbf{3}},\mathbf{1})_{-2/3}\right)$	$\mathbb{P}^1_1(Y_6)$
$\mathbb{P}^1_3\left((\overline{\mathbf{3}},\mathbf{1})_{1/3}\right)$	$\mathbb{P}^1_0(Y_6)$	$\mathbb{P}^1_0\left((\overline{\mathbf{3}},\mathbf{1})_{-2/3}\right)$	$\mathbb{P}^1_3(Y_6)+\mathbb{P}^1_4(Y_6)$
$\mathbb{P}^1_1((\mathbf{1},\mathbf{1})_1)$	$\sum_{i=0}^{2}\mathbb{P}^1_i(Y_6)+\mathbb{P}^1_4(Y_6)$	$\mathbb{P}^1_2((\mathbf{1},\mathbf{1})_1)$	$\mathbb{P}^1_3(Y_6)$

(C.1.53)

The intersection numbers in the fiber over Y_6 are as follows:

	$\mathbb{P}^1_0(Y_6)$	$\mathbb{P}^1_1(Y_6)$	$\mathbb{P}^1_2(Y_6)$	$\mathbb{P}^1_3(Y_6)$	$\mathbb{P}^1_4(Y_6)$
$\mathbb{P}^1_0(Y_6)$	-2	1	1	0	0
$\mathbb{P}^1_1(Y_6)$	1	-2	0	1	0
$\mathbb{P}^1_2(Y_6)$	1	0	-2	0	1
$\mathbb{P}^1_3(Y_6)$	0	1	0	-2	1
$\mathbb{P}^1_4(Y_6)$	0	0	1	1	-2

(C.1.54)

C.2 Induced line bundles in F-theory Standard Models

In this section, we give details on how we identify the root bundles in the largest currently-known class of globally consistent F-theory Standard Model constructions without chiral exotics and gauge coupling unification [32]. More details can be found in the earlier works [82, 40]. We provide details on the employed G_4-flux in C.2.1. Subsequently, we outline our computational techniques in C.2.2 and summarize the resulting root bundle constraints in C.2.3. Finally, we construct root bundle solutions in compactifications over a particular 3-fold base space B_3 in C.2.4.

C.2.1 G_4-flux and matter surfaces

U(1)-flux We associate to the section $s_1 = V(e_4)$ a $U(1)$-flux. To this end, we employ the Shioda map to turn s_1 into $\sigma \in H^{(1,1)}(\widehat{Y}_4)$:

$$\sigma = \left([e_4] - [v] - \left[\widehat{\pi}^* \left(\overline{K}_B \right) \right] + \frac{1}{2} [e_1] + \frac{1}{3} [e_2] + \frac{2}{3} [u] \right) \Big|_{\hat{Y}_4} . \tag{C.2.1}$$

In this expression, $[e_4] = \gamma(V(e_4)) \in H^{(1,1)}(\widehat{Y}_4)$ denotes the image of the divisor $V(e_4) \subseteq X_5$ under the cycle map γ. Furthermore, recall that $\widehat{\pi}\colon \widehat{Y}_4 \twoheadrightarrow B_3$. The $U(1)$-flux is then given by

$$G_4^{U(1)} \equiv \omega \wedge \sigma \in H^{(2,2)}(\widehat{Y}_4) , \qquad \omega \in \pi^*(H^{(1,1)}(B_3)) . \tag{C.2.2}$$

Matter surface flux To the matter surface $S^{(1)}_{(\mathbf{3},\mathbf{2})_{1/6}}$ over the quark-doublet curve $C_{(\mathbf{3},\mathbf{2})_{1/6}}$ (cf. C.1) one can associate a *gauge invariant* flux

$$G_4^{(\mathbf{3},\mathbf{2})_{1/6}} \equiv \left[S^{(1)}_{(\mathbf{3},\mathbf{2})_{1/6}} \right] + \frac{1}{2} \cdot \left[\mathbb{P}^1_1((\mathbf{3},\mathbf{2})_{1/6}) \right] + \frac{1}{3} \cdot \left[\mathbb{P}^1_3((\mathbf{3},\mathbf{2})_{1/6}) \right] + \frac{2}{3} \cdot \left[\mathbb{P}^1_4((\mathbf{3},\mathbf{2})_{1/6}) \right] . \tag{C.2.3}$$

Total flux expression One can now consider a linear combination of these fluxes

$$G_4(a,\omega) = a \cdot G_4^{(\mathbf{3},\mathbf{2})_{1/6}} + \omega \wedge \sigma \in H^{(2,2)}(\widehat{Y}_4) . \tag{C.2.4}$$

The parameters $a \in \mathbb{Q}$ and $\omega \in \pi^* \left(H^{(1,1)}(B_3) \right)$ are subject to flux quantization, D_3-tadpole cancelation, masslessness of the $U(1)$-gauge boson and exactly three chiral families on all matter curves. These conditions are solved base-independently by

$$\omega = \frac{3}{\overline{K}^3_{B_3}} \cdot \overline{K}_{B_3} , \qquad a = \frac{15}{\overline{K}^3_{B_3}} . \tag{C.2.5}$$

This leads to

$$G_4 = \frac{-3}{\overline{K}_B^3} \cdot \left(5[e_1] \wedge [e_4] - \overline{K}_B \wedge (3[e_1] - 2[e_2] - 6[e_4] + \overline{K}_B - 4u + v)\right). \tag{C.2.6}$$

For this G_4, it was verified in [32], that the integral over all matter surfaces $S_{\mathbf{R}}$ and complete intersections of toric divisors is integral. This is a necessary condition, for this algebraic cycle to be integral. A sufficient check is computationally very demanding and currently beyond our arithmetic abilities. Therefore, we proceed under the assumption that this G_4-flux candidate 6.2.25, is indeed integral and thus a proper G_4-flux.

We next look at

$$\begin{aligned}\mathcal{A}' = -3\cdot (5V(e_1, e_4) - 3V(e_1, t_1) - 2V(e_2, t_2) - 6V(e_4, t_3) \\ +V(t_4, t_5) - 4V(t_6, u) + V(t_6, v))|_{\widehat{Y}_4} \in \mathrm{CH}^2(\widehat{Y}_4, \mathbb{Z}),\end{aligned} \tag{C.2.7}$$

where $t_i \in H^0(X_5, \alpha^*(\overline{K}_B))$ and $\alpha\colon X_5 = B_3 \times \mathbb{P}_{F_{11}} \twoheadrightarrow B_3$. Note that $\gamma(\mathcal{A}') = \overline{K}_B^3 \cdot G_4$. Therefore, this gauge potential would induce chiral exotics, unless we "devide" it by $\xi = \overline{K}_B^3$. Hence, we are led to consider gauge potentials $A = \widehat{\gamma}(\mathcal{A}) \in H^4_D(\widehat{Y}_4, \mathbb{Z}(2))$ with

$$\gamma(\mathcal{A}) = G_4\,, \qquad \xi \cdot \widehat{\gamma}(\mathcal{A}) \sim \widehat{\gamma}(\mathcal{A}')\,. \tag{C.2.8}$$

Hence, we can infer that the line bundles induced from $A = \widehat{\gamma}(\mathcal{A})$ are $\overline{K}_{B_3}^3$-th roots of the ones induced from $A' = \widehat{\gamma}(\mathcal{A}')$. The divisors $D_{\mathbf{R}}(\mathcal{A}')$ are then $\overline{K}_B^3$-th roots of the $D_{\mathbf{R}}(\mathcal{A}')$. In the following, we outline the arithmetic identification of the divisors $D_{\mathbf{R}}(\mathcal{A}')$.

Matter surfaces As C.2.7 is gauge invariant, it suffices to focus on the following matter surfaces (cf. C.1)

$$
\begin{aligned}
&S^{(1)}_{(\mathbf{3},\mathbf{2})_{1/6}} = V(s_3, s_9, e_4)\,, \quad S^{(1)}_{(\overline{\mathbf{3}},\mathbf{1})_{-2/3}} = V(s_5, s_9, e_3)\,, \quad S^{(1)}_{(\mathbf{1},\mathbf{1})_1} = V(s_1, s_5, v)\,,\\
&S^{(1)}_{(\mathbf{1},\mathbf{2})_{-1/2}} = V(s_3, s_2 s_5^2 + s_1^2 s_9 - s_1 s_5 s_6, s_1 e_2 e_3 e_4 u + s_5 w,\\
&\qquad s_2 s_5 e_2 e_3 e_4 u + s_5 s_6 w - s_1 s_9 w, s_2 e_2^2 e_3^2 e_4^2 u^2 + s_6 e_2 e_3 e_4 u w + s_9 w^2)\,,\\
&S^{(1)}_{(\overline{\mathbf{3}},\mathbf{1})_{1/3}} = V(s_9, s_3 s_5^2 - s_2 s_5 s_6 + s_1 s_6^2, s_5 e_1 e_4^2 u + s_6 e_3 v,\\
&\qquad s_1 s_6 e_1 e_4^2 u - s_3 s_5 e_3 v + s_2 s_6 e_3 v, s_1 e_1^2 e_4^4 u^2 + s_2 e_1 e_3 e_4^2 u v + s_3 e_3^2 v^2)\,.
\end{aligned}
\tag{C.2.9}
$$

Note that $S^{(1)}_{(\mathbf{1},\mathbf{2})_{-1/2}}$ and $S^{(1)}_{(\overline{\mathbf{3}},\mathbf{1})_{1/3}}$ are not complete intersections. In C.2.2, we explain how one can compute topological intersection numbers of cycles with them. Moreover, we can simplify the expressions for those two matter surfaces.

$$
\begin{aligned}
&S^{(1)}_{(\mathbf{1},\mathbf{2})_{-1/2}} = V(s_3, u s_1 e_2 e_3 e_4 + w s_5, u^2 s_2 e_2^2 e_3^2 e_4^2 + u w s_6 e_2 e_3 e_4 + w^2 s_9)\,,\\
&S^{(1)}_{(\overline{\mathbf{3}},\mathbf{1})_{1/3}} = V(s_9, u s_5 e_1 e_4^2 + v s_6 e_3, u^2 s_1 e_1^2 e_4^4 + u v s_2 e_1 e_3 e_4^2 + v^2 s_3 e_3^2) - V(s_9, s_5, s_6)\,.
\end{aligned}
\tag{C.2.10}
$$

Therefore, we can express all matter surfaces as pullbacks from elements in $\mathrm{CH}^2(X_5)$:

$$
\begin{aligned}
S^{(1)}_{(\mathbf{3},\mathbf{2})_{1/6}} &= V(s_3, e_4) - V(e_1, e_4)|_{\hat{Y}_4}\,,\\
S^{(1)}_{(\mathbf{1},\mathbf{2})_{-1/2}} &= V(s_3, p_1) - V(e_1, p_1) - V(s_3, v)|_{\hat{Y}_4}\,,\\
S^{(1)}_{(\overline{\mathbf{3}},\mathbf{1})_{-2/3}} &= V(s_5, e_3) - V(v, e_3)|_{\hat{Y}_4}\,,\\
S^{(1)}_{(\overline{\mathbf{3}},\mathbf{1})_{1/3}} &= V(s_9, q_1) + V(e_2, e_3) - V(e_2^2, q_1) - V(e_3, s_9) - V(u, q_1)\Big|_{\hat{Y}_4}\,,\\
S^{(1)}_{(\mathbf{1},\mathbf{1})_1} &= V(s_1, v) - V(v, w)|_{\hat{Y}_4}\,,
\end{aligned}
\tag{C.2.11}
$$

where $p_1 = u s_1 e_2 e_3 e_4 + w s_5$ and $q_1 = u s_5 e_1 e_4^2 + v s_6 e_3$. We exploit this in C.2.2 to compute the actual intersection loci.

Finally in C.2.2, we make use of the fact that we know that the matter surfaces are particular $\mathbb{P}^1$-fibrations over the matter curves. The matter surface flux originates from

the matter surface $S_{(\mathbf{3},\mathbf{2})_{1/6}}$. This allows us to derive the divisors $D_{\mathbf{R}}(\mathcal{A}')$ intuitively from intersections in the fiber and intersections in the base. The former is facilitated by knowledge of the intersection numbers listed in C.1.

C.2.2 Computational strategies

Euler characteristic of structure sheaf of intersection variety

The twisted cubic – a non-complete intersection Let us start with a simple and instructive example that involves a non-complete intersection. We consider $\mathbb{P}^3$ with homogeneous coordinates $[x:y:z:w]$ and focus on the hypersurface $Y = V(xw - yz)$. In this hypersurface Y, we consider the twisted cubic

$$S = V(xz - y^2, yw - z^2) \cap Y = V(xz - y^2, yw - z^2, xw - yz) \cong \mathbb{P}^1\,, \tag{C.2.12}$$

and a union of two lines

$$\mathcal{A} = V(x) \cap Y = V(x, xw - yz) = V(x, y) \cup V(x, z)\,. \tag{C.2.13}$$

Crucially, note that S is not a complete intersection and cannot be expressed as any sort of pullback from $\mathbb{P}^3$. In order to compute the topological intersection number $S \cdot \mathcal{A}$, we notice that this intersection number coincides with the Euler characteristic of the structure sheaf of the intersection variety $V(x, xz - y^2, yw - z^2, xw - yz)$.

Let us denote the coordinate ring of $\mathbb{P}^3$ by R. Then an f.p. graded (left) R-module, which sheafifies to the structure sheaf in question, is given by

$$R(-2)^{\oplus 3} \oplus R(-1) \xrightarrow{\begin{pmatrix} xw - yz & xz - y^2 & yw - z^2 & x \end{pmatrix}^T} R \twoheadrightarrow O_{S\cdot\mathcal{A}} \to 0\,. \tag{C.2.14}$$

Denote this sequence by $F_1 \xrightarrow{M_1} R \twoheadrightarrow O_{S\cdot\mathcal{A}} \to 0$. A minimal free resolution is given by

$$0 \to F_3 \xrightarrow{M_3} F_2 \xrightarrow{M_2} F_1 \xrightarrow{M_1} R \twoheadrightarrow O_{S\cdot\mathcal{A}} \to 0\,, \tag{C.2.15}$$

where $F_2 = R(-3)^{\oplus 5}$, $F_3 = R(-4)^{\oplus 2}$ and

$$M_2 = \begin{pmatrix} -wz & y & 0 & \\ -y & w & x & 0 \\ -y & w & 0 & yz - w^2 \\ -x & 0 & 0 & xz - yw \\ 0 & x & 0 & y^2 - xw \end{pmatrix}, \qquad M_3 = \begin{pmatrix} 0 & 0 & x & -y & -w \\ x & -y & y & -w & -z \end{pmatrix}. \tag{C.2.16}$$

The vector bundles $\widetilde{F}_i$ has the following sheaf cohomologies:

	$\mathcal{O}_{\mathbb{P}^3}(-4)^{\oplus 2}$	$\mathcal{O}_{\mathbb{P}^3}(-3)^{\oplus 5}$	$\mathcal{O}_{\mathbb{P}^3}(-2)^{\oplus 3} \oplus \mathcal{O}_{\mathbb{P}^3}(-1)$	$\widetilde{F}_0 \equiv \widetilde{R} \cong \mathcal{O}_{\mathbb{P}^3}$
h^0	0	0	0	1
h^1	0	0	0	0
h^2	0	0	0	0
h^3	2	0	0	0

(C.2.17)

It follows that $h^i(\mathbb{P}^3, \mathcal{O}_{S\cdot\mathcal{A}}) = (3, 0, 0, 0)$, i.e. $S \cdot \mathcal{A} = \chi(\mathcal{O}_{S\cdot\mathcal{A}}) = 3$. Equivalently, we find

$$V(xw - yz, xz - y^2, yw - z^2, x) = V(x, y, z)\,, \tag{C.2.18}$$

which allows us to conclude $S \cdot \mathcal{A} = 3 \cdot V(x, y, z)$.

Application to Higgs matter surface We employ this technique as a consistency check on intersections with the non-complete matter surfaces. For instance, let us work out the topological intersection number of $B = V(e_1, e_4, p_{F_{11}})$ with (cf. C.2.9 for p_i)

$$S \equiv S^{(1)}_{(\mathbf{1},\mathbf{2})_{-1/2}} = V(p_1, p_2, p_3, p_4, p_5)\,. \tag{C.2.19}$$

in the elliptic fibration $\widehat{Y}_4$ over the base space $B_3 = P_{39}$ (cf. C.2.4). To construct the structure sheaf of the variety $V(p_1, p_2, p_3, p_4, p_5, e_1, e_4)$, we model the coordinate ring of

X_5 as $R = \mathbb{Q}[s_1, s_2, s_3, s_5, s_6, s_9, u, v, w, e_1, e_2, e_3, e_4]$ with $\mathbb{Z}^6$-grading[1]

	s_1	s_2	s_3	s_5	s_6	s_9	u	v	w	e_1	e_2	e_3	e_4
$\overline{K}_{B_3}$	1	1	1	1	1	1							
H							1	1	1				
E_1							-1		-1	1			
E_2							-1	-1			1		
E_3								-1			-1	1	
E_4							-1			-1			1

(C.2.20)

Then, an f.p. graded (left) R-module $O_{S\cdot B}$ which sheafifies to $\mathcal{O}_{S\cdot B}$ is given by

$$\begin{pmatrix} R(-\overline{K}_{B_3}) \\ R(-3\overline{K}_{B_3}) \\ R(-\overline{K}_{B_3} - H + E_1) \\ R(-2\overline{K}_{B_3} - H + E_1) \\ R(-\overline{K}_{B_3} - 2H + 2E_1) \\ R(-E_1 + E_4) \\ R(-E_4) \end{pmatrix}^T \xrightarrow{\begin{pmatrix} p_1 & p_2 & p_3 & p_4 & p_5 & e_1 & e_4 & p_{F_{11}} \end{pmatrix}^T} R \twoheadrightarrow O_{S\cdot B} \to 0\,. \tag{C.2.21}$$

Denote this sequence by $F_2 \xrightarrow{M_1} F_1 \twoheadrightarrow O_{S\cdot B} \to 0$. A minimal free resolution is given by

$$0 \to F_7 \xrightarrow{M_6} F_6 \xrightarrow{M_5} F_5 \xrightarrow{M_4} F_4 \xrightarrow{M_3} F_3 \xrightarrow{M_2} F_2 \xrightarrow{M_1} F_1 \twoheadrightarrow O_{S\cdot B} \to 0\,, \tag{C.2.22}$$

where $\mathrm{rk}(F_1) = \mathrm{rk}(F_7) = 1$, $\mathrm{rk}(F_6) = 6$, $\mathrm{rk}(F_2) = 7$, $\mathrm{rk}(F_3) = \mathrm{rk}(F_5) = 19$, $\mathrm{rk}(F_4) = 25$.[2]

We compute the Euler characteristics of the $\widetilde{F}_i$ by computing their sheaf cohomologies. The latter is performed by use of the Künneth formula. Namely, since $X_5 = P_{39} \times \mathbb{P}_{F_{11}}$,

[1] We could use the actual coordinate ring for the fibration over P_{39}. This ring has 18 indeterminates and is $\mathbb{Z}_{14}$-graded. As a consequence, the resulting computations take longer than the ones performed with the simpler ring. Both lead to the same result.

[2] The twists of these free modules and the mapping matrices are huge. We therefore omit them here.

and

$$H^k\left(X_5, L\right) = H^k(P_{39} \times \mathbb{P}_{F_{11}}, L) = \bigoplus_{i+j=k} H^i(P_{39}, L) \otimes H^j(\mathbb{P}_{F_{11}}, L)\,. \tag{C.2.23}$$

we can easily compute the cohomologies in question from line bundle cohomologies on P_{39} and $\mathbb{P}_{F_{11}}$. The Euler characteristics of the vector bundles $\widetilde{F}_i$ are

$$\chi(\widetilde{F}_1) = 1\,, \qquad \chi(\widetilde{F}_2) = -50\,, \qquad \chi(\widetilde{F}_3) = -82\,, \qquad \chi(\widetilde{F}_4) = 384\,, \tag{C.2.24}$$

$$\chi(\widetilde{F}_5) = 699\,, \qquad \chi(\widetilde{F}_6) = 266\,, \qquad \chi(\widetilde{F}_7) = 0\,. \tag{C.2.25}$$

It follows that

$$\begin{aligned} S \cdot B = \chi(\widetilde{O}_{S\cdot B}) &= \chi(\widetilde{F}_1) - \chi(\widetilde{F}_2) + \chi(\widetilde{F}_3) - \chi(\widetilde{F}_4) + \chi(\widetilde{F}_5) - \chi(\widetilde{F}_6) + \chi(\widetilde{F}_7) \\ &= 1 - (-50) + (-82) - 384 + 699 - 266 + 0 = 18\,. \end{aligned} \tag{C.2.26}$$

Line bundles from Chow ring of toric ambient space

Let us repeat the intersection computation $S \cdot B$ by using

$$S \equiv S^{(1)}_{(\mathbf{1},\mathbf{2})_{-1/2}} = V(s_3, p_1) - V(e_1, p_1) - V(s_3, v)|_{\hat{Y}_4}\,, \tag{C.2.27}$$

instead. Similarly, $B = V(e_1, e_4)|_{\hat{Y}_4}$. We define $S', T' \in \mathrm{CH}^2(X_5, \mathbb{Z})$ via

$$S' = V(s_3, p_3) - V(e_1, p_3) - V(s_3, v), \qquad T' = V(e_1, e_4)\,. \tag{C.2.28}$$

Then, it follows $S \cdot_{\widehat{Y}_4} T = S' \cdot_{X_5} T' \cdot_{X_5} V(p_{F_{11}})$. Explicitly, we find

$$\begin{aligned} &V(s_3, p_3) \cdot_{X_5} V(e_1, e_4) = V(s_3, s_5 w, e_1, e_4) = V(s_3, s_5, e_1, e_4)\,, \\ &V(e_1, p_3) \cdot_{X_5} V(e_1, e_4) = \emptyset\,, \qquad V(s_3, v) \cdot_{X_5} V(e_1, e_4) = \emptyset\,. \end{aligned} \tag{C.2.29}$$

From a primary decomposition, we find $\langle s_3, s_5, e_1, e_4, p_{F_{11}}\rangle = \langle e_1, e_4, s_3, s_5, s_9\rangle$. Note that $e_1 = e_4 = 0$ fixes all other homogeneous coordinates of $P_{F_{11}}$. Hence

$$\pi_* \left(S \cdot_{\widehat{Y}_4} T \right) = V\left(s_3, s_5, s_9\right) . \tag{C.2.30}$$

If we consider $B_3 = P_{39}$, then it follows from C.2.26 that $V(s_3, s_5, s_9)$ must be a divisor of degree 18 on $C_{(\mathbf{1},\mathbf{2})_{-1/2}}$. Indeed, this is true because $\overline{K}^3_{P_{39}} = 18$. It is not too hard to repeat this computation and find that $\mathcal{A}'$ in C.2.7 gives

$$D_{(\mathbf{3},\mathbf{2})_{1/6}}\left(\mathcal{A}'\right) = 3 \cdot V(\overline{K}_B, s_3, s_9)\,, \tag{C.2.31}$$

$$D_{(\mathbf{1},\mathbf{2})_{-1/2}}\left(\mathcal{A}'\right) = -3\left[5V(s_3, s_5, s_9) - 2V(\overline{K}_B, s_3, P_H)\right]\,, \tag{C.2.32}$$

$$D_{(\overline{\mathbf{3}},\mathbf{1})_{-2/3}}\left(\mathcal{A}'\right) = 3 \cdot V(\overline{K}_B, s_5, s_9)\,, \tag{C.2.33}$$

$$D_{(\overline{\mathbf{3}},\mathbf{1})_{1/3}}\left(\mathcal{A}'\right) = -3\left[5V(s_3, s_6, s_9) - 2V(\overline{K}_B, s_9, P_R)\right]\,, \tag{C.2.34}$$

$$D_{(\mathbf{1},\mathbf{1})_1}\left(\mathcal{A}'\right) = 3 \cdot V(\overline{K}_B, s_1, s_5)\,. \tag{C.2.35}$$

In this expression, we are using

$$P_H = s_2 s_5^2 + s_1(s_1 s_9 - s_5 s_6)\,, \qquad P_R = s_3 s_5^2 + s_6(s_1 s_6 - s_2 s_5)\,. \tag{C.2.36}$$

By considering $\overline{K}^3_B$-th roots and adding spin bundles on the matter curves, one arrives at the root bundle expressions summarized in C.2.3.

Line bundles from fiber structure

Finally, let us present a third way to compute the induced line bundles. Even though this approach is equivalent, it provides more intuition than the brute-force intersection computations in $\mathrm{CH}^*(X_5)$. To this end we make use of the genesis of the G_4-flux and the fiber structure of $\widehat{Y}_4$, which we outlined in C.1.

Let us apply this strategy for the Higgs curve. We first recall that $\mathcal{A}'$ in C.2.7 can be

thought of as

$$\mathcal{A}' = \mathcal{A}'_{(\mathbf{3},\mathbf{2})_{1/6}} + \mathcal{A}'_{U(1)} = 15 \cdot \mathcal{A}_{(\mathbf{3},\mathbf{2})_{1/6}} + 3 \cdot \pi^* \left(\overline{K}_B \right) \cdot \sigma \in CH^2(\widehat{Y}_4, \mathbb{Z}) \,, \tag{C.2.37}$$

where (in abuse of notation) σ denotes the canonical lift of the 1-form associated to the section $s_1 = V(e_4)$ via the Shioda map. On general grounds, it now follows that

$$\pi_*(S_{\mathbf{R}} \cdot \mathcal{A}'_{U(1)}) = q_{U(1)} \cdot 3\overline{K}_B \Big|_{C_{\mathbf{R}}} \,. \tag{C.2.38}$$

For the Higgs curve, we have $q_{U(1)} = -1/2$. Thus,

$$\pi_* \left(S_{(\mathbf{1},\mathbf{2})_{-1/2}} \cdot \mathcal{A}'_{U(1)} \right) = -\frac{3}{2} \cdot \overline{K}_B \Big|_{C_{(\mathbf{1},\mathbf{2})_{-1/2}}} \,. \tag{C.2.39}$$

Note that (c.f. 6.2.22) $C_{(\mathbf{1},\mathbf{2})_{-1/2}} \cdot C_{(\mathbf{3},\mathbf{2})_{1/6}} = Y_1 \cup Y_2$. Hence, the intersection number of the Higgs matter surface and $\mathcal{A}'_{(\mathbf{3},\mathbf{2})_{1/6}}$ is found in the fiber over Y_1 and Y_2:

$$\mathcal{A}'_{(\mathbf{3},\mathbf{2})_{1/6}} \Big|_{Y_1} \cdot S_{(\mathbf{1},\mathbf{2})_{-1/2}} \Big|_{Y_1} = (1/2, 2/3, 0, 1, 1/3, 0) \cdot (0, 1, 1, 1, 1, 0) = -1/2 \,, \tag{C.2.40}$$

$$\mathcal{A}'_{(\mathbf{3},\mathbf{2})_{1/6}} \Big|_{Y_2} \cdot S_{(\mathbf{1},\mathbf{2})_{-1/2}} \Big|_{Y_2} = (0, 1/2, 2/3, 1, 1/3, 0) \cdot (0, 0, 0, 0, 0, 1) = +1/2 \,. \tag{C.2.41}$$

This implies

$$D_{(\mathbf{1},\mathbf{2})_{-1/2}} \left(\mathcal{A}'_{(\mathbf{3},\mathbf{2})_{1/6}} \right) = 15 \cdot \left[-\frac{1}{2} Y_1 + \frac{1}{2} Y_2 \right] \,. \tag{C.2.42}$$

We now use $Y_1 + Y_2 = \overline{K} \Big|_{C_{(\mathbf{1},\mathbf{2})_{-1/2}}}$ (c.f. 6.2.22) to conclude that

$$\begin{aligned} D_{(\mathbf{1},\mathbf{2})_{-1/2}} \left(\mathcal{A}'_{(\mathbf{3},\mathbf{2})_{1/6}} \right) &= 15 \cdot \left[-\frac{1}{2} Y_1 + \frac{1}{2} Y_2 \right] - \frac{3}{2} \cdot \overline{K} \Big|_{C_{(\mathbf{1},\mathbf{2})_{-1/2}}} \\ &= 6 \, \overline{K} \Big|_{C_{(\mathbf{1},\mathbf{2})_{-1/2}}} - 15 Y_1 \,. \end{aligned} \tag{C.2.43}$$

Noting that $Y_1 = V(s_3, s_5, s_9)$, and $P_H = s_2 s_5^2 + s_1(s_1 s_9 - s_5 s_6)$, we thus find

$$D_{(\mathbf{1},\mathbf{2})_{-1/2}}\left(\mathcal{A}'_{(\mathbf{3},\mathbf{2})_{1/6}}\right) = -3\left[5V(s_3, s_5, s_9) - 2V(\overline{K}_B, s_3, P_H)\right] . \tag{C.2.44}$$

This is exactly the result that we found in C.2.32. Similarly, the line bundle expressions found in C.2.2 for $C_{(\mathbf{1},\mathbf{1})_1}$, $C_{(\overline{\mathbf{3}},\mathbf{1})_{-2/3}}$, $C_{(\overline{\mathbf{3}},\mathbf{1})_{1/3}}$ can be verified by using this strategy. For the quark-doublet curve, the situation is more involved since the matter surface flux is defined over this very matter curve so that self-intersections are to be taken into account. Equivalently, we can give a quick argument by noting that the divisor in question must be a linear combination of the Yukawa loci on $C_{(\mathbf{3},\mathbf{2})_{1/6}}$. Any of these Yukawa loci Y_1, Y_2, Y_3 admits a pullback description:

$$\mathcal{O}_{C_{(\mathbf{3},\mathbf{2})_{1/6}}}(Y_1) \cong \mathcal{O}_{C_{(\mathbf{3},\mathbf{2})_{1/6}}}(Y_3) \cong \overline{K}_{B_3}\Big|_{C_{(\mathbf{3},\mathbf{2})_{1/6}}} , \quad \mathcal{O}_{C_{(\mathbf{3},\mathbf{2})_{1/6}}}(Y_2) \cong 2\overline{K}_{B_3}\Big|_{C_{(\mathbf{3},\mathbf{2})_{1/6}}} . \tag{C.2.45}$$

Therefore, the bundle must be of the form $n \cdot \overline{K}_{B_3}\Big|_{C_{(\mathbf{3},\mathbf{2})_{1/6}}}$ and the prefactor n is fixed by the chiral index. This gives $D_{(\mathbf{3},\mathbf{2})_{1/6}}\left(\mathcal{A}'_{(\mathbf{3},\mathbf{2})_{1/6}}\right) = 3 \cdot \overline{K}_{B_3}\Big|_{C_{(\mathbf{3},\mathbf{2})_{1/6}}}$.

C.2.3 Root bundle constraints

By repeating the intersection computations, we obtain the root bundle constraints as functions of $\overline{K}_B^3$ (c.f. 6.2.37). Since we analyze the case $\overline{K}_B^3 = 18$ in more detail momentarily, let us list the root bundles for such base spaces explicitly:

curve	g	P	d	BN-theory
$C_{(\mathbf{3},\mathbf{2})_{1/6}} = V(s_3, s_9)$	10	$P^{\otimes 36}_{(\mathbf{3},\mathbf{2})_{1/6}} = \overline{K}_{B_3}\big\vert^{\otimes 24}_{C_{(\mathbf{3},\mathbf{2})_{1/6}}}$	12	h^0 h^1 ρ 3 0 10 4 1 6 5 2 0
$C_{(\mathbf{1},\mathbf{2})_{-1/2}} =$ $V\left(s_3, s_2 s_5^2 + s_1(s_1 s_9 - s_5 s_6)\right)$	82	$P^{\otimes 36}_{(\mathbf{1},\mathbf{2})_{-1/2}} = \overline{K}_{B_3}\big\vert^{\otimes 66}_{C_{(\mathbf{1},\mathbf{2})_{-1/2}}} \otimes \mathcal{O}_{C_{(\mathbf{1},\mathbf{2})_{-1/2}}}(-30 \cdot Y_1)$	84	h^0 h^1 ρ 3 0 82 4 1 78 $\vdots$ $\vdots$ $\vdots$ 10 7 12
$C_{(\overline{\mathbf{3}},\mathbf{1})_{-2/3}} = V(s_5, s_9)$	10	$P^{\otimes 36}_{(\overline{\mathbf{3}},\mathbf{1})_{-2/3}} = \overline{K}_{B_3}\big\vert^{\otimes 24}_{C_{(\overline{\mathbf{3}},\mathbf{1})_{-2/3}}}$	12	h^0 h^1 ρ 3 0 10 4 1 6 5 2 0
$C_{(\overline{\mathbf{3}},\mathbf{1})_{1/3}} =$ $V\left(s_9, s_3 s_5^2 + s_6(s_1 s_6 - s_2 s_5)\right)$	82	$P^{\otimes 36}_{(\overline{\mathbf{3}},\mathbf{1})_{1/3}} = \overline{K}_{B_3}\big\vert^{\otimes 66}_{C_{(\overline{\mathbf{3}},\mathbf{1})_{1/3}}} \otimes \mathcal{O}_{C_{(\overline{\mathbf{3}},\mathbf{1})_{1/3}}}(-30 \cdot Y_3)$	84	h^0 h^1 ρ 3 0 82 4 1 78 $\vdots$ $\vdots$ $\vdots$ 10 7 12
$C_{(\mathbf{1},\mathbf{1})_1} = V(s_1, s_5)$	10	$P^{\otimes 36}_{(\mathbf{1},\mathbf{1})_1} = \overline{K}_{B_3}\big\vert^{\otimes 24}_{C_{(\mathbf{1},\mathbf{1})_1}}$	12	h^0 h^1 ρ 3 0 10 4 1 6 5 2 0

The parameter ρ from Brill-Noether theory [150] provides a measure of how likely it is to find a degree d line bundle with certain number of global sections – the larger ρ is, the more likely such bundles exist. Notably, this parameter does not take the root bundle constraints into account. See [128, 48] for an application of Brill-Noether theory to F-theory and further explanations.

In F-theory Standard Model constructions, the toric base spaces must satisfy $\overline{K}_B^3 \in \{6, 10, 18, 30\}$ [32]. Therefore, let us list the root bundle constraints for these values of $\overline{K}_B^3$. For ease of presentation, we will merely list the constraints on $C_{(\mathbf{3},\mathbf{2})_{1/6}}$ and $C_{(\mathbf{1},\mathbf{2})_{-1/2}}$:

$\overline{K}^3_{B_3}$	curve	g	P	d	BN-theory		
					h^0	h^1	ρ
6	$C_{(\mathbf{3},\mathbf{2})_{1/6}} = V(s_3, s_9)$	4	$P^{\otimes 12}_{(\mathbf{3},\mathbf{2})_{1/6}} = \overline{K}_{B_3}\big\vert^{\otimes 12}_{C_{(\mathbf{3},\mathbf{2})_{1/6}}}$	6	3	0	4
					4	1	0
					5	2	-6
	$C_{(\mathbf{1},\mathbf{2})_{-1/2}} =$				h^0	h^1	ρ
					3	0	28
					4	1	24
	$V\left(s_3, s_2 s_5^2 + s_1(s_1 s_9 - s_5 s_6)\right)$	28	$P^{\otimes 12}_{(\mathbf{1},\mathbf{2})_{-1/2}} = \overline{K}_{B_3}\big\vert^{\otimes 30}_{C_{(\mathbf{1},\mathbf{2})_{-1/2}}} \otimes \mathcal{O}_{C_{(\mathbf{1},\mathbf{2})_{-1/2}}}(-30 \cdot Y_1)$	30	$\vdots$	$\vdots$	$\vdots$
					7	4	0
10	$C_{(\mathbf{3},\mathbf{2})_{1/6}} = V(s_3, s_9)$	6	$P^{\otimes 20}_{(\mathbf{3},\mathbf{2})_{1/6}} = \overline{K}_{B_3}\big\vert^{\otimes 16}_{C_{(\mathbf{3},\mathbf{2})_{1/6}}}$	8	h^0	h^1	ρ
					3	0	6
					4	1	2
					5	2	-4
	$C_{(\mathbf{1},\mathbf{2})_{-1/2}} =$				h^0	h^1	ρ
					3	0	46
					4	1	42
	$V\left(s_3, s_2 s_5^2 + s_1(s_1 s_9 - s_5 s_6)\right)$	46	$P^{\otimes 20}_{(\mathbf{1},\mathbf{2})_{-1/2}} = \overline{K}_{B_3}\big\vert^{\otimes 42}_{C_{(\mathbf{1},\mathbf{2})_{-1/2}}} \otimes \mathcal{O}_{C_{(\mathbf{1},\mathbf{2})_{-1/2}}}(-30 \cdot Y_1)$	48	$\vdots$	$\vdots$	$\vdots$
					8	5	6
18	$C_{(\mathbf{3},\mathbf{2})_{1/6}} = V(s_3, s_9)$	10	$P^{\otimes 36}_{(\mathbf{3},\mathbf{2})_{1/6}} = \overline{K}_{B_3}\big\vert^{\otimes 24}_{C_{(\mathbf{3},\mathbf{2})_{1/6}}}$	12	h^0	h^1	ρ
					3	0	10
					4	1	6
					5	2	0
	$C_{(\mathbf{1},\mathbf{2})_{-1/2}} =$				h^0	h^1	ρ
					3	0	82
					4	1	78
	$V\left(s_3, s_2 s_5^2 + s_1(s_1 s_9 - s_5 s_6)\right)$	82	$P^{\otimes 36}_{(\mathbf{1},\mathbf{2})_{-1/2}} = \overline{K}_{B_3}\big\vert^{\otimes 66}_{C_{(\mathbf{1},\mathbf{2})_{-1/2}}} \otimes \mathcal{O}_{C_{(\mathbf{1},\mathbf{2})_{-1/2}}}(-30 \cdot Y_1)$	84	$\vdots$	$\vdots$	$\vdots$
					10	7	12
30	$C_{(\mathbf{3},\mathbf{2})_{1/6}} = V(s_3, s_9)$	16	$P^{\otimes 60}_{(\mathbf{3},\mathbf{2})_{1/6}} = \overline{K}_{B_3}\big\vert^{\otimes 36}_{C_{(\mathbf{3},\mathbf{2})_{1/6}}}$	18	h^0	h^1	ρ
					3	0	16
					4	1	12
					5	2	6
	$C_{(\mathbf{1},\mathbf{2})_{-1/2}} =$				h^0	h^1	ρ
					3	0	136
					4	1	132
	$V\left(s_3, s_2 s_5^2 + s_1(s_1 s_9 - s_5 s_6)\right)$	136	$P^{\otimes 60}_{(\mathbf{1},\mathbf{2})_{-1/2}} = \overline{K}_{B_3}\big\vert^{\otimes 102}_{C_{(\mathbf{1},\mathbf{2})_{-1/2}}} \otimes \mathcal{O}_{C_{(\mathbf{1},\mathbf{2})_{-1/2}}}(-30 \cdot Y_1)$	138	$\vdots$	$\vdots$	$\vdots$
					13	10	6

C.2.4 Limit roots in base space P_{39}

We consider the smooth, complete toric 3-fold base P_{39}, whose Cox ring is $\mathbb{Z}^8$-graded

x_1	x_2	x_3	x_4	x_5	x_6	x_7	x_8	x_9	x_{10}	x_{11}
1	-2	1	0	0	0	0	0	0	0	0
0	1	0	-2	1	0	0	0	0	0	0
0	2	0	-3	0	1	0	0	0	0	0
0	-1	0	1	0	0	1	0	0	0	0
0	1	0	-1	0	0	0	1	0	0	0
0	-1	0	2	0	0	0	0	1	0	0
0	0	0	1	0	0	0	0	0	1	0
0	-1	0	3	0	0	0	0	0	0	1

(C.2.46)

and whose Stanley-Reisner ideal is given by

$$\begin{aligned} I_{\mathrm{SR}} = \langle & x_8x_{11}, x_7x_{11}, x_6x_{11}, x_5x_{11}, x_4x_{11}, x_2x_{11}, x_9x_{10}, x_7x_{10}, x_6x_{10}, x_5x_{10}, \\ & x_4x_{10}, x_2x_{10}, x_8x_9, x_6x_9, x_5x_9, x_4x_9, x_2x_9, x_7x_8, x_5x_8, x_4x_8, x_2x_8, x_6x_7, \\ & x_5x_7, x_4x_7, x_4x_6, x_2x_6, x_2x_5, x_1x_3\rangle\,. \end{aligned} \tag{C.2.47}$$

P_{39} is a particular triangulation of the 39-th polytope in the Kreuzer-Skarke list of toric threefolds [2], hence the name. It follows that $\overline{K}^3_{P_{39}} = 18$. Furthermore, for $D_i = V(x_i)$, we find non-trivial topological intersection numbers

	D_i	D_3	D_6	D_{11}
$D_i \cdot \overline{K}^2_{P_{39}}$	3	3	6	6

(C.2.48)

The remaining divisors have vanishing topological intersection numbers. Even more, for $D_i \in \{D_4, D_5, D_7, D_9\}$, we find $D_i \cdot V(s_i) \cdot V(s_j) = \emptyset$ for any $s_i, s_j \in H^0(P_{39}, \overline{K}_{P_{39}})$. The divisors D_2, D_8, D_{10} intersect the generic curve $V(s_i, s_j)$ trivially but admit non-trivial

intersections with non-generic curves.

In 6.4.2, we discussed roots on the quark-doublet curve $C_{(\overline{\mathbf{3}},\mathbf{2})_{1/6}}$. Here, we provide details on the limit roots on $C_{(\overline{\mathbf{3}},\mathbf{1})_{1/3}} = V\left(s_9, s_3 s_5^2 + s_6(s_1 s_6 - s_2 s_5)\right)$. We use

$$s_1 \to s_6 - s_3\,, \qquad s_2 \to s_5 - \prod_{i=1}^{11} x_i\,, \qquad s_9 \to \prod_{i=1}^{11} x_i\,, \tag{C.2.49}$$

and *generic* s_3, s_5, s_6 to deform this curve into

$$C^{\bullet}_{(\overline{\mathbf{3}},\mathbf{1})_{1/3}} = V\left(\prod_{i=1}^{11} x_i, s_5 - s_6\right) \cup V\left(\prod_{i=1}^{11} x_i, s_3 - s_6\right) \cup V\left(\prod_{i=1}^{11} x_i, s_5 + s_6\right) \equiv Q_1 \cup Q_2 \cup Q_3\,. \tag{C.2.50}$$

It is important to verify that this curve is nodal so that we can apply the limit root techniques outlined in 6.3. A computationally favorable description is that a point p is a node if and only if the Jacobian matrices vanish identically at p but the Hessian matrix does not [195]. Therefore, it is readily verified that for example, the points $V(x_1, s_5 - s_6, s_3 - s_6)$ are indeed nodes.

Consequently, we proceed to identify roots $P^{\bullet}_{(\overline{\mathbf{3}},\mathbf{1})_{1/3}}$ that solve the root bundle constraint in C.2.3 and admit exactly three sections. For this, it suffices to construct solutions to

$$\left(P^{\bullet}_{(\overline{\mathbf{3}},\mathbf{1})_{1/3}}\right)^{\otimes 6} = \overline{K}_{B_3}\Big|^{\otimes 11}_{C^{\bullet}_{(\overline{\mathbf{3}},\mathbf{1})_{1/3}}} \otimes \mathcal{O}_{C^{\bullet}_{(\overline{\mathbf{3}},\mathbf{1})_{1/3}}}(-5\cdot Y_3)\,, \quad h^0\left(C^{\bullet}_{(\overline{\mathbf{3}},\mathbf{1})_{1/3}}, P^{\bullet}_{(\overline{\mathbf{3}},\mathbf{1})_{1/3}}\right) = 3\,, \tag{C.2.51}$$

where $Y_3 = V(s_3, s_6, s_9)$. We notice that $Y_3 \cap Q_1 = Y_3 \cap Q_3 = \emptyset$, which implies

$$\begin{aligned}
\left(P^{\bullet}_{(\overline{\mathbf{3}},\mathbf{1})_{1/3}}\right)^{\otimes 6}\Big|_{Q_1} &= \overline{K}_{B_3}\Big|_{Q_1}^{\otimes 11}\,, \\
\left(P^{\bullet}_{(\overline{\mathbf{3}},\mathbf{1})_{1/3}}\right)^{\otimes 6}\Big|_{Q_2} &= \overline{K}_{B_3}\Big|_{Q_2}^{\otimes 11} \otimes \mathcal{O}_{Q_2}(-5\cdot Y_3) = \overline{K}_{B_3}\Big|_{Q_2}^{\otimes 11} \otimes \overline{K}_{B_3}\Big|_{Q_2}^{\otimes(-5)} = \overline{K}_{B_3}\Big|_{Q_2}^{\otimes 6}\,, \\
\left(P^{\bullet}_{(\overline{\mathbf{3}},\mathbf{1})_{1/3}}\right)^{\otimes 6}\Big|_{Q_3} &= \overline{K}_{B_3}\Big|_{Q_3}^{\otimes 11}\,.
\end{aligned} \tag{C.2.52}$$

These observations allow us to draw a weighted graph, which encodes roots $P^{\bullet}_{(\overline{\mathbf{3}},\mathbf{1})_{1/3}}$ on $C^{\bullet}_{(\overline{\mathbf{3}},\mathbf{1})_{1/3}}$. This graph is displayed in 18.

We find it important to mention that this graph is non-planar. This is remarkable because all other dual graphs considered in this work are planar. To our knowledge, there does not seem to be any result in the literature which suggests that the dual graph of a nodal curve is necessarily planar. In fact, most of the literature, such as [194] and [195], only discuss examples of nodal curves with planar dual graphs. Although there are well-known planarity criterion theorems, such as the Kuratowski's theorem [215], we resorted to excessive computational checks to verify that $C^{\bullet}_{(\overline{\mathbf{3}},\mathbf{1})_{1/3}}$ has a non-planar dual graph 18. A more minimalistic example of this sort is the nodal curve whose dual graph is $K_{3,3}$. There are many interesting questions concerning planarity that arise in graph theory, such as criterion theorems [189, 190], enumeration [191], and other variants of planarity [192, 193]. However, the significance of non-planarity for the geometry of nodal curves is unknown. We hope to return to this interesting question in the future.

Turning back to solving C.2.51, we note that the degrees of the roots encoded by 18 are listed in 19. In particular, the total degree is $d = 84$, as expected for $\chi(P^{\bullet}_{(\overline{\mathbf{3}},\mathbf{1})_{1/3}}) = 3$ on this $g = 82$ curve. Recall that we identify the number of global sections from 6.3.8, i.e. we add the number of sections on all curve components except the exceptional $\mathbb{P}^1$s, which are colored in blue. Therefore, it suffices to focus on the curves $C_1^{Q_1}$, $C_3^{Q_1}$, $C_1^{Q_2}$,

$C_3^{Q_2}$, $C_6^{Q_2}$, $C_1^{Q_3}$ and $C_3^{Q_3}$. Each curve $C_1^{Q_1}$ and $C_1^{Q_3}$ admits 36 roots whereas $C_6^{Q_2}$ only admits a unique root. These roots each have one section. It follows from 6.3.3 that of the roots on $C_3^{Q_1}$, $C_1^{Q_2}$, $C_3^{Q_2}$ and $C_3^{Q_3}$, each curve admits at least 35 roots which have no sections. We have thus found at least $36^2 \cdot 35^4$ solutions to C.2.51. In future works, we wish to investigate which of these root bundles stem from F-theory gauge potentials in $H_D^4(\widehat{Y}_4, \mathbb{Z}(2))$.

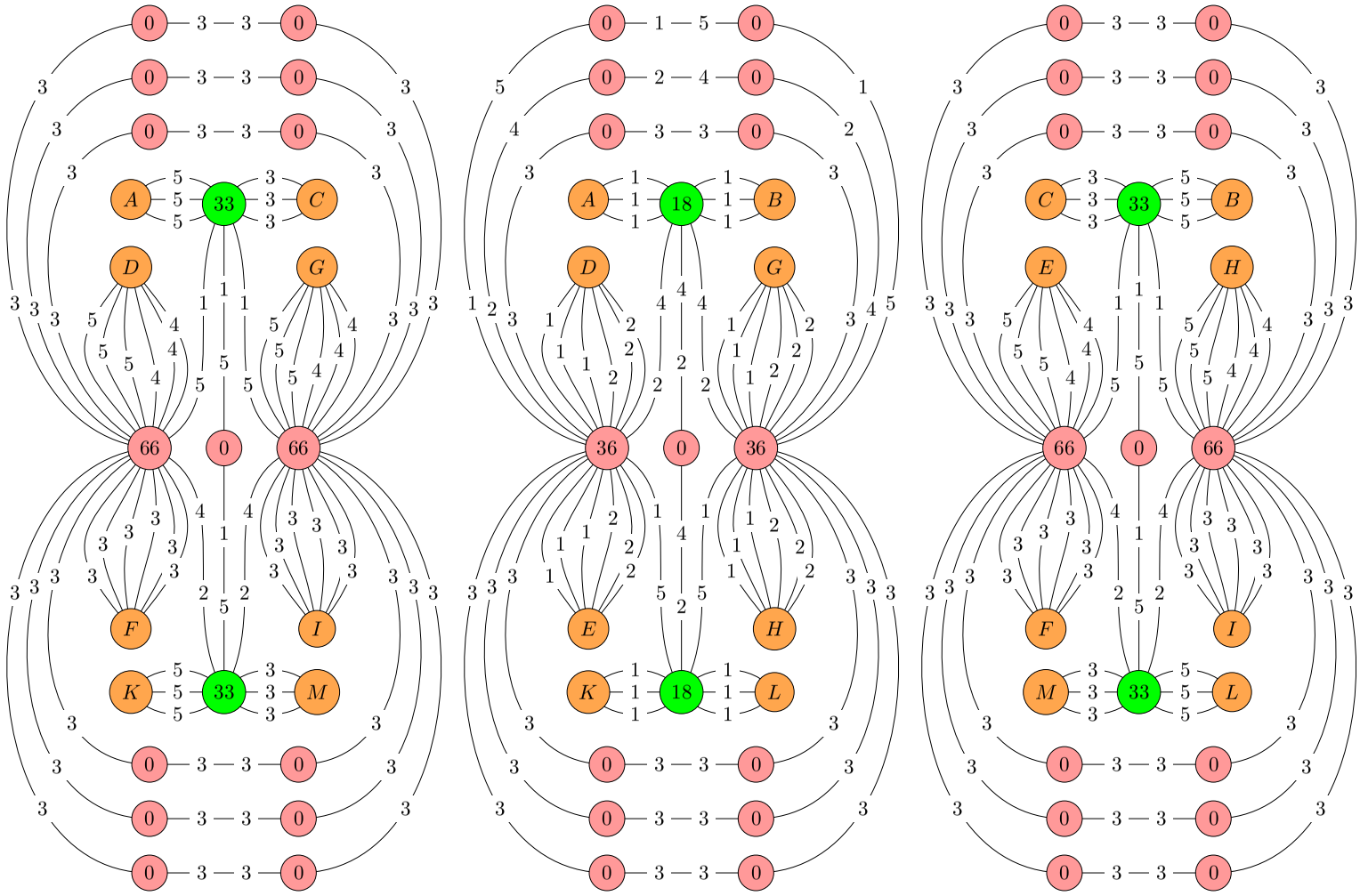

Figure 18: Weighted diagram of roots $P^{\bullet}_{(\overline{\mathbf{3}},\mathbf{1})_{1/3}}$ on $C^{\bullet}_{(\overline{\mathbf{3}},\mathbf{1})_{1/3}}$ which solve C.2.51.

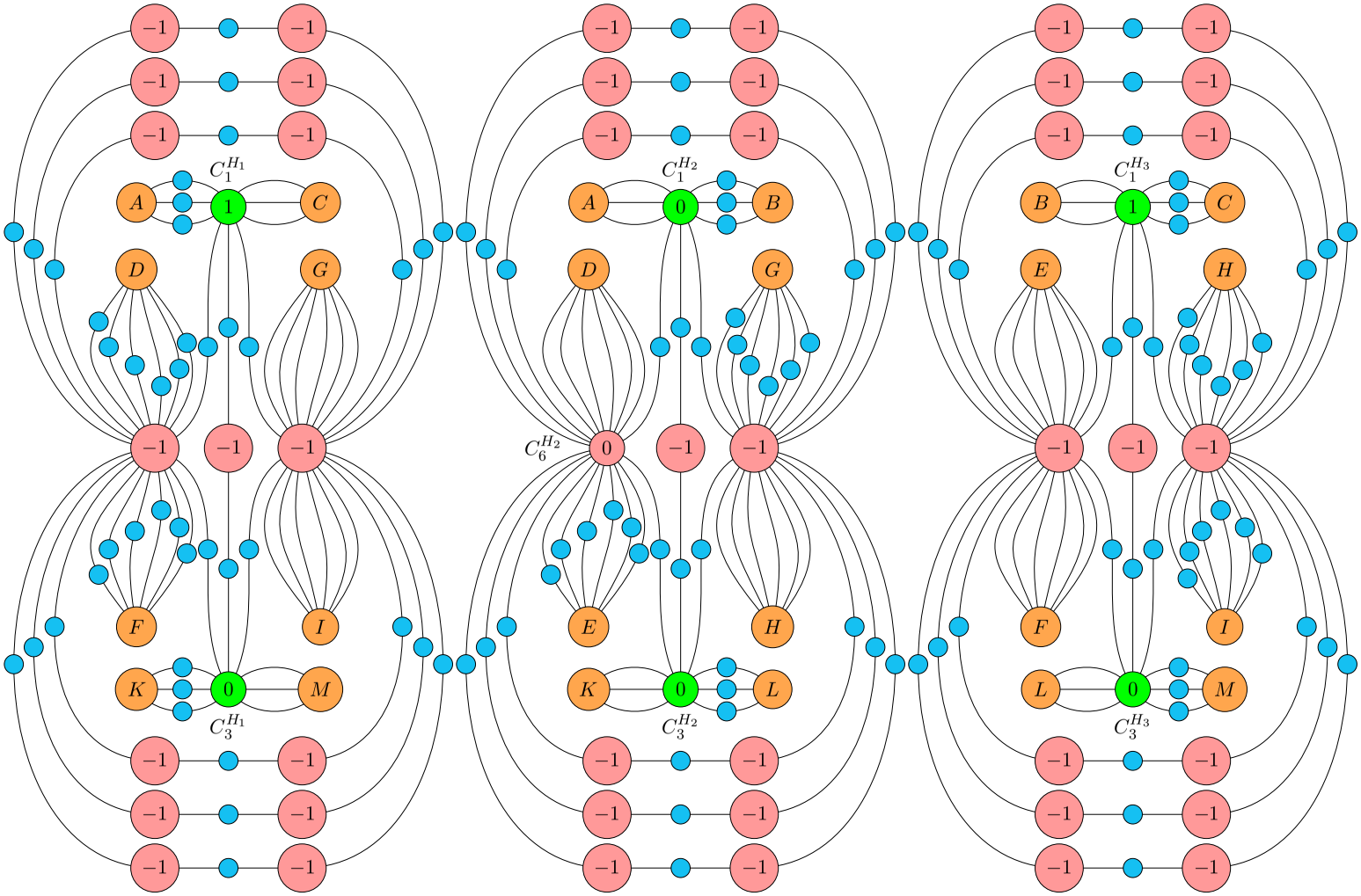

Figure 19: Degrees of roots $P^{\bullet}_{(\overline{\mathbf{3}},\mathbf{1})_{1/3}}$ on $C^{\bullet}_{(\overline{\mathbf{3}},\mathbf{1})_{1/3}}$ encoded by 18. Exceptional $\mathbb{P}^1$s are indicated in blue and each carries a line bundle of degree $d = 1$.

CHAPTER D: Chapter 7 Appendix

BIBLIOGRAPHY

[1] L. Lin, *Gauge fluxes in F-theory compactifications*, Ph.D. thesis, U. Heidelberg (main), 2016. 10.11588/heidok.00021601.

[2] M. Kreuzer and H. Skarke, *Classification of reflexive polyhedra in three-dimensions*, *Adv. Theor. Math. Phys.* **2** (1998) 853 [hep-th/9805190].

[3] J. Polchinski, *String theory. Vol. 1: An introduction to the bosonic string*, Cambridge Monographs on Mathematical Physics, Cambridge University Press (12, 2007), 10.1017/CBO9780511816079.

[4] J. Polchinski, *String theory. Vol. 2: Superstring theory and beyond*, Cambridge Monographs on Mathematical Physics, Cambridge University Press (12, 2007), 10.1017/CBO9780511618123.

[5] M.B. Green, J.H. Schwarz and E. Witten, *SUPERSTRING THEORY. VOL. 1: INTRODUCTION*, Cambridge Monographs on Mathematical Physics (7, 1988).

[6] M.B. Green, J.H. Schwarz and E. Witten, *Superstring Theory Vol. 2: 25th Anniversary Edition*, Cambridge Monographs on Mathematical Physics, Cambridge University Press (11, 2012), 10.1017/CBO9781139248570.

[7] L.E. Ibanez and A.M. Uranga, *String theory and particle physics: An introduction to string phenomenology*, Cambridge University Press (2, 2012).

[8] R. Blumenhagen, D. Lüst and S. Theisen, *Basic concepts of string theory*, Theoretical and Mathematical Physics, Springer, Heidelberg, Germany (2013), 10.1007/978-3-642-29497-6.

[9] E. Witten, *String theory dynamics in various dimensions*, *Nucl. Phys. B* **443** (1995) 85 [hep-th/9503124].

[10] T. Kaluza, *Zum Unitatsproblem der Physik*, *Sitzungsberichte der Koniglich Preusischen Akademie der Wissenschaften (Berlin* (1921) 966.

[11] O. Klein, *Quantentheorie und funfdimensionale Relativitatstheorie*, *Zeitschrift fur Physik* **37** (1926) 895.

[12] O. Klein, *The Atomicity of Electricity as a Quantum Theory Law*, *nat* **118** (1926) 516.

[13] P. Candelas, G.T. Horowitz, A. Strominger and E. Witten, *Vacuum Configurations for Superstrings*, *Nucl. Phys. B* **258** (1985) 46.

[14] E. Calabi, *On kähler manifolds with vanishing canonical class*, in *Algebraic Geometry and Topology*, R.H. Fox, ed., pp. 78–89, Princeton University Press (2015), DOI.

[15] S. Yau, *On the ricci curvature of a compact kahler manifold and the complex monge-ampere equation, i**, *Communications on Pure and Applied Mathematics* **31** (1978) 339.

[16] J. Dai, R.G. Leigh and J. Polchinski, *New Connections Between String Theories*, *Modern Physics Letters A* **4** (1989) 2073.

[17] M. Berkooz, M.R. Douglas and R.G. Leigh, *Branes intersecting at angles*, *Nucl. Phys.* **B480** (1996) 265 [hep-th/9606139].

[18] G. Aldazabal, S. Franco, L.E. Ibanez, R. Rabadan and A.M. Uranga, *D = 4 chiral string compactifications from intersecting branes*, *J. Math. Phys.* **42** (2001) 3103 [hep-th/0011073].

[19] G. Aldazabal, S. Franco, L.E. Ibanez, R. Rabadan and A.M. Uranga, *Intersecting brane worlds*, *JHEP* **02** (2001) 047 [hep-ph/0011132].

[20] L.E. Ibanez, F. Marchesano and R. Rabadan, *Getting just the standard model at intersecting branes*, *JHEP* **11** (2001) 002 [hep-th/0105155].

[21] R. Blumenhagen, B. Kors, D. Lüst and T. Ott, *The standard model from stable intersecting brane world orbifolds*, *Nucl. Phys.* **B616** (2001) 3 [hep-th/0107138].

[22] M. Cvetič, G. Shiu and A.M. Uranga, *Three family supersymmetric standard - like models from intersecting brane worlds*, *Phys. Rev. Lett.* **87** (2001) 201801 [hep-th/0107143].

[23] M. Cvetič, G. Shiu and A.M. Uranga, *Chiral four-dimensional N=1 supersymmetric type 2A orientifolds from intersecting D6 branes*, *Nucl. Phys.* **B615** (2001) 3 [hep-th/0107166].

[24] R. Blumenhagen, M. Cvetic, P. Langacker and G. Shiu, *Toward realistic intersecting D-brane models*, *Ann. Rev. Nucl. Part. Sci.* **55** (2005) 71 [hep-th/0502005].

[25] D. Lust, *Intersecting brane worlds: A Path to the standard model?*, *Class. Quant. Grav.* **21** (2004) S1399 [hep-th/0401156].

[26] T. Weigand, *F-theory*, *PoS* **TASI2017** (2018) 016 [1806.01854].

[27] C. Vafa, *Evidence for F theory*, *Nucl. Phys. B* **469** (1996) 403 [hep-th/9602022].

[28] W. Taylor and Y.-N. Wang, *A Monte Carlo exploration of threefold base geometries for 4d F-theory vacua*, *JHEP* **01** (2016) 137 [1510.04978].

[29] W. Taylor and Y.-N. Wang, *The F-theory geometry with most flux vacua*, *JHEP* **12** (2015) 164 [1511.03209].

[30] J. Halverson and J. Tian, *Cost of seven-brane gauge symmetry in a quadrillion F-theory compactifications*, *Phys. Rev. D* **95** (2017) 026005 [1610.08864].

[31] J. Halverson, C. Long and B. Sung, *Algorithmic universality in F-theory compactifications*, *Phys. Rev. D* **96** (2017) 126006 [1706.02299].

[32] M. Cvetič, J. Halverson, L. Lin, M. Liu and J. Tian, *Quadrillion F-Theory Compactifications with the Exact Chiral Spectrum of the Standard Model*, *Phys. Rev. Lett.* **123** (2019) 101601 [1903.00009].

[33] W. Taylor, *TASI Lectures on Supergravity and String Vacua in Various Dimensions*, 1104.2051.

[34] T. Weigand, *Lectures on F-theory compactifications and model building*, *Class. Quant. Grav.* **27** (2010) 214004 [1009.3497].

[35] A. Maharana and E. Palti, *Models of Particle Physics from Type IIB String Theory and F-theory: A Review*, *Int. J. Mod. Phys. A* **28** (2013) 1330005 [1212.0555].

[36] T.W. Grimm and H. Hayashi, *F-theory fluxes, Chirality and Chern-Simons theories*, *JHEP* **03** (2012) 027 [1111.1232].

[37] S. Krause, C. Mayrhofer and T. Weigand, *Gauge Fluxes in F-theory and Type IIB Orientifolds*, *JHEP* **08** (2012) 119 [1202.3138].

[38] V. Braun, T.W. Grimm and J. Keitel, *Geometric Engineering in Toric F-Theory and GUTs with U(1) Gauge Factors*, *JHEP* **12** (2013) 069 [1306.0577].

[39] M. Cvetič, A. Grassi, D. Klevers and H. Piragua, *Chiral Four-Dimensional F-Theory Compactifications With SU(5) and Multiple U(1)-Factors*, *JHEP* **04** (2014) 010 [1306.3987].

[40] M. Cvetic, D. Klevers, D.K.M. Peña, P.-K. Oehlmann and J. Reuter, *Three-Family Particle Physics Models from Global F-theory Compactifications*, *JHEP* **08** (2015) 087 [1503.02068].

[41] L. Lin, C. Mayrhofer, O. Till and T. Weigand, *Fluxes in F-theory Compactifications on Genus-One Fibrations*, *JHEP* **01** (2016) 098 [1508.00162].

[42] L. Lin and T. Weigand, *G 4 -flux and standard model vacua in F-theory*, *Nucl. Phys. B* **913** (2016) 209 [1604.04292].

[43] S. Krause, C. Mayrhofer and T. Weigand, *G_4 flux, chiral matter and singularity resolution in F-theory compactifications*, *Nucl. Phys. B* **858** (2012) 1 [1109.3454].

[44] M. Cvetič, L. Lin, M. Liu and P.-K. Oehlmann, *An F-theory Realization of the Chiral MSSM with $\mathbb{Z}_2$-Parity*, *JHEP* **09** (2018) 089 [1807.01320].

[45] M. Bies, C. Mayrhofer, C. Pehle and T. Weigand, *Chow groups, Deligne cohomology and massless matter in F-theory*, 1402.5144.

[46] M. Bies, C. Mayrhofer and T. Weigand, *Gauge Backgrounds and Zero-Mode Counting in F-Theory*, *JHEP* **11** (2017) 081 [1706.04616].

[47] M. Bies, *Cohomologies of coherent sheaves and massless spectra in F-theory*, Ph.D. thesis, Heidelberg U., 2, 2018. 1802.08860. 10.11588/heidok.00024045.

[48] M. Bies, M. Cvetič, R. Donagi, L. Lin, M. Liu and F. Ruehle, *Machine Learning and Algebraic Approaches towards Complete Matter Spectra in 4d F-theory*, *JHEP* **01** (2021) 196 [2007.00009].

[49] M. Bies, M. Cvetič, R. Donagi, M. Liu and M. Ong, *Root Bundles and Towards Exact Matter Spectra of F-theory MSSMs*, 2102.10115.

[50] M. Bies, M. Cvetič and M. Liu, *Statistics of Limit Root Bundles Relevant for Exact Matter Spectra of F-Theory MSSMs*, 2104.08297.

[51] J.H. Schwarz, *An SL(2,Z) multiplet of type IIB superstrings*, *Phys. Lett. B* **360** (1995) 13 [hep-th/9508143].

[52] A. Sen, *F theory and orientifolds*, *Nucl. Phys. B* **475** (1996) 562 [hep-th/9605150].

[53] M.R. Gaberdiel and B. Zwiebach, *Exceptional groups from open strings*, *Nucl. Phys. B* **518** (1998) 151 [hep-th/9709013].

[54] M.R. Gaberdiel, T. Hauer and B. Zwiebach, *Open string-string junction transitions*, *Nucl. Phys. B* **525** (1998) 117 [hep-th/9801205].

[55] O. DeWolfe and B. Zwiebach, *String junctions for arbitrary Lie algebra representations*, *Nucl. Phys. B* **541** (1999) 509 [hep-th/9804210].

[56] K. Kodaira, *On the structure of compact complex analytic surfaces, ii*, *American Journal of Mathematics* **88** (1966) 682.

[57] A. Grassi and D.R. Morrison, *Anomalies and the Euler characteristic of elliptic Calabi-Yau threefolds*, *Commun. Num. Theor. Phys.* **6** (2012) 51 [1109.0042].

[58] A. Grassi and D.R. Morrison, *Group representations and the Euler characteristic of elliptically fibered Calabi-Yau threefolds*, math/0005196.

[59] R. Donagi and M. Wijnholt, *Model Building with F-Theory*, *Adv. Theor. Math. Phys.* **15** (2011) 1237 [0802.2969].

[60] C. Beasley, J.J. Heckman and C. Vafa, *GUTs and Exceptional Branes in F-theory - I*, *JHEP* **01** (2009) 058 [0802.3391].

[61] C. Beasley, J.J. Heckman and C. Vafa, *GUTs and Exceptional Branes in F-theory - II: Experimental Predictions*, *JHEP* **01** (2009) 059 [0806.0102].

[62] R. Donagi and M. Wijnholt, *Breaking GUT Groups in F-Theory*, *Adv. Theor. Math. Phys.* **15** (2011) 1523 [0808.2223].

[63] E. Dudas and E. Palti, *Froggatt-Nielsen models from E(8) in F-theory GUTs*, *JHEP* **01** (2010) 127 [0912.0853].

[64] D.R. Morrison and C. Vafa, *Compactifications of F theory on Calabi-Yau threefolds. 2.*, *Nucl. Phys.* **B476** (1996) 437 [hep-th/9603161].

[65] T.W. Grimm and T. Weigand, *On Abelian Gauge Symmetries and Proton Decay in Global F-theory GUTs*, *Phys. Rev.* **D82** (2010) 086009 [1006.0226].

[66] D.R. Morrison and D.S. Park, *F-Theory and the Mordell-Weil Group of Elliptically-Fibered Calabi-Yau Threefolds*, *JHEP* **10** (2012) 128 [1208.2695].

[67] M. Cvetič, T.W. Grimm and D. Klevers, *Anomaly Cancellation And Abelian Gauge Symmetries In F-theory*, *JHEP* **02** (2013) 101 [1210.6034].

[68] C. Mayrhofer, E. Palti and T. Weigand, *U(1) symmetries in F-theory GUTs with multiple sections*, *JHEP* **03** (2013) 098 [1211.6742].

[69] J. Borchmann, C. Mayrhofer, E. Palti and T. Weigand, *SU(5) Tops with Multiple U(1)s in F-theory*, *Nucl. Phys.* **B882** (2014) 1 [1307.2902].

[70] S. Krippendorf, D.K. Mayorga Peña, P.-K. Oehlmann and F. Ruehle, *Rational F-Theory GUTs without exotics*, *JHEP* **07** (2014) 013 [1401.5084].

[71] C. Lawrie, S. Schafer-Nameki and J.-M. Wong, *F-theory and All Things Rational: Surveying U(1) Symmetries with Rational Sections*, *JHEP* **09** (2015) 144 [1504.05593].

[72] S. Krippendorf, S. Schafer-Nameki and J.-M. Wong, *Froggatt-Nielsen meets Mordell-Weil: A Phenomenological Survey of Global F-theory GUTs with U(1)s*, *JHEP* **11** (2015) 008 [1507.05961].

[73] A.P. Braun, A. Collinucci and R. Valandro, *Hypercharge flux in F-theory and the stable Sen limit*, *JHEP* **07** (2014) 121 [1402.4096].

[74] J. Marsano, H. Clemens, T. Pantev, S. Raby and H.-H. Tseng, *A Global SU(5) F-theory model with Wilson line breaking*, *JHEP* **01** (2013) 150 [1206.6132].

[75] K.-S. Choi, *On the Standard Model Group in F-theory*, *Eur. Phys. J.* **C74** (2014) 2939 [1309.7297].

[76] L. Lin and T. Weigand, *Towards the Standard Model in F-theory*, *Fortsch. Phys.* **63** (2015) 55 [1406.6071].

[77] L.M. Krauss and F. Wilczek, *Discrete Gauge Symmetry in Continuum Theories*, *Phys. Rev. Lett.* **62** (1989) 1221.

[78] T. Banks and N. Seiberg, *Symmetries and Strings in Field Theory and Gravity*, *Phys. Rev.* **D83** (2011) 084019 [1011.5120].

[79] L. Ibáñez and G. Ross, *Discrete gauge symmetry anomalies*, *Physics Letters B* **260** (1991) 291.

[80] R. Barbier et al., *R-parity violating supersymmetry*, *Phys. Rept.* **420** (2005) 1 [hep-ph/0406039].

[81] Y. Kao and T. Takeuchi, *Single-Coupling Bounds on R-parity violating Supersymmetry, an update*, 0910.4980.

[82] D. Klevers, D.K. Mayorga Pena, P.-K. Oehlmann, H. Piragua and J. Reuter, *F-Theory on all Toric Hypersurface Fibrations and its Higgs Branches*, *JHEP* **01** (2015) 142 [1408.4808].

[83] T.W. Grimm, A. Kapfer and D. Klevers, *The Arithmetic of Elliptic Fibrations in Gauge Theories on a Circle*, *JHEP* **06** (2016) 112 [1510.04281].

[84] V. Braun and D.R. Morrison, *F-theory on Genus-One Fibrations*, *JHEP* **08** (2014) 132 [1401.7844].

[85] L.B. Anderson, I.n. García-Etxebarria, T.W. Grimm and J. Keitel, *Physics of F-theory compactifications without section*, *JHEP* **12** (2014) 156 [1406.5180].

[86] I.n. García-Etxebarria, T.W. Grimm and J. Keitel, *Yukawas and discrete symmetries in F-theory compactifications without section*, *JHEP* **11** (2014) 125 [1408.6448].

[87] C. Mayrhofer, E. Palti, O. Till and T. Weigand, *Discrete Gauge Symmetries by Higgsing in four-dimensional F-Theory Compactifications*, *JHEP* **12** (2014) 068 [1408.6831].

[88] C. Mayrhofer, E. Palti, O. Till and T. Weigand, *On Discrete Symmetries and Torsion Homology in F-Theory*, *JHEP* **06** (2015) 029 [1410.7814].

[89] M. Cvetič, R. Donagi, D. Klevers, H. Piragua and M. Poretschkin, *F-theory vacua with $\mathbb{Z}_3$ gauge symmetry*, *Nucl. Phys. B* **898** (2015) 736 [1502.06953].

[90] P. Candelas and A. Font, *Duality between the webs of heterotic and type II vacua*, *Nucl. Phys. B* **511** (1998) 295 [hep-th/9603170].

[91] V. Bouchard and H. Skarke, *Affine Kac-Moody algebras, CHL strings and the classification of tops*, *Adv. Theor. Math. Phys.* **7** (2003) 205 [hep-th/0303218].

[92] W. Buchmuller, M. Dierigl, P.-K. Oehlmann and F. Ruehle, *The Toric SO(10) F-Theory Landscape*, *JHEP* **12** (2017) 035 [1709.06609].

[93] M. Cvetic and L. Lin, *The Global Gauge Group Structure of F-theory Compactification with U(1)s*, *JHEP* **01** (2018) 157 [1706.08521].

[94] W. Decker, G.-M. Greuel, G. Pfister and H. Schönemann, "SINGULAR 4-2-0 — A computer algebra system for polynomial computations." http://www.singular.uni-kl.de, 2020.

[95] K. Dasgupta, G. Rajesh and S. Sethi, *M theory, orientifolds and G - flux*, *JHEP* **08** (1999) 023 [hep-th/9908088].

[96] D.K. Mayorga Pena and R. Valandro, *Weak coupling limit of F-theory models with MSSM spectrum and massless U(1)'s*, *JHEP* **03** (2018) 107 [1708.09452].

[97] E. Witten, *On flux quantization in M theory and the effective action*, *J. Geom. Phys.* **22** (1997) 1 [hep-th/9609122].

[98] S. Sethi, C. Vafa and E. Witten, *Constraints on low dimensional string compactifications*, *Nucl. Phys. B* **480** (1996) 213 [hep-th/9606122].

[99] H.K. Dreiner, C. Luhn and M. Thormeier, *What is the discrete gauge symmetry of the MSSM?*, *Phys. Rev. D* **73** (2006) 075007 [hep-ph/0512163].

[100] T.W. Grimm, T.G. Pugh and D. Regalado, *Non-Abelian discrete gauge symmetries in F-theory*, *JHEP* **02** (2016) 066 [1504.06272].

[101] V. Braun, M. Cvetic, R. Donagi and M. Poretschkin, *Type II String Theory on Calabi-Yau Manifolds with Torsion and Non-Abelian Discrete Gauge Symmetries*, *JHEP* **07** (2017) 129 [1702.08071].

[102] M. Cvetič, J.J. Heckman and L. Lin, *Towards Exotic Matter and Discrete Non-Abelian Symmetries in F-theory*, *JHEP* **11** (2018) 001 [1806.10594].

[103] V. Braun, T.W. Grimm and J. Keitel, *Complete Intersection Fibers in F-Theory*, *JHEP* **03** (2015) 125 [1411.2615].

[104] P.-K. Oehlmann, J. Reuter and T. Schimannek, *Mordell-Weil Torsion in the Mirror of Multi-Sections*, *JHEP* **12** (2016) 031 [1604.00011].

[105] Y. Kimura, *Discrete Gauge Groups in F-theory Models on Genus-One Fibered Calabi-Yau 4-folds without Section*, *JHEP* **04** (2017) 168 [1608.07219].

[106] S. Ashok and M.R. Douglas, *Counting flux vacua*, *JHEP* **01** (2004) 060 [hep-th/0307049].

[107] R. Blumenhagen, F. Gmeiner, G. Honecker, D. Lüst and T. Weigand, *The Statistics of supersymmetric D-brane models*, *Nucl. Phys.* **B713** (2005) 83 [hep-th/0411173].

[108] L.B. Anderson, J. Gray, A. Lukas and E. Palti, *Heterotic Line Bundle Standard Models*, *JHEP* **06** (2012) 113 [1202.1757].

[109] V. Braun, Y.-H. He, B.A. Ovrut and T. Pantev, *A Heterotic standard model*, *Phys. Lett.* **B618** (2005) 252 [hep-th/0501070].

[110] V. Bouchard and R. Donagi, *An SU(5) heterotic standard model*, *Phys. Lett.* **B633** (2006) 783 [hep-th/0512149].

[111] A. Collinucci and R. Savelli, *On Flux Quantization in F-Theory*, *JHEP* **02** (2012) 015 [1011.6388].

[112] K. Intriligator, H. Jockers, P. Mayr, D.R. Morrison and M.R. Plesser, *Conifold Transitions in M-theory on Calabi-Yau Fourfolds with Background Fluxes*, *Adv. Theor. Math. Phys.* **17** (2013) 601 [1203.6662].

[113] T.W. Grimm, *The N=1 effective action of F-theory compactifications*, *Nucl. Phys.* **B845** (2011) 48 [1008.4133].

[114] T.W. Grimm, M. Kerstan, E. Palti and T. Weigand, *Massive Abelian Gauge Symmetries and Fluxes in F-theory*, *JHEP* **12** (2011) 004 [1107.3842].

[115] D.S. Park, *Anomaly Equations and Intersection Theory*, *JHEP* **01** (2012) 093 [1111.2351].

[116] W. Stein et al., *Sage Mathematics Software (Version 8.4)*. The Sage Development Team, 2018.

[117] F. Bonetti and T.W. Grimm, *Six-dimensional (1,0) effective action of F-theory via M-theory on Calabi-Yau threefolds*, *JHEP* **05** (2012) 019 [1112.1082].

[118] M. Demirtas, C. Long, L. McAllister and M. Stillman, *The Kreuzer-Skarke Axiverse*, 1808.01282.

[119] O.J. Ganor, *A Note on zeros of superpotentials in F theory*, *Nucl. Phys.* **B499** (1997) 55 [hep-th/9612077].

[120] P. Berglund, T. Hubsch and L. Parkes, *Gauge Neutral Matter in Three Generation Superstring Compactifications*, *Mod. Phys. Lett. A* **5** (1990) 1485.

[121] P. Berglund and T. Hubsch, *Twisted three generation compactification*, *Phys. Lett. B* **260** (1991) 32.

[122] R. Donagi, Y.-H. He, B.A. Ovrut and R. Reinbacher, *Moduli dependent spectra of heterotic compactifications*, *Phys. Lett. B* **598** (2004) 279 [hep-th/0403291].

[123] R. Donagi, Y.-H. He, B.A. Ovrut and R. Reinbacher, *The Particle spectrum of heterotic compactifications*, *JHEP* **12** (2004) 054 [hep-th/0405014].

[124] V. Bouchard, M. Cvetič and R. Donagi, *Tri-linear couplings in an heterotic minimal supersymmetric standard model*, *Nucl. Phys.* **B745** (2006) 62 [hep-th/0602096].

[125] E.I. Buchbinder, A. Lukas, B.A. Ovrut and F. Ruehle, *Heterotic Instantons for Monad and Extension Bundles*, *JHEP* **02** (2020) 081 [1912.07222].

[126] E.I. Buchbinder, A. Lukas, B.A. Ovrut and F. Ruehle, *Instantons and Hilbert Functions*, 1912.08358.

[127] J. Gray and J. Wang, *Jumping Spectra and Vanishing Couplings in Heterotic Line Bundle Standard Models*, *JHEP* **11** (2019) 073 [1906.09373].

[128] T. Watari, *Vector-like pairs and Brill–Noether theory*, *Phys. Lett. B* **762** (2016) 145 [1608.00248].

[129] A.P. Braun, A. Collinucci and R. Valandro, *G-flux in F-theory and algebraic cycles*, *Nucl. Phys.* **B856** (2012) 129 [1107.5337].

[130] J. Marsano and S. Schafer-Nameki, *Yukawas, G-flux, and Spectral Covers from Resolved Calabi-Yau's*, *JHEP* **11** (2011) 098 [1108.1794].

[131] T.W. Grimm and H. Hayashi, *F-theory fluxes, Chirality and Chern-Simons theories*, *JHEP* **1203** (2012) 027 [1111.1232].

[132] C. Mayrhofer, E. Palti and T. Weigand, *Hypercharge Flux in IIB and F-theory: Anomalies and Gauge Coupling Unification*, *JHEP* **09** (2013) 082 [1303.3589].

[133] G. Curio and R.Y. Donagi, *Moduli in N=1 heterotic / F theory duality*, *Nucl.Phys.* **B518** (1998) 603 [hep-th/9801057].

[134] R. Donagi and M. Wijnholt, *Gluing Branes, I*, *JHEP* **1305** (2013) 068 [1104.2610].

[135] R. Donagi and M. Wijnholt, *Gluing Branes II: Flavour Physics and String Duality*, *JHEP* **05** (2013) 092 [1112.4854].

[136] L.B. Anderson, J.J. Heckman and S. Katz, *T-Branes and Geometry*, *JHEP* **05** (2014) 080 [1310.1931].

[137] Y.-H. He, *Deep-Learning the Landscape*, 1706.02714.

[138] D. Krefl and R.-K. Seong, *Machine Learning of Calabi-Yau Volumes*, *Phys. Rev. D* **96** (2017) 066014 [1706.03346].

[139] F. Ruehle, *Evolving neural networks with genetic algorithms to study the String Landscape*, *JHEP* **08** (2017) 038 [1706.07024].

[140] J. Carifio, J. Halverson, D. Krioukov and B.D. Nelson, *Machine Learning in the String Landscape*, *JHEP* **09** (2017) 157 [1707.00655].

[141] F. Ruehle, *Data science applications to string theory*, *Phys. Rept.* **839** (2020) 1.

[142] D. Klaewer and L. Schlechter, *Machine Learning Line Bundle Cohomologies of Hypersurfaces in Toric Varieties*, *Phys. Lett. B* **789** (2019) 438 [1809.02547].

[143] C.R. Brodie, A. Constantin, R. Deen and A. Lukas, *Machine Learning Line Bundle Cohomology*, 1906.08730.

[144] C.R. Brodie, A. Constantin, R. Deen and A. Lukas, *Topological Formulae for the Zeroth Cohomology of Line Bundles on Surfaces*, 1906.08363.

[145] C.R. Brodie, A. Constantin, R. Deen and A. Lukas, *Index Formulae for Line Bundle Cohomology on Complex Surfaces*, 1906.08769.

[146] M. Bies, "SheafCohomologyOnToricVarieties." https://github.com/homalg-project/ToricVarieties_project/tree/master/SheafCohomologyOnToricVarieties, 2020.

[147] M. Bies, M. Cvetič, R. Donagi, L. Lin, M. Liu and F. Rühle, "Database." https://github.com/Learning-line-bundle-cohomology/Database, 2020.

[148] M. Bies, "H0Approximator." https://github.com/homalg-project/ToricVarieties_project/tree/master/H0Approximator, 2020.

[149] M. Cvetič and L. Lin, *TASI Lectures on Abelian and Discrete Symmetries in F-theory*, *PoS* **TASI2017** (2018) 020 [1809.00012].

[150] Brill, *Ueber die algebraischen Functionen und ihre Anwendung in der Geometrie. (Zus. mit Noether)*, *Mathematische Annalen* **7** (1874) 269.

[151] D. Mumford, *Curves and their Jacobians*, The Ziwet Lectures, University of Michigan Press (1975).

[152] P.A. Griffiths and J. Harris, *Principles of algebraic geometry*, Wiley classics library, Wiley, New York, NY (1994).

[153] P. Griffiths and J. Harris, *On the variety of special linear systems on a general algebraic curve*, *Duke Math. J.* **47** (1980) 233.

[154] I. Bacharach, *Ueber den Cayley'schen Schnittpunktsatz*, *Mathematische Annalen* **26** (1886) 275.

[155] C. Arthur, "On the Intersection of Curves." online, 1889.

[156] D. Eisenbud, M. Green and J. Harris, *Cayley-Bacharach theorems and conjectures*, *Bulletin of the American Mathematical Society* **33** (1996) 295.

[157] D.R. Grayson and M.E. Stillman, "Macaulay2, a software system for research in algebraic geometry." Available at `http://www.math.uiuc.edu/Macaulay2/`.

[158] W. Bosma, J. Cannon and C. Playoust, *The Magma algebra system. I. The user language*, *J. Symbolic Comput.* **24** (1997) 235.

[159] B.R. Greene, D.R. Morrison and M.R. Plesser, *Mirror manifolds in higher dimension*, *Commun. Math. Phys.* **173** (1995) 559 [`hep-th/9402119`].

[160] A.P. Braun and T. Watari, *The Vertical, the Horizontal and the Rest: anatomy of the middle cohomology of Calabi-Yau fourfolds and F-theory applications*, *JHEP* **01** (2015) 047 [`1408.6167`].

[161] B.R. Greene, K.H. Kirklin, P.J. Miron and G.G. Ross, *A Superstring Inspired Standard Model*, *Phys. Lett.* **B180** (1986) 69.

[162] L.B. Anderson, J. Gray, Y.-H. He and A. Lukas, *Exploring Positive Monad Bundles And A New Heterotic Standard Model*, *JHEP* **02** (2010) 054 [`0911.1569`].

[163] L.B. Anderson, J. Gray, A. Lukas and E. Palti, *Two Hundred Heterotic Standard Models on Smooth Calabi-Yau Threefolds*, *Phys. Rev.* **D84** (2011) 106005 [`1106.4804`].

[164] T.L. Gomez, S. Lukic and I. Sols, *Constraining the Kahler moduli in the heterotic standard model*, *Commun. Math. Phys.* **276** (2007) 1 [`hep-th/0512205`].

[165] V. Bouchard and R. Donagi, *On heterotic model constraints*, *JHEP* **08** (2008) 060 [`0804.2096`].

[166] D.R. Morrison and C. Vafa, *Compactifications of F theory on Calabi-Yau threefolds. 1*, *Nucl.Phys.* **B473** (1996) 74 [`hep-th/9602114`].

[167] D.R. Morrison and C. Vafa, *Compactifications of F theory on Calabi-Yau threefolds. 2.*, *Nucl.Phys.* **B476** (1996) 437 [`hep-th/9603161`].

[168] The Toric Varieties project authors, "The `ToricVarieties` project." (`https://github.com/homalg-project/ToricVarieties_project`), 2019–2020.

[169] The Sage Developers, "Sagemath, the Sage Mathematics Software System (Version 8.5)." `http://www.sagemath.org`, 2018.

[170] L. Caporaso, C. Casagrande and M. Cornalba, *Moduli of Roots of Line Bundles on Curves*, *Transactions of the American Mathematical Society* **359** (2007) 3733 [`math/0404078`].

[171] G. Farkas and M. Kemeny, *The Prym–Green conjecture for torsion line bundles of high order*, *Duke Mathematical Journal* **166** (2017) 1103–1124 [`1509.07162`].

[172] H. Hayashi, R. Tatar, Y. Toda, T. Watari and M. Yamazaki, *New Aspects of Heterotic–F Theory Duality*, *Nucl. Phys. B* **806** (2009) 224 [`0805.1057`].

[173] R. Donagi and M. Wijnholt, *Higgs Bundles and UV Completion in F-Theory*, *Commun. Math. Phys.* **326** (2014) 287 [`0904.1218`].

[174] J.J. Heckman, *Particle Physics Implications of F-theory*, *Ann. Rev. Nucl. Part. Sci.* **60** (2010) 237 [`1001.0577`].

[175] S. Greiner and T.W. Grimm, *On Mirror Symmetry for Calabi-Yau Fourfolds with Three-Form Cohomology*, *JHEP* **09** (2016) 073 [`1512.04859`].

[176] S. Greiner and T.W. Grimm, *Three-form periods on Calabi-Yau fourfolds: Toric hypersurfaces and F-theory applications*, *JHEP* **05** (2017) 151 [`1702.03217`].

[177] M.F. Atiyah, *Riemann surfaces and spin structures*, *Annales Scientifiques de L'Ecole Normale Superieure* **4** (1971) 47.

[178] D. Mumford, *Theta characteristics of an algebraic curve*, *Ann. Sci. Ecole Norm. Sup* **4** (1971) 181.

[179] D.S. Freed and E. Witten, *Anomalies in string theory with D-branes*, *Asian J. Math.* **3** (1999) 819 [`hep-th/9907189`].

[180] H.B. Lawson and M.L. Michelsohn, *Spin geometry*, *Princeton Mathematical Series* **38** (1990) .

[181] Y.-H. He, R.-K. Seong and S.-T. Yau, *Calabi–Yau Volumes and Reflexive Polytopes*, *Commun. Math. Phys.* **361** (2018) 155 [`1704.03462`].

[182] D. Mumford and G.M. Bergman, *Lectures on Curves on an Algebraic Surface*, *Annals of Mathematics Studies* **59** (1966) .

[183] E. Freitag, *Complex Analysis 2: Riemann Surfaces, Several Complex Variables, Abelian Functions, Higher Modular Functions*, Universitext, Springer Berlin Heidelberg (2011).

[184] S. Natanzon and A. Pratoussevitch, *Higher spin klein surfaces*, *Moscow Mathematical Journal 16* (2016) 95 [1502.06546].

[185] R. Hartshorne, *Deformation Theory*, *Graduate Studies in Mathematics* (2009) .

[186] G. Greuel, C. Lossen and E. Shustin, *Introduction to Singularities and Deformations*, *Springer Monographs in Mathematics* (2007) .

[187] T.J. Jarvis, *The Picard group of the moduli of higher spin curves*, *The New York Journal of Mathematics* **7** (2001) 23 [math/9908085].

[188] T.J. Jarvis, *Geometry of the moduli of higher spin curves*, *International Journal of Mathematics* **11** (1998) 637 [math/9809138].

[189] K. Wagner, *Über eine Eigenschaft der ebenen Komplexe*, *Mathematische Annalen* **114** (1937) 570.

[190] S. Mac Lane, *A combinatorial condition for planar graphs*, *Fundamenta Mathematicae* **28** (1937) 22.

[191] O. Gimenez and M. Noy, *Asymptotic enumeration and limit laws of planar graphs*, *Journal of the American Mathematical Society* **22** (2009) 309.

[192] A. Chmeiss and P. Jégou, *A generalization of chordal graphs and the maximum clique problem*, *Information Processing Letters* **62** (1997) 61 .

[193] S. Felsner, *Geometric Graphs and Arrangements: Some Chapters from Combinatorial Geometry*, *Advanced Lectures in Mathematics* (2012) .

[194] S. Busonero, M. Melo and L. Stoppino, *Combinatorial aspects of nodal curves*, math/0602553.

[195] E. Arbarello, M. Cornalba and P. Griffiths, *Geometry of algebraic curves*, *Grundlehren der mathematischen Wissenschaften* **2** (2011) 79.

[196] M. Bies, M. Cvetič, R. Donagi, M. Liu and M. Ong, *Root Bundles and Towards Exact Matter Spectra of F-theory MSSMs*, 2102.10115.

[197] C. Lucia, C. Cinzia and C. Maurizio, *Moduli of roots of line bundles on curves*, *Trans. Amer. Math. Soc. 359* (2007) [math/0404078].

[198] V.V. Batyrev, *Dual polyhedra and mirror symmetry for Calabi-Yau hypersurfaces in toric varieties*, *J. Alg. Geom.* **3** (1994) 493 [alg-geom/9310003].

[199] E. Perevalov and H. Skarke, *Enhanced gauged symmetry in type II and F theory compactifications: Dynkin diagrams from polyhedra*, *Nucl. Phys. B* **505** (1997) 679 [hep-th/9704129].

[200] Cox, D.A. and Katz, S., *Mirror Symmetry and Algebraic Geometry*, Mathematical surveys and monographs, American Mathematical Society (1999).

[201] F. Rohsiepe, *Lattice polarized toric K3 surfaces*, hep-th/0409290.

[202] A.P. Braun, C. Long, L. McAllister, M. Stillman and B. Sung, *The Hodge Numbers of Divisors of Calabi-Yau Threefold Hypersurfaces*, 1712.04946.

[203] D. Cox, J. Little and H. Schenck, *Toric Varieties*, Graduate studies in mathematics, American Mathematical Soc. (2011), 10.1090/gsm/124.

[204] M. Kreuzer, *Toric geometry and Calabi-Yau compactifications*, *Ukr. J. Phys.* **55** (2010) 613 [hep-th/0612307].

[205] R. Blumenhagen, B. Jurke, T. Rahn and H. Roschy, *Cohomology of Line Bundles: A Computational Algorithm*, *J. Math. Phys.* **51** (2010) 103525 [1003.5217].

[206] S.-Y. Jow, *Cohomology of toric line bundles via simplicial Alexander duality*, *Journal of Mathematical Physics* **52** (2011) 033506 [1006.0780].

[207] R. Blumenhagen, B. Jurke, T. Rahn and H. Roschy, *Cohomology of Line Bundles: Applications*, *J. Math. Phys.* **53** (2012) 012302 [1010.3717].

[208] R. Blumenhagen, B. Jurke and T. Rahn, *Computational Tools for Cohomology of Toric Varieties*, *Adv. High Energy Phys.* **2011** (2011) 152749 [1104.1187].

[209] Jurke , B. and Rahn, T. and Blumenhagen, R. and Roschy, H., *cohomCalg ++ Koszul Extension - Manual v0.31*, May, 2011.

[210] "cohomCalg package." https://github.com/BenjaminJurke/cohomCalg, 2010.

[211] T. Rahn and H. Roschy, *Cohomology of Line Bundles: Proof of the Algorithm*, *J.Math.Phys.* **51** (2010) 103520 [1006.2392].

[212] L.B. Anderson, Y.-H. He and A. Lukas, *Heterotic Compactification, An Algorithmic Approach*, *JHEP* **07** (2007) 049 [hep-th/0702210].

[213] L.B. Anderson, *Heterotic and M-theory Compactifications for String Phenomenology*, Ph.D. thesis, Oxford U., 2008. 0808.3621.

[214] R. Hartshorne, *Algebraic Geometry*, Graduate Texts in Mathematics, Springer (1977).

[215] C. Kuratowski, *Sur le problème des courbes gauches en Topologie*, *Fundamenta Mathematicae* **15** (1930) 271.